

**School of Electrical Engineering and Computing
International Centre for Radio Astronomy Research
Curtin Institute of Radio Astronomy**

**Small Reverberation Chambers for Radio Frequency Emission
Measurements: a Radio Astronomy Feasibility Study**

Chittawan Choeyesakul

**This thesis is presented for the Degree of
Doctor of Philosophy
of
Curtin University**

June 2015

To the best of my knowledge and belief, this thesis contains no material previously published by any other person except where due acknowledgement has been made. This thesis contains no material which has been accepted for the award of any other degree or diploma in any university.

Chittawan Choeyesakul

Chittawan Choeyesakul

Commander, Royal Thai Navy

24 June 2015

ABSTRACT

Radio frequency emission measurements are performed to establish compliance with standards, or for problem identification. Emission limit values for radio astronomy applications are extremely low, and the sensitivity of instrumentation in a typical EMC laboratory is often insufficient for required measurements. The Square Kilometre Array (SKA) is a new, extremely powerful radio telescope to be built in Western Australia and South Africa. It will operate in the frequency range from 50 MHz to 20 GHz and emission from its electrical and electronic components must be tightly controlled to avoid self-interference. For example, emission limit values up to 80 dB more stringent than the commonly-used MIL-STD-461F are in place.

Reverberation chambers are, in principle, well suited for testing equipment used in radio astronomy, because of their better sensitivity compared with other environments, such as anechoic chambers or open area test sites. Emission measurements in conventional reverberation chambers require a stirrer to change the field distribution and to shift resonance frequencies. Accurate measurements can only be made in a frequency range with high enough mode density, i.e. above a certain frequency which is dependent on the physical size of a chamber. This frequency is referred to as the “lowest usable frequency” (LUF). A room would need dimensions in the order of at least 20 m by 12 m to be usable as a reverberation chamber at 50 MHz.

The objective of this research was to develop a technique for accurate and sensitive emission measurements in reverberation chambers below their conventional LUF, allowing much smaller and more economical rooms to be used. A number of modifications to the design and operation of a conventional reverberation chamber were made to achieve this goal. These were:

1. Stirrer design: gaps between resonance frequencies in cavities are wider at lower frequencies, and the ability of the stirrer to shift resonances becomes an important design criterion. A double C-shaped stirrer was compared to a commonly used Z-shaped stirrer, and was found to perform better at low frequencies.

2. Multiple receive antennas: at low frequencies the field distribution is not statistically uniform and isotropic over one stirrer revolution. In this research, placing antennas at several locations ensured that each cavity mode excited a maximum signal in at least one antenna, and improved the performance of the reverberation chamber significantly.
3. Movement of the equipment under test (EUT): placing the EUT at different positions ensured that each cavity mode was excited and thus generated a strong signal in one, or several, of the receiving antennas.
4. Validation procedure: the concept of statistically uniform and isotropic fields as used in conventional reverberation chambers (in which the EUT always produces the same signal in the receiving antenna regardless of EUT position) was replaced by a formalism which identifies and selects preferred data sets yielding accurate field measurements.

Analytical approaches and computer simulations were used as tools to understand the reverberation chamber field distributions, and to guide the design and evaluation of a one-fifth scale model reverberation chamber. Tests made on the model validate the usability of the modified chamber for emission measurements at low frequencies.

The conclusion of this thesis is that, while testing with an under-sized chamber takes longer (in the order of 10 - 30 times), and requires a more complex validation procedure, the sensitivity is much better than for anechoic chamber measurements (by up to 20 - 30 dB). The uncertainty, at low frequencies down to the first resonance frequency, is better than for a conventional reverberation chamber. After a consideration of frequency and dimensional scaling of resonance “Q” (quality) factors, the thesis shows that similar performance gains can be expected for a full-size reverberation chamber.

ACKNOWLEDGEMENTS

This journey of many years has been exhilarating and fulfilling, but challenging and demanding. I would not have made it this far without the many people who have travelled alongside me, even if only for a little while.

I would like to express my sincere gratitude to my supervisor, Dr Franz Schlagenhauer. I will forever be indebted for trusting my abilities and fully supporting my thesis candidacy, travel arrangements and research. Words will not suffice in describing the extensive role that Prof. Peter Hall, my co-supervisor, has played in nurturing my fledgling career as a researcher. Their suggestions have never been a mistaken. The greatest lesson that both my supervisors have taught me is that the best presentations and papers are the ones that are the simplest and most succinct.

I am also thankful to many others from ICRAR/CIRA and other institutions, with whom I have had the pleasure of discussing my work through random chats in the corridor, or in official discussions and meetings. In particular, I thank Mr Jonathan Tickner, Mr David Emrich, Mr Mark Waterson, Dr Adrian Sutinjo, Dr Budi Juswardy, Dr John Flexman, Dr Shantanu Padhi, and Mr Brian Crosse. I would never have finished my works without their help.

I would like to thank Dr André Fletcher of the UWA School of Physics, for his careful proofreading of various drafts of this thesis.

To my fellow ICRAR slaves and postgraduate students past and present, including Dr Tim Colegate, Dr John Goldsmith, Mr Aziz Jiwani, Dr Hayden Rampadarath, Mr Tom Russell, Mrs Divya Palaniswamy; thanks for keeping me sane. It is good to know that I am not alone on this way. Special thanks go to Dr Tim Colegate for sharing his thesis.

I never forget to say thank you to my father, my mother, my sister and my brother for their helpful guidance, suggestions and encouragement throughout this study. I would like to thank all people of my family (including my grandfather and my grandmother who passed away) and my friends in Thailand for always cheering me up. Also, I give special thanks to my wife for supporting me along this long journey.

Additionally, I would like to express my thank to my commander and colleagues in Royal Thai Navy. Especially and particularly, Admiral Panlop

Tamisanon, who allowed me to study in Australia. I would also like to thank the Royal Thai Navy for providing financial support in the form of a research fund and my scholarship. Finally, thanks to Captain Kerchai Vajanaporn and Captain Apichai Sompolgrunk for taking care of me during my stay in Australia.

Chittawan Choeksakul
Commander, Royal Thai Navy

TABLE OF CONTENTS

	Page
Declaration.....	iii
Abstract.....	v
Acknowledgements.....	vii
Table of Contents.....	ix
List of Tables.....	xii
List of Figures.....	xiii
List of Abbreviations.....	xvii
List of Symbols.....	xix
Chapter 1 Introduction.....	1
1.1 Thesis Motivation.....	1
1.2 Preamble.....	3
1.2.1 Navy.....	3
1.2.2 Radio Astronomy.....	6
1.3 Purpose of the Research.....	14
1.3.1 Reverberation Chamber for Radio Astronomy.....	15
1.3.2 Thesis Objectives.....	18
1.4 Literature Review.....	18
1.5 Research Methodology.....	32
1.6 Structure of the Thesis.....	34
1.7 Original Research in this Thesis.....	37
1.8 Thesis Contributions.....	38
Chapter 2 From Basic EMC to Reverberation Chambers for RA.....	39
2.1 Electromagnetic Compatibility.....	39
2.1.1 Early EMC prior to WW2.....	41
2.1.2 WW2 – Emergence of EMC Issues.....	43
2.1.3 Birth of Modern EMC.....	44
2.2 Standard Development of Radiated Emission Measurements for RA.....	46
2.2.1 Principle of a Radiated Emission Measurements.....	46
2.2.2 Standardised Approaches to Emission Measurements.....	47
2.2.3 Four Methods for Radiated Emission Measurements.....	51
2.3 Method of Conventional RC.....	55
2.3.1 Origin of RC.....	57
2.3.2 Procedures for Radiated Emission Measurements (Conventional RC).....	70
2.4 New Ideas in this Research.....	75
2.4.1 Theories Supporting the Methodology.....	75
2.4.2 Summary of New Ideas in this Research.....	82
2.5 Chapter Summary.....	85

	Page
Chapter 3 MIMO RC: Designs and Applied Implementations	87
3.1 Novel Designs and Implementations	88
3.1.1 Conceptual Designs	88
3.1.2 Choice of Simulation Program	91
3.1.3 Composite Q Factors (Q_g) of chambers.....	94
3.1.4 Scaled Model	103
3.2 Design Characteristics	104
3.2.1 Receiving Antenna	104
3.2.2 Stirrer.....	110
3.2.3 Working Volume & Field Uniformity.....	115
3.3 Assembly of Components and Control Software.....	119
3.3.1 Hardware	119
3.3.2 Software.....	122
3.4 Chapter Summary	125
Chapter 4 Field Uniformity of a MIMO RC	127
4.1 Introduction.....	127
4.2 Setups and Procedures	131
4.2.1 Setups	131
4.2.2 Procedures	133
4.3 Measured Results	137
4.3.1 Conventional Validation Measurements	137
4.3.2 MIMO Validation Measurements.....	140
4.4 Analysis of the Measured Results.....	143
4.4.1 Analysis	143
4.4.2 Simulated Field Distribution	144
4.5 Chapter Summary	147
Chapter 5 MIMO Radiated Emission Measurements	149
5.1 Introduction.....	149
5.2 Procedure Developments	150
5.2.1 Procedure to move the EUT	150
5.2.2 Procedure to process the Measured Signals	156
5.3 MIMO Radiated Emission Measurements.....	160
5.3.1 The EUT for Measurements	160
5.3.2 Measuring CVF, CLF, AVF, and IL	161
5.3.3 Setting Up for MIMO Radiated Emission Measurements ...	163
5.3.4 Processing Received Signals by using Mean Values	165
5.3.5 Processing Received Signals by using Maximum Values....	170
5.4 Scientific Validation of the Results: Sensitivity and Accuracy	172
5.5 Summary of MIMO RC procedures for Emission measurements.	176
5.6 Chapter Summary	178

	Page
Chapter 6 Conclusion and Scope for Future Work.....	179
6.1 Introduction.....	179
6.2 Practical Outcomes and Considerations.....	179
6.3 Implications/Utilisation of the Study to Related Areas	181
6.4 Problems and Suggestions for Future Research.....	182
6.5 A Final Word	182
References.....	183
Appendix A Computational Electromagnetic Modelling (ANSOFT HFSS)	191
Appendix B MATLAB Automating System for Collecting the Data.....	198
Appendix C The GUI Code for Post-Processing the Data.....	201
Appendix D Manual for MIMO RC (Guideline to apply MIMO RC to the Actual Room)	207
Appendix E Key Measured Results	212
Appendix F Conventional Validation Procedure from IEC standard	220
Appendix G Publications	224

LIST OF TABLES

Table	Page
1-1 Comparison of EMC units for RA and NAVY	12
1-2 Advantages and Disadvantages of the RC method.....	16
1-3 Objectives of this thesis	18
2-1 Resonant frequency comparisons (2013).....	67
3-1 Implementation of SISO, MISO, SIMO, and MIMO	89
3-2 Three different materials for investigations.....	95
3-3 Simulated Composite Q -factor	96
3-4 Composite Q -factors, for copper	99
3-5 Characteristics of the scaled model and the CIRA shielded room	104
4-1 Implementations of SISO - MIMO Validation Procedures	128
4-2 MIMO RC procedures	129
4-3 Comparison of all equations	136
4-4 Field uniformity tolerance requirements	143
5-1 KPIs suggested from the “6 dB band” criterion (at a particular frequency).....	158
5-2 KPIs after applying the “6 dB band” criterion to 9 EUT positions	167
F-1 Field uniformity tolerance requirements	223

LIST OF FIGURES

Figure	Page
1-1 Smart 80 RC, ETS-LINDGREN, 80 MHz-18 GHz.	3
1-2 HTMS Makut Rajakumarn, a frigate operated by the Royal Thai Navy...	4
1-3 MIL-STD-461F, Table V, Table IV.	5
1-4 Karl Jansky (1932): investigating RFI for telephone service, the signals turned out to be of astronomical origin.....	8
1-5 Grote Reber and his radio telescope (1937): after looking for astronomical signals, he found galactic RF emission....	8
1-6 Importance of EMC to control interference at an RA site.....	11
1-7 The SKA Low Frequency Aperture Array located in MRO, Image credit: Swinburne Astronomy Productions.....	13
1-8 Radio Quiet Zones at MRO site, Western Australia,.....	14
1-9 Examples of making emission measurements	16
1-10 The CIRA shielded room expected to be a RC.....	17
1-11 Number of useful research selected for good starting this thesis (excluding text books, standards, and online resources).	19
1-12 DSTO Reverberation Chamber.....	21
1-13 Schematic View of Source Stirring Reverberation Chamber: SSRC (no need for a stirrer).	25
1-14 The Vibrating Intrinsic Reverberation Chamber: VIRC (no need for a stirrer)	26
1-15 Research flow adopted for this thesis.	35
2-1 Applications and methods of EMC.....	40
2-2 Map of the transatlantic telegraph cable route (1858).....	41
2-3 Cooperation of IEC and CISPR.....	50
2-4 MIL-STD-461F, RE102 limit for ground application	51
2-5 Anechoic Chamber, Curtin University, WA, Australia.....	53
2-6 Schematic view of Symmetrical TEM Cell	54
2-7 Concept of radiated emission measurements in the RC method	56
2-8 Rectangular waveguide and some of its resonant modes	57
2-9 The cutoff TE and TM modes of a rectangular waveguide	61
2-10 Reference excitation for rectangular cavity modes	61
2-11 The cutoff TM modes of a rectangular cavity.	63
2-12 Z-Stirrer, ETS-LINDGREN, 1.5 m x 1.5 m x 7 m, for 80 MHz.	64
2-13 C-LUF compared to 1 st resonance	65
2-14 Probability Density Function (PDF) of Gaussian, Rician, and Rayleigh distributions (medium SNR).....	66
2-15 Effect of composite Q factor (Q_g).....	69
2-16 A conventional reverberation chamber's working volume validated by 8 probes placed at the corners (3 polarisations measured at each corner)....	71
2-17 An example of Standard Deviation of data for E -field components.	72
2-18 IEC Standard: setup for measuring Chamber Validation Factor	73
2-19 Field distributions at dominant modes related to the excitation position..	76
2-20 Simulated Reflection Coefficient (S_{11}) of 2 excitation cases from Fig. 2-19.	77

Figure	Page
2-21 <i>E</i> -field at TM ₁₁₀ , 441 MHz. <i>E</i> -field has only Z component when position of excitation is as in case A (Fig. 2-19).	78
2-22 <i>E</i> -field at TE ₁₀₁ and TE ₀₁₁ , 371 MHz. <i>E</i> -field has only Y component when position of excitation is as in case B (Fig. 2-19).	78
2-23 <i>E</i> -field at 1,457 MHz, case A (Fig. 2-19).	79
2-24 Poor S ₁₁ performance of Z-stirrer at dominant mode: case A (Fig. 2-19).	80
2-25 <i>E</i> -field of S ₁₁ , case A (Fig. 2-19)	80
2-26 An EUT placed in the model, and moved.	81
2-27 Simulated S ₂₁ over one revolution of Z-stirrer after a “1 W” EUT is placed, comparison for two positions of EUT.	81
2-28 Microwave oven, an example of moving the EUT (using infrared thermal imaging inside a microwave oven [80]).	83
2-29 Summary of all procedures for a conventional RC and MIMO RC to make radiated emission measurements (above the conventional LUF).	86
3-1 CIRA shielded room (3.6m by 2.4m by 2.4m) expected to be a RC	88
3-2 4 types of basic communication channels	89
3-3 Comparison of concepts, from conventional RC to MIMO RC	90
3-4 Computational Electromagnetic Modelling Methods	91
3-5 Model of the CIRA room and its scaled model (in ANSOFT HFSS).	94
3-6 Calculated Composite <i>Q</i> -Factors of the Shielded Room	97
3-7 Calculated Composite <i>Q</i> -factors of the 1:5 Scaled Model	98
3-8 Calculated composite <i>Q</i> -Factors	100
3-9 Comparison between measured and calculated <i>Q_g</i> , Scaled Model.	101
3-10 Scaled model (1:5) of the CIRA Shielded Room	103
3-11 MIMO-LUF (1 st resonance), C-LUF, transition region of the scale model ...	104
3-12 A top-loaded monopole specifically designed to be used in the 1:5 Scaled Model.	107
3-13 Characteristics of the top-loaded monopole placed in the vertical plane.	107
3-14 Examples of field distributions as below the 60 th mode frequency)	108
3-15 Half-wave electric field (in relation to Fig. 3-14)	108
3-16 Nine top-loaded monopole antennas mounted on the 1:5 scaled Model.	109
3-17 Comparison of Reflection coefficientS (S ₁₁) at port 1 (scaled Model).	109
3-18 Position of the stirrer in the Scaled Model (ANSOFT HFSS)	111
3-19 Simulated S ₁₁ from receiving antenna port 1, Double C stirrer, case A (Fig. 2-19).	111
3-20 <i>E</i> -field of of 8 marked resonances, when the Double C stirrer is applied.	112
3-21 Comparison of simulated S ₁₁ (resonances) for the Z-stirrer & Double C stirrer, one revolution, 45-degree/step, case A (Fig. 2-19)	113
3-22 Measured S ₁₁ from receiving antenna case A (Fig. 2-19), Double C stirrer, case A (Fig. 2-19).	113
3-23 Measured Voltage over the stirrers’ revolution, case N2 (Fig. 2-26).	114
3-24 Conventional Working Volume validated by probes at each corner.	116
3-25 Working Volume of the Scaled Model	116
3-26 The Validation Set; rotatable H-shaft with cone antennas	117
3-27 The 1:5 scaled model with all tools and the Validation Set	118
3-28 Characteristics of the cone antennas	118

Figure	Page
3-29 Schematic diagram of the automating system	119
3-30 The scaled model set up for automated measurements.....	120
3-31 Concepts of Conventional RC and MIMO RC — equivalent to basic communication channels	121
3-32 Processing steps from collecting to post-processing	123
3-33 GUI version 6.0 (as of 30 June 2014).....	125
4-1 The Working Volume defined by the Validation Set	132
4-2 Setting up for validation procedures.....	132
4-3 Connection diagram of the validation procedures	133
4-4 Setting up for the SISO validation procedure.....	137
4-5 Signals received by antenna port 1, X-polarisation	138
4-6 Maximum received signals (from 8 corners of the working volume) by receiving antenna port 1, X-polarisation.....	139
4-7 STDs of X, Y, Z and total following the IEC standard	139
4-8 Setting up for the MIMO validation procedure	141
4-9 Standard deviations of X, Y, Z and total for MIMO validation procedure	142
4-10 Comparison of σ_z between the conventional RC and MIMO RC.....	144
4-11 The Scaled Model without stirrer-this can be called a Source Stirring Reverberation Chamber (SSRC).....	144
4-12 Measured STD of the Scaled Model, with and without the stirrer	145
4-13 Field distributions at 650 MHz, Y-Polarisation.....	146
5-1 Canonical 12-face/axis orientations for a typical EUT for TEM cells	150
5-2 Concept of a Uniform Field Area (UFA), in ACs	151
5-3 The Biconical Noise Source	152
5-4 Characterisations of the Biconical Noise Source.....	152
5-5 The Biconical Noise Source placed for 3 positions \times 3 polarisations	153
5-6 Maxima of eight SISO results (without CVF)	153
5-7 Comparisons of SIMO and MIMO results (Q_g is not compensated).....	154
5-8 Example of the “6 dB band” strategy at a particular frequency.....	158
5-9 Diagram of the EUT: Slot Noise Source	160
5-10 Characteristics of the EUT: Slot Noise Source.....	161
5-11 Setting up for CVF measurements	162
5-12 Measured CVF and IL of the Scaled Model, combination of ants. 1 and 2 ...	163
5-13 Pattern of moving the EUT over $N_p = 9$ positions.....	164
5-14 Setting up for moving the EUT over 9 positions	164
5-15 Receiving antenna 1 only, EUT position 1, over 1 stirrer revolution	165
5-16 All 9 receiving antennas (mean value in each case), EUT position 1; 1 st EUT Position, 1 stirrer revolution	166
5-17 All 9 EUT positions (maximum of means from all 9 receiving antennas in each case).....	166
5-18 KPI strategy that 67% (or 6 out of 9 data points) must lie inside 6 dB	167
5-19 Common and modified means (6 dB band) for all 9 results of Fig. 5-17..	168
5-20 The Radiated Power of the EUT, from the processed results in Fig. 5-19	168
5-21 Radiated power (CVF method), when EUT placed in different polarisations	169
5-22 The Radiated Power determined by Equation 5.1, EUT is placed in Z-Polarisation.	170

Figure	Page
5-23 Radiated power (IL method), when the EUT is placed in different polarisations.	171
5-24 Comparison of Radiated power (absolute values) between MIMO RC, Conventional RC, and AC results.....	171
5-25 Comparison of Radiated power (relative differences) between MIMO RC, Conventional RC, and AC results.....	172
5-26 Performance of Double C Stirrer from Fig. 3-20.....	173
5-27 Sensitivities of MIMO RC and AC.....	173
5-28 Field distribution is changed when the Tx position is moved.....	176
5-29 MIMO RC procedure for emission measurements	177
A-1 ANSOFT HFSS V.13 is deployed to make a model of the actual shielded room (3.6m by 2.4m by 2.4m).....	192
A-2 Dimensions of the existing shielded room (in mm)	193
A-3 A model of the existing shielded room in ANSOFT HFSS	194
A-4 Dimensions of the 1:5 Scaled Model (in mm) with positions of 9 receiving antennas, stirrer, and calibrating set.....	195
A-5 A model of the 1:5 scaled model in ANSOFT HFSS	196
A-6 Feeding Ports used with all models in this research in ANSOFT HFSS simulation program	197
B-1 All 15 sub codes of the Automating System for collecting the data.	199
B-2 MIMO Automating System for collecting the data.	200
C-1 All 15 sub codes of MATLAB Analysis System for post-processing the recorded data. *All files are available on the CD	202
C-2 MIMO Analysis System for post-processing the data.	203
C-3 Validation Procedure Analysis on GUI version 6.0.....	205
C-4 Emission Measurement Analysis on GUI version 6.0.	206
D-1 The actual Shielded Room with its 1:1 model in ANSOFT HFSS	209
D-2 Expected conditions of the actual Shielded Room when MIMO RC technique is applied.....	210
D-3 Pattern on moving EUT for 9 positions in the actual Shielded Room	211
E-1 MIMO Validation Procedure: Raw data, from each cone to receiving antennas, only X-polarisation (the maxima are used)	213
E-2 MIMO Validation Procedure: Raw data, from each cone to receiving antennas, only Y-polarisation (the maxima are used)	214
E-3 MIMO Validation Procedure: Raw data, from each cone to receiving antennas, only Z-polarisation (the maxima are used).....	215
E-4 MIMO emission measurement: Z-polarisation, 1 st EUT position, 2 nd – 9 th antennas	216
E-5 Measured S_{11} from receiving antenna port 2, Double C stirrer	217
E-6 Received signals over one stirrer revolution, when Port 1 is used as Tx..	217
E-7 Received signals over one stirrer revolution, when Port 2 is used as Tx..	218
E-8 The forwarded power go through the antenna port 1	218
E-9 The forwarded power go through the antenna port 2	219
E-10 The forward power, combination between ports 1 and 2	219

LIST OF ABBREVIATIONS

AC	Anechoic Chamber
ASKAP	Australian SKA Pathfinder
ATCA	Australia Telescope Compact Array
AVF	Antenna Validation Factor
BER	Bit Error Rate
BPSK	Binary Phase Shift Keying
CVF	Chamber Validation Factor
CDF	Cumulative Distribution Function
CISPR	Comité International Spécial des Perturbations Radioélectriques
CIRA	Curtin Institute of Radio Astronomy
CLF	Chamber Loading Factor
C-LUF	Conventional Lowest Usable Frequency
CMC	Combined Mode Chamber
CSIRO	Commonwealth Scientific and Industrial Research Organisation
CW	Continuous Wave
EA	Electronic Attack
ECCM	Electronic Counter-countermeasures
ECM	Electronic Countermeasures
EM	Electromagnetic
EMC	Electromagnetic Compatibility
EMI	Electromagnetic Interference
EMP	Electromagnetic Pulse
EP	Electronic Protection
ES	Electronic Support
ESM	Electronic Support Measures
EUT	Equipment Under Test
EVN	European VLBI Network
EW	Electronic Warfare
FDTD	Finite Difference Time-Domain
FEM	Finite Element Method
FRI	Frequency Range of Interest
GTEM	Gigahertz Transverse Electromagnetic
GUI	Graphic User Interface
HFSS	High Frequency Structure Simulator
HTMS	His Thai Majesty's Ship
ICRAR	International Centre for Radio Astronomy Research
IEC	International Electrotechnical Commission
IEEE	Institute of Electrical and Electronics Engineers
IF	Image Frequency
IL	Insertion Loss
ISM	Industrial, Scientific or Medical
ISO	International Organization for Standardisation
KPI	Key Performance Indicator
LBA	Long Baseline Array
LUF	Lowest Usable Frequency

MIL-STD	Military Standard
MIMO	Multiple-Input Multiple-Output
MIMO LUF	Multiple-Input Multiple-Output Lowest Usable Frequency
MISO	Multiple-Input Single-Output
MoM	Method of Moments
MRO	Murchison Radioastronomy Observatory
MSRC	Mechanics Stirring Reverberation Chamber
MWA	Murchison Widefield Array
NIST	National Institute of Standards and Technology
OATS	Open Area Test Site
PC	Personal Computer
PDE	Partial Differential Equations
PDF	Probability Density Function
RA	Radio Astronomy
RC	Reverberation Chamber
RE	Radiated Emission
RF	Radio Frequency
RFI	Radio Frequency Interference
RA	Radio Astronomy
Rx	Receive (antenna)
SE	Shielding Effectiveness
SIMO	Single-Input Multiple-Output
SISO	Single-Input Single-Output
SKA	Square Kilometre Array
SMA	Subminiature version A
SNR	Signal-to-Noise Ratio
SSRC	Source Stirring Reverberation Chamber
STD	Standard Deviation
TE	Transverse Electric (EM mode)
TEM	Transverse Electromagnetic
TM	Transverse Magnetic (EM mode)
Tx	Transmit (antenna)
UFA	Uniform Field Area
USSR	Union of Soviet Socialist Republics
VIRC	Vibrating Intrinsic Reverberation Chamber
VLBA	Very Long Baseline Array
WLAN	Wireless LAN
WV	Working Volume

LIST OF SYMBOLS

C	Speed of light
\vec{E}	Electric field (E field)
E_x, E_y, E_z	Electric field X, Y, Z polarisation
f_0	Fundamental frequency
$f_{m,n,l}$	Frequency of mode m, n, l
L	Length
H	Height
\vec{H}	Magnetic field (H field)
H_x, H_y, H_z	Magnetic field X, Y, Z polarisation
S_{ij}	S-parameter characterisation between port i and j of a network
Q	Quality factor
Q_g	Composite Quality factor
V	Voltage
V_{pl}	Voltage measurement from 1 st polarisation
λ	Wavelength
λ_c	Cutoff Wavelength
∇	Curl (Operator)
$m, n, \text{ and } l$	Third index, nomenclature for modes in a cavity
P_{AveRec}	Average received power
P_{Input}	Forward power
P_L	Time-average power dissipated in the cavity
$P_{Radiated}$	Radiated power
S	Surface
V	Volume
W	Width
W_e, W_m	Energies stored in electric and magnetic fields
ω	Angular frequency
η	Efficiency
η_{Tx}, η_{Rx}	Antenna efficiency factor (transmitting, receiving)
σ	Electric conductivity
σ_x	Standard Deviation, X polarisation
μ	Permeability, $\mu = \mu_0 \times \mu_r$
μ_0	Permeability of free space
μ_r	Relative permeability
ϵ	Permittivity, $\epsilon = \epsilon_0 \times \epsilon_r$
ϵ_0	Permittivity of free space
ϵ_r	Relative permittivity
$\vec{}$	Vector
\leftrightarrow	Normalised value
$\langle \rangle$	Arithmetic mean value
γ	Propagation constant
k	Wavenumber
h	$\sqrt{\gamma + k}$

“As Radio Astronomy requires the detection of very weak electromagnetic waves from very distant sources, the author believes the techniques in this thesis, which will help increase sensitivity of large radio telescope antennas, will also be useful when applied to long-range telecommunication systems.”

Commander Chittawan Choeyesakul, the author

CHAPTER 1

INTRODUCTION

1.1 Thesis Motivation

During the 2004 Indian Ocean tsunami disaster, the author's role in the Royal Thai Navy was to command a group of hundreds of people to assist in search and rescue efforts. Leading the team into deep forest on an island, line-of-sight radio communications systems failed, forcing the author to command the group by voice alone. This caused major problems in accurately carrying out tasks and in maintaining control. A particular example occurred when one of his colleagues shouted that another tsunami would come; then, hundreds of people tried to run away to the hills, attempting to survive, and the author could not control the rescue team because they were too far away. That led to an inspiration of the author to learn more about radio communications. This kind of situation could have been avoided with a better understanding of communications.

After this inspiring story, the author engaged in studies and found that every long-range radio communication system encounters many problems. One of the major problems is radio frequency interference (RFI), which can be minimised by understanding the nature of electromagnetic signals, specifically in an area known as electromagnetic compatibility (EMC). This is an engineering field in which relatively few engineers work. For example, EMC plays an important role in hospitals, airports, or generally where sensitive equipment, such as receivers or probes, is used in harsh environments. It can also play an important role in the Navy, e.g. in warships, where multiple transmitters and receivers are used at the same time for internal communication, or for contacting other ships, aircraft and land bases. A common situation is the measurement of weak signals among interference from other nearby systems, e.g. the military (Navy) is usually working in such an isolated area that many electromagnetic devices within the Navy itself prevent the successful detection of weak radio signals from distant sources. Studying similar cases to those in the Navy can make the task less complicated.

One practical case study, similar to the Navy situation, is that in radio astronomy (RA). A RA telescope is a highly sensitive system usually located in an isolated area measuring extremely weak signals, while dealing with interference from within the observing site itself. This process is very similar to that in the NAVY. Studying EMC for the most demanding applications for RA should also help with designing NAVY communications and detection systems. At the Curtin University node of the International Centre for Radio Astronomy Research (ICRAR) in Perth, Western Australia, EMC is being researched by focusing on the measuring of extremely weak electromagnetic signals, up to 80 dB more sensitive [1] than usually found in NAVY work. EMC experts at ICRAR seek to minimise RFI to make sure that all electrical and electronic equipment close by, or at, radio astronomy sites have a very low level of electromagnetic emission. Demanding very high sensitivity emission measurements typical of RA requires a plausible set of modified applications for the methods of EMC.

There are many applications and methods of EMC that limit or avoid electromagnetic interference. Measuring in a completely controlled environment is suitable to high sensitive RA requirements. Reverberation Chamber (RC) is chosen among many available EMC methods (details are in Chapter 2). The method of RC can provide more sensitive measurements than other kinds of EMC measurements, enabling the detection of extraordinarily weak signals (and which can also benefit immunity tests). The RC method could deliver a way of making emission measurements of very high sensitivity, reliability, and repeatability at a lower cost than with other techniques. This type of chamber is compact and cheap compared to other methods. The advantages of this method can be applied to the communities of RA, and of the Navy (and can also be applied to immunity tests with high field strength levels). This research has been conducted at ICRAR to examine the possibility of emission measurements with the method of reverberation chambers (RCs). However, this method comes with a serious limitation—the lowest usable frequency (LUF). Fig. 1-1 shows an example of a RC used for automotive tests.

The purpose of this thesis is to investigate feasibility to extend the lowest operation frequency of RCs by modifying the current procedures of the RC method. A novel approach to signal processing is adapted from the conventional method to boost

the performance, due to the fact that the cost of computer equipment is steadily decreasing. As for the results, this research has found a novel RC that can provide better results at low frequencies.



Figure 1-1: Smart 80 RC, ETS-LINDGREN, 80 MHz-18 GHz, $\approx 7 \text{ m} \times 15 \text{ m} \times 8 \text{ m}$.

1.2 Preamble

1.2.1. Navy

Military EMC design can be quite complicated. The combination of interference from a variety of the military platform's own equipment, with those from external threats, lead to stringent demands in specifying military EMC requirements, which are different from non-military ones; i.e., military requirements are usually more stringent than those in commercial environments. In general, Navy EMC requirements are grouped according to two environments, which are:

1) **Navy Fixed Land Based:** This environment includes command, office, and residential buildings. Commercial emission requirements are possibly not suitable and insufficient to protect land based military communications receivers. In general, military receivers are much more sensitive than commercial ones. Military environments are often crowded, where equipment is located in close proximity to sensitive radio receivers, generally more closely and with more serious consequences, than in the commercial environment.

2) **NAVY Mobile Based:** These environments include ships, aircraft, submarines and vehicles. The Navy requirements are affected by many more factors, e.g. sea depth and saltiness, Earth's magnetic field and ionospheric layer, etc. All electronic equipment needs specified emission measurements; these emission limits help prevent the electronic equipment from producing noise that could compromise other receivers on the platform, e.g., for the case of interfering radar and EMP signals. Thus, the emission concerns in the Navy are usually aimed to protect multiple channels over a much wider range of operating frequencies.

Figure 1-2 shows a frigate operated by the Royal Thai Navy, HTMS Makut Rajakumarn. She is armed with multiple receivers and transceivers; her operation frequency ranges, for those installed devices, are from HF (2 MHz) to Ku band (18 GHz). All devices are operating at the same time. Thus, better sensitivity, stability, reliability, and repeatability than those for the usual applications of EMC are required.



Figure 1-2: HTMS Makut Rajakumarn, a frigate operated by the Royal Thai Navy.

EMC applications for the Navy: In 1967, the USS Forrestal disaster brought EMC to the attention of military forces, with the deaths of 134 sailors, and many more got injured (more details in Chapter 2). After that, a standard on the subject of EMC

for military uses was released in the USA; this standard was used as a kind of proxy for a variety of applications. The military standard (more details in Chapter 2) provided both for test procedures and recommended requirements. The standard was updated over the years, to MIL-STD-461F [2] in the present day; this standard is widely used by various Navies around the world. The requirements drawn from the standard are partly shown in Fig. 1-3. Obviously, from these figures, the requirements for Navy Surface ships and submarines are the most demanding, as compared to Army and Air Force applications.

TABLE V. Requirement matrix.

Equipment and Subsystems Installed In, On, or Launched From the Following Platforms or Installations	Requirement Applicability																	
	CE101	CE102	CE106	CS101	CS103	CS104	CS105	CS106	CS109	CS114	CS115	CS116	RE101	RE102	RE103	RS101	RS103	RS105
Surface Ships	A	A	L	A	S	S	S	A	L	A	S	A	A	A	L	A	A	L
Submarines	A	A	L	A	S	S	S	A	L	A	S	L	A	A	L	L	A	L
Aircraft, Army, Including Flight Line	A	A	L	A	S	S	S			A	A	A	A	A	L	A	A	L
Aircraft, Navy	L	A	L	A	S	S	S			A	A	A	L	A	L	L	A	L
Aircraft, Air Force		A	L	A	S	S	S			A	A	A	A	L	L	A	A	
Space Systems, Including Launch Vehicles		A	L	A	S	S	S			A	A	A	A	L	L	A	A	
Ground, Army		A	L	A	S	S	S			A	A	A	A	L	L	A	A	
Ground, Navy		A	L	A	S	S	S			A	A	A	A	L	A	A	A	L
Ground, Air Force		A	L	A	S	S	S			A	A	A	A	L	L	A	A	

Legend:

- A: Applicable
- L: Limited as specified in the individual sections of this standard
- S: Procuring activity must specify in procurement documentation

TABLE IV. Emission and susceptibility requirements.

Requirement	Description
CE101	Conducted Emissions, Power Leads, 30 Hz to 10 kHz
CE102	Conducted Emissions, Power Leads, 10 kHz to 10 MHz
CE106	Conducted Emissions, Antenna Terminal, 10 kHz to 40 GHz
CS101	Conducted Susceptibility, Power Leads, 30 Hz to 150 kHz
CS103	Conducted Susceptibility, Antenna Port, Intermodulation, 15 kHz to 10 GHz
CS104	Conducted Susceptibility, Antenna Port, Rejection of Undesired Signals, 30 Hz to 20 GHz
CS105	Conducted Susceptibility, Antenna Port, Cross-Modulation, 30 Hz to 20 GHz
CS106	Conducted Susceptibility, Transients, Power Leads
CS109	Conducted Susceptibility, Structure Current, 60 Hz to 100 kHz
CS114	Conducted Susceptibility, Bulk Cable Injection, 10 kHz to 200 MHz
CS115	Conducted Susceptibility, Bulk Cable Injection, Impulse Excitation
CS116	Conducted Susceptibility, Damped Sinusoidal Transients, Cables and Power Leads, 10 kHz to 100 MHz
RE101	Radiated Emissions, Magnetic Field, 30 Hz to 100 kHz
RE102	Radiated Emissions, Electric Field, 10 kHz to 18 GHz
RE103	Radiated Emissions, Antenna Spurious and Harmonic Outputs, 10 kHz to 40 GHz
RS101	Radiated Susceptibility, Magnetic Field, 30 Hz to 100 kHz
RS103	Radiated Susceptibility, Electric Field, 2 MHz to 40 GHz
RS105	Radiated Susceptibility, Transient Electromagnetic Field

Figure 1-3: MIL-STD-461F [2], Table V: Requirement Matrix, Table IV: Emission and Susceptibility Requirements. CE - Conducted Emissions, CS - Conducted Susceptibility, RE - Radiated Emissions, and RS - Radiated Susceptibility.

However, the standard does not help in every environment. From experiments, done by the author, working in harsh environments (such as the 2004 tsunami incident) might require more sensitive methods/requirements than stated in MIL-STD-461F. The standard does not state the use of the RC method for emission measurements, even though it could provide more sensitive measurements. Studying EMC for emission measurements in RA, which requires one of the most sensitive environments, could be extended to military applications.

1.2.2. Radio Astronomy

Astronomy is the study of celestial objects, e.g. stars, pulsars, black holes, galaxies, and even the whole Universe; for example, visible light, emitted from another Galaxy, can travel through space, and be observed on the Earth's surface. In fact, those celestial objects emit not only visible light but also: radio waves, infrared, ultraviolet, X-ray, and gamma-ray radiation. Varieties of those emissions also can be detected on Earth.

Radio Astronomy (RA) is a subset of astronomy which studies electromagnetic emission, in the form of radio waves, from celestial sources. Radio astronomers observe radio waves with wavelengths longer than 1 mm (much below visible light in the frequency domain). Those radio waves are often called “astronomical signals”, which require a radio telescope for their detection.

Radio Telescopes are used to collect and process astronomical signals. These signals can be used to visualise objects in space. Astronomical images can look very different compared to visible light ones. A radio telescope consists of three general components:

- **Antenna(s)** to collect the astronomical signals. Antennas can be parabolic dishes, cones, dipoles, or other shapes.
- **Amplifier(s)** to increase astronomical signals to a measurable level. The amplifiers are usually extremely sensitive; however, thermal noise is usually one of the main concerns in the operation of amplifier(s).
- **Receiver(s)** to measure (and record) the received astronomical signals. Most radio telescopes now record the measured signals in some digital form. Then, astronomers can process and analyse the signals later.

The sensitivity of the radio telescopes is one of the key factors in successfully detecting astronomical signals. Many factors can deteriorate the sensitivity of radio telescopes; these require engineering knowledge to avoid or mitigate those effects; e.g. radio telescopes must be located at *dry* sites to minimise the water vapour absorption at higher frequencies. Also, the sites must be located at *remote places* to minimise any unwanted signals from other sources that can cause radio-frequency interference (RFI). However, the dominant noise usually comes from electrical devices on the sites themselves, resulting in the requirement of EMC to minimise these interferers (explained in Chapter 2).

History of Radio Astronomy (related to EMC): In the 1860s, scientists considered that celestial objects could emit electromagnetic signals, according to Maxwell's equations [4, 5]. Nikola Tesla and Oliver Lodge made several attempts to detect the emission from the Sun, but those attempts failed due to the limitations of their instruments. It was not until about 70 years later that radio waves were first detected from space.

In the early 1930s, Karl Jansky, who was an engineer with Bell Telephone Laboratories, accidentally discovered the first astronomical signal. He was using a large directional antenna to investigate signals that interfered with transatlantic voice transmissions (Fig. 1-4). Jansky noticed that an unknown source was emitting a signal which repeatedly peaked every 23 hours and 56 minutes, i.e., this unknown signal peaked at every turn of the Earth's rotation (i.e., once per sidereal day). As a result, Jansky concluded that the source of the emission might be interstellar, and in our Milky Way Galaxy (later, in the 1950s, the astronomical signal that Jansky found was designated Sagittarius A, which is one of the brightest known radio sources).

In 1937, Grote Reber, who was interested in extending Jansky's work, designed and built a 32-ft paraboloidal transit dish antenna in an area near his mother's house in Wheaton, Illinois, USA (Fig. 1-5). He also designed and built sensitive receivers to place at the focal point of the dish antenna. In effect, Reber built his own radio telescope, which was significantly more advanced than Jansky's. Reber finished his telescope in September 1937. Reber failed in his first and second attempts to detect astronomical signals (at 900 and 3,300 MHz), due to poor receivers and automobile ignition noise interference. However, his third attempt was finally successful (in 1938,

at 160 MHz), and he could confirm the previous discovery of Jansky's (for his third attempt, Reber worked at night to avoid the interference and noise). As a result, he detected the Galactic radio signal in 1939, made the first radio emission maps (of our Milky Way Galaxy), and detected solar radio emission in 1943 [107].

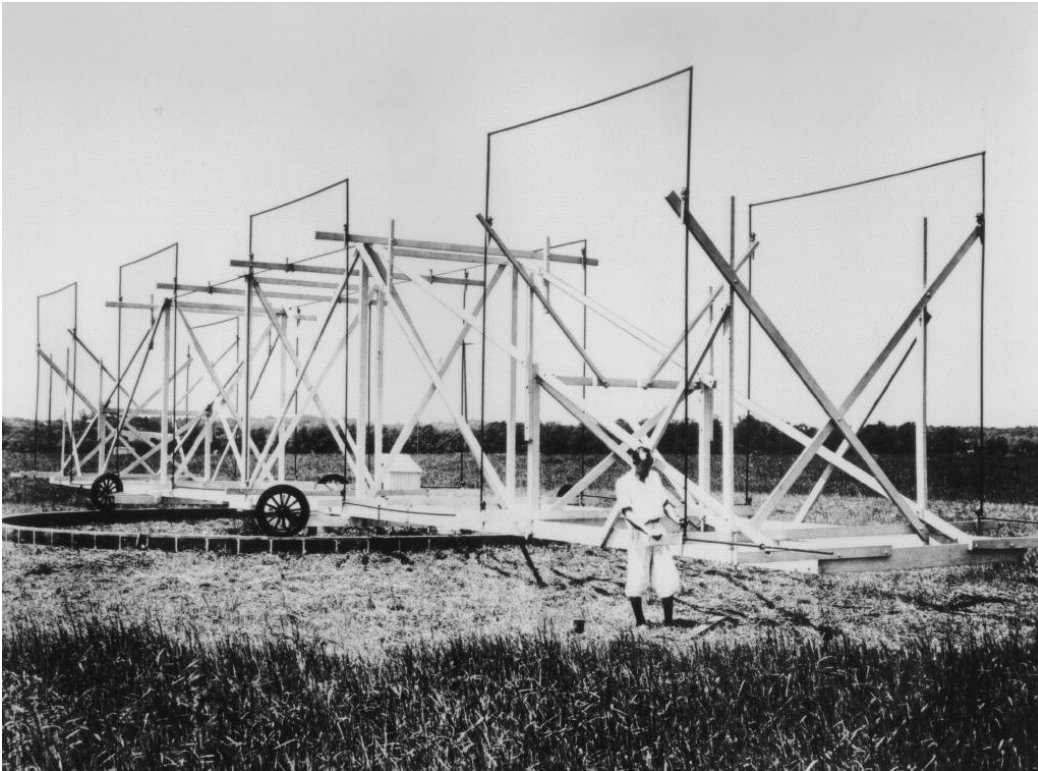


Figure 1-4: Karl Jansky (1932): investigating RFI for telephone service, the signals turned out to be of astronomical origin.



Figure 1-5: Grote Reber and his radio telescope (1937): after looking for astronomical signals, he found galactic RF emission.

Techniques: [3] Radio astronomers work to search for astronomical signals, which are electromagnetic waves. Theoretically, all matter is made of atoms. Every atom consists of one or more electrons which are orbiting the nucleus comprised of protons and neutrons. By changing their speed, location, or direction, they radiate electromagnetic waves. Each type of electromagnetic radiation is produced under certain conditions. By detecting and studying electromagnetic waves emitted from celestial sources, astronomers can understand the conditions that produced them, and so improve their understanding of objects far out in space. All those electromagnetic waves (or astronomical signals) are very faint and carry less energy compared to visible light (which has photons in its electromagnetic spectrum of 2-3 eV, or $3.2\text{-}4.8 \times 10^{-19}$ Joules); radio astronomers thus require a highly sensitive radio telescope to detect faint radio sources. Using only one large radio telescope might not be sensitive enough; then, techniques to link multiple telescopes are necessary. In this thesis, two general techniques using multiple radio telescopes to detect astronomical signals are briefly explained.

1) Radio Interferometry & Aperture Synthesis: developed in its coherent form in 1946 by Martin Ryle [102], a British radio astronomer, and independently by Joseph L. Pawsey and Ruby Payne-Scott, Australian radiophysicists. Modern connected-element radio interferometers consist of two or more separated radio telescopes, investigating the same celestial object, that are connected together using any type of physical connections, e.g. fibre optics. The separation distance between any two radio telescopes is called a "baseline": many more different baselines yield a better quality image. This method allows the telescope array to possibly have sub-arcsecond synthesised beams. As a result, the method generates much more data than a single-antenna radio telescope; then, a process called Aperture Synthesis is used to increase angular resolution. This effectively creates a combined telescope that is as large as the size of the maximum baseline in the array.

An example of an aperture synthesis telescope is the Australia Telescope Compact Array (ATCA), which consists of five moveable 22-metre dish antennas (they can be moved on a railroad track over 3 km, i.e., they can be spaced up to a distance of 6 km apart), and another (6th) telescope 3 km from the end of the track. Its operating frequencies are from 600 MHz to 90 GHz.

2) Very Long Baseline Interferometry (VLBI) [108]: while radio interferometer techniques allow local radio telescopes to work together through physical connections, VLBI (Very Long Baseline Interferometry) effectively allows the linking of multiple radio telescopes from all around the world, without the need of physical connection between the antennas. The received data from multiple telescopes (array antennas) are processed along with recorded timing data. This technique achieves very high angular resolutions by using extremely long baselines. The method allows the telescope array to potentially have sub-milliarcsecond synthesised beams at high frequencies.

Examples of well-known VLBI arrays are: the Very Long Baseline Array (VLBA—with telescopes in North America), the European VLBI Network (EVN—with telescopes in Europe, China, South Africa and Puerto Rico), and the Long Baseline Array (LBA—with telescopes in Australia). Although these arrays are usually operated independently, they occasionally can work together (this is known as Global VLBI), and the sensitivity is then even better.

It is clear that the techniques above were developed to increase the sensitivity of radio telescopes. This may bring the radio astronomer into situations involving RFI, and hence Electromagnetic Compatibility (EMC).

EMC for Radio Astronomy (RA): the higher sensitivity of telescope arrays means that there is more chance to be affected by RFI from other unwanted electromagnetic signals (or noise). From Fig. 1-6, increasing sensitivity might increase interference or noise from unwanted sources as well, and so unwanted emissions from all electronic devices near the telescopes must be very low to avoid interference: e.g., from amplifiers, power lines, solar panels, or the antenna array (coupling). Thus, all electric and electronic devices near the telescope must have their emissions checked against very low emission levels. This leads to the requirement of a high sensitivity emission measurement method for RA.

To apply the EMC method to RA, it must be noted that RA power is expressed in terms of flux density, with a unit called a Jansky (Jy) [4]. There are very few engineers outside of RA who know what a Jy is. The Jansky is also known as a “flux

unit”, and is defined as $10^{-26} \text{ W m}^{-2} \text{ Hz}^{-1}$ (or, $-230 \text{ dBm m}^{-2} \text{ Hz}^{-1}$). For example, “Sagittarius A”, one of the strongest cosmic sources found by Jansky, emits about 0.5-1 Jy over 1-10 GHz [5], while other sources, e.g. “Pulsars”, require up to a 10,000 times higher sensitivity at 4.85 GHz [101]. To convert Jy to dBm, many factors are involved, such as bandwidth, frequency, and antenna characteristics. Some assumptions are required regarding those factors. For an example, $30 \text{ dB}\mu\text{V/m @ 120 kHz} \triangleq 32 \mu\text{V/m}$; $P = \frac{E^2}{377\Omega} = \frac{(32 \times 10^{-6})^2}{377} = 2.65 \times 10^{-12} \text{ W/m}^2 \text{ @ 120 kHz}$, or $= 2.21 \times 10^{-17} \text{ W m}^{-2} \text{ Hz}^{-1}$, or $= -137 \text{ dBm m}^{-2} \text{ Hz}^{-1}$.

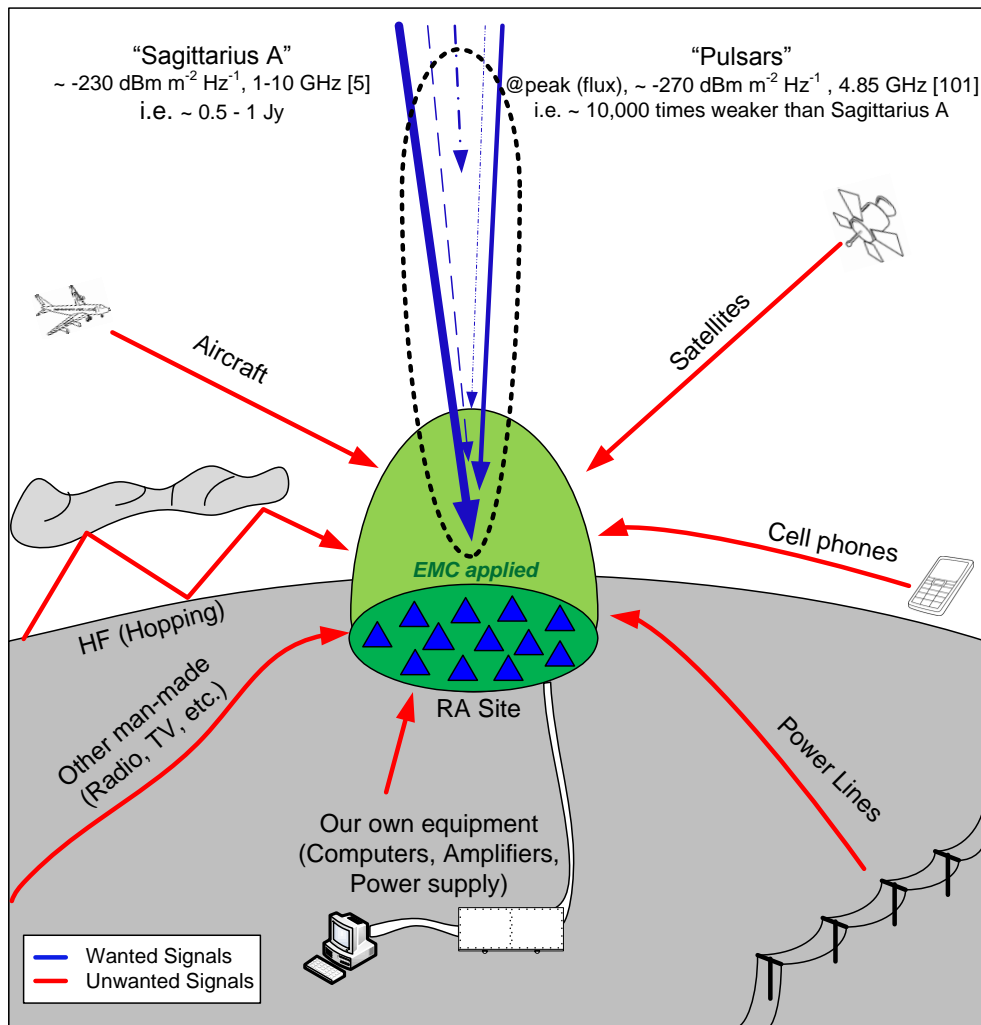


Figure 1-6: Importance of EMC to control interference at an RA site.

Unlike limit values for NAVY (using MIL-STD-461), the Jy is a bandwidth-normalised unit (i.e. /Hz), whereas the limits in MIL-STD-461 versions D and later (explained in Chapter 2) are absolute levels that must be measured in a specified

bandwidth. RA seems to speak in a different language to that in common engineering (EMC); see Table 1-1.

However, building the most powerful radio telescope can only be a success if EMC/RFI problems are solved. Fortunately, the International Telecommunication Union (ITU) established a “Radio Quiet Zone (RQZ) concept” [6, 98], which provides for cooperation between engineers and radio astronomers. Conceptually, an RQZ manages the area around the RA site into zones/layers; use of transmitters is restricted in the zones, depending on the distance from the centre of the RA site. Thus, adopting EMC techniques in each zone is made easier. Each RA site establishes its own RQZ and associates rules; the RA site at Murchison Radioastronomy Observatory (MRO), which this thesis will take as a study case, will be used as the exemplar RQZ from this point.

Table 1–1: Comparison of EMC units for RA and NAVY.

	Radio Astronomy	Common EMC (for Commercial and Military)
Common Unit	Jansky (Jy)	Total radiated power: dBW, dBm, dB μ W
Definition	$1 \text{ Jy} = 10^{-26} \text{ W/m}^2/\text{Hz}$ $1 \text{ Jy} = -260 \text{ dBW/m}^2/\text{Hz}$ $1 \text{ Jy} = -230 \text{ dBm/m}^2/\text{Hz}$ $1 \text{ Jy} = -200 \text{ dB}\mu\text{W/m}^2/\text{Hz}$	$1 \text{ dBW} = 10 \log_{10} (\text{power in Watts})$ $1 \text{ dBm} = 10 \log_{10} (\text{power in Milliwatts})$ $1 \text{ dB}\mu\text{W} = 10 \log_{10} (\text{power in Microwatts})$

EMC for Radio Astronomy at the MRO site, Western Australia: Radio astronomy has played a major role in Australia for a long time; three well-known radio telescopes are given here as examples. The first one was at Dover Heights in Sydney, one of the early telescopes used following the Second World War. The second is the Parkes radio telescope, made famous by the film “*The Dish*” [99], opened in 1961, and still operating today. The third is the Australia Telescope Compact Array (ATCA) near Narrabri, northern New South Wale. In the present day, Australia is at the forefront of Radio Astronomy research. Two new radio telescopes have been built at the MRO in Western Australia, namely the Australian SKA Pathfinder Project (ASKAP) [8], and the Murchison Widefield Array (MWA) [1]. ASKAP is designed to be a high-speed survey instrument with high dynamic range. The MWA is designed to be an all-sky, wide beam, low frequency radio telescope, and is run by the Curtin Institute of Radio Astronomy (CIRA) of the Curtin

University, Perth, Western Australia. Both ASKAP and MWA are precursors to the Square Kilometre Array (SKA). The SKA project is a global science and engineering project led by the International SKA Organisation [7], based in the United Kingdom. The SKA, due for completion in 2024, will be the world's largest and most sensitive radio telescope, made up of thousands of antennas linked together by high bandwidth optical fibre. The SKA will be co-hosted in two locations, with central array sites in Australia and South Africa. ASKAP and MWA will provide key results and techniques to the international effort to design and develop the SKA, as well as being world-leading precursor telescopes in their own right. The precursors and the SKA will give astronomers remarkable insights into the formation of the early Universe. Fig. 1-7 shows an artist's view of a SKA installation for low frequency radio astronomy observations.



Figure 1-7: The SKA Low Frequency Aperture Array located in MRO, Image credit: Swinburne Astronomy Productions.

The MRO site [8] is located in a remote part of Australia, and is protected from RFI. The MRO is in an area with low population density, to ensure that RFI from residents is significantly lower than in other parts of the world. The MRO is a 12,600 hectare purpose-established radio astronomy observatory, meaning that the site is free from the impact of growing human settlement. A Radio Quiet Zone (RQZ) has been implemented to ensure RA observations are made in a suitably low-interference environment, by demanding very low radiation emission powers from intentional radio communications [103], e.g. TV, radio stations, or mobile phones; and also from

unintentional radio emissions [1], e.g. electrical devices such as motors, generators or arc welders. Equipment used at the MRO site must meet stringent requirements for limiting RFI from intentional and unintentional radio emissions. Figure 1-8 shows the ASKAP-MRO-0001 RFI [1] Standards for unintentional emission from Equipment to be deployed at the MRO. The table inset shows the requirement of emission measurement to be up to 80 dB more sensitive than the MIL-STD-461F standard (NAVY) [2]. This requires a challenging involvement in the Electromagnetic Compatibility (EMC) assessment – and testing – of all deployed equipment.

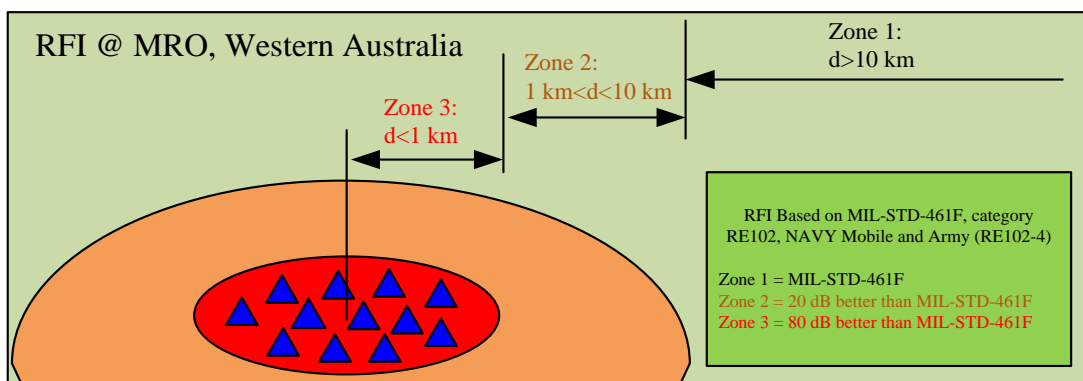


Figure 1-8: RFI Zone at MRO site, Western Australia; fundamental thresholds for emissions as a function of distance [1].

For the compliance tests in an EMC laboratory, this means measuring very weak signals, ideally more sensitively than possible with standard test instrumentation. The Reverberation Chamber (RC) method could provide a more sensitive facility to test equipment planned to be installed near the RA site at the MRO.

1.3 Purpose of the Research

The RA site at the MRO is concerned with the measurement of extremely weak electromagnetic signals. Radiated emissions are a concern for RA applications, as the sites are located in an isolated area. Then, electrical and electronic equipment close to, or at, an RA site must have very low electromagnetic emission in order not to interfere with RA signals. Thus, the task of the research becomes more about focusing on RA testing related to applications of EMC; i.e., an electronic device or system must be tested against stringent emission limits at a test facility, which has the capacity to measure very weak signals, before it can be installed at an RA site. Consideration is given to 4 test methods/environments (explained in Chap. 2); i.e.,

Reverberation Chamber (RC), TEM cells, Anechoic Chamber (AC), and Open Area Test Site (OATS). Here, the favoured RC method is explained conceptually.

1.3.1. Reverberation Chamber for Radio Astronomy

A Reverberation Chamber, RC [9] is a shielded room allowing measurements to be made in a controlled environment free of ambients. RC is physically a shielded and resonant cavity primarily consisting of at least a metallic paddle (stirrer) and an antenna; the antenna is the primary path in and out of the chamber for energy transfer. A stirrer, generally a metallic paddle, is usually installed in RCs and rotated. This is basically a resonant cavity in which the electromagnetic field pattern can be changed by moving a metallic stirrer, thus creating pseudo-uniform field characteristics. The RC method provides high sensitivity, repeatability, and reliability of radiated emission measurement at a lower cost than for other methods (no absorber is required). A high quality factor (Q) allows the chamber to measure weaker emissions compared to an OATS or an AC. The statistical results of the RC method provide emission measurements with good stability, repeatability and reliability. RC can measure all radiated signal directions/polarisations of the Equipment Under Test (EUT), Fig. 1-9, when compared to OATS, TEMs cell, or an AC. The RC method is the only one capable of measuring indirect signals by controlling the reflecting signals, while the other methods measure the direct signal by controlling the environment.

RC for a radiated emission measurement [9] consists of a receiving antenna, equipped with one or several stirrers to generate a statistically uniform and statistically isotropic field, and the EUT as a source. During a revolution of the stirrer, boundary conditions for the electromagnetic field inside the cavity change, and resonant frequencies and locations for field maxima and minima also change. This leads to uniform (within a certain margin) field strength within a given working volume, over a complete stirrer revolution. The uniform field is the key to the accuracy of the RC method. In fact, a field with acceptably low uncertainty can be achieved only above a certain frequency, known as the Lowest Usable Frequency (LUF), which is related to the size of the chamber: the larger the chamber, the lower the LUF, i.e., the physical dimensions of a RC affect its operation frequency.

Advantages and Disadvantages of the RC method: from the brief details given, the RC method can provide many advantages, especially highly sensitive emission measurements which can suit the RA requirements. The serious disadvantages are the required dimensions of the chamber at low frequencies, which depend on the LUF, see Table 1-2.

Table 1-2: Advantages and Disadvantages of the RC method.

Advantages	Disadvantages
<ul style="list-style-type: none"> • Sensitivity • Reliability • Repeatability • Low cost • Isotropy 	<ul style="list-style-type: none"> • The Lowest Usable Frequency (LUF) • Large dimensions for low frequency (independent of EUT size)

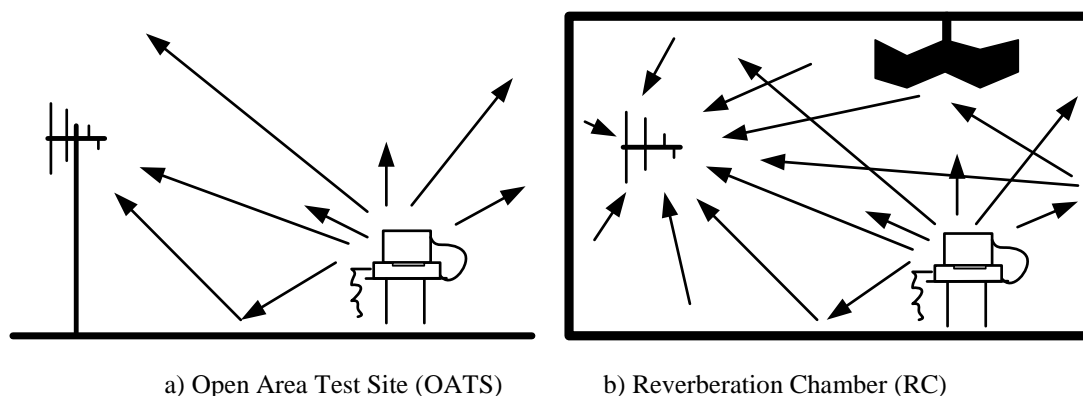


Figure 1-9: Examples of making emission measurements.

Limitations of the conventional RC method: the RC method could make more sensitive emission measurements for all requirements of both RA and NAVY. However, the chamber has to be large to achieve a uniform field distribution at low frequencies, within the working volume during one revolution of the stirrer. In reality, most RCs are of similar size as ACs, but RCs are used at higher frequencies, though the cost per square metre for RC is cheaper than for AC (no need for any absorber on the walls; an RF absorber can cost around \$1,000 per square metre).

Problems when the conventional RC applied for RA at the MRO: a conventional RC with an LUF of as low as 50 MHz - the lowest frequency of concern at the MRO in Australia - would need to have dimensions of at least 20 m by 12 m by 9 m, which could be a seriously obstructive requirement. It would not be able to

achieve a uniform field distribution below the LUF by following the conventional procedure defined in the standards [9]. This leads to the main objectives in this dissertation — to reduce the dimensions of the RC for use at a given frequency.

Hypothesis, the hypothesis of this research is that if more resonances, below the LUF, are excited and/or stirred by the stirrer, a better uniform field distribution could be achieved below the LUF as well. If the problem of field distribution below the LUF is solved, RC will be usable below the LUF.

This research was prompted by available resources at CIRA, where an existing shielded room is planned to be converted into a RC to be used as a test facility for EMC measurements for RA equipment at the MRO site. This will provide better sensitivity than an anechoic chamber currently used. The CIRA shielded room (Fig. 1-10) has dimensions of 3.6 m by 2.4 m by 2.4 m, resulting in an expected LUF of 290 MHz (explained in Chapter 2); however, emission measurements for RA applications at the MRO might start at as low a frequency as 50 MHz. Thus, the aim of this thesis is to reduce the conventional LUF of a RC towards much lower values.



Figure 1-10: The CIRA shielded room (3.6 m × 2.4 m × 2.4 m) expected to be a RC, details are in Appendix A.

1.3.2. Thesis Objectives

The Primary objective is to conduct emission measurements with higher sensitivity than currently possible with standard methods. This can be done by using a reverberation chamber, but to be of practical value a RC must be used well below the conventional LUF (C-LUF), allowing much smaller and more economical RCs to be used for radiated emission measurements. In other words, this thesis is to study the possibility to reduce the linear dimensions of a RC by 3-6 times. Scaled hardware and simulation models are used to assure the feasibility. A number of modifications to the design and operation of a conventional RC were made to achieve this goal (details are in Sect. 1.5).

To conclude, the objectives of this thesis are listed in Table 1-2:

Table 1-2: Objectives of this thesis.

Objective	What we have, or what a standard says	What we want, or possible compromise
(a) [main] – Lowest Usable Frequency (LUF)	-RC is usable only above the 3-6 times first chamber resonance.	-Make the RC usable below the C-LUF (the first chamber resonance would be ideal); the region between the first chamber resonance to the C-LUF is called the transition region (explained in Chapter 2).
(b) – Field Uniformity	-Achieving field uniformity of better than 3dB ($f > 400$ MHz) can only be done above the C-LUF.	-Use multiple receiving antennas, and move EUT to excite more resonances and increase field uniformity below the C-LUF.
(c) – Stirrer	-Stirrer gives poor performance below the C-LUF.	-Design a new stirrer to perform better at low frequencies.
(d) – Procedure	-Following guidelines from the standard, e.g. [9].	- Conventional procedure will be replaced by a formalism which identifies and selects preferred data sets, yielding accurate field measurements.

1.4 Literature Review

The author has studied the publications related to this research, and found that reducing the linear dimensions of RC (or reduce the LUF) by up to a factor of 3-6 times has never been done before due to poor propagation and insufficient mode density for conventional stirring techniques to be effective. Numerous articles have been published

on RCs but not all are related to the particular topics of this thesis and included in the list of references. There was a constant trickle of papers over the past years, but a large number of relevant articles have been published very recently. Fig. 1-11 show the number of relevant papers vs. publication year, and demonstrates that research on RCs continues, and even accelerates; highlighting this thesis and the underlying research is quite “timely”. Here, historical reviews are briefly discussed.

The RC Method has existed for a few decades, starting from around the beginning of the 1970s [10, 11], as researchers were concerned about methods of measuring electromagnetic radiation for industrial, scientific, and medical equipment. Initially, RC was introduced with the use of a shielded enclosure for measurements of radiated power (EUT was inside, although it was powered from outside) [11] — it should be noted that immunity testing on RC method was first introduced 2 years later [12]. Two vanes, made as large as possible, were installed to change the boundary conditions inside the enclosure. It could generate natural multipath environments, resulting in more sensitive emission measurements than can be done in AC (shown in Sect. 5.4), in a free space environment. The RC method was recommended for very few applications. Not until around the mid-1980s, did using RCs become one of the well-known EMI/EMC measurement methods [13]. In 2014, there were some standards available for the RC method; IEC Standard no. 61000-4-21: 2011 [9] was the most accepted and cited by many publications. It was used as a basis and benchmark for both immunity tests and emission measurements; however, this standard limited the method to be used only above the conventional LUF. The details are included in Sect. 2.3.1 (Origin of RC).

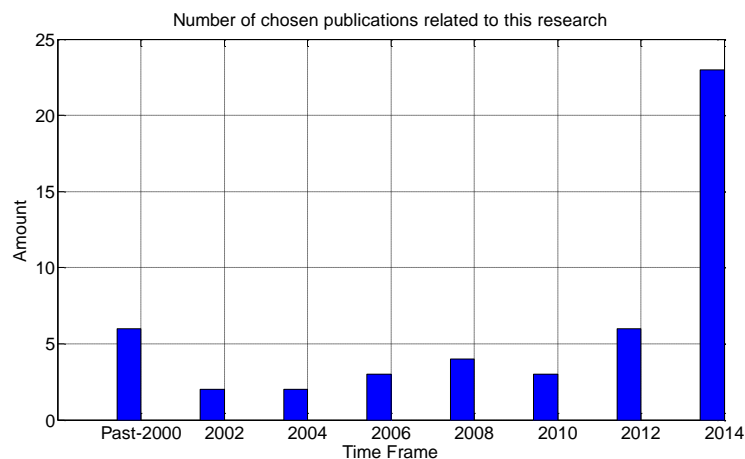


Figure 1-11: Number of useful research selected for good starting this thesis (excluding text books, standards, and online resources).

Although the RC method specified in the standards is not flexible, the RC concept is flexible enough to be modified for a specified purpose. Thus, while some researchers were following standards, there were quite a few who worked on the RC method for their own purposes, which were far different from the procedures stated in the standards. The author groups those useful related articles into five groups: 1) LUF and Field Distribution, 2) Stirrer, 3) Computer Simulation and Tools, 4) Example Applications, and 5) MIMO system for RC.

LUF and Field Distribution: In 2002, P-S. Kildal *et al.* (a group of researchers called the "BLUETEST" group) reviewed the use of RCs, and their validations, advantages, and disadvantages [14]. Setting up for measurements was also initially discussed in the concept by comparing to ACs. The LUF was discussed, as it should be one of the first concerns. The operating only under overmoded condition (i.e. above the LUF) became one of the well-known limitations of RCs. This research was still being referenced in a recent version (2011) of the IEC Standard [9].

In 2003, Elin Broström's research produced a helpful reference for a RC in an undermoded condition [15]. The methods used in this Master's thesis broke down at lower frequencies than those where conventional reverberation techniques could be applied. The conclusions suggest that a Bessel K distribution could be used to determine those frequencies in the undermoded range (below the LUF) that should be avoided due to uniformity and isotropy problems. Problem of LUF was confirmed again with this thesis.

In 2007, there was some work presented on RCs. F. Schlagenhauser and P. Kay showed how to give a Graphical Presentation for a Hybrid TEM/Reverberation Chamber without loss of insight into the problem [16]. Also, this paper confirmed that, below the LUF in normal cases, there always would be one component dominating the others, which was the behaviour found in TEM cells. Above the LUF, all 3 field components were uniform, which was the behaviour found in a RC.

In 2009, P. Kay's Thesis [17] investigated the effect of using stirrers (a basic structure in RCs) to shift the resonance frequencies of modified TEM cells; this method was called the hybrid-reverberation chamber. Thus, the usable frequency range of a TEM cell can be extended into the transition region (frequency range from the 1st resonance to the LUF). The results also show the possibility of decreasing the

LUF of a RC. This effect, however, was not the main purpose of his research.

In 2009, A. Walters *et al.* also worked on the transition region [18], but with a different approach. Their work intended to lower the LUF of a RC by installing a septum (a basic structure of TEM cells) in a RC; this was renamed as a Combined Mode Chamber (CMC). As a result, the chamber (Fig. 1-12) could still work at the same conventional LUF (30 MHz), but it could also work as a TEM cell from 1 MHz to 15 MHz (i.e., 1st resonance). It was still not usable in the transition region, i.e., between 15 and 30 MHz. It must be noted that this paper did not provide any information on the field uniformity in the transition region.



Figure 1-12: DSTO Reverberation Chamber [19].

In 2010, J.W. Nijenhuis was interested in why the measured LUF is usually higher than calculated. Their research [20] followed the IEC standard and compared the simulated LUF with the measured LUF. The paper gave partial details of Q-Factors: wall, antenna and composite. The highlight of this paper was that the simulated LUF of a given chamber is 200 MHz, but the measured LUF is up to 350 MHz. This paper found that, not only the LUF, but also the differences of the E-fields (i.e., measured vs. simulated) were present in almost all corners of the chamber. Unfortunately, they gave no reason for this phenomenon. This was one of many papers which stated that simulated results might not be similar to measured results. This further reinforced a belief in the need for an experimental path in this thesis.

In 2011, A. Cozza, defined the role of losses of the RC [21]. This paper investigated overmoded condition (above the LUF). All the information and setting up in this paper followed the IEC standard, e.g. probe, antennas, validation, and the stirrer was stepped over 100 positions/revolution. The Composite Q-Factor of a RC was observed when emptied and loaded. As the LUF was around 550 MHz, the Frequency Range of Interested (FRI) in the paper was up to 3 GHz. In summary, with the cavity loaded by absorbers, the composite Q-Factor decreased from around 5,000 to 2,000 at the LUF, and it was much more attenuated, from around 25,000 down to 9,000, at 3 GHz.

In 2012, in another attempt to reduce the LUF of the RCs, Y. Cui *et al.* installed a "groove" at the top of the room, in order to improve the field uniformity [22]. The results showed that the RC had a conventional LUF at 87 MHz, but that the LUF increased up to about 430 MHz when the "groove" was installed. This was reasonable, because installing the groove decreased the space in the chamber. However, when the Q-factor was measured with the cavity loaded by installing some absorbers, this brought the LUF back to normal.

To conclude, no way was found to reduce the LUF while following the standard [9]; to reduce the LUF (or using smaller dimensions for the chamber), a new procedure should be developed; this requires an understanding of the stirring of the field distribution below the LUF (i.e., in the undermoded condition).

Stirrer: During the 1990s, most of the research was to understand how the fields were stirred; for example: studying the dimensions of stirrers [23], or applying electronic stirring instead of a physical stirrer [24].

In 2005, J. Clegg *et al.* studied stirrer designs [25], and found the following useful facts: 1) all stirrers have a poor performance at low frequencies; 2) the structure of a stirrer is more important than its size (but, this does not mean that size does not matter); 3) increasing the radius of a stirrer slightly improves its performance more than increasing its height; and 4) optimisation does improve the performance, but this is relatively small compared to changing the whole structure. This paper concluded that the shape of the stirrer affected performance the most.

After that, studies of the stirrer structure seemed to have it frozen as a Z-shape, which performed well in an overmoded condition. From the author's experience, the

size, structure, and position of the stirrer are all important. In other words, understanding the field distribution is the most important consideration in designing a stirrer.

In 2012, a comparison was made between 2 different stirrers: a very small but complicated structure, and a normal-sized but simple structure. The simulated results showed that using the normal-sized one gave better performance than the smaller stirrer [26], even though the structure of the larger one was just simple. This is in good agreement with the author's experience during the research for this thesis, that stirrer need not be a very complicated structure, and that understanding the field distribution is more important for designing the stirrer, especially at low frequencies.

In the same year, S. Pfennig *et al.* determined the number of independent stirrer positions [27]. They used a Pearson correlation technique on a simulated model of a RC, whose LUF was about 200 MHz and the 1st resonance was about 70 MHz. The research used a commercial simulation program, FEKO (MoM method). The Z-stirrer was deployed and showed that, at lower frequencies, the performance of the stirrer dramatically dropped compared to higher frequencies. A. Adardour *et al.* investigated the effect of this stirrer on the 1st resonance [28]. An interesting issue was found that the stirrer could shift the 1st resonance by only 1.6 MHz, or 0.66%, for one revolution of the stirrer.

To conclude, the Z-stirrer is not suitable in an undermoded condition (below the LUF); a new design of stirrer is needed, along with an understanding of the field distribution below the LUF. A computer simulation program should be chosen to design the stirrer, and other fittings.

Computer Simulation and Tools: There are quite a few simulation methods available for engineering design (as explained in Chapter 3). For RCs, there are usually 2 methods which have been used: MoM and FDTD/FEM. In 2002, Perini and Cohen [29] developed and discussed Method of Moments (MoM) simulations to estimate the field strength; their research was supported by experimental data that showed fair agreement with the numerical predictions. At that time, the methods of Finite Difference Time Domain (FDTD) and Finite Element Method (FEM) were still difficult to run on PC computers.

In 2008, R. Serra and F. Canavero introduced a one-dimensional plot to

understand the statistical behaviour of RCs. [30]. This plot needed to be considered along with the presence of stirrer, and losses in the walls, in the model; however, this was quite difficult to understand, as there were too many factors in the RC – even a 3-D plot might not have been useful. This was why W. J. Krzysztofik, and S. Wolny proposed a 3-D plot to design a small RC for handset testing [31]. Their paper simulated a small RC: $1\text{ m} \times 0.75\text{ m} \times 1\text{ m}$. The LUF was 708.5 MHz, while the 1st resonance was at 187.9 MHz. As a result, Finite Difference Time Domain (FDTD) and Finite Element Method (FEM) were suggested for designing a RC, as they could allow the behaviour of RCs to be modelled even though they required intensive computational resources.

In 2012, J.-S. Kim *et al.* [32] researched on the stirrer effect, based on previous work [25]. This paper contained simulated results only; an FDTD simulation program was used to model a RC with LUF at about 500 MHz ($1.6\text{ m} \times 1.4\text{ m} \times 2.0\text{ m}$), and 3 stirrers of different size and symmetry were studied. It was concluded that the performance of the stirrer would improve, if the size and asymmetry were increased.

In 2012, H. Zhao *et al.* compared various simulation methods used to model RCs [33]. Comparison between the MoM, FDTD, and FEM methods was discussed. The FEM was stated to be the best, but required more computational resources, such as CPU, RAM, etc. This research also investigated hybrid methods, i.e., hybrid numerical modelling and a hybrid method of FDTD. They concluded that the FEM method was the most preferred.

RC Simulation programs can be summed up in two main methods: Finite Element Method, FEM (or Finite Difference Time Domain, FDTD) and the Method of Moments, MoM. As a result, it was decided to use the FEM method, and the reasons are explained in Sect. 3.1.2.

Example Applications: some researchers are working on modifications of the RC method, which are totally different to the procedures stated in standards [9]. For instance, research on electronic stirring, instead of using a physical stirrer, was started around 1994 by D. A. Hill [24], although this idea was not really developed until many years later.

In 2000, Perini and Cohen discussed an alternative way to stir the modes in a RC by using a 2-wire septum-like structure with phase shifting applied as excitation

in order to change the fields inside the test chamber [34]. The paper explained the central problem at low frequencies; the waves physically did not fit into their chamber, and modes other than the TEM mode were evanescent.

In 2010, there were quite a few modifications of RCs researched in that year. They were totally different from established RC standards at that time. L. Shuanggang *et al.* studied a Source Stirring Reverberation Chamber (SSRC) [35], which changed the excitation source to create an evenly homogeneous and isotropic field; this is different from a traditional Mechanical Stirring RC (MSRC). This paper showed the use of 8 transmitting antennas and 8 probes for receiving antennas. The results could reduce the LUF from about 125 MHz to about 60 MHz without installing any physical stirrer. Note that all the antennas and probes were perfectly symmetrical in placements to the room, which was why LUF related to STDs was so good (Fig. 1-13). It was still doubted that the field might not be uniform inside the working volume.

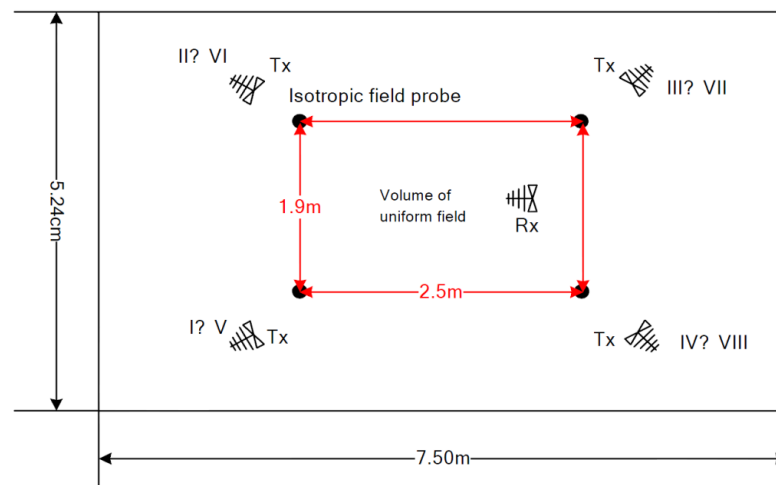


Figure 1-13: Schematic View of Source Stirring Reverberation Chamber: SSRC (no need for a stirrer) [35].

In 2010, F. B.J. Leferink *et al.* produced a special RC called a VIRC (Vibrating Intrinsic Reverberation Chamber) [36]. There was no stirrer, but the walls were made of flexible conducting material (Fig. 1-14). Their paper claimed that there were many advantages arising from this technique; such as lowering the LUF, and that the chamber can be folded to be easily stored. In particular, the LUF of the VIRC was 150 MHz, as compared to 174 MHz (three times the 1st resonance, 58 MHz) for a conventional RC of the same size. However, the field strength was within a 0-6 dB

range at the LUF (according to the IEC standard, it should be within 4 dB). Besides, there were some interesting points: 1) the EUT was placed at the wall, not at the middle of the chamber or working volume; 2) this chamber could be used with mode “stir” only. It could not be used with mode “tune” due to its structure (the terms “mode stir” and “mode tune” are explained in Sect. 2.3.1); moreover, 3) the LUF was not reduced as much as required in the objectives of this thesis.



Figure 1-14: The Vibrating Intrinsic Reverberation Chamber: VIRC (no need for a stirrer) [36].

In 2012, A. Cozza *et al.* produced a technique using 8 receiving antennas called "Multiple-Antenna Stirring" [37]. The main concern of their research was to speed up the measurement time, and the technique might be able to reduce the LUF. This stirring technique was specified only for mode “stir” (explained in Sect. 2.3). Also, the position of each antenna was placed randomly. Moreover, the paper did not state the dimensions of the chamber, nor the LUF. This technique did not intend to move the EUT, and the conclusion was that it needed to be optimised in future work (but it was not clearly stated how). Apart from that, the LUF was claimed to be a little bit better than using a conventional RC.

Z. Bo *et al.* carried out a research specifically on the comparison between RCs with ACs for EM measurements [38]. This paper said that emission measurement in a RC was just feasible, while susceptibility testing is very good. The paper tried to compare measured results between AC and RC to support these conclusions. However, this problem had already been found and stated in Sects. E.6 and E.7 of the standard [9], and the solution already existed.

E. Amador *et al.* provided a new probabilistic approach that could give a better result even with 30 positions of the stirrer, as compared to 150 positions for a traditional process [39]. The FRI was 850 MHz to 1.5 GHz. The paper explained that this new method was based on the GTEM cell technique, and that the E-field components followed a Rayleigh distribution well. This agreed with the new version of the standard IEC 61000-4-21: 2011 [9], which stated that only 12 positions of the stirrer were recommended (above the LUF). However, it must be noted that this paper did not give any details on the chamber dimensions.

F. Moglie *et al.* made a new design of the stirrer [40]. The stirrer can be built up from 2 to 8 strips; all were very complicated stirrers (each had a narrow and long strip). It was found that the stirrer had a limitation of independent positions (more strips, more repeating). It should be noted that this paper showed only simulated results. G. Gradoni *et al.* [41] developed another new design of the working volume (WV) which used the same concept of WV, but focused on a pulsed mode. This work could make the RC work well compared to the conventional one. However, the research showed only simulated results to understand the sequence at 15 and 150 ns after the pulse was generated. There was nothing reported about the LUF, and, in general, it was not much different from conventional RCs.

D. Senic *et al.* were measuring the Shielding Effectiveness (SE) in a RC by combining with a Gigahertz Transverse Electromagnetic (GTEM) cell [42]. The RC had a LUF at 1.4 GHz, with 3 removable front panels (each had a different dimension for a slot). The RC had its stirrer rotated 5 degrees per step. The average received power was then calculated. The SE was calculated by comparing the average power with that for an open front panel. The important lesson was that the RC with no load (i.e., empty) showed strong signal fluctuations that could not be resolved. Two cylindrical containers with fresh water were then added to load the RC. It was noted that, with an empty RC, both two and four cylindrical water containers gave the same SE. The benefit of having the RC loaded was the short time period for the averaging function to obtain the desired results.

Q. Wang *et al.* presented a new way to obtain an accurate immunity test using RCs, and compared the results with GTEM chambers [43]. In their results, the two methods agreed, with the same observed trends. A Pearson correlation coefficient was

chosen to evaluate their correlations. The coefficient was 0.81, which showed a high level of agreement. The paper also confirmed that RC obtained very good repeatability.

V. M. Primiani *et al.* modified a RC with an SSRC (Source Stirring Reverberation Chamber) technique [44]. This research installed up to 20 conical wire antennas placed on a cubic metallic support of 1 m side (5 faces are used, with 4 antennas per face), set up as transmitting antennas. A horn antenna placed in the working volume was set up as the receiving antenna. A network analyser was used to collect the S_{21} parameter, forward transmission coefficient (gain), of this Multiple-Input Single-Output (MISO) system (with opened ports for the unused transmitting antennas). The LUF of the chamber was 900 MHz. Again, this SSRC could not work in “tune” mode; it could only be used in “stir” mode (more details in Sect. 2.3). An important point was that this paper did not show the STD to confirm the field uniformity - CDF, polar and anisotropy plots were given instead. These plots showed that the SSRC produced a good Rayleigh distribution for the FRI. The paper did not intend to lower the LUF, but it was stated that this would be a goal for future work.

R. Vogt-Ardatjew *et al.* worked on using a Dual Vibrating Intrinsic RC (Dual-VIRC, each is $1.5 \times 1.2 \times 1.0$ m) to measure the reflection coefficient (S_{11}) of an antenna [45]. This was another type of RC with no stirrer [36]. The paper stated that any antenna in a RC should not need any high gain, but that the losses should be low and be restricted to small dimensions. This paper suggested using a conical, or discone, antenna in RCs. This research showed a very good example of using RCs to measure antenna characteristics, and why the average value should be preferred, over the maximum value. The same setting was continually used in SE measurements by S. V. D. Beek *et al.* [46]. This paper found that the dynamic range of a Dual-VIRC was more than 80 dB over the 300 MHz – 18 GHz range, which was well suited to measuring SE.

J. Carlsson *et al.* provided another method of using RCs to measure SE [47]. This paper put a smaller RC in a bigger RC to measure the SE of the smaller one. One side of the smaller RC had a circular slot (which could be changed to 5 different sizes). One transmitting antenna and one receiving antenna were placed outside the smaller RC, and one more receiving antenna was placed inside the smaller RC. The

final result was obtained by comparing the received powers of both receiving antennas. The difference from the standard was that this method swapped the value of the input power with the received power, so that the final values this method provided had a different meaning; i.e., higher values meant a worse SE, while the general method has the opposite meaning. Apart from this, the results agreed well in theory.

There were at least two papers that explained their results by CDF and PDF, and not with STD. Firstly, A. Manicke *et al.* investigated transient effects in a RC excited by short pulses [48]. The time domain was used to explain the behaviours, instead of the frequency domain. The paper contained both simulated and measured results. Secondly, M. Magdowski *et al.* made an alternative way to level the field for immunity tests [49]. A RC with a LUF of 1 GHz (1st resonance was at 160 MHz) was deployed. As a result, the RC could provide very good dynamic range.

There are many more research articles available on various applied approaches to the RC method; they showed the possibility of designing a modified version of RC specified with the purpose of reducing the LUF. From previous work, exciting more resonances seems to better affect the LUF (explained in Sect. 2.4).

MIMO System for RC: MIMO stands for Multiple-Input Multiple-Output which is one of the basic types of communication links (explained in Chapter 3). In 2004, P.-S. Kildal *et al.* did early research on using MIMO in RCs [50, 51]. This paper was mobile phone communications testing—which is not central to this thesis, but the mechanisms might well be. Their papers adopted MIMO techniques for multipath effects. There were good examples of using fixed wall antennas (the walls were used as the ground planes of the antennas, for all 3 polarisations) that were not suggested by any standard. There were 6-element monopole circular array receiving antennas. A network analyser was connected to the transmitting and receiving antennas. The results were discussed in terms of correlations; the variable positions of antennas provided different values of the field distribution inside the RC. However, the papers did not provide any information or results related to the LUF. They only focused on the multipath effect. To conclude, there were 2 interesting results: (1) using 3 transmitting antennas could provide better signal capacity than only one transmitting antenna (from 5 bits/sec/Hz to 8 bits/sec/Hz); and (2) when 6 receiving antennas were placed closer to one another, the performance was worse. Their

research on using the MIMO technique in RCs was further developed and discussed in their 2005 paper [52]. There were some small fixed-wall antennas and platform stirring for moving the EUT (a mobile phone). This setup was for emission measurement. However, this test did not relate to reduce the LUF, but only to check the Bit Error Rate (BER) of a mobile phone when in a Rayleigh environment. The paper also showed a cumulative plot to confirm the Rayleigh distribution. The paper claimed that the RCs were still able to produce a Rayleigh distribution even when the Multiple-Input Multiple-Output (MIMO) technique was applied and the Q-factor was low.

In 2006, A.A.H. Azremi *et al.* studied the field distribution [53, 54 and 26] of a Single-Input Multiple-Output (SIMO) system. Their first 2 papers were to confirm that using three small fixed wall receiving antennas for three polarisations provided good agreement for antenna efficiency measurements [53, 54]. The chamber and the antennas were used again [55] to study the Rayleigh distribution of SIMO RCs (1 transmitting, 3 receiving antennas), and 3 distributions at 3 receiving antennas were plotted, and explained in terms of PDF. Their variances were almost the same at 0.2-0.5, and it could be concluded that even when using the SIMO RCs, there was still a Rayleigh distribution. In opposite way, C. L. Holloway *et al.* found another way to make RCs simulate a Rician distribution [56]. However, their purpose of simulating a Rician distribution was for measuring the BER of wireless devices, and not for reducing the LUF.

In 2010, in a paper from the "BLUETEST" team [57], C. Orlenius *et al.* modified RCs by installing an active MIMO-WLAN system. The installation for measurement had 2 RCs connected to a 3-by-3 MIMO system. A router and a laptop were installed in each RC, and the measured results were investigated using 1-by-1 SISO and 3-by-3 MIMO. The throughput showed that, using MIMO, the repeatability was better than SISO in every channel. However, this work did not intend to reduce the LUF.

In 2011, there was another paper from NIST [58]; for this work, K. A. Remley *et al.* adopted the MIMO technique with a RC. The paper, however, focused on multipath in the propagation environment only. The hypothesis was to check the BER when the signal was modulated by Binary Phase Shift Keying (BPSK) at 2.4 GHz. The results showed that MIMO could provide a better BER than a conventional RC.

However, this was not a real MIMO technique, as there was only one receiver, and no real-time processing of MIMO. It could be called MISO (Multiple-Input Single-Output) only. The Q-factor was around 3,000, but there was no LUF information.

In 2012, D. Jianjin *et al.* adopted a MISO technique to reduce the LUF [59]. They called their technique “Source Stirring and Mechanical Stirring”. The paper used multiple (8) antennas to reduce the LUF. The results showed that the LUF was reduced from 120 MHz to 80 MHz, or 1.5 times lower than the conventional LUF. It, however, must be noted that all 8 antennas were placed close to the walls in a symmetrical pattern (similar to [35]) of a cubic shape to cover the WV. There was still doubt that, in practice, the field might not be really uniform inside the WV.

C. L. Holloway *et al.* gave a validation of using RCs to measure total and radiation efficiency of antennas [60]. This was a step forward from previous work, which estimated the efficiency of the 2 antennas under test without the need for any reference antenna. The purpose of this paper was to validate the previous use of 2 antennas (again in the RCs) by showing comparisons with other methods.

C. Choeyesakul, F. Schlagenhauer, and P. Hall (as part of this thesis work) developed a Double C stirrer [61] which showed better performance than a Z-stirrer, and was more suitable for use with MIMO RCs. The double C stirrer worked well above the LUF, and also down to the first resonance. This type of stirrer could play an important role in any work requiring an investigation of RCs in the transition region (below the LUF).

In 2013, there was another useful research using MIMO technique in a RC that came from the "BLUETEST" group [62]. R. Rehammar *et al.* measured 4x4 MIMO capability in RCs. An EUT designed for 4 ports was installed in 2 different size RCs, in which 4 receiving antennas were installed, and 50 ohm-loads were connected to terminate unused ports. The conclusion was that RCs, even different in size, could achieve better repeatability when the MIMO technique was adopted, indicating the stability of this technique. This paper also stated that RC was a very good tool for EM measurements; especially to simulate an ideal environment well suited for techniques of mobile phone. Note that Pearson correlations between antenna elements were also reported and discussed.

In conclusion, the RC method can provide good sensitivity, reliability, repeatability, and stability measurements. The LUF (Lowest Usable Frequency) is one of RCs concerns; i.e., as larger the chamber, as lower the LUF. This constraint obstructs applying the method for RA applications as stated in the objectives. The LUF depends mainly on the field uniformity, which is related to the field distribution. Stirring fields as much as possible is the key technique to extend the usable frequencies. A conventional RC is assumed to be configured with at least one stirrer to achieve field uniformity by stirring the field distribution. However, other than using mechanical stirrers, there are some techniques, which can produce a valid test; these techniques can also achieve a statistically uniform and statistically isotropic environment. Examples include the optimisation of the stirrer, stirring the source (moving the source), flexible walls (moving boundaries [36, 45, or 46]), moving transmitting or receiving antennas [26, 35, 44, 52, or 59] and changing the frequency over some bandwidth (single-tone frequency variation or band-limited noise excitation [24]), modification of the WV, installing new structure (a septum, groove, or wires [18, 22, or 34]), or a combination of these. It is, however, important to state that some of these alternative methods of stirring are good for specified measurements, but may not be applicable to certain EMC tests, e.g. frequency stirring cannot easily be used in emission measurements, flexible walls or moving boundaries cannot be used with any mode-tuned operations.

The literature review above shows that applying innovative ideas to the conventional RC method for specified applications to RA (or the NAVY) is possible. RC can be used below the LUF (or smaller dimensions than usual), if the field uniformity below the LUF is increased; the field uniformity can be increased, if the field distributions are stirred well by an appropriate technique(s). According to the ultimate requirements of this research, a combination of some special techniques might possibly be required to achieve the desired goals.

1.5 Research Methodology

Ultimately, this research is investigating a fundamentally different mode of RC operation — to extend beyond the limitations of the LUF — with the CIRA shielded room. It has been found that rotating the stirrer alone does not achieve acceptably

uniform field strength below the LUF, although the behaviour improves with increasing frequency. To further reduce the LUF significantly, a combination of methods, and a fundamentally new method, to operate a RC are needed in order to stir the field distributions below the LUF. Thus, this research does not follow the standards, but uses the standard [9] as a reference when comparing experimental results.

Strategies: conceptually, a conventional RC can be considered as a Single-Input and Single-Output (SISO) communication channel, as there are only 2 antennas; a transmitting (EUT) and a receiving antenna. The idea of this research is related to the concept of Multiple-Input and Multiple-Output (MIMO) communication channels, which is often used to improve the performance of communication links. Basically, the performance of a communication channel can often be improved if several antennas are available for transmitting and receiving the signal, and the pair with the lowest path loss is selected. Applied to a RC, the EUT (being the signal source) is moved around the chamber (e.g. rotated on a turntable), and several selectable receiving antennas are used. The modified RC, in this configuration, can be called a MIMO RC, which involves a number of strategies, as follows:

- Studying field distributions below the conventional LUF;
- Use of multiple receiving antennas to select and arrange the field distribution;
- Increase stirrer performance below the conventional LUF;
- Rotation of the EUT to further change the field distributions;
- Use of wall-mounted antennas to have more space in the chamber for multiple antennas;
- Establish a new calibration procedure for everyone to build their own modified (MIMO) RC.

Methodologies: Studying the feasibility to reduce the LUF will be done on a scaled model and simulating models. Studies will be made on a scaled model based on the CIRA shielded room (Fig. 1-10). In this thesis, design and operation are based on computer simulations for guiding, designing, and understanding during the research (explained in Sect. 3.1.2). Once design guidelines have been established and analysis tools developed, the techniques can be adapted later to the actual shielded room at ICRAR (Appendix D). In addition, the outcome of this research can be

applied by everyone to build their own MIMO RC, including in the NAVY. The methodologies can be summarised as follows:

- Prototype of MIMO RC is done on a scaled model of CIRA shielded room; design and operation is supported by simulation program;
- After designs and procedures are found, MIMO RC procedures can be concluded for adopting on the CIRA shielded room and can benefit to other existing RCs.
- Prototype of MIMO RC is modification on a conventional RC in purpose of lowering the LUF by adopting three aspects:
 1. Improvement of the performance when using multiple positions for the receiving antenna (detecting the signals);
 2. Improvement of the performance when moving and/or rotating the EUT (exciting the resonances);
 3. Stirrer design, under special consideration of its ability to shift resonance frequencies below the LUF.

These three aspects lead to the introduction of a novel RC, which requires a sacrifice of measurement time, and would probably lead to a larger measurement uncertainty and reduced repeatability, although it can provide an improvement of the LUF. MIMO RC, thus, requires longer measurement time and a more sophisticated approach to signal processing (received signal depends not only on the stirrer angle, but also on the location of the receiving antenna and the EUT); therefore, measurement automation is necessary. An automated system (controlling not only the stirrer, but also the receiving antenna and the EUT) for validation procedure and emission measurement are introduced in this thesis, as well as a Graphical User Interface (GUI) for post-processing.

1.6 Structure of the Thesis

To extend the performance of a RC to low frequencies (or reduce its dimensions for the same usable frequencies), this thesis explains an approach to the signal processing that can be adopted on any existing RC by using the concept of MIMO communication. This concept is considered; then the theory is studied, investigated, and evaluated to test on a simulation program. A simulation program is chosen

carefully, among many choices in the market, to confirm the new approach. Ultimately, this thesis offers the demonstration of complete measurements (including validation) to support the hypothesis, theory, and simulated results. Measurements are done on a model of the CIRA shielded room at ICRAR/CIRA, Curtin University, Western Australia, where requirements to use an available chamber as a RC for emission measurements are about 3-6 times below its conventional LUF. This thesis is written in 6 Chapters; starting from a discussion on conventional RC, to the development of Multiple-Input and Multiple-Output (MIMO) RC, as Fig. 1-15.

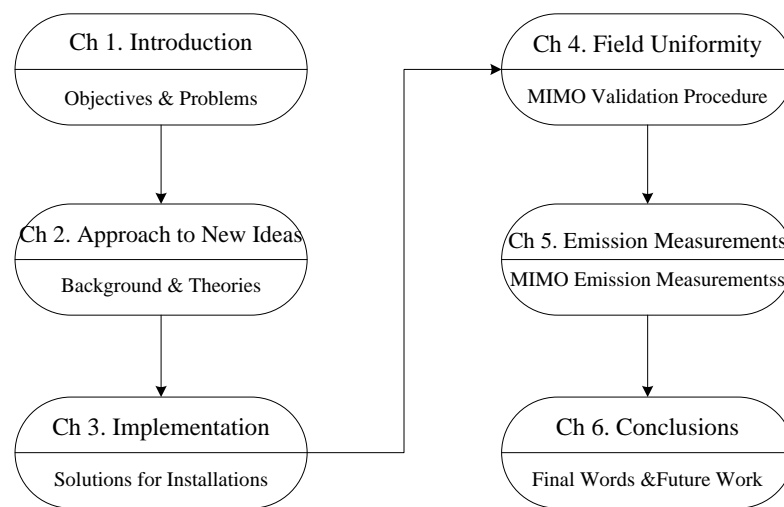


Figure 1-15: Research flow adopted for this thesis.

Chapter 2 gives the history of EMC since before WW1 to the modern EMC at the present day. Four methods for applications of modern EMC are summed up, including summary of related standards. Use of conventional RC is explained, and the limitation of conventional RC is pointed out for an understanding of the relevant problems. The goal to reduce the LUF becomes covering the transition region instead. Novel ideas on RC are revealed, studied, and summarised in Sect. 2.4.

Chapter 3 is a study of the hypothesis on the shielded room. This Chapter presents the characteristics of the CIRA shielded room expected to be a RC, but the room is too small to work at as low frequencies as required. In other words, this demands the use of the room below the conventional LUF (C-LUF). Instead of testing the MIMO technique on the actual shielded room, a RC model is made in this Chapter [61]. Setting up, implementation and programming are also presented in this Chapter. The decision made to choose a simulation program is described in this

Chapter. The simulation models are made carefully in every detail; for example the SMA (Subminiature version A) port, stirrer, WV, etc. This can be very useful for other work related to conventional RC and/or MIMO RC.

Chapter 4 demonstrates applying the MIMO technique on the RC model. This Chapter starts with a confirmation of the conventional validation procedure. The scaled model cannot pass the conventional validation procedure below the C-LUF, as the field is not uniform. As expected, the MIMO technique (when multiple receiving antennas are installed with a fixed position of the EUT) can increase field uniformity even in the transition region. As a result, the MIMO validation procedure is found. The benefit could be for any RC to work at lower frequencies, although these are not been as low as the first resonance.

Chapter 5 shows confirmation of the idea of smaller RC dimensions; i.e., being used from its first resonance. This Chapter demonstrates making radiated emission measurements of a noise source as EUT. The total radiated power is determined by using both peak values and mean values. This Chapter has developed a “6 dB strategy” [63] to manage data measured from moving the EUT in the WV in a pattern to find an exact result. There are also comparisons of results from MIMO RC with AC, which confirms that MIMO RC is usable in the transition region. This Chapter clarifies that the results from MIMO RC will never be worse than those from conventional RC. The thesis is summarised in Chapter 6, including outcomes, utilisations and suggestions.

The re-useable simulation of the 1:5 scaled model and the shielded room are made by the author (see Appendix A). Flow charts to control MIMO RC, instrument (spectrum analyser), stepper motor, and other devices are shown in Appendix B. The code can be reused easily; for instance, the number of receiving antennas can be selected by changing the parameter “PORTS”. Appendix C shows more flow charts, written for a Graphic User Interface (GUI). All measured data from Appendix B can be analysed using these codes. These GUI codes should be very useful for a wide range research that contains a large quantity of raw data, and for processing those data and displaying many results simultaneously (also allowing the user to save the results). Appendix D gives guidelines for adopting the MIMO RC technique to other RCs, by using the CIRA shielded room as an example. All procedures are summarised

as a “lab manual” for a typical RC, which will be used as a MIMO RC. Appendix E contains the key measured results from Chapters 4 and 5. In addition, Appendices F and G give a summary of the conventional validation procedure [9], and list of publications related to this research.

1.7 Original Research in this Thesis

In this thesis, MIMO technique is demonstrated to extend usability of RC from the conventional LUF (C-LUF) by 3-6 times down to the MIMO-LUF (around the 1st resonance) for emission measurements. The high-level engineering techniques are:

1. Studying the field distributions in a conventional RC below the LUF. This thesis reveals that following the conventional procedures (fixed position of receiving antenna and EUT) cannot excite enough modes, and achieve proposed uniform field distributions below the LUF (Chapter 2);
2. Moving EUT (Multiple Input technique, MI) and using multiple receiving antennas (Multiple Output technique, MO) can excite more resonances, later on, select and arrange the field distributions to increase field uniformity in the transition region, i.e., from the 1st resonance to the C-LUF (Chapters 4 and 5);
3. Development of double C stirrer for undermoded condition, below the C-LUF. The double C stirrer is more effective than Z-stirrer especially below the C-LUF. The double C stirrer can shift amplitude and resonance of the first resonance more than 10%, while Z-stirrer is almost unable to affect the first resonance (Chapter 3);
4. Reveal feasibility to extend usability from C-LUF to MIMO-LUF when techniques of multiple receiving antennas and moving the EUT are applied. This thesis also introduces procedures for the MIMO RC. Complete measurements are shown to assure the MIMO RC technique by using both maximum (peak) values and mean (average) values (Chapter 5);
5. Providing guidelines to adapt method of MIMO RC to a shielded room, or other existing RC (Appendix D).

Notably, this thesis confirms the feasibility of the MIMO RC technique, using both electromagnetic simulation and measured results from a scaled model of the MIMO RC and its fittings.

1.8 Thesis Contributions

The key contributions of this thesis are:

1) Outcomes: the lowest usable frequencies of the prototype MIMO RC were 1/3 those obtained with a conventional RC chamber, which means that a MIMO RC:

- can be used from the first resonance;
- requires smaller dimensions;
- becomes cheaper;
- is a more accessible method;
- can be easily applied for immunity tests by setting reverse signal directions (however, immunity tests are not included in this thesis).

2) Impact on relevant areas: The established design guidelines and developed analysis tools in the thesis can be used to applications of RA, the NAVY and other areas requiring sensitive measurements. This work can also impact existing RCs in terms of adopting techniques to extend the usable frequencies.

3) Publications: some peer-reviewed papers have been accepted. One of them received the best student paper award (in 2012) from the EMC Society of Australia. There were academic posters including presentations for academic conferences in the subjects of EMC and the NAVY (Appendix G).

The work in this thesis was carried out between 2011 and 2015, at CIRA/ICRAR, Curtin University. Although the author visited some researchers working in related fields, there is no specific contribution of others to this thesis. The author, under the guidance of his supervisor and co-supervisor, developed all the hardware and programming. However, some ICRAR staff helped in supporting this research; specifically, Mr Jonathan Tickner helped in building and assembling all physical models, and the technical skills of Mr David Emrich helped the author to build the Validation Set (details are in Chapters 3 and 4).

CHAPTER 2

FROM BASIC EMC TO REVERBERATION CHAMBERS FOR RADIO ASTRONOMY

2.1. Electromagnetic Compatibility

Electromagnetic compatibility (EMC) may not come up in daily conversation, but its effects are apparent almost everywhere due to the ubiquitous use of electronic circuits. A commonly quoted phrase in this subject is “Electromagnetic Interference (EMI) is the absence of EMC”; thus, the definition of EMI should be clearly stated before considering EMC.

Electromagnetic Interference, or EMI, is an interference that affects an electrical or electronic device by galvanic, inductive or capacitive coupling, or by electromagnetic radiation. The interference may interrupt, or decrease, the effective performance of the device. EMI can arise either intentionally or unintentionally. The source may be any object, artificial or natural, such as any electrical or electronic device, lightning activity, or even the Sun. It often affects the reception of AM radio, but can also affect mobile phone, FM radio and television reception.

The definition of EMC is “the ability of an equipment or system to function satisfactorily in its electromagnetic environment without introducing intolerable electromagnetic disturbances to anything in that environment” [64]. EMC includes system design configurations and clear concepts and doctrines to ensure this ability.

While the definition of EMC is flexible, depending on the meaning of the words “satisfactorily”, “intolerability”, and “environment”, EMC is a requirement in all situations. Modern approaches to EMC are mostly driven by compliance with standards. Over the past 100 years, EMC has moved from reacting to one-off electromagnetic compatibility problems to attempting to defeat them through “standardisation”. In fact, standards are used as a “proxy” approach; standards are not the reality, but they are used to represent reality. Therefore, complying with a standard allows a reasonable expectation that few incompatibilities will happen when the equipment is being used in respective environments.

A number of standardisation bodies develop test methods for electromagnetic compatibility. There are numerous applications available for making EMC tests, depending on considerations such as: size of the test equipment, frequency of interest, test limits, type of the field (E -field, H -field), characteristics of the test signal (in the frequency and time domains). Each method has its own advantages and disadvantages, and no method is perfectly ideal for all tests. For example, the traditional RC method contains some serious limitations (e.g. limited use at low frequencies, complicated validation procedure), although with techniques like those described in this thesis, the RC method can provide many advantages (e.g. sensitivity, repeatability). In practice, nowadays (2015), EMC is considered to cover Immunity and Emission characteristics/requirements for radiated and conducted signals, with four test environments (test sites), as shown in Fig. 2-1. This thesis focuses on emission measurements of radiated signals in environment of a reverberation chamber, other test sites are briefly explained in Sect. 2.2.

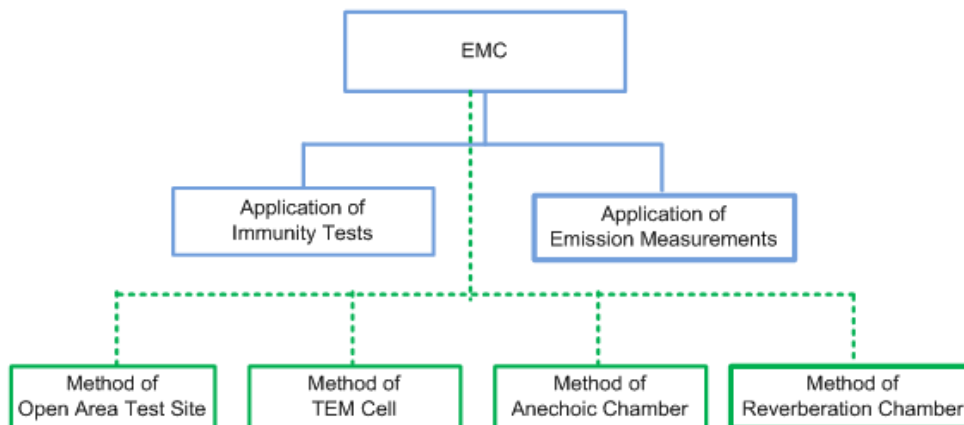


Figure 2-1: Applications and methods of EMC.

The purpose of this Chapter is to give a brief background of EMC (emission and immunity), review the application of emission measurements, explain the method of conventional RC, reveal its problems, and sum up all the new ideas in this research. All the information will be grouped into four subtopics:

- History of EMC from prior WW2 to modern EMC (Sect. 2.1);
- Standard development of emission measurements and methods (Sect. 2.2);
- Conventional RC (Sect. 2.3);
- New ideas in this thesis (Sect. 2.4).

Please note that the history of EMC in this thesis may contain some military jargon. Although the military were at the forefront in the immunity part of EMC, RFI (emission) started in the 1910s and 1930s in the commercial world, on interference to wireless communication. However, the author believes that the advancements of EMC came after the development of electric devices, most of which were initially developed for military purposes. Also, the requirements for RA at the MRO are based on MIL-STD-461F [2] (Sect. 2.2.2). In this section, history of EMC is summarized as an account of developments in both emission and immunity.

2.1.1. Early EMC prior to WW2:

Before the world knew what EMC was, there were some big projects which suffered from “signal interference”, or RF noise. One of these RFI incidents happened in 1858, on a transatlantic telegraph cable [65] — an undersea cable running from Valentia Island, western Ireland to Heart's Content, Newfoundland. The cable failed due to RF interference effects arising from the poor electrical insulation (shielding) of the system. The second incident occurred in the first transatlantic wireless radio transmissions performed by Guglielmo Marconi in 1901, across the Atlantic Ocean from Poldhu, England, to St. Johns, Newfoundland. After 14 days, this system was forced to be suspended after complaints of interference, due to uncontrolled bandwidth, from ship radio communications (Fig. 2-2).



Figure 2-2: Map of the transatlantic telegraph cable route (1858) and transatlantic wireless radio transmissions (1901).

The early need for EMC to eliminate RF interference was when people first noticed “noise” on telephone circuits [66, 67, and 68]. These circuits often became unreliable when telephone lines were running parallel to power transmission lines; electrical interference between telephone and power lines was a common occurrence. To understand this problem, EMC became a common procedure in the 1920s, when engineers began to recognise that the noise power was proportional to the bandwidth of the system. There are two types of fluctuation noise in electronic circuits - thermal and shot noise. The first is due to random temperature-dependent motion of charge flowing through an electrical conductor; the second is due to the variations in electrical current as discrete charges are randomly emitted. It was during this time that engineers began working with the performance measure generally known as the “signal-to-noise ratio,” or SNR.

In the military (e.g. in aircraft), radio transceivers had been used in airborne applications since 1912; it was recognised that receiving radio signals in close proximity to ignition sources was problematic [69]. During this time, the development of direction finders (known as “radio compasses”) in the 1930s also led to the recognition of interference [70].

Two well-known cases of RFI had a significant impact on the birth of RA. During investigations by Karl Jansky for a U.S. telephone service with a large directional antenna, the telecommunication signals were disturbed by astronomical galactic RF noise. In the second case, Grote Reber failed in his first and second attempts to detect astronomical signals in 1937, due to automobile ignition noise interference.

Advent of EMC: It should be noted that possibly the first EMC legislation began as early as 1892, when the German Parliament voted to create the "Laws of Telegraphy in the German Empire." These described how to deal with cases of interference in electrical installations, although it was only a kind of a “manual” [71]. This might have been the first law in the world that dealt with influences of electromagnetic disturbances. However, there was no significant evidence of applying this first EMC law. In 1912, the first international attempt was proposed to control the bandwidth of a RF emission. International agreement was reached on bandwidth allocation for maritime use [72]; however, there was no requirement for control of spurious or harmonic (bandwidth) emissions at the transmitter output until 1932 [73].

Some time before WW2, there was the initial study on Electromagnetic Interference (EMI) made when a radio was first installed on a vehicle. The IRE (Institute of Radio Engineers) 1932 Proceedings included a paper on electrical interference in car radios [74]. During this time, the subject of EMC was also related to Electrostatic Discharge (ESD), which arose in hazardous environments, e.g. in coalmines, or gas stations.

In summary, many interference problems were encountered in this period of time; however, a RF community needed the development of “EMC tools” to state what really caused the problems.

2.1.2. WW 2 – Emergence of EMC Issues

Regardless of the losses and damages caused by the war, the WW2 period saw great and significant developments in electronic engineering, including EMC. Electronic devices played major roles in WW2 in some battles, called the ‘Battle of Beams’. Controlling of bandwidth and signal power in communication systems required EMC. Powerful transmitters, sensitive receivers, and sufficient antenna directionality enabled the development of Radio Detection and Ranging (RADAR). Radar cross-section as a function of wavelength, air-surface, air-air and anti-aircraft gun control radar were subjects of research and development in almost all countries engaged in the war.

An improvement in signal power and a good understanding of bandwidth (BW) enabled the construction of a well-known navigation system called “Knickebein” [75], a radio navigation system using two transmitted beams arranged so that one transmits dots and the other transmits dashes. As a result, the overlapping beams created a centre line of continuous notes, and, following this note, pilots were able to navigate accurately in the dark of night over ranges of up to 200 nautical miles.

Although, there was not yet any consideration given to EMC testing of communications or other equipment for early developments, these developed technologies already brought great complexity into Electronic Warfare (EW). Radar jamming and anti-jamming technology came after the developments of the radar world; EW consisted of Electronic Support Measures (ESM), Electronic Countermeasures (ECM), and Electronic Counter-countermeasures (ECCM).

ESM involved the detecting of signal power; for example, to detect a RADAR signal from a source (target). ECM was for offensive and defensive purposes; for example, using Chaff to interfere with the RADAR signal from being used. ECCM was an anti-jamming system; for example, by increasing the frequency range and reducing its jamming susceptibility by spreading the power of the radar signals. ESM, ECM, and ECCM, in current times, have been made obsolete, and replaced by Electronic Support (ES), Electronic Attack (EA), and Electronic Protection (EP), respectively [75].

Since WW2, the knowledge of controlling the BW, radiated power, and of modulating the signal was an opening to a more “sensitive” electronic systems era; for example, the missile and space ages. Techniques of radio interferometry & aperture synthesis were also developed during this time (starting in 1946), in Australia and the UK. The US *Moonbounce* project could also use the benefit of sensitive electronic systems to collect radiation from USSR radars reflected from the Moon’s surface.

To conclude, during WW2, there was the birth of really practical EMC for military and RA use; it also saw the introduction of many other electronic systems, e.g. analogue “computers” which were developed for instrumentation control applications.

2.1.3. Birth of Modern EMC

During the Vietnam War (1955–1975), the use of electromagnetic devices played a major role. This was the first time for the U.S. Navy to appoint Electronic Warfare Officers (EWOs), or “Crows”, who played a major role in this conceptual change in air tactics. As late as December 1965, with the development of the first Radar Homing and Warning (RHAW) system, the AN/APR-25 (developed in 1965) was used to equip F-100F aircraft. This RHAW system not only detected radar emissions, but also displayed the relative bearing of the emitter, and gave warnings to the crew if the aircraft was being tracked by threat radars. Four two-seat U.S. F-100Fs were fitted with suites comprising RHAW, radar signal analysis and missile launch warning receiver systems, manned by experienced F-100 pilots and EWOs, and flown on missions over North Vietnam. As a result, the F-100Fs destroyed a number of SAM (Surface-Air Missile) sites, SA-2. The development of technologies to control

the bandwidth and power of systems was related to the knowledge of EMC, but not yet on issues of reliability or repeatability, so that later become a significant problem.

By 1967, EMC had been recognised as an issue in the integration of electronic systems, which had little connection between standard developers in different parts of the world; most nations had no product-level regulation and different services used different specifications. As from 1967, the USS Forrestal disaster brought EMC to the attention of military forces. The USS Forrestal was an aircraft carrier which was operating in the Vietnam War, where it used F-4 Phantom aircraft loaded with Zuni rockets, which used an electrical signal to initiate launch. Accidentally, in July 1967, one of the F-4 Phantoms on the carrier's deck launched a Zuni rocket without any warning, which crossed the deck and struck the full belly fuel tank of another aircraft. The ensuing explosion and fire of the aircraft's 1000 lb bomb caused a chain reaction of fires and explosions ultimately resulting in the loss of 134 sailors and injury of a further 62 [76]. The flight deck was penetrated by the heat and explosions, causing fire to spread throughout the ship; the fires continued to burn on three levels below the flight deck for many hours afterwards.

The actual cause of this disaster is unknown, but two possible explanations for this incident are related to EMC. Firstly, it was a problem of shielding effectiveness, as a faulty cable shield allowed the extremely high power ship's transmitters to trigger the launch command lines [77]. Secondly, there was an electrical transient which happened during weapon loading, resulting in the activation of a false launch signal. For both these theories, EMC was a key suspect.

During that time, the need for more sensitivity, and wider frequency coverage, for EMC methods had been dramatically increasing not only in the military; for example, a new technique in RA, Very Long Baseline Interferometry (VLBI), was developed in the 1970s; it achieved RFI-resistant cross-correlation by using the natural filtering effect of interferometry to suppress interferences in "fringe washing". From the many demands for a more sensitive EMC method, the reverberation chamber (RC) was initially developed in the 1970s, for the purpose of measuring more sensitive levels of electromagnetic radiation [10, 11].

To conclude, EMC became an issue of primary importance in all engineering disciplines, and will remain so as the number of chips, computers, and radio

transmissions grows, and the sensitivity of electronic circuits increases (this is a side-effect of lower power consumption circuits). The process of establishing EMC with electronic equipment consists of two parts: emission measurements and immunity tests. The first part is to make measurements to determine if any undesired signals being radiated from the equipment exceed limits set forth by the relevant agency. The second part is to expose the electronic equipment to selected levels of electromagnetic fields, at various frequencies, to determine if the equipment can perform satisfactorily in its intended operational environment. The main goal of this thesis is to develop a prototype of MIMO RC, focusing on its application to radiated emission measurements.

2.2. Standard Development of Radiated Emission Measurements for RA

2.2.1. Principle of Radiated Emission Measurements

An IEC standard [9] defines the meaning of radiated emission as the “phenomenon by which energy emanates from a source in the form of waves or particles”. Basically, most electronic equipment is, in some situations, interfered by electromagnetic radiation. The radiation can be from natural or man-made sources, and can be intentional or unintentional. Examples of intentional radiators are cell phones, walkie-talkies, and wireless communications, while transistors, welders, lights, and switches are examples of unintentional radiators. Thus, emission measurements quantify the amount of intentional and unintentional RF power radiated by the EUT within the measurement bandwidth. The radiated power from the EUT must not be stronger than the prescribed limits, or that EUT fails the test.

For RA application, emission measurements are of more concern and more demanding than immunity tests. While immunity tests determine the quality of the EUT, which is often an economic subject, emission measurements are related to issues of government and law. For instance, a cheap television set is easily interrupted from using a mobile phone nearby, so the television should undergo immunity tests, and the mobile phone will need emission measurements. In this domain, the mobile phone owner is the “source”, and the television owner is the “victim”; issues of government and law might be consulted by the victim.

2.2.2. Standardised Approaches to Emission Measurements

Two separate standards, military [2] and commercial [9], are combined in this research. The limit values come from the military standard [2], while the procedures of the RC method are modified based on the international standard [9]. Both standards are reviewed here, as follows:

Military Standards: the first concerns about EMI began before WW1, when a radio was firstly installed in a vehicle [72, 79]. However, it had to wait until 1934 that the US Army Signal Corps released the first EMI standard: SCL-49, "Electrical Shielding and Radio Power Supply in Vehicles." This document offered a solution to not disturb radio reception installed in a vehicle, by shielding the ignition system. In the 1940s, military standards were concerned with RFI, which was involved with making suppression components for electrical machinery and internal combustion engines. In the 1950s and 1960s, each major US military agency imposed its own EMI and EMC specifications for limits on equipment for conducted and radiated emissions of electronic systems and equipment. For instance, the US Air Force used MIL-I-26600 and MIL-I-826, the Navy used MIL-I-16910 and MIL-I-17623, and the Army used MIL-E-55301. These specifications limited the amount of conducted and radiated emissions, and set susceptibility levels for systems and equipment. The specifications also set forth the test configurations and techniques needed to demonstrate compliance with the requirements. At this time, shielded Anechoic Chamber, AC, (Sect. 2.2.3) did not exist, so making measurements across a wide frequency range was likely to contain errors. In 1960, the US Department of Defense (DoD) created a comprehensive Defense Radio Frequency Compatibility Program (later renamed Electromagnetic Compatibility Program) which focused the Military Services R&D programs "to provide a means whereby electromagnetic compatibility should be 'built into' military communications-electronics equipment in the research and development stage".

Before 1967, US military EMC specifications were separated among the Navy, Army, and Air force. After the USS Forrestal disaster in 1967, MIL-STD-461 was created, along with its sister documents MIL-STD-462 and MIL-STD-463. It was the first "tri-service" EMI/EMC standard; MIL-STD-461 described the EMI requirements.

MIL-STD-462 recommended the measurement methodology, and relevant definitions and acronyms were given in MIL-STD-463. These standards have been kept up to date until 1993, when the Tri-Service EMC Committee issued an updated MIL-STD-461 and MIL-STD-462, revision D. At this time, MIL-STD-463 was eliminated and merged into the American National Standards Institute (ANSI) C63.14 "Standard Dictionary for Technologies of Electromagnetic Compatibility (EMC), Electromagnetic Pulse (EMP) and Electrostatic Discharge (ESD)". In 1999, the 461 and 462 standards were combined and published as MIL-STD-461E, which was later updated in 2007 to the currently used standard: MIL-STD-461F.

Until now, MIL-STD-461 has been refined considerably over the last 40 years. It has gone through revisions A through F, and many different notices. The present version (at May 2014) is MIL-STD-461F [2], and specifies an AC method to measure radiated emission measurements (RE102), which cover a range of 10 kHz to 18 GHz. A RC test method is allowed as an alternative one only for RS103, which is for radiated susceptibility tests. The author's understanding is that ACs are the preferred means of demonstrating compliance with MIL-STD-461F, for reasons of convenience (facilities are well established internationally) and comparison with historical results.

International Standards, IEC and CISPR: The International Electrotechnical Commission (IEC) is a not-for-profit, non-governmental organisation, officially founded on 26 June 1906 in London. Early standards development was driven by what we now regard as the electrical power industry. In 1930, the IEC established some well-known electrical units; for example, Hertz (Hz), for the unit of frequency; Gauss (G), for the unit of magnetic flux density; Weber, for the unit of magnetic flux. In 1938, the IEC published the first edition of the International Electrotechnical Vocabulary, prepared by TC1 – a milestone. It contained more than 2,000 terms in English, French, German, Italian, Spanish and Esperanto, with definitions in the first two of these languages.

In 1934, representatives of 6 countries in Europe (Belgium, the Netherlands, Luxembourg, France, Germany, and the UK) also founded the Comité International Spécial des Perturbations Radioélectriques (CISPR), or International Special Committee on Radio Interference, to decide how the subject of RFI should be dealt with internationally. This committee was established after an ad-hoc meeting of

interested international organisations in Paris in 1933 [80]. The first meeting was held in 1934, but meetings were suspended during WW2; in 1946, meetings resumed, and Australia, Canada and the US joined CISPR at that time.

In 1950, CISPR was brought under the IEC with the standing as a technical committee, but retained its own organisation. During the 1960s to early 1970s, CISPR established eight Working Groups, and CISPR specifications were extended to cover frequencies up to 1,000 MHz. IEC (including CISPR) had released many standards over these decades, but the boundaries between the activities of CISPR and IEC were still uncertain.

Until 1973, IEC work on RFI and EMC was restricted to CISPR's emission measurement techniques and limit-setting activities. Various IEC technical committees (TCs) had representation on CISPR: for example, TC-12: Radio Communication was set up in 1926; TC-20: Electric Cables was created in 1933. TC-77 was established in 1973 because of a need for more work on EMC test and measurement methods, and for greater coordination between various equipment committees. TC-77 has three sub-committees: 1) SC-77A: low frequency phenomena (up to 9 kHz, emissions and immunity), 2) SC-77B: high frequency phenomena (Continuous and Transient phenomena, including Electrostatic Discharge), and 3) SC-77C: high power fields (including high altitude nuclear detonations). CISPR, in 1973, also formed six sub-committees (SCs) along the lines of seven principal product families. Sub-Committee A (SC A) was on radio interference measurements and statistical methods. The subjects of Industrial, Scientific or Medical (ISM), motor vehicles, radio and TV receivers, household appliances and fluorescent lighting are the scope of SCs B, D, E and F. The work of SC C was on high voltage lines.

In 2014, the cooperation of IEC and CISPR is as shown in Fig. 2-3 [80]. CISPR has updated six sub committees, which are responsible for different areas, defined as: SC-A: measurement of radio interference and statistical methods; SC-B: measurement of interference regarding ISM equipment, high voltage equipment, or traction devices; SC-D: interference in motor vehicles (both gasoline and electric); SC-F: interference in household appliances, tools, and lighting equipment; SC-H: limitations to protect radio frequencies; and SC-I: electromagnetic compatibility of Information

Technology (IT) equipment (e.g. computers), multimedia / hi-fi devices and radio equipment (receivers).

IEC TC-77 undertakes the majority of technical work relating to immunity tests and emission measurements. One of the notable exceptions in the present CISPR/TC77 differentiation is the IEC 61000-4-21 standard [9] for reverberation chambers, which was processed in parallel through CISPR sub-committee A (measurement methods) and IEC SC-77B (high frequency sub-committee under IEC technical committee TC-77).

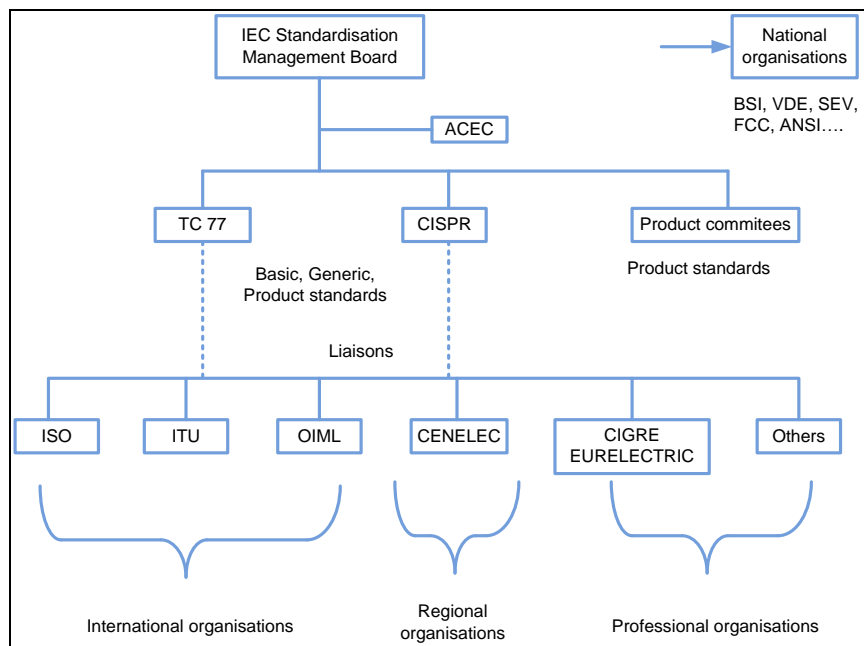


Figure 2-3: Cooperation of IEC and CISPR [80].

Analysis: Typically, emission requirements for equipment on RA sites [78], such as the MRO, are very demanding, and the respective measurements are a challenge for an EMC laboratory; they are not only more sensitive than the MIL-STD requirements, but it also depends on location of each EUT from the centre of the site as Fig. 1-8 (while only one set of limit values is required for common use). As more sensitive emission measurements are required, this research uses the RC method (Sect. 2.3) in the application of emission measurements to improve the sensitivity of a test facility although MIL-STD has not stated using of RC method.

There are 2 standards involved in this research; one is for the application, and the other is for the method. For the application, emission limit values for equipment to be used at the MRO are referred to the MIL-STD 461F [2] limit values (Fig. 2-4). For

the method, IEC 61000-4-21 [9] describes the performance requirements for RC on an international level, although there are a number of standardisation bodies which develop the RC method. Therefore, for EMC tests for RA sites at the MRO, there is a combination of at least 2 different standards, i.e., the military [2] and international [9] standards.

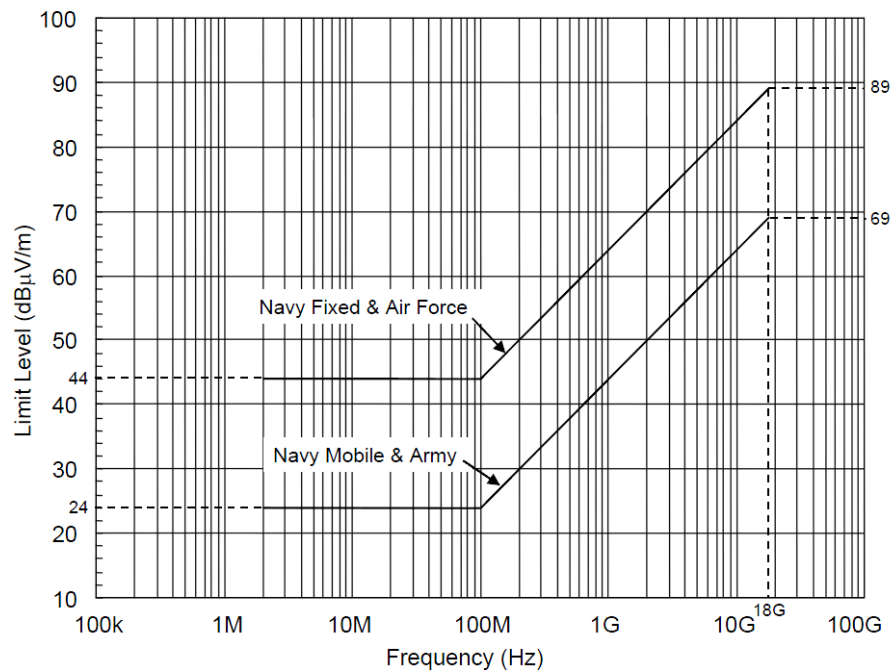


Figure 2-4: MIL-STD-461F, RE102 limit for ground application [2].

To conclude: for RA sites, e.g. the MRO, special EMC limits are defined, while measurement methods are normally referred to an international standard; i.e., technical methods based on the RC method referred to IEC standards, but emission limits are based on MIL-STD-461F. Note, MIL-STD-461F does not specify using a RC for radiated emission measurements (RE102), while IEC 61000-4-21:2011 allows the use of RC as low as 100 MHz. Thus, this thesis is not just about combining both standards, but also about how to, apply them by making up new solutions and limit values.

2.2.3. Four Methods for Radiated Emission Measurements

From the above EMC standards, there are 4 main methods for radiated emission measurements: Open Area Test Site (OATS), Anechoic Chamber (AC), Transverse Electro Magnetic cell (TEM cell, GTEM cell), and Reverberation Chamber (RC).

Open Area Test Site (OATS): this is the most common method, and one that can provide the most accurate results, depending on the EUT setup and site imperfections. This method has some common limitations (Fig. 1-9) related to high ambient noise levels, reflections, and weather. Some of these limitations can be eliminated by good calibration. As a result, a good OATS can be more accurate than the AC (but the OATS cannot be more sensitive than the AC). Nowadays, this method is rarely used, and especially not as a reference.

Anechoic Chamber (AC): anechoic chambers (“an-echoic” means echo-free or no-reflection), was developed by American acoustics expert Leo Beranek, and was originally used for acoustics to minimise the reflections in a room. In the EMC context, an AC is used to absorb reflections of electromagnetic waves by installing absorbers to dampen reflections (i.e. by reducing standing waves, resulting in the elimination of resonances), according to the recommendations of each application. Therefore, it can be said that the AC method is close to OATS, but in ideal conditions. The AC can be used for many EMC applications, e.g., emission measurements and immunity tests. The AC method has limitations at low frequencies, i.e., it requires large absorbers; then, the chamber dimensions depend on measurement distance and the operating frequency range.

To make emission measurements in an AC (Fig. 2-5), the EUT must be rotated, as only one signal direction can be measured each time. Then the measured results are calculated from the collected measurement data. It must be noted that the signals measured in the AC method yield only the maximum values, as this method measures only the peak value at each orientation direction of the EUT, whereas the RC method provides a statistically averaged result which is better in terms of stability, repeatability and reliability. Besides, the cost per square metre for ACs is more expensive than for RCs due to the requirements of absorbers, and more sensitive antennas and instruments.

An AC itself cannot use the benefit of the Q-factor to increase the level of “signal” power sent from the EUT; thus, more sensitive measurement can be done only by installing more sensitive devices:

- (i) For receivers, the noise floor of the instrument must be extremely low, leading to higher costs;



Figure 2-5: Anechoic Chamber (AC), Curtin University, WA, Australia.

- (ii) For antennas, the antenna dimensions do matter for working at low frequencies (where larger antennas are required); also important is having a large beamwidth, and maintaining a very good reflection coefficient, and
- (iii) For absorbers, they must absorb as much as possible over the entire range of operation frequencies. The absorber quality should be frequency independent so that very accurate measurements can be done.

To summarise: in general, the AC method is similar to OATS under ideal conditions, which is the simplest method with the widest range of operation frequencies; AC does not give the most sensitive results, and is not the cheapest method. RC, for similar dimensions, requires a lower cost per square metre. However, the AC method is currently the “most” commonly used method.

TEM Cells: the Transverse Electro Magnetic cell (TEM cell, also known as the Crawford Cell) can be traced back to the work published by Myron Crawford, of the (then) U.S. National Bureau of Standards (NBS), in 1974 [81]. TEM cells are based on the concept of a coaxial line, where the distance between the outer conductor and

inner conductor is expanded in order to put in the EUT. In contrast to the AC, no RF-absorptive lining is used to damp resonances.

For immunity tests, the test field, generated between the outer and inner conductor (by the septum, see Fig. 2-6), is well defined in intensity and polarisation, and is uniform over a relatively small proportion of the total cell volume. For emission measurements, on the other hand, the EUT's radiated power corresponds to a signal between the septum and ground.

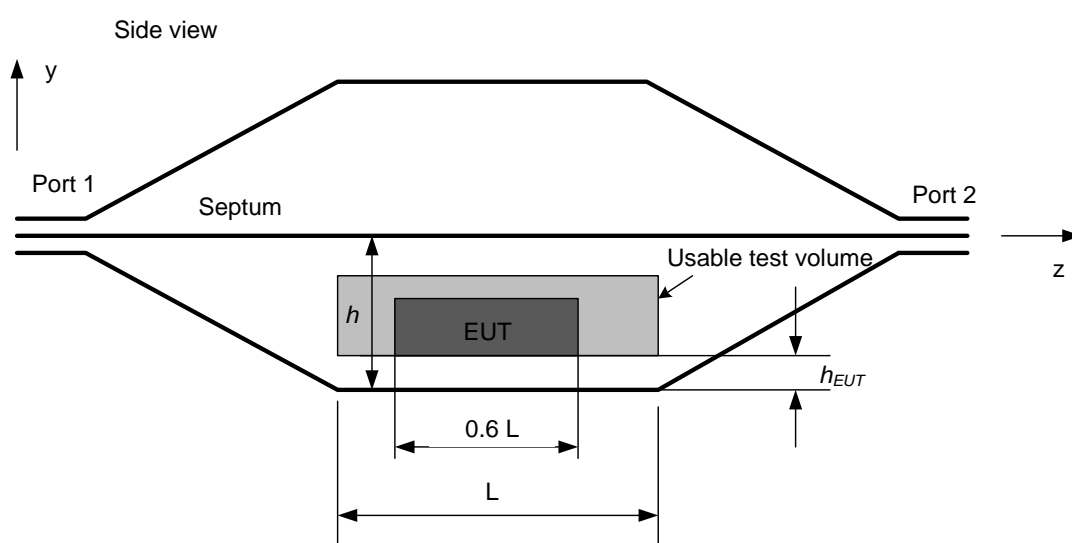


Figure 2-6: Schematic view of Symmetrical TEM Cell [82].

One of the most pressing concerns with the method of the TEM cell is that TEM cells illuminate the EUT with only a single polarisation of TEM wave, so re-orientation of the EUT is required for another polarised measurement. Tilting the EUT may not be an option for this method (according to the standard [82]), and three polarisations of EUT are required to find the sum square value by [82]:

$$S = \sqrt{V_{p1}^2 + V_{p2}^2 + V_{p3}^2}, \quad (\text{V}) \quad (2.1)$$

where S is the root sum square of measured voltages, in Volts, and V_{p1} , V_{p2} , V_{p3} are the voltage measurements from the 3 polarisations, respectively.

Besides, there are two more serious limitations with the TEM cell method. Firstly, TEM behaviour breaks down as the excitation frequency approaches the first resonance of the enclosure. They are applicable only to frequencies lower than the

first cavity resonance of the shell. Moreover, TEM cells are only suitable for measuring relatively small EUTs, because the frequency range across which the TEM field is established is determined by the first cavity resonance of the enclosure. For example, a cell approximately 30 cm x 90 cm x 90 cm has a maximum usable frequency of 200 MHz. Such a cell could accommodate an EUT of approximately 10 cm x 30 cm x 30 cm, based on the commonly accepted “rule of thumb” that the EUT should not occupy more than approximately 1/3 of the distance between the shell and septum.

Although TEM cells can make more sensitive emission measurements compared to AC or OATS, they can be problematic that the dimensions of TEM cells dominate the highest usable frequency and maximum EUT size. Although the GTEM chamber was later developed in 1990 [104] (with a specified cavity shape — the rectangular prism) to extend the highest operation frequency of the TEM chamber (up to about a few GHz), it still comes with problems of uniformity along the cell, positioning, and test volume size [83].

Reverberation Chamber (RC): As this method is studied in this thesis, the details will be explained in the following Section.

2.3. Method of Conventional Reverberation Chamber [9]

A Reverberation Chamber (RC) is a highly conductive shielded cavity, installed with a mechanism for “stirring” (i.e. perturbing) its modes, to perform electromagnetic (EM) measurements (for both emissions and immunity) on an EUT. Any cavity that fits this definition can be considered a RC (also called a mode-stirred chamber, or mode-tuned/mode-stirred reverberation chamber, or stirred-mode cavity). A high quality factor (Q) allows the generation of strong signals with very low source power; measurements can be made more “sensitive” compared with an OATS or AC, and immunity tests can also be done at low cost, as high field strengths can be generated with low amplifier power. The RC method provides a statistical result, which is good in terms of measurement “stability”, “repeatability” and “reliability”. Besides, the cost per square metre of a RC is cheaper than for a AC (as there is no need for absorber).

Research on electromagnetic RCs has been performed for more than 50 years. The author has reviewed many research articles, and found that there are quite a few applications that can be done in RCs; for example, (1) radiated immunity of components and large systems, (2) **radiated emissions**, (3) shielding characterisations of cables, connectors, and materials, (4) antenna measurements (including efficiency), (5) field probe calibration, (6) characterisation of material properties, (7) biological and biomedical effects, (8) tests of wireless devices including simulations of various wireless “multipath” environments.

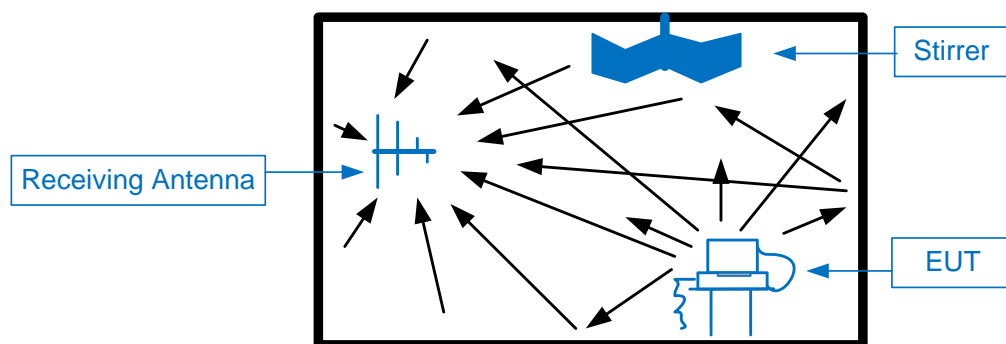


Figure 2-7: Concept of radiated emission measurements in the RC method.

The concept of making emission measurements in a RC (in typical uses) is as simple as placing an EUT in a shielded cavity. Then, operate the EUT as normal (the walls will reflect the signals inside the cavity), and measure the radiated signal from the EUT with a receiving antenna. Figure 2-7 illustrates the concept of making radiated emission measurements in a RC (conventional).

Although the application of radiated emission measurements in a shielded room can also be done with other methods (for instance, using ACs), an advantage of RCs is the ability to generate a statistically isotropic, homogeneous, and unpolarised field (so rotation of the EUT is not required). As for the results, the RC method is the only one capable of measuring indirect signals (see Fig. 2-7), whereas the other methods measure direct signals by controlling or eliminating the indirect path losses. For example, RCs can capture emissions from all directions of a cubic to check all 6 faces of EUT, while OATS and AC test with a full 360 degree rotation can only cover 4 sides. However, the field distribution in a RC must be confirmed to be sufficiently uniform, before making any emission measurements, otherwise measurement results are not reliable (i.e., EUT position has an effect on the result).

In order to make the field uniform, the field distribution (for any mode) in the cavity cannot be fixed (standing wave), but it must be stirred (i.e. perturbed) by rotating the stirrer. Moreover, the energy losses due to the walls, cables and other structures (including the stirrer) also impact the performance of the chamber due to the influence on the quality “Q-Factor”. As a result, the sum total of all measured signals at the receiving antenna does not equal the radiated power from the EUT. Thus, the Chamber Validation Factor, CVF (described in Sect. 2.3.2) is an important parameter needed to calculate the radiated power from the EUT, from the measured signals.

2.3.1 Origin of RC

To explain the method of a conventional RC, the behaviour of electromagnetic propagation along a *rectangular waveguide* is a good start. Generally, waveguides are metal conduits used to confine and direct RF signals; rectangular waveguides (Fig. 2-8) are more common, and are also related to this research. The idea of a waveguide for electromagnetic waves was first suggested in 1897 by Lord Rayleigh [105]. A waveguide behaves much like a High Pass Filter. It will support waves above a certain cutoff frequency. If the operating frequency lies below the waveguide cutoff frequency, propagation does not take place, and the wave is said to be evanescent. The cutoff wavelength (λ_c) for a rectangular waveguide is given in Eq. 2.2.

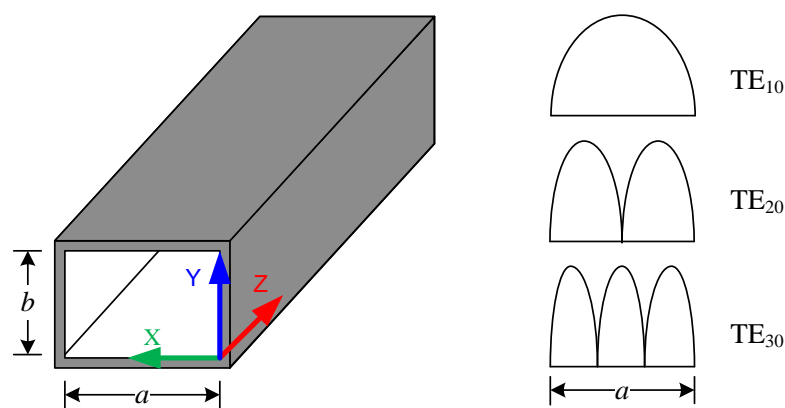


Figure 2-8: Rectangular waveguide and some of its resonant modes.

$$\lambda_c = \frac{2}{\sqrt{\left[\left(\frac{m}{a}\right)^2 + \left(\frac{n}{b}\right)^2\right]}}, \quad \mu_r, \epsilon_r = 1: \quad (2.2)$$

where m = number of half-wavelengths along the broad side dimension (i.e. the width), n = number of half-wave lengths along the shorter side (i.e. the height), a and b are the broad side dimension and shorter side dimensions, respectively.

Power loss can occur in the walls of the waveguide due to induced currents; in order to reduce this loss, walls are designed with as low a resistance as possible (i.e. with a high Q-factor). The Q-factor is defined by Eq. 2.3.

$$Q = \omega \left(\frac{\text{energy stored per unit length}}{\text{energy loss per unit length/ second}} \right), \quad (2.3)$$

One of the most important differences in the operation of a waveguide, compared to a transmission line, is the mode of propagation. In a transmission line, both the magnetic and electric components of the electromagnetic field are perpendicular to the direction of wave propagation; this mode of propagation is called TEM (transverse electromagnetic). There are infinitely many static modes that any waveguide can support, but the TEM mode is not one of them. Static waveguide modes are designated either TE (transverse electric) or TM (transverse magnetic), followed by 2 suffixes identifying the mode (m, n).

TE mode stands for transverse electric mode, where the electric field (E field) is perpendicular to the direction of propagation, and the magnetic field (H field) is along the direction of propagation [84]. In a rectangular waveguide, the TE₁₀ mode (the cutoff TE mode) is the dominant one; the longer dimension a is a half-wave length; i.e., the index 1 indicates that only 1 half-wave length along the a axis (Fig. 2-8). Electric and magnetic fields in rectangular waveguides can be derived from *Maxwell's equations* (Eqs. 2.4-2.5) via the *Helmholtz equation* (Eqs. 2.6-2.7). For example, only the magnetic field along the Z -axis needs to be derived (Eqs. 2.8 through 2.10), after applying the relevant *boundary conditions* (Eqs. 2.11 through 2.13) as follows:

Starting from the assumption that the waveguide is source free interior of the *Maxwell's equations* can be written as:

$$\nabla \times \bar{E} = -j\omega\mu\bar{H}, \quad (2.4)$$

$$\nabla \times \bar{H} = j\omega\epsilon\bar{E}. \quad (2.5)$$

Taking the curl of the equations above, they become the wave equations, or *Helmholtz equations* for \bar{E} and \bar{H} :

$$0 = \nabla^2 \bar{E} + \omega^2 \mu \epsilon \bar{E}, \quad (2.6)$$

$$0 = \nabla^2 \bar{H} + \omega^2 \mu \epsilon \bar{H}. \quad (2.7)$$

A constant $k = \sqrt{\omega^2 \mu \epsilon}$ is defined and called the wavenumber of the medium; its units are 1/m. So, in free space, the Helmholtz equation for \bar{H} , for example, can be written as:

$$0 = \nabla^2 \bar{H} + k^2 \bar{H}. \quad (2.8)$$

For TE waves in a waveguide, $E_z = 0, H_z \neq 0$, and the propagation constant (γ) is equal to $\sqrt{h^2 - k^2}$; where $h^2 = \left(\frac{m\pi}{a}\right)^2 + \left(\frac{n\pi}{b}\right)^2$, and $k \neq 0$. So, $\gamma = \sqrt{h^2 - k^2} = j\beta = j\sqrt{\omega^2 \mu \epsilon - \left(\frac{m\pi}{a}\right)^2 - \left(\frac{n\pi}{b}\right)^2}$ for both: TE and TM: To apply, one must first find H_z , which can be solved from:

$$0 = \left(\frac{\partial^2}{\partial x^2} + \frac{\partial^2}{\partial y^2} + \frac{\partial^2}{\partial z^2} + k^2\right) H_z(x, y, z). \quad (2.9)$$

For TE waves, $H_z(x, y, z) = H_z^0(x, y)e^{-\gamma z}$, where $H_z^0(x, y)$ satisfies the following second-order partial differential equation (PDE):

$$0 = \left(\frac{\partial^2}{\partial x^2} + \frac{\partial^2}{\partial y^2} + k^2\right) H_z^0(x, y). \quad (2.10)$$

The solution for $H_z^0(x, y)$ must satisfy the following *boundary conditions*:

1) In the X-direction:

$$\frac{\partial H_z^0}{\partial x} = 0 \quad \rightarrow \quad (E_y = 0); \quad \text{at} \quad x = 0, a, \quad (2.11)$$

2) In the Y-direction:

$$\frac{\partial H_z^0}{\partial y} = 0 \quad \rightarrow \quad (E_x = 0); \quad \text{at} \quad y = 0, b. \quad (2.12)$$

It is readily verified that the appropriate solution for $H_z^0(x, y)$ is:

$$H_z^0(x, y) = H_0 \cos\left(\frac{m\pi}{a}x\right) \cos\left(\frac{n\pi}{b}y\right). \quad (\text{A/m}) \quad (2.13)$$

This thesis shows only the derivation of \bar{H} , as the remaining fields can be derived in a similar way; the other field components are as follows:

$$E_x^0(x, y) = \frac{j\omega\mu}{h^2} \left(\frac{n\pi}{b}\right) H_0 \cos\left(\frac{m\pi}{a}x\right) \sin\left(\frac{n\pi}{b}y\right), \quad (\text{V/m}) \quad (2.14)$$

$$E_y^0(x, y) = -\frac{j\omega\mu}{h^2} \left(\frac{m\pi}{a}\right) H_0 \sin\left(\frac{m\pi}{a}x\right) \cos\left(\frac{n\pi}{b}y\right), \quad (\text{V/m}) \quad (2.15)$$

$$E_z^0(x, y) = 0, \quad (\text{V/m}) \quad (2.16)$$

$$H_x^0(x, y) = \frac{\gamma}{h^2} \left(\frac{m\pi}{a} \right) H_0 \sin \left(\frac{m\pi}{a} x \right) \cos \left(\frac{n\pi}{b} y \right), \quad (\text{A/m}) \quad (2.17)$$

$$H_y^0(x, y) = \frac{\gamma}{h^2} \left(\frac{n\pi}{b} \right) H_0 \cos \left(\frac{m\pi}{a} x \right) \sin \left(\frac{n\pi}{b} y \right). \quad (\text{A/m}) \quad (2.18)$$

TM mode stands for transverse magnetic mode, where the magnetic field is perpendicular to the direction of propagation, and the electric field is along the direction of propagation [84]. In analogy to TE mode, it can be shown that the TM mode has $E_z(x, y, z) = E_z^0(x, y)e^{-\gamma z}$, and that:

$$E_x^0(x, y) = -\frac{\gamma}{h^2} \left(\frac{m\pi}{a} \right) E_0 \cos \left(\frac{m\pi}{a} x \right) \sin \left(\frac{n\pi}{b} y \right), \quad (\text{V/m}) \quad (2.19)$$

$$E_y^0(x, y) = -\frac{\gamma}{h^2} \left(\frac{n\pi}{b} \right) E_0 \sin \left(\frac{m\pi}{a} x \right) \cos \left(\frac{n\pi}{b} y \right), \quad (\text{V/m}) \quad (2.20)$$

$$E_z^0(x, y) = E_0 \sin \left(\frac{m\pi}{a} x \right) \cos \left(\frac{n\pi}{b} y \right), \quad (\text{V/m}) \quad (2.21)$$

$$H_x^0(x, y) = \frac{j\omega\epsilon}{h^2} \left(\frac{n\pi}{b} \right) E_0 \sin \left(\frac{m\pi}{a} x \right) \cos \left(\frac{n\pi}{b} y \right), \quad (\text{A/m}) \quad (2.22)$$

$$H_y^0(x, y) = -\frac{j\omega\epsilon}{h^2} \left(\frac{m\pi}{a} \right) E_0 \cos \left(\frac{m\pi}{a} x \right) \sin \left(\frac{n\pi}{b} y \right), \quad (\text{A/m}) \quad (2.23)$$

$$H_z^0(x, y) = 0, \quad (\text{A/m}) \quad (2.24)$$

The cutoff TE and TM modes are shown as plots in Fig. 2-9. The cutoff TE mode is TE₁₀; and the next mode (TE₂₀) has twice as many half-waves as the TE₁₀ mode. If a and b are different to one another, TE₀₁ and TE₁₀ will have different frequencies and also different propagation patterns. The cutoff TM mode is TM₁₁, which is $\sqrt{5}$ times the dominant mode frequency in a 2:1 waveguide. Propagation of EM waves takes place due to the waveguide; hence, a TEM mode is not possible.

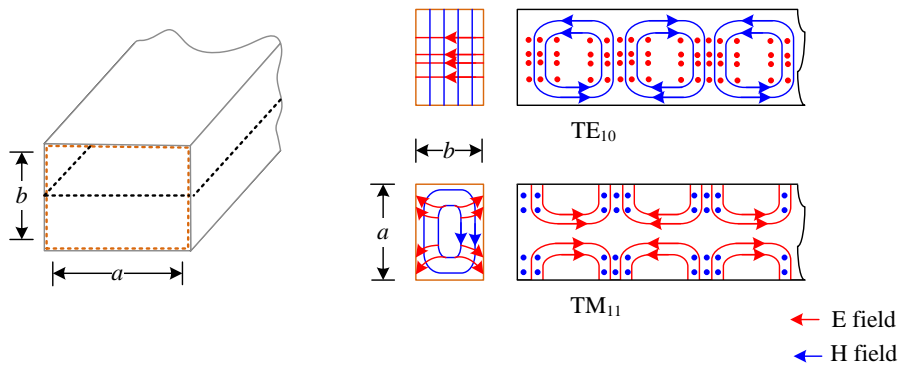


Figure 2-9: The cutoff TE and TM modes of a rectangular waveguide.

Cavity resonator: Consider a rectangular waveguide with both ends closed by a conducting wall. Waves are trapped inside, and are reflected between the two ends. The cavity will resonate at a characteristic frequency. The cavity dimensions are assigned as a , b , and d (Fig. 2-10). Both TE and TM modes become more complicated to be designated in this cavity, as “direction of propagation” can be chosen along any dimension, e.g., a TE mode with respect to the Z axis could be a TM mode with respect to the Y axis. Usually, the longest dimension is chosen as the “direction of propagation” to avoid confusion; thus, the Z axis is the “direction of propagation” in this Section (Figure 2-10). As a result, the conducting end walls at $Z=0$ and $Z=d$ give rise to multiple reflections, leading to standing waves being set up in the cavity.

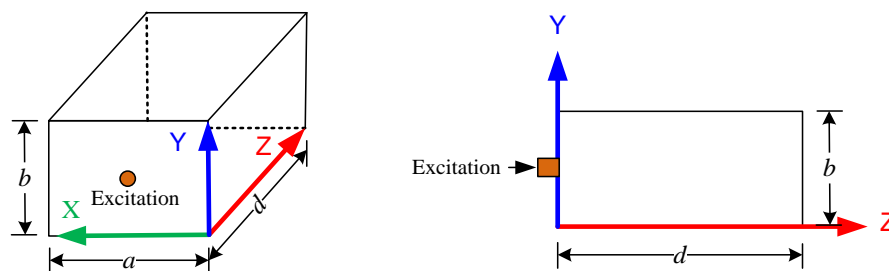


Figure 2-10: Reference excitation for rectangular cavity modes.

The nomenclature for modes in a cavity introduces a third index: m , n , and l , for example TE_{011} . The first two indices are the transverse mode numbers, which are the same as those for a waveguide. The third index is the longitudinal mode caused by the interference pattern of the forward travelling and reflected waves. In other words, the third index is equal to the number of half-wavelengths along the length of the waveguide (for TE modes, either m or n can be zero, but not l ; for TM modes, neither m nor n can be zero, but l can). According to [85, 86], the resonance frequencies ($f_{m,n,l}$) of a cavity can be calculated from the associated wavelengths:

$$\lambda_{m,n,l} = \frac{2}{\sqrt{\left[\left(\frac{m}{a}\right)^2 + \left(\frac{n}{b}\right)^2 + \left(\frac{l}{d}\right)^2\right]}}, \quad f_{m,n,l} = \frac{c}{\lambda_{m,n,l}}, \quad \mu_r, \epsilon_r = 1, \quad (2.25)$$

where l , m , and n are the mode indices, a , b , and d are the chamber dimensions, and c is the speed of wave propagation in the enclosure.

From Maxwell's equations again, waves in a rectangular cavity for TE modes have field components as shown in Eqs. 2.26 through 2.31, and TM modes have components as shown in Eqs. 2.32 through 2.37 [84]:

$$E_x(x, y, z) = \frac{j\omega\mu}{h^2} \left(\frac{n\pi}{b}\right) H_0 \cos\left(\frac{m\pi}{a}x\right) \sin\left(\frac{n\pi}{b}y\right) \sin\left(\frac{l\pi}{d}z\right), \quad (\text{V/m}) \quad (2.26)$$

$$E_y(x, y, z) = -\frac{j\omega\mu}{h^2} \left(\frac{m\pi}{a}\right) H_0 \sin\left(\frac{m\pi}{a}x\right) \cos\left(\frac{n\pi}{b}y\right) \sin\left(\frac{l\pi}{d}z\right), \quad (\text{V/m}) \quad (2.27)$$

$$E_z(x, y, z) = 0, \quad (\text{V/m}) \quad (2.28)$$

$$H_x(x, y, z) = -\frac{1}{h^2} \left(\frac{m\pi}{a}\right) \left(\frac{l\pi}{d}\right) H_0 \sin\left(\frac{m\pi}{a}x\right) \cos\left(\frac{n\pi}{b}y\right) \cos\left(\frac{l\pi}{d}z\right), \quad (\text{A/m}) \quad (2.29)$$

$$H_y(x, y, z) = -\frac{1}{h^2} \left(\frac{n\pi}{b}\right) \left(\frac{l\pi}{d}\right) H_0 \cos\left(\frac{m\pi}{a}x\right) \sin\left(\frac{n\pi}{b}y\right) \cos\left(\frac{l\pi}{d}z\right), \quad (\text{A/m}) \quad (2.30)$$

$$H_z(x, y, z) = H_0 \cos\left(\frac{m\pi}{a}x\right) \cos\left(\frac{n\pi}{b}y\right) \sin\left(\frac{l\pi}{d}z\right), \quad (\text{A/m}) \quad (2.31)$$

$$E_x(x, y, z) = -\frac{1}{h^2} \left(\frac{m\pi}{a}\right) \left(\frac{l\pi}{d}\right) E_0 \cos\left(\frac{m\pi}{a}x\right) \sin\left(\frac{n\pi}{b}y\right) \sin\left(\frac{l\pi}{d}z\right), \quad (\text{V/m}) \quad (2.32)$$

$$E_y(x, y, z) = -\frac{1}{h^2} \left(\frac{n\pi}{b}\right) \left(\frac{l\pi}{d}\right) E_0 \sin\left(\frac{m\pi}{a}x\right) \cos\left(\frac{n\pi}{b}y\right) \sin\left(\frac{l\pi}{d}z\right), \quad (\text{V/m}) \quad (2.33)$$

$$E_z(x, y, z) = E_0 \sin\left(\frac{m\pi}{a}x\right) \sin\left(\frac{n\pi}{b}y\right) \cos\left(\frac{l\pi}{d}z\right), \quad (\text{V/m}) \quad (2.34)$$

$$H_x(x, y, z) = \frac{j\omega\epsilon}{h^2} \left(\frac{n\pi}{b}\right) E_0 \sin\left(\frac{m\pi}{a}x\right) \cos\left(\frac{n\pi}{b}y\right) \cos\left(\frac{l\pi}{d}z\right), \quad (\text{A/m}) \quad (2.35)$$

$$H_y(x, y, z) = -\frac{j\omega\epsilon}{h^2} \left(\frac{m\pi}{a}\right) E_0 \cos\left(\frac{m\pi}{a}x\right) \sin\left(\frac{n\pi}{b}y\right) \cos\left(\frac{l\pi}{d}z\right), \quad (\text{A/m}) \quad (2.36)$$

$$H_z(x, y, z) = 0, \quad (\text{A/m}) \quad (2.37)$$

where $h^2 = \left(\frac{m\pi}{a}\right)^2 + \left(\frac{n\pi}{b}\right)^2 + \left(\frac{l\pi}{d}\right)^2$ for Equations 2.26 through 2.37.

In practice, there will always be some currents induced in the cavity walls, which will dissipate the energy. The rate of energy dissipation is characterised by the quality factor, or Q-factor: The resonant modes (integer mode numbers) in a cavity will present high Q values. Fields can also exist in non-integer mode numbers, but the energy will be dramatically damped (low Q values), because the currents in the walls will be relatively large. The Q-factor of the cavity for each mode can be calculated from:

$$Q = 2\pi \frac{c}{\lambda_r} \left(\frac{\text{energy stored in cavity; electric and magnetic fields}}{\text{Energy dissipated in one period of the } f_r} \right) = \frac{\omega W}{P_L}, \quad (2.38)$$

$$W_e = \frac{\epsilon_0}{4} \int \left\{ |E_x|^2 + |E_y|^2 + |E_z|^2 \right\} dv, \quad (2.39)$$

$$W_m = \frac{\mu_0}{4} \int \left\{ |H_x|^2 + |H_y|^2 + |H_z|^2 \right\} dv, \quad (2.40)$$

$$P_L = \oint P_{av} ds, \quad (2.41)$$

where λ_r is a resonant wavelength where the stored energy is constant with time, W is the total energy stored in electric and magnetic fields (i.e., $W_e + W_m$), P_L is the time-average power dissipated in the cavity (regardless of where the power comes from), and ω is the angular frequency.

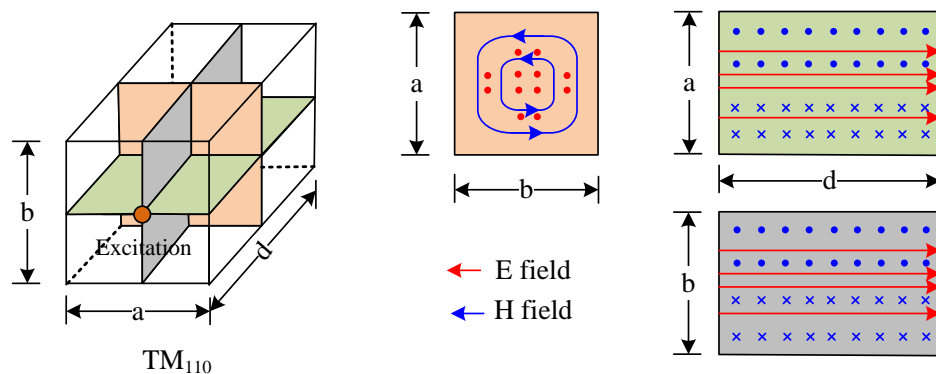


Figure 2-11: The cutoff TM modes of a rectangular cavity.

However, one of the most important differences in the cavity operation, as compared to a waveguide, is the propagation of modes. Close to a given resonant mode frequency, the associated field distribution in space can be best excited by EM

power injection at certain calculable cavity positions. *In other words, using multiple feeding positions can cover (excite) many more propagation modes in the cavity.*

Conventional RC: the RC method is adopted from the concept of field distribution in a cavity. Conceptually, when the EUT and receiving antenna are placed in the resonant location(s), the antenna can easily measure the signal radiated from the EUT. However, emission measurement cannot be done in a cavity, as the bandwidth of any resonance frequency is usually narrow, and the resonance locations are fixed (the propagation pattern forms a standing wave). In other words, the pattern of the field distribution is very important for the RC method. To change a cavity to be a typical RC will require the stirring of the field distribution, and the shifting of the resonance frequencies in the cavity. Thus, the rotating of a metallic paddle, called the stirrer, to shift resonant frequencies (so as to cover the range of operation frequencies) and to stir the field distribution, is necessarily required for the method of conventional RC. The stirrer, in other words, is one of the major differences between a RC and a cavity.

By IEC 61000-4-21:2011 [9], symmetries in the design and placement of the stirrer are not recommended, in order to maximise the highest number of independent positions that it can generate. The stirrers should be adequate to provide the desired field uniformity. Rotating the stirrer can stir the field distribution, and shift the resonance frequencies in an area in the chamber called the working volume; this depends on the position, structure and size of the stirrer (more than one stirrer may be needed in some cases). In general, a stirrer(s) is designed to have good performance over a range of operating frequencies. One of most popular stirrer structures is the Z-shape (Fig. 2-12), or any shape bent like the letter “Z”. However, it is also known that the Z stirrer is not good in stirring resonances at low frequencies.



Figure 2-12: Z-Stirrer, ETS-LINDGREN, 1.5 m x 1.5 m x 7 m, for 80 MHz and above.

Operation Modes of RC: there are two modes for the RC method, depending on the rotation of the stirrer: “mode-tuned” and “mode-stirred”. While mode-stirred operation allows the stirrer to run continuously during measurements, mode-tuned operation makes measurements at discrete stirrer steps, employed in the course of moving the stirrer through a full revolution. The minimum number of stirrer steps suggested by [9] is 12 for all frequencies. The author’s review found that mode-stirred operation yields only mean values, or maximum values. Apart from alignment problems, mode-stirred data cannot be analysed in terms of the orientation angles of the stirrer, as the stirrer is being rotated continuously; it might then be impossible to study the field distribution at each stirrer position. Thus, in this research, only mode-tuned operation will be discussed and applied.

Conventional Lowest Usable Frequency (C-LUF) is the lowest frequency at which the required isotropicity and uniformity are met in a particular region (called the working volume, or WV). The chamber mode density and the effectiveness of the mechanical stirrer determine the C-LUF; the C-LUF typically occurs at the 60th resonant cavity mode, or at a frequency slightly above three times the first chamber resonance [9]. Above the C-LUF, there are enough resonance frequencies to be stirred to cover the whole FRI over one stirrer revolution. However, when the Q-factor of the chamber is very high, the stirrer is not very effective, or other factors affect its performance, the C-LUF may be higher (it may be up to 6 times the first chamber resonance, see Fig.e 2-13).

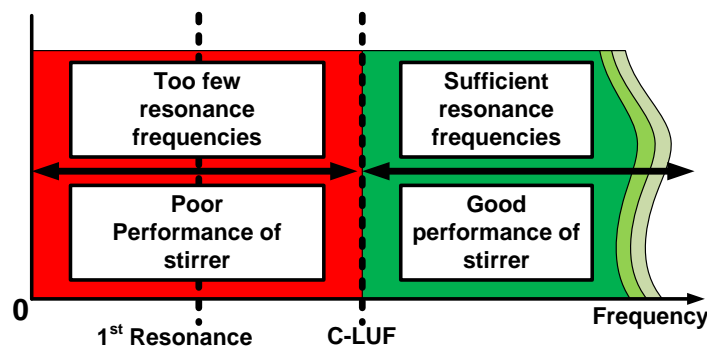


Figure 2-13: C-LUF compared to 1st resonance.

Above the 60th mode, the field distribution is a Rayleigh distribution, not a Rician distribution. This means that measuring the indirect path loss can be achieved, and there is no dominance of direct path loss (i.e., $A = 0$ in Eq. 2.43) which

dominates signals along other directions. This (Rayleigh) distribution allows RC to generate multipath environments.

To describe the difference between the Rayleigh and Rician distributions, this thesis will refer to direct and indirect propagation (environments) in a wireless system. In the case of RC, there is mainly a Rayleigh field distribution [55], which is a pure (i.e. no direct coupling) environment. The Gaussian field distribution represents a strong direct coupling environment (perfect balance), which does not occur in any RC, while the Rician environment is somewhere between these two environments. The Probability Density Functions (PDF) of the Gaussian, Rician and Rayleigh distributions are shown in Eqs. 2.42 through 2.44, respectively. From these equations, the difference between the Rician and Rayleigh PDFs is the variable A . A represents the dominant, stationary (nonfading) signal component, such as that along a line-of-sight propagation path. The effect of a dominant signal arriving with many weaker multipath signals gives rise to the Rician distribution; when A is 0, the Rician distribution becomes a Rayleigh distribution. In other words, in a RC, if the dominant signal becomes weaker (or fades away), the Rician distribution will degenerate to a Rayleigh distribution.

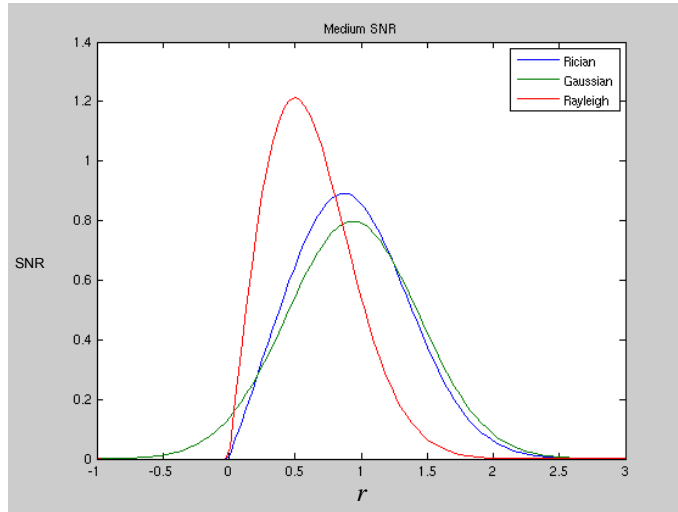


Figure 2-14: Probability Density Function (PDF) of Gaussian, Rician, and Rayleigh distributions (medium SNR) [55].

$$p_{\text{Gaussian}}(r) = \frac{1}{\sigma\sqrt{2\pi}} \times e^{-\left(\frac{(r-\mu)^2}{2\sigma^2}\right)}, \quad (r \in \mathbb{R}, \mu = \text{mean}), \quad (2.42)$$

$$p_{\text{Rician}}(r) = \frac{r}{\sigma^2} \times e^{-\left(\frac{(r^2+A^2)}{2\sigma^2}\right)} \times I_0\left(\frac{A \times r}{\sigma^2}\right), \quad (0 \leq A, r \leq \infty), \quad (2.43)$$

$$p_{\text{Rayleigh}}(r) = \frac{r}{\sigma^2} \times e^{-\left(\frac{r^2}{2\sigma^2}\right)}, \quad (0 \leq r \leq \infty), \quad (2.44)$$

where r is variable (in this thesis r is the field amplitude), σ^2 is the time-average power of the received signal; A is the peak amplitude of the dominant signal, and I_0 is the modified Bessel function of the first kind and zero-order.

Thus, the C-LUF is expected to be above the 60th mode due to the requirement of a sufficiently high number density of resonance frequencies, and also to generate a Rayleigh environment. The C-LUF can be defined as the lowest frequency at which the specified “field uniformity” can be achieved over a defined volume — called the “working volume” (this is described further in Sect. 2.3.2: Procedures). According to [85, 86], for a rectangular cavity, the 60th mode can be calculated from Eq. 2.45:

$$N \approx \frac{8\pi}{3}LWH \frac{f^3}{c^3} - (L + W + H) \frac{f}{c} + \frac{1}{2}, \quad (2.45)$$

where L , W , and H are the chamber dimensions, N is the number of modes up to a certain frequency f , and c is the speed of wave propagation in the enclosure.

The C-LUF can also be calculated from Eq. 2.25, with an estimate of the 60th mode at the frequency of $f_{4,2,2}$. The author has found that the LUF calculated from both Eq. 2.25 and Eq. 2.45 are not very different; Table 2-1 shows measured C-LUFs compared to the calculated C-LUFs (the higher result from Eq. 2.25 and Eq. 2.45) of some RCs in the market. The actual shielded room at CIRA is also compared in this Table. The CIRA room is roughly of the same size as the smallest Schaffner chamber, and its C-LUF could be expected at around 290 MHz.

Table 2-1: Resonant frequency comparisons (2013).

Dimensions (m)			1 st resonance	60 th mode freq.	C-LUF	Owner
L	W	H	(@calculation)	(@calculation)	(@ advertised)	
2.7	1.5	1.3	114.39 MHz	377.4 MHz	500 MHz	www.teseq.com
1.5	0.8	1	212 MHz	624.6 MHz	800 MHz	www.teseq.com
30	11	6	14.52 MHz	59.65 MHz	30 MHz	DSTO (Air OPT. division)
4	2.5	2.55	70.75 MHz	225.1 MHz	200 MHz	www.schaffner.com
3.1	7	2.55	52.91 MHz	174.7 MHz	100 MHz	www.schaffner.com
12.5	5.5	4	29.79 MHz	104.4 MHz	80 MHz	www.schaffner.com
32	25	15	7.61 MHz	29.82 MHz	85-98 MHz	www.ramayes.com
44	20	16	8.23 MHz	27.52 MHz	81-93 MHz	www.ramayes.com
29.5	22.9	13.3	8.27 MHz	33.05 MHz	94-108 MHz	www.ramayes.com
3.6	2.4	2.4	75.11 MHz	291.5 MHz	-	CIRA, Curtin Uni.

The Quality (Q) factor is a measure of the ability of a RC to store energy relative to its rate of dissipation. The ability of a chamber to store energy is determined by the factors of frequency, volume, and losses present in the chamber. The presence of losses at every resonance frequency affects the measurement of received powers. Without the EUT in place, the dominant loss mechanism in an empty chamber is due to the chamber walls and antennas. However, losses from antennas and other structures are often relatively small, and negligible compared to those from the walls. Thus, higher conductivity materials, such as copper or aluminium, are used to construct the chamber walls to lower the chamber losses. Besides, the EUT, the required support equipment, or any absorbing material present, may load the chamber and reduce its Q -factor, resulting in weaker measured signals. Therefore, the Q -factor should be monitored, as it can affect to measurement's sensitivity.

There are some ways to determine the Composite Q -factor (Q_g) of a chamber. Firstly, it can be approximately calculated by considering just 3 factors: the antenna, the walls and the EUT (Eq. 2.46). Secondly, Eq. 2.47 (which is derived from Eq. 2.38) is to determine the Q_g by comparing average received power to input power. Thirdly, Eq. 2.48 also shows another way to determine the Q_g by measuring 3 dB bandwidth. In addition, it must be noted that there have been attempts to try other ways to find the Q -factor, for example [87], although this research would not include.

$$\frac{1}{Q_g} = \frac{1}{Q_1} + \frac{1}{Q_2} + \frac{1}{Q_3}, \quad (2.46)$$

$$Q_g = \frac{16 \pi^2 V}{\eta_{Tx} \eta_{Rx} \lambda^3} \left\langle \frac{P_{AveRec}}{P_{input}} \right\rangle, \quad (2.47)$$

$$Q_g = \frac{f_{m,n,l}}{BW_Q}. \quad (2.48)$$

Here, Q_1 is the coefficient for the walls, Q_2 is the coefficient for the receiving antenna, Q_3 is the coefficient for the EUT, V is the chamber volume, λ is the wavelength, η_{Tx} , η_{Rx} are the antenna efficiency factors (see Eq. 2.50), $\langle \frac{P_{AveRec}}{P_{input}} \rangle$ is the average ratio of the received power to the input power over one revolution of the stirrer, BW_Q is the bandwidth across which the modes of the chamber are correlated (wider BW for a lossy chamber), and $f_{m,n,l}$ is the frequency of mode m, n, l .

Figure 2-15 shows that the measured power in a RC is not the radiated power from the EUT, due to some power lost by the effect of Q_g ; i.e., lost due to the presence of the antenna, the walls and the EUT itself (in this case, the EUT is another antenna). The black curve is the S_{12} when two antennas are set as shown in Fig. 2-15 (a); this environment represents OATS (and AC) method. Then, the similar setup is covered in a shielded aluminum cavity as shown in Fig. 2-15 (b) to represent RC environment, and the S_{12} becomes the red curve. There are two interesting conclusions from these results. Firstly, RC method can provide more sensitive measurement than OATS and AC methods. Although some certain frequencies RC gives lower sensitive results than OATS (or AC), these can be fixed by installing a mechanic stirrer(s). Secondly, the red curve shows that, even RC, the maximum received signal cannot be higher than the blue curve; this is due to the composite Q -factor (Q_g) of the chamber. Therefore, an emission measurement procedure is required to determine radiated power of the EUT from the received signal.

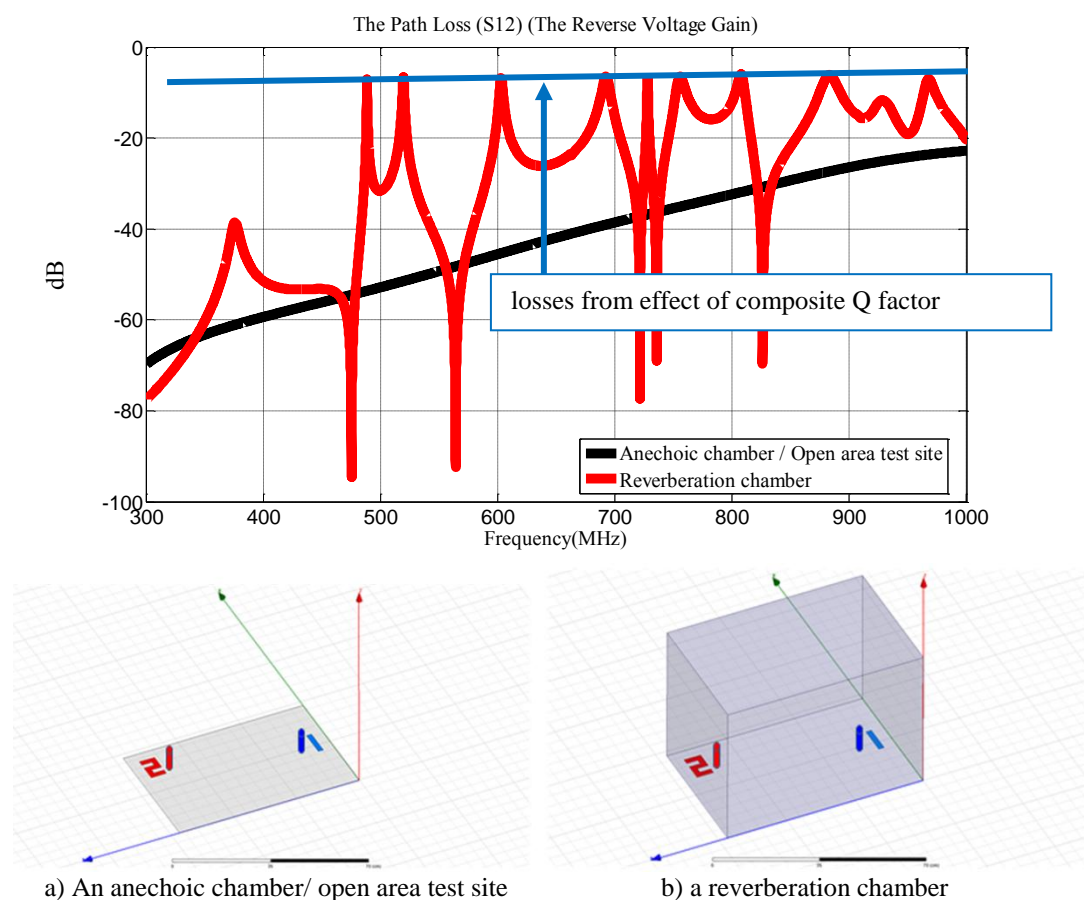


Figure 2-15: Effect of composite Q -factor (Q_g) [61].

There are quite a few factors involved in making emission measurements using the method of conventional RC, but all those factors are combined together in the procedures for users by the standards. A summary of the mode tuned procedures, described in the next Section is taken from Annex B of IEC 61000-4-21 [9], in order to explain what a conventional RC is, and to compare with the process of a modified RC in Chapters 3, 4, and 5. These conventional procedures will be summarised up until the calculation of radiated power from the EUT.

2.3.2 Procedures for Radiated Emission Measurements (Conventional RC)

IEC61000-4-21:2011 [9] does not recommend a minimum size RC test chamber for making radiated emission measurements. The chamber should be large enough to accommodate the EUT, the stirrers and the measurement antennas. The critical factor is that if a chamber fulfils the “validation procedure”, then this demonstrates that it provides the required electromagnetic environment at the desired level of statistical confidence; this is the definition of C-LUF. Above the C-LUF, when the chamber is excited with RF energy by the EUT, the resulting multi-mode electromagnetic environment can be “stirred” by the mechanical stirrer. The resulting field is statistically uniform, statistically isotropic (i.e., the measured power having arrived from all aspect angles), and statistically randomly polarised (i.e., with all possible directions of polarisation) when averaged over a sufficient number of positions of the stirrer. Thus, for making emission measurements, RC must have passed a validation procedure beforehand. In other words, there are 2 steps for making emission measurements: a validation procedure (without the EUT placed in the WV) and emission measurements (with the EUT placed in the WV).

Validation Procedure: [2, 9, 88] The outcome from the chamber validation is to determine if the combinations of all installed structures in the chamber produce sufficient stirring of the cavity modes to generate an (Rayleigh) environment that is statistically uniform and isotropic (this requires checking the field uniformity: σ). This validation can also determine the C-LUF (the lowest frequency at which σ meets the requirement).

The setup for making the validation procedure of a conventional RC is shown in Fig. 2-16. The “working volume” (dotted lines) is the volume of space in the chamber, which is suitable for achieving uniform fields for the purpose of an emission measurement. In other words, (from an extract taken from [9] page 24) the validation procedure is “to verify that the same magnitude, within a defined uncertainty interval, occurs for all polarisations and for all directions of arrival at all locations within the working volume, for a given number of stirrer steps.”

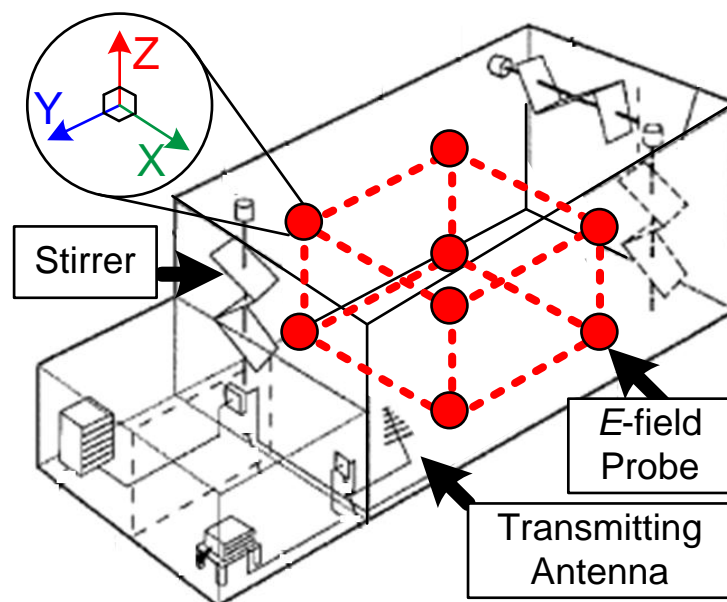


Figure 2-16: A conventional reverberation chamber’s working volume validated by 8 probes placed at the corners (with 3 polarisations measured at each corner).

The conventional procedure for field uniformity validation is summarised in Appendix F of this thesis. An example of the STD result is shown in Fig. 2-17, which shows that the C-LUF of the chamber is approximately at 120 MHz. Above the C-LUF, the field is sufficiently uniform (i.e. STD is below the limit proposed by the standard) for the chamber to be usable for making emission measurements.

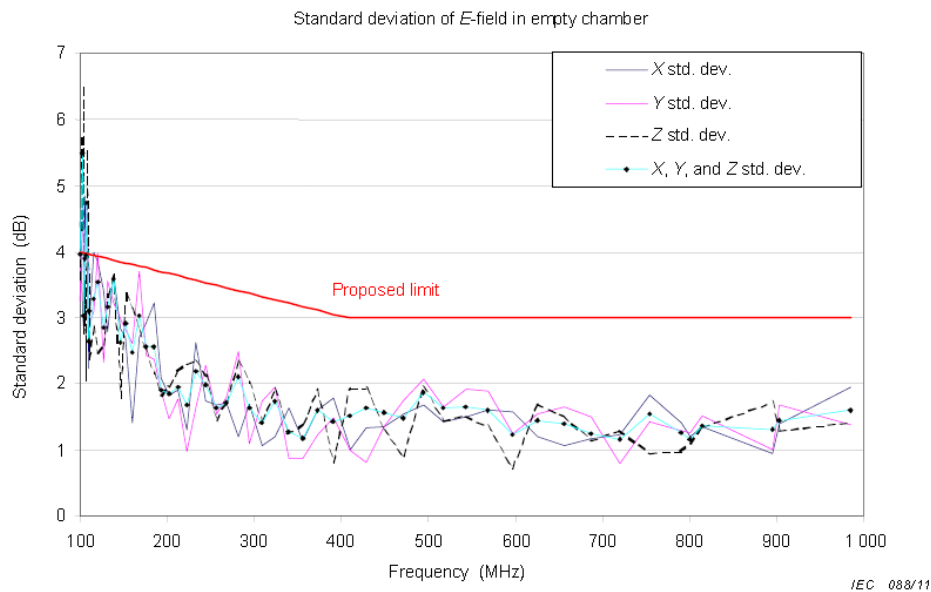


Figure 2-17: An example of Standard Deviation of data for E -field components of 8 probes, from [9], chamber dimensions are 3 m \times 7 m \times 15 m.

Emission measurements: When the chamber passes the validation procedure, the EUT can be placed in the working volume. Then, measurements can be done over one revolution of the stirrer. After that, the mean value of the received antenna signals will be the output of the measurement. However, the mean value is still not the radiated power of the EUT, as the presence of the antenna, wall, and the EUT in the chamber degrades the Q_g and also the field uniformity (see Eq. 2.50). Thus, the Chamber Validation Factor (CVF) must be determined before making emission measurements.

Chamber Validation Factor: (CVF): this is a compensation for all power losses; in fact, the CVF is just a “ratio” to convert the measured result to the radiated power. The CVF is applied to the normalised average received power over one stirrer rotation with the EUT and supporting equipment present. The CVF for each frequency can be calculated using a validation procedure. For a conventional RC validation procedure, the CVF should be measured before “each” emission measurement, while the field uniformity can be confirmed only with one measurement in an empty chamber. The setup to calculate the CVF is as shown in Fig. 2-18.

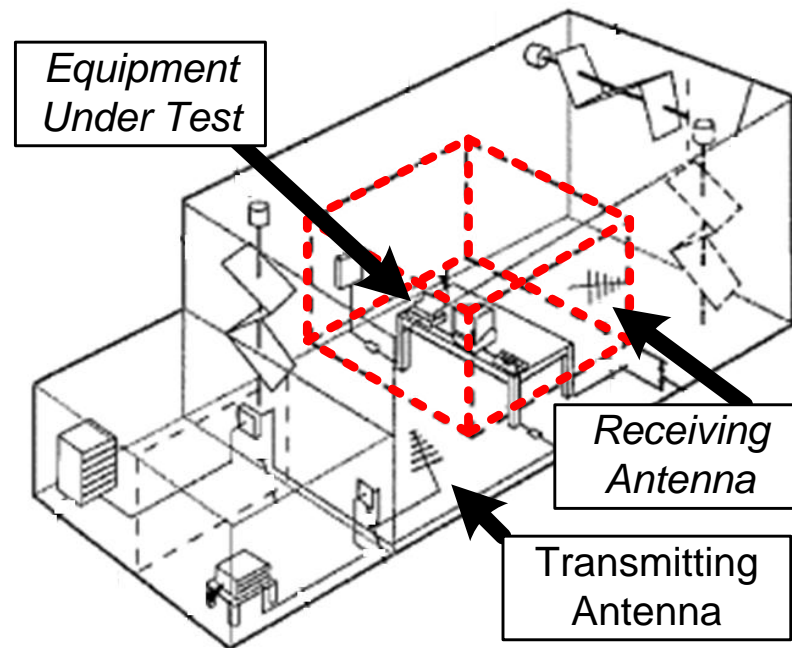


Figure 2-18: IEC Standard: setup for measuring Chamber Validation Factor.

- 1) Place the EUT and supporting equipment within the chamber working volume.
- 2) Place the receiving antenna (Rx) at a location within the working volume (being careful to place the Rx antenna at the required distance from the EUT).
- 3) Beginning at the lowest test frequency, adjust the RF source level to inject an appropriate input power, P_{input} , into the transmitting antenna (Tx).
- 4) Operate the chamber and the stirrer, taking into account the possible addition of criteria defined in the Field Uniformity Validation, that are required to meet the homogeneity criterion.
- 5) Record the maximum amplitude and average amplitude of the received power (P_{MaxRec} , P_{AveRec}), and the input power, P_{Input} .
- 6) Repeat the above procedure for each frequency in the FRI.
- 7) Calculate the Chamber Validation Factor (CVF) for each frequency using the following equation:

$$CVF = \left\langle \frac{P_{AveRec}}{P_{Input}} \right\rangle_n, \quad (2.49)$$

where

- CVF is the normalised average received power over one stirrer rotation with the EUT and supporting equipment present,
- P_{AveRec} is the average received power over one stirrer rotation,
- P_{Input} is the forward transmitted power over one stirrer rotation, and
- n is the number of antenna locations. Only one location is required; however, multiple locations may be evaluated and the data averaged over the number of locations.

Total Radiated Power: the received signals over one stirrer revolution are analysed after an emission measurement is made, but neither the mean nor the maximum of those received signals is the total radiated power from the EUT. The total radiated power of the EUT can be calculated from:

$$P_{Radiated} = \frac{P_{AveRec} \times \eta_{Tx}}{CVF}, \quad (2.50)$$

where

- $P_{Radiated}$ is the radiated power (in W) from the device within the measurement BW,
- CVF is the Chamber Validation Factor (Eq. 2.49),
- P_{AveRec} is the received power (in W) as measured by the reference antenna averaged over the number of stirrer steps, and
- η_{Tx} is the antenna efficiency factor (dimensionless) for the Tx antenna used in validating the chamber, and can be assumed to be 0.75 for a log periodic antenna and 0.9 for a horn antenna.

Instead of P_{AveRec} , the maximum received power over one stirrer revolution can be recorded and be used to determine $P_{Radiated}$ [9]. Although it is not stated in this Chapter, this is demonstrated in Chapter 5.

In conclusion, characteristics of a conventional RC are: 1) Rayleigh environment, and 2) flexible placement of the EUT due to field uniformity. To use a RC well below its C-LUF, the validation and operation methodology has to be changed.

2.4. New Ideas in this Research

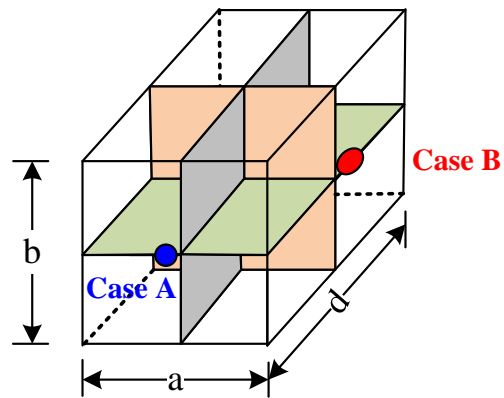
The aim of this thesis is to make radiated emission measurements with the RC at frequencies below the C-LUF; from the C-LUF down to at least the first (lowest) chamber resonance frequency (i.e. to cover the “transition region”). The idea is as simple as to excite more resonances in this region and to design a better stirrer, but this is not possible in practice. The fact is that, following the conventional RC procedures (Sect. 2.3), the number of resonance frequencies over one revolution of the stirrer would never cover the complete transition region, and the field uniformity in the WV would never meet the requirement (i.e. the proposed limit in Fig. 2-17), as it may not follow a Rayleigh distribution. In other words, the radiated signals for the 3 polarisations are different from one another; i.e., one polarised signal dominates the other field components. These are fundamental problems, which necessarily occur in field distributions at low mode density. The reasons are too few resonance frequencies, and too poor a performance of the Z stirrer (or a stirrer with a similar to Z shape) to shift the initial resonance frequencies to cover the transition region. Following procedures from the standards fails to reduce the C-LUF significantly.

The best approach is to excite more/all resonances below the C-LUF, and perturb them by the stirrer to cover the transition region; i.e., moving the receiving antennas and the EUT to excite more resonances could allow the RC to be usable below the C-LUF. In other words, lower measurement precision (i.e. field uncertainty) and a sacrifice in measurement time cannot be avoided.

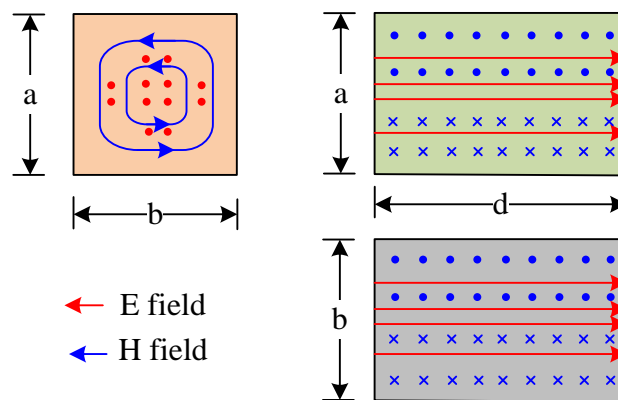
2.4.1. Theories Supporting the Methodology

Moving position of antenna: From Sect. 2.3.1, it can be interpreted that a fixed position of Tx cannot excite all modes in the cavity. When carefully choosing different antenna positions, different modes, which happen to exist at different frequencies, are excited. To investigate the theory, simulation modelling is used (detailed in Chapter 3). Figure 2-19 shows the dimensions of the model, $a, b = 0.48$ m, and $d = 0.72$ m. Two cases of exciting positions are shown in Fig. 2-19 (a). According to Eqs. 2.26-2.37, the dominant mode of case A is $TM_{110} = 441$ MHz, as shown in Fig. 2-19 (b), while the dominant mode of case B is TE_{101} or TE_{011} (371 MHz) as in Fig. 2-19 (c). It must be noted that resonant frequencies of TE_{101} and

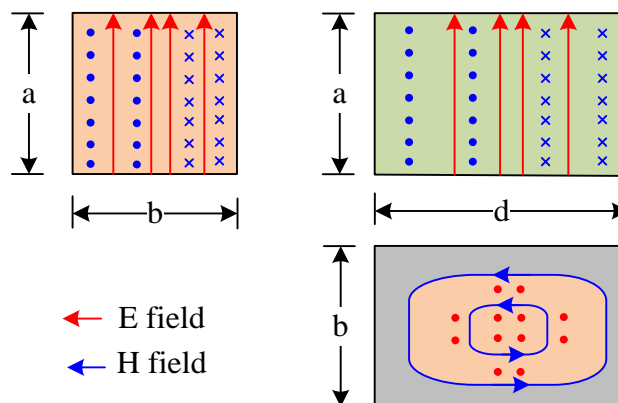
TE_{011} are similar as this model is a symmetrical cavity; however, their field distributions are different depending on feeding plane.



a) Two cases of feeding positions.



b) Case A: TM_{110} is the dominant mode.



c) Case B: TE_{101} or TE_{011} are dominant modes (this is a symmetrical cavity, $a=b$).

Figure 2-19: Field distributions at dominant modes related to the excitation position.

From the simulation modelling in Fig. 2-19, Reflection Coefficients (S_{11}) of the dominant modes can be calculated, and are shown in Fig. 2-20.

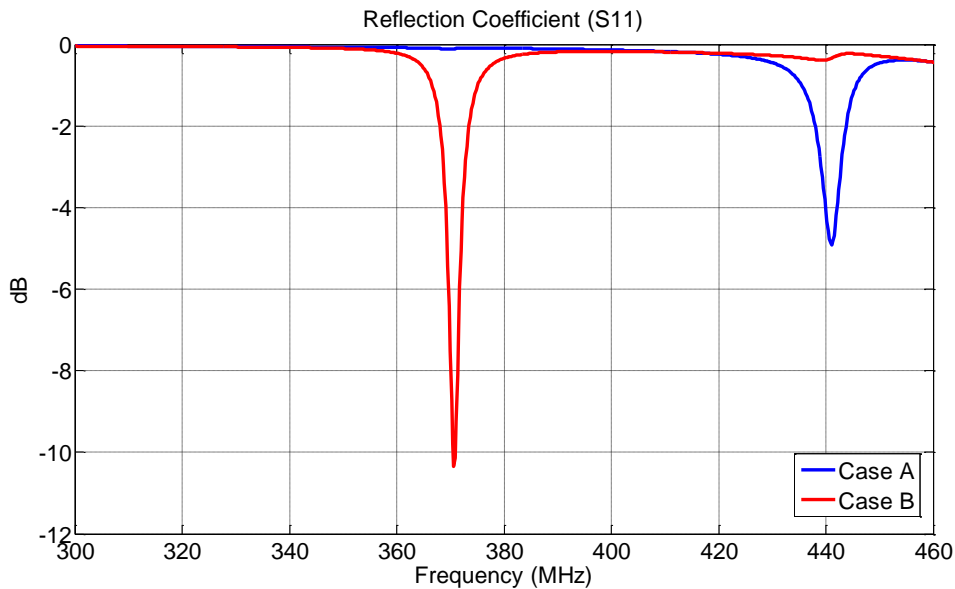


Figure 2-20: (Simulated) Reflection Coefficient (S_{11}) of 2 excitation cases from Fig. 2-19.

The 3-D plots in Figs. 2-21 and 2-22 show clearly that the resonance regions of the 2 cases are different; the resonant region excited in case A does not include the feeding position of case B (Fig. 2-22). Note: to avoid confusion, the E-field is chosen to be the reference (same as in the conventional RC method). Figure 2-21 shows that the E-field of case A has only a Z-component; i.e., E-field = 0 for the 4 wall surfaces: $y = 0, b$ and $x = 0, a$. The maximum of the E-field occurs at the centre of the 2 wall planes $Z = 0, d$. Case B, in contrast, can be explained in the same way as case A, but with the resonance region oriented along a different axis (X). It is obvious from Figs. 2-20 through 2-22 that: (a) the dominant mode excited in case A is at 441 MHz (the mode at 371 MHz is not excited), (b) the dominant mode in case B is at 371 MHz (the mode at 441 MHz is not excited). Thus, with a single transmitting antenna, not all resonant modes can be excited. It can be concluded that “changing the excitation position is required in order to excite all resonant modes.”

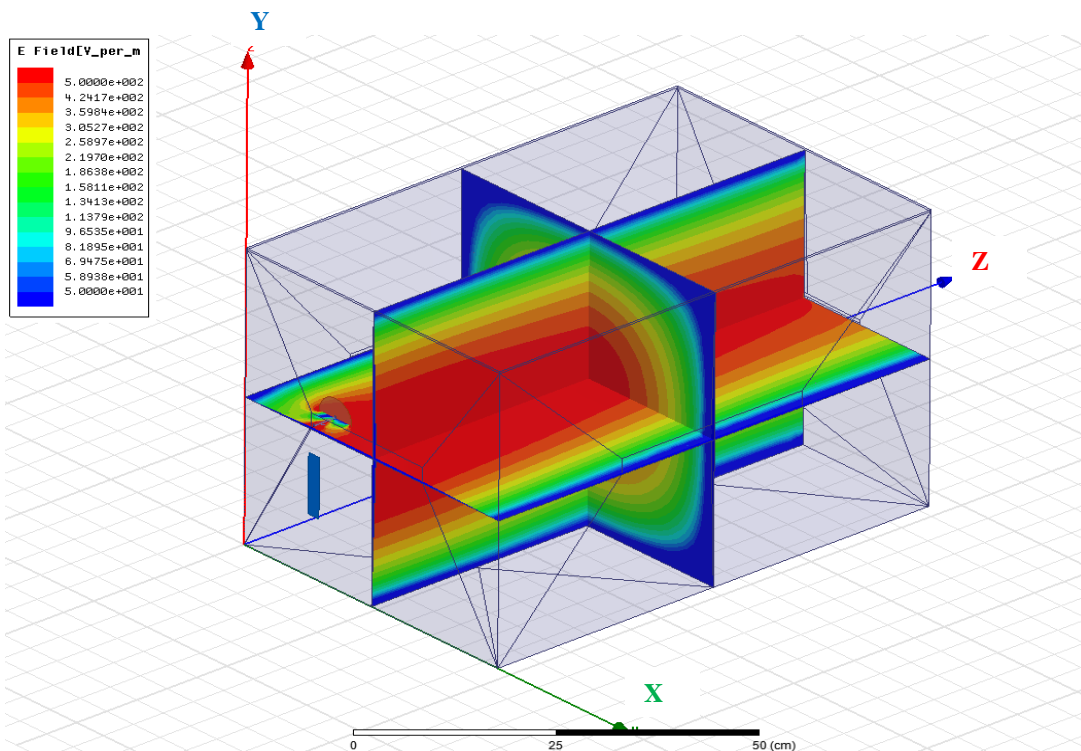


Figure 2-21: E -field at TM_{110} , 441 MHz. E -field has only a Z component when the position of excitation is as in case A (Fig. 2-19).

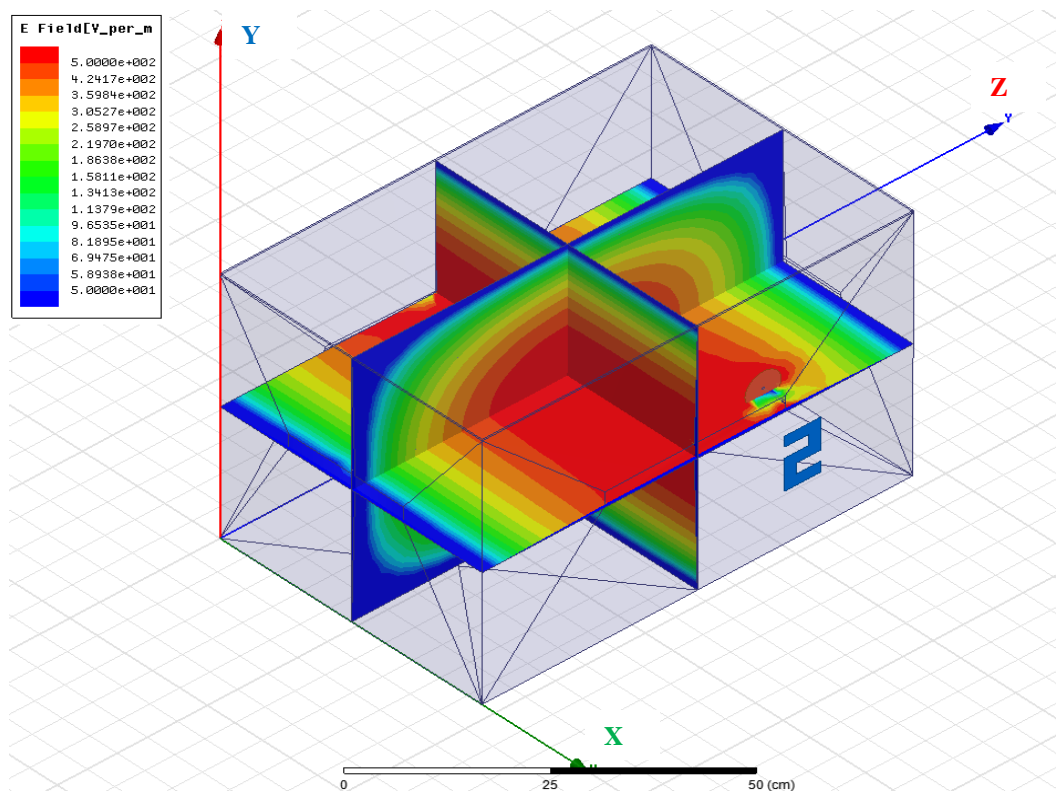


Figure 2-22: E -field at TE_{101} or TE_{011} , 371 MHz. E -field has only a Y component when the position of excitation is as in case B (Fig. 2-19).

Performance of Z stirrer: a Z-shaped stirrer is applied to case A to investigate the field distribution. Figure 2-23 shows that the Z-stirrer can perform well at high frequencies, 1,457 MHz (predicted C-LUF) in this case. *E*-fields cover all the areas well in response to revolution of Z stirrer. In contrast, at low frequencies, the performance of the Z stirrer is poor, as shown in Fig. 2-24. It is obvious that, over one revolution of the Z stirrer, the resonance (441 MHz) can be stirred only in between 405 MHz to 436 MHz; i.e., approximately 7%. Moreover, Fig. 2-25 shows that *E*-fields do not cover all the areas over revolution of Z stirrer. This is because the structure of the Z stirrer has not been designed to use below the C-LUF. It should be noted that field distribution at 405 MHz in Fig. 2-25 (1) looks similar to TM_{110} (Fig. 2-21), while field distribution at 436 MHz in Fig. 2-25 (4) looks similar to TE_{101} (Fig. 2-25). More plots and analysis are provided in Sect. 3.2.2.

To alter the field distributions and shift resonance frequencies below the C-LUF, a new design of stirrer is therefore required. The new stirrer must be able to stir field distributions and amplitudes of all resonances below the C-LUF (i.e. in the transition region).

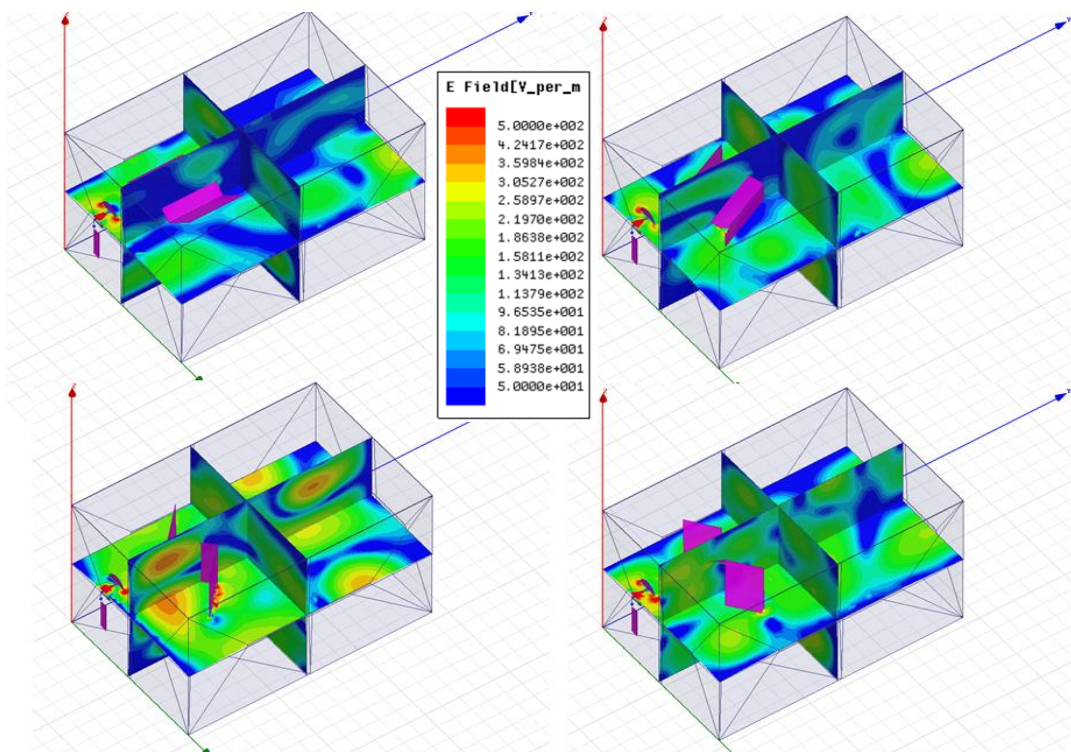


Figure 2-23: *E*-field at 1,457 MHz, case A (Fig. 2-19).

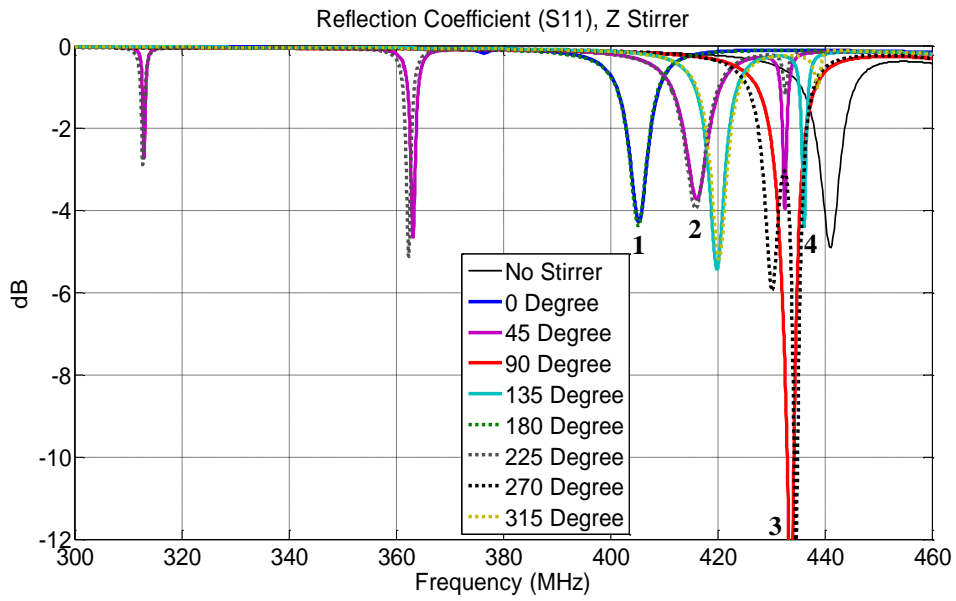


Figure 2-24: Poor S_{11} performance of Z-stirrer at dominant mode: case A (Fig. 2-19).

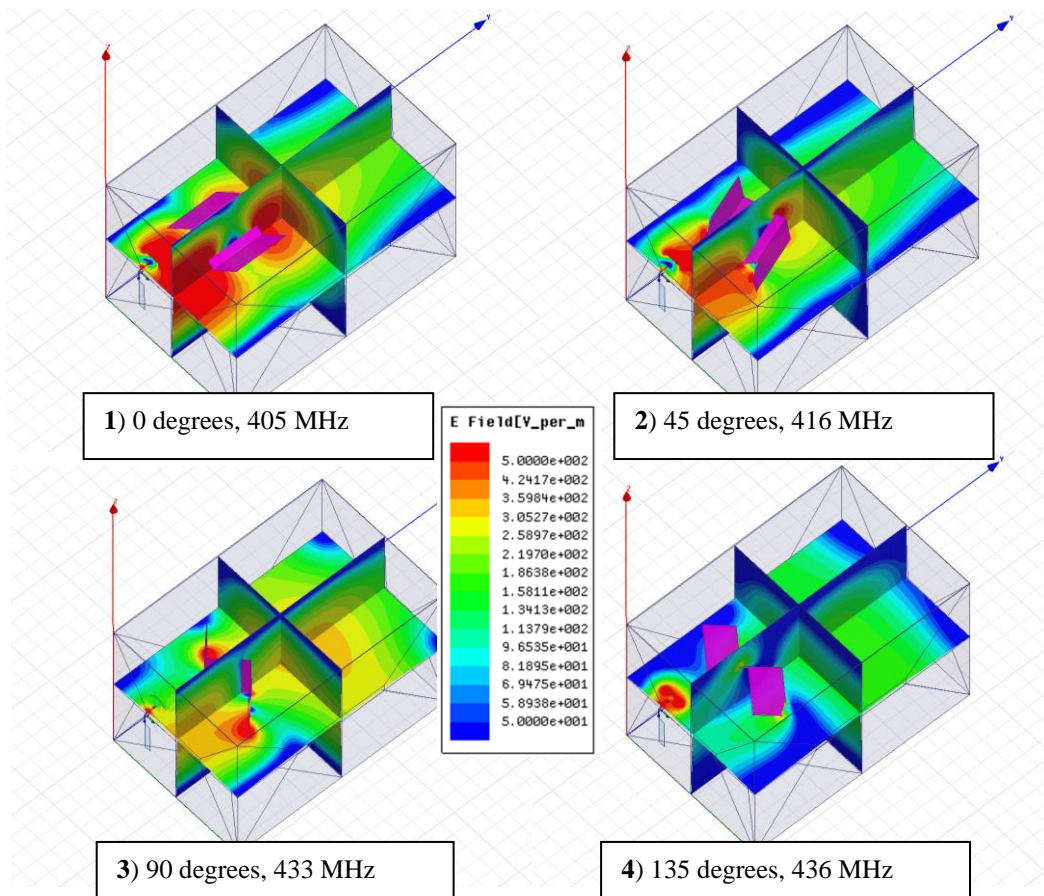


Figure 2-25: E -field of S_{11} , case A, as marked in Fig. 2-19.

Effect of Moving the EUT: when the field is uniform (above the C-LUF), the EUT can be placed anywhere in the working volume. On the other hand, when the field is not uniform, different measured results are expected from the placement of the EUT at different positions. This can be confirmed by a simulation modelling (explained in Chapter 3). An EUT, a monopole antenna, placed on top of a rectangular box, is modeled; the monopole antenna is fed by 1-Watt input power from inside the cavity. Then, the EUT is placed to investigate the effect of moving the EUT position. The EUT is placed at N1 and N2, as in Fig. 2-26, and the simulated results for one stirrer revolution are shown in Fig. 2-27. These results show that different resonances are excited when the EUT is moved. Therefore, there is a possibility to stir resonances, below the C-LUF, by moving the EUT. Shortcoming when operating as conventional RC, but can be used to excite more modes.

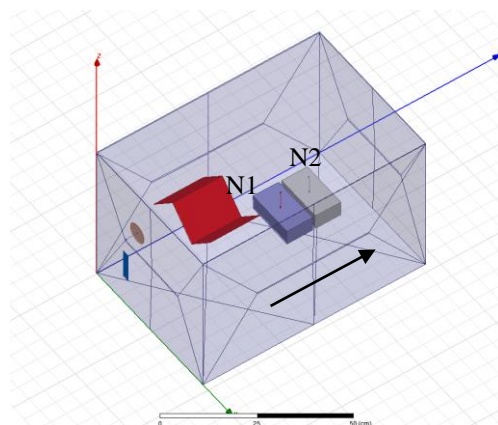


Figure 2-26: An EUT placed in the model, and moved.

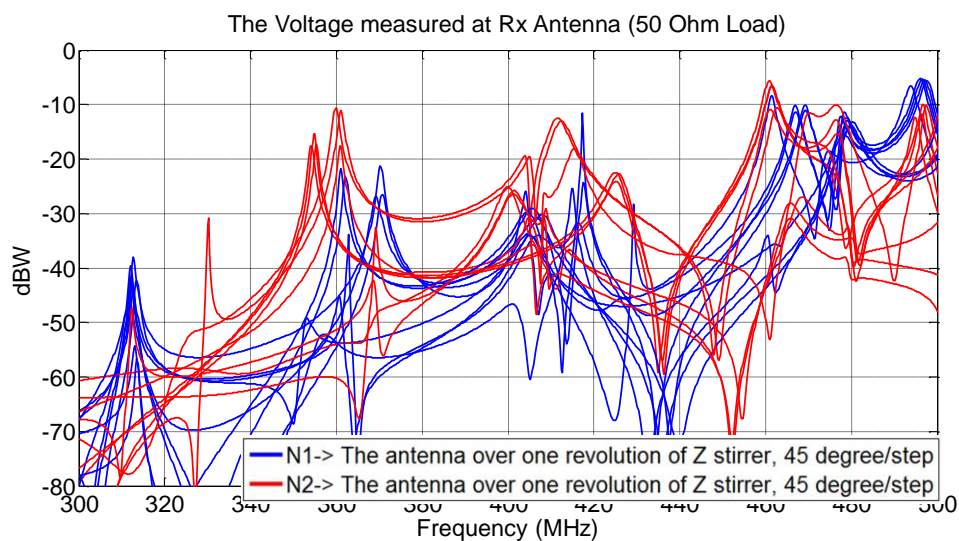


Figure 2-27: Simulated S_{21} over one revolution of Z-stirrer after a “1 W” EUT is placed, comparison for two positions of EUT.

Effect of Composite Q factor (Q_g): From Eq. 2.47, at low frequencies, the Q_g of a cavity is low, resulting in low sensitivity for making emission measurements below the C-LUF (Fig. 2-27). In addition, Eq. 2.48 tells that using multiple antennas can further decrease the Q_g as shown in Eq. 2.51:

$$\frac{1}{Q_g} = \frac{1}{Q_1} + \frac{1}{Q_2} + \frac{1}{Q_3}, \quad \frac{1}{Q_2} = \frac{1}{Q_{Ant1}} + \frac{1}{Q_{Ant2}} + \frac{1}{Q_{Ant3}} + \dots \dots, \quad (2.51)$$

where Q_g is the composite Q factor; Q_1 is coefficient for the walls; Q_2 is the coefficient for the receiving antenna; Q_3 is coefficient for the EUT.

Eq. 2.51 demonstrates that Q_g can be lower when more antennas are installed in the chamber. Thus, a solution to avoid decreasing the Q_g is required, after installation of multiple receiving antennas, in order to increase the sensitivity of emission measurements.

2.4.2. Summary of New Ideas in this Research

Below the C-LUF, more resonance frequencies can be excited by moving the antenna and EUT. Figs. 2-19 and 2-20 show that different antenna positions can excite different modes. More resonance frequencies can also be excited when the EUT is moved. In other words, when more resonances are excited and a new (better) design of stirrer is made, field uniformity can be expected to be better than that for the conventional method. However, the technique of placing multiple Rx antennas, and moving the EUT (this is called Multiple-Input Multiple-Output, MIMO technique), makes the usage of the RC no longer conforming to a conventional RC method. In this scenario, the modified RC is called a MIMO RC.

In order to make the RC work in the transition region (i.e., below the C-LUF), this thesis will adopt a MIMO technique on a conventional RC. There are quite a number of things found and explained in Chapter 3; a list of these is summarised, with short explanations, as follows:

- 1) Moving positions of Antennas (Multiple Outputs: MO): As a fixed position of a receiving antenna cannot achieve the required field uniformity, moving the position of the receiving antenna should be able to increase the field

uniformity. In practice, moving the receiving antenna position is equivalent to using multiple antennas simultaneously. Chapter 4 shows that using 9 receiving antennas, with three measured polarisations, can increase the field uniformity in the transition region. This strategy makes a RC become a Single-Input Multiple-Output (SIMO) RC.

- 2) Moving position of EUT (Multiple Inputs: MI): the EUT is moved inside the working volume. This is necessary as the field uniformity of a SIMO RC at some frequencies is still poor; changing the EUT position should increase the chance of smoothing the measured result. A microwave oven is an example of moving the EUT to smooth the field (and the results) on the food, when the stirrer cannot by itself achieve enough field uniformity. Fig. 2-28 shows that the food will not be evenly cooked without using the turntable. As a result, a SIMO RC becomes a MIMO RC; Chapter 5 will explain how moving the EUT in a pattern of 9 positions will adequately smooth the measured results for making MIMO emission measurements.

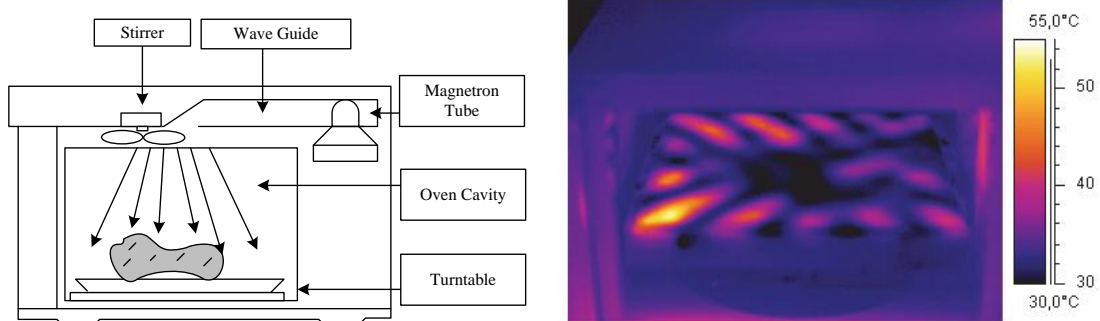


Figure 2-28: Microwave oven, an example of moving the EUT (using infrared thermal imaging inside a microwave oven [89]).

- 3) Designing a stirrer for use in the transition region: due to poor performance of the Z-stirrer below the C-LUF, this thesis introduces the use of the double C stirrer. The double C stirrer can perform very well in the transition region. Chapter 3 shows that the double C stirrer can shift the 1st resonance frequency (both in frequency and amplitude) up to 10.95%.
- 4) New procedure using MIMO validation: Implementation of MI, MO and of the double C stirrer transforms a conventional RC into a MIMO RC. The new validation procedure is called a MIMO validation procedure, which, however,

has much more measured data compared to that from a conventional validation procedure; i.e., the MIMO validation procedure for a MIMO RC gives 216 sets (8 corners \times 3 polarisations \times 9 antennas) of SISO data, while only 24 sets of SISO data (8 corners \times 3 polarisations \times 1 antenna) are collected from a conventional validation procedure. A new method is required to process the measured results (as explained in Chapter 4).

- 5) New procedure of MIMO emission measurement: In a MIMO RC, when the EUT is moved along 9 positions, MIMO emission measurements will provide 81 sets of SISO data (9 positions of EUT \times 9 antennas), which is 81 times more than that from a conventional RC. A new procedure is required to process the measured data to determine the correct result (as explained in Chapter 5).
- 6) Programming under concept of “save, load, and analyse” for MIMO RC: While a typical RC can give the final result after making an emission measurement, MIMO RC might not be able to do the same, as moving the EUT is required. All the measured data must be saved for later analysis. In this thesis, a MATLAB protocol is chosen for saving all the measured data, and for making the measurement system work in an automated manner. Appendix B shows the flowcharts used for obtaining and saving all the data, and Appendix C shows programming (GUI) flowcharts for post-processing all those collected data.
- 7) Maximise Composite Q factor (Q_g): Using MIMO RC at low frequencies leads to lower sensitivity, as the Q_g decreases after installation of multiple antennas. Chapter 3 proposes the use of reflective switch as to avoid significantly decreasing the Q_g at low frequencies (below the C-LUF).

2.5. Chapter Summary

Electromagnetic Compatibility (EMC) has been known for more than 100 years (Sect. 2.1); EMC, from the author's point of view is "to confirm that the EUT is good enough for doing its job under an assigned circumstance". "Good" means at least as good as the limit assigned from a chosen standard reference, which can be at the local or international level, and "to confirm" can be done by choosing at least 1 environment/method of EMC testing.

EMC has 2 applications: Immunity Tests, and Emissions Measurements. The application of Radiated Emission Measurement testing is more important for Radio Astronomy (RA), as the sites are typically located in isolated areas; noise levels for equipment at the Murchison Radioastronomy Observatory (MRO) requires sensitive methods up to 80 dB more than the usual EMC requirements. In Section 2.2, for making radiated emission measurements for equipment at the MRO, the Reverberation Chamber (RC) [9, 14] method is chosen due to its sensitivity. Besides, the cost per square metre of a RC can be considered cheap comparing to Anechoic Chamber (AC).

From background knowledge of RCs (Sect. 2.3), a mode-tuned operation has been selected for application to radiated emission measurements. Mode-tuned operation is more suitable for the requirements of this thesis, especially for doing validations.

A RC must pass a validation procedure before it is used for making emission measurements. Procedures for conventional RCs are summarised in Fig. 2-29. However, these procedures limit the usability of a RC, as they determine the limitation of the Conventional LUF, C-LUF. Conventional RCs can be used only above the C-LUF, where the field becomes sufficiently uniform. The C-LUF is usually 3 to 6 times above the first chamber resonance. The "field is uniform" means a fixed-position antenna can measure the signals coming from every direction at the same time (i.e. it is in a Rayleigh field environment). It can be concluded that conventional procedures use a fixed-position receiving antenna to achieve the requirement of field uniformity for all points in the working volume. In other words, the conventional procedures aim to allow the flexible placement of the EUT in the working volume. Following these procedures, the EUT can be placed anywhere in the working volume, but with a sacrifice of the usability of the RC below the C-LUF.

In contrast, using multiple receiving antennas and moving the EUT (as shown in Sect. 2.4), excite more resonances, and increase the field uniformity below the C-LUF. Each receiving antenna added in the RC can increase the chance of better field uniformity, as well as allow for moving the EUT among more positions. This modified method is called the “Multiple-Input Multiple-Output Reverberation Chamber, MIMO RC”. Procedures for MIMO RCs are summarised and compared to those of conventional RCs in Figure 2-29. Details will be in the following Chapters.

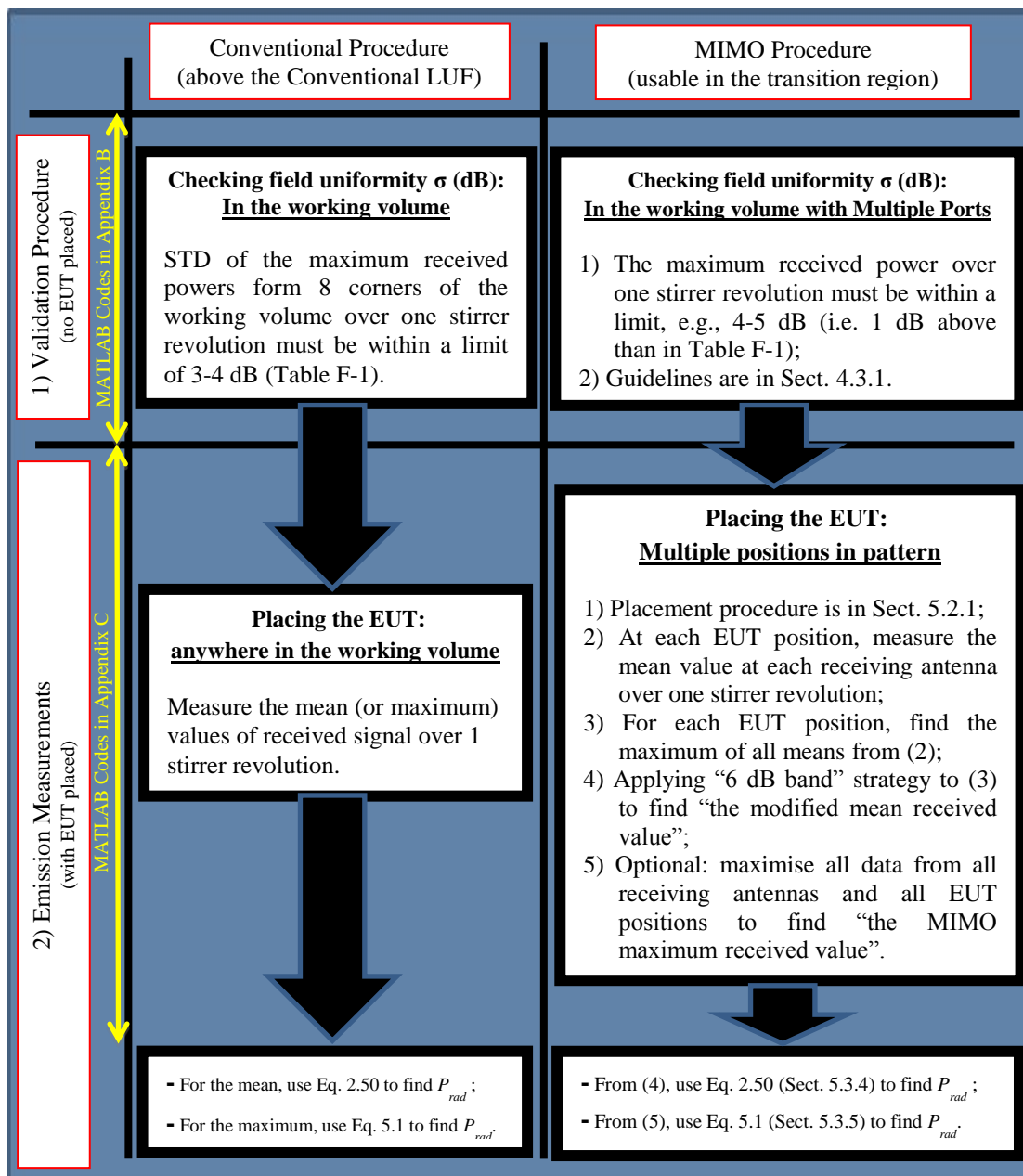


Figure 2-29: Summary of all procedures for a “conventional” RC and MIMO RC to make radiated emission measurements (above the conventional LUF).

CHAPTER 3

MIMO REVERBERATION CHAMBER: DESIGNS AND APPLIED IMPLEMENTATIONS

“Reverberation chambers are best suited for measurements that do not require directional information about the signal source. Measurement results are statistical rather than deterministic. The chamber’s interior dimensions will determine the lowest attainable frequency and the largest allowable EUT size.”

- ETS-LINDGREN, (2013)

The purpose of emission measurements in a RC is to obtain a predictable correlation between radiated power of EUT and received signal over one revolution of stirrer. High mode density and at least one resonance are required for accuracy and sensitivity. Following the procedures given in the standards [9], conventional RCs become unusable in the transition region (i.e., from the 1st resonance to the 60th mode, the conventional LUF, C-LUF). Optimisation of essential components of a RC, such as stirrer geometry or chamber shape, can reduce the C-LUF only marginally. For using a RC well below the C-LUF, it is necessary to understand the principal behaviour of the field distribution and modify the mode of operation. The problematical issues that limit conventional RCs from being used in the transition region are:

- 1) Field distribution: there are too few resonances to generate a statistically uniform and isotropic field;
- 2) Z-stirrer: this well-known stirrer has poor performance below the C-LUF;
- 3) Composite Q -factor (Q_g): at lower frequencies, Q_g decreases (the RC method requires high Q_g to make more sensitive measurements).

To solve these problems, a Multiple-Input Multiple-Output (MIMO) RC is designed, and expected to extend the usable frequencies of the RC down to its first resonance. In practice, a MIMO RC requires multiple receiving antennas, a new design of the stirrer, a solution for the Q_g , and moving the EUT to excite more resonances in the transition region. Implementations and designs of MIMO RCs are demonstrated in this Chapter, by the end of which all the necessary tools will have been described for the simulations and measurements of the following Chapters. From this point onwards, this research will not follow any of the conventional RC standards/procedures.

3.1 Novel Designs and Implementations

Future EMI measurements for MRO equipment are planned in the shielded room (Fig. 3-1) at ICRAR/CIRA, Curtin University, Western Australia. The 1st resonance of the shielded room is at 70 MHz, and the C-LUF is about 300 MHz, while the RA requirement at MRO is from as low a frequency as 50 MHz; the room is too small. This situation is an ideal opportunity for testing the concept of MIMO RC. After applying MIMO RC concept, the shielded room can be expected to work in the transition region, i.e. from 70 MHz (henceforth known as the MIMO-LUF) to the C-LUF, and above as in a conventional RC.



Figure 3-1: CIRA shielded room (3.6 m by 2.4 m by 2.4 m), expected to be a RC.

A scaled model of the shielded room has been made, and analysed as a prototype of a MIMO RC to investigate its feasibility to be used below the C-LUF, as stated in the objectives; then, designed procedures and developed tools found on the scaled model can be adopted for the shielded room, or used as guidelines for other MIMO RCs.

3.1.1. Conceptual Designs

What is a MIMO communication channel? Basically, there are 4 types of communication channels, as shown in Fig. 3-2. The simplest is a Single-Input Single-Output (SISO) communication channel; however, the performance of the data link can be improved if several antennas are available at both ends, and the pair with the lowest path loss is selected/switched to. The use of multiple antennas at both ends is named a Multiple-Input Multiple-Output (MIMO) communication link [106].

To Implement a MIMO communication channel in a RC: a conventional RC can be considered as a SISO communication channel, as there are only 2 fixed-position

antennas: a transmitting and a receiving antenna. From Chapter 2, it was found that different positions of antennas can excite different modes (Sect. 2.4.1); installing more than one antenna could allow more resonances to be excited (or detected), and thus increase the field uniformity in the transition region. Furthermore, if multi-position antennas cannot achieve enough field uniformity, moving the EUT could encourage this to be achieved. The idea is roughly related to the concept of MIMO communication links (Table 3-1). Although moving the EUT is not exactly as same as using Multiple-Input channels, the procedures are similar. The main difference is that conventionally in a MIMO system multiple input antennas are used simultaneously; in the MIMO RC emission measurements for various EUT positions are made consecutively, where each position represents feeding one of multiple input antennas. Thus, the modified RC is named a “MIMO RC”, for which MO (Multiple-Output) means that several receiving antennas are used to pick up the emission, and MI (Multiple-Input) is equivalent to moving the EUT during an emission measurement. However, a MIMO RC does “not” choose only the lowest path lost; instead, a MIMO RC collects all the measured data, which are processed later. A MIMO RC, in this case, requires much more time to complete measurements, than a conventional RC.

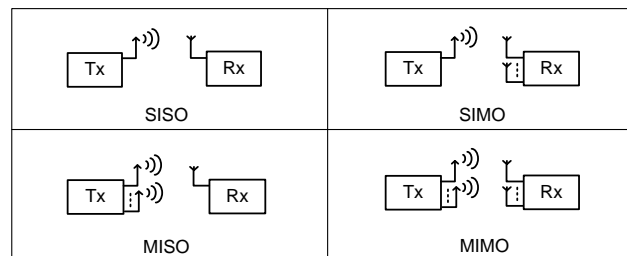


Figure 3-2: 4 types of basic communication channels.

TABLE 3-1: Implementation of SISO, MISO, SIMO, and MIMO Links.

	SISO (conventional)	MISO	SIMO	MIMO
EUT	1 position	Multiple positions	1 position	Multiple positions
Antennas	1 Antenna	1 Antenna	Multiple positions	Multiple positions

The validation procedure of a MIMO RC (i.e. without a EUT) is a SIMO communication link (Fig. 3-3). The signal directions in a SISO RC and a MIMO RC are in opposite directions, i.e., the role of Tx and Rx antennas are swapped (more details are given in Sect. 3.2.3). Measuring in opposite directions should not cause any difference, as S_{12} is equal to S_{21} (assuming reciprocity). This validation procedure

is more intuitive for emission measurements, whereas the conventional validation procedure is more compatible with immunity testing. This MIMO RC validation procedure, which uses a SIMO link, will be described in Chap. 4, and MIMO emission measurements will be demonstrated in Chap. 5.

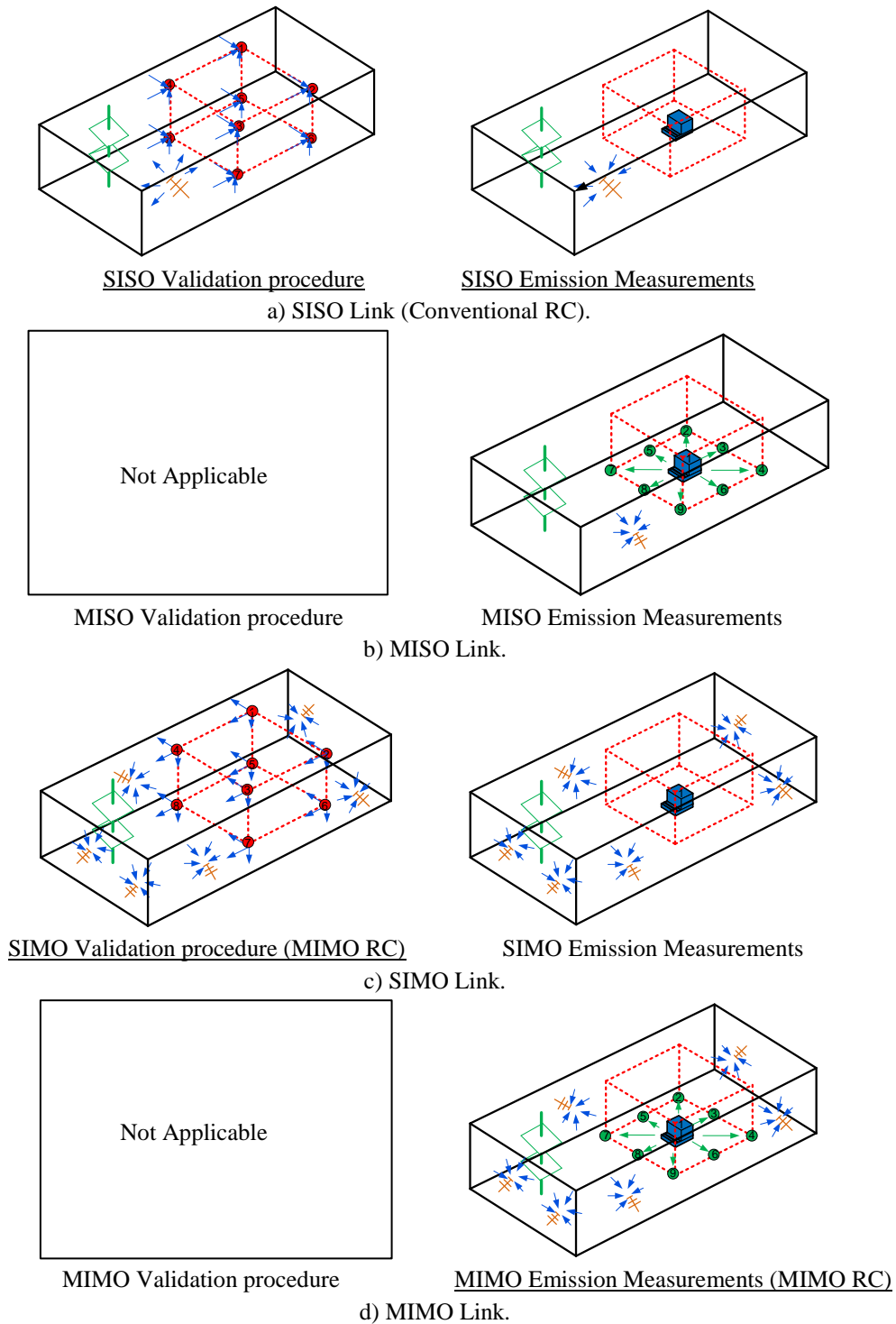


Figure 3-3: Comparison of concepts, from conventional RC to MIMO RC.

A 1:5 scaled model of the shielded room at ICRAR/CIRA was made to study the idea of using a MIMO RC to investigate the feasibility of its use below the C-LUF. Once design guidelines have been established, and analysis tools developed, solutions can be given for applying these developed techniques to the CIRA shielded room. Simulation modelling is still necessary, as this is an easier way to progress in the design: placements, positioning, investigating field distributions, and the effect of Q_g . Thus, the choice of computational electromagnetic modelling must be decided on carefully, in order to get the most reliable results.

3.1.2. Choice of Simulation Program

Computational Electromagnetic Modelling can be categorised into 4 types, as shown in Fig. 3-4: Analytical Calculation and Ray Tracing are not suitable for the analysis of a simulated model of a MIMO RC. Analytical Calculation is hardly possible, although it is useful for determining bounds on the problems (for instance, calculating reference values for an empty cavity). Ray Tracing is only suitable for high frequencies; it is not compatible with the objectives of this thesis. Thus, a decision must be made on either the Differential, or the Integral, form of Maxwell's equations; i.e., Finite-Difference Time-Domain (FDTD), Finite Element Method (FEM), or Method of Moments (MoM).

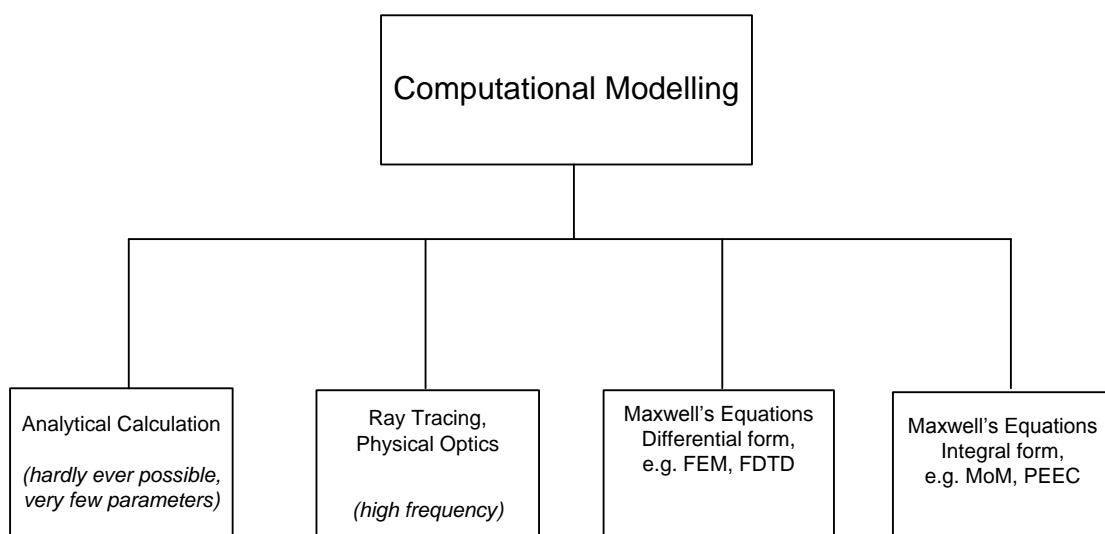


Figure 3-4: Computational Electromagnetic Modelling Methods.

Finite-Difference Time-Domain (FDTD): this is the simplest technique, and the easiest to understand. Maxwell's equations, in partial differential form, are transformed into central-difference equations, discretised, and implemented in software. The equations are solved in a cyclic manner; i.e., the electric field is solved, then the magnetic field is solved, and the process is repeated over and over again.

Finite Element Method (FEM): yields approximate solutions of partial differential equations (PDEs) which are numerically stable. The FEM can be a good choice for solving PDEs over complex domains, or when the demanded accuracy varies over the entire domain.

Both FEM and FDTD are PDE techniques; FEM is in the frequency domain, and FDTD is in the time domain. For these methods, the computation time scales proportionally with the number of unknowns because characteristics of matrix. These PDE methods use a mesh over the entire solution volume, and solve for the electric field throughout that region. For instance, for FEM, the model is run across its entire volume for each frequency of interest to show the electromagnetic fields in the region; thus, PDE methods require substantial computational power to solve problems.

Method of Moments (MoM): is a numerical computational method of solving linear PDEs which have been formulated as integral equations (IEs); i.e. in boundary integral form. However, because of these imposed boundary conditions, this technique is not useful for the complex 3D volumes of non-metallic surfaces. This method requires calculating only boundary values, rather than values distributed throughout the space. Conceptually, it works by constructing a "mesh" over the modelled surface. However, for many problems, MoM is significantly less efficient than volume-discretisation methods (e.g. FEM).

Choice of Finite Element Method (FEM): the decision was made that the FEM technique should be the best for modelling MIMO RCs, based on its expected accuracy below the C-LUF. In FEM, the model domain is bounded, and the boundary conditions are used to find the solutions for all the finite elements, which is suitable for the MIMO RC concept. The reasons are listed below:

- 1) In a RC, the standing waves (or “modes”) are spatially moved throughout the chamber volume by the mechanical stirring mechanism, which alters the boundary conditions of the system. The MIMO RC

method is mainly concerned with the transition region, where there are fewer resonances than in a conventional RC; thus, the results at/near resonances become more important. FEM could be suitable for a closed cavity problem (using a volume mesh method), as the computations can deal well with undamped systems, especially near resonances; while MoM simulation is a surface current technique, which may be unreliable near resonances;

- 2) The RC method uses a kind of low-loss cavity over revolutions of a stirrer. The chamber is equipped with some complementary objects, which are non-metallic. Thus, the FEM method, which meshes over the entire 3D model, could be more suitable to a RC, to provide accurate results such as the pattern of field distribution, and the resonance frequencies;
- 3) The simulation program must be used to design the other fittings of a MIMO RC: such as the antennas, noise sources, and stirrers. The FEM methods could provide accurate results for all of them, especially in terms of S-parameters;
- 4) According to literature reviews, it was recommended by [17, 29, 30, 33, 90, and 91] that the Differential Form could give the most accurate results for the RC method; however, this form requires a good PC, and a longer time to obtain a stable result in return. It may take several days to finish a model, if the computer is low on speed or memory.

In conclusion: both MoM and FEM/FDTD use Maxwell's equations, but in different forms. Both MoM and FEM/FDTD have their own advantages, and also some drawbacks. In 2011, there were many engineering simulation programs using MoM; for instance: [92, 93, 94]; while there were only a few with FDTD/FEM. However, in 2014, FDTD/FEM became widely used for engineering design, in the same way as MoM. It is possible that FEM/FDTD and MoM might be completely combined in the near future; for instance, a MoM-FDTD/FEM hybrid method was first introduced in June 2014 [93] with the suggestion that "*The MoM is used for the efficient modelling of open boundary radiating structures where no 3D space*

discretisation is required. The FEM is used for the efficient modelling of inhomogeneous dielectric bodies in terms of field distributions inside the volume.”

In this thesis, the ANSOFT HFSS simulation program (FEM) was chosen at the start of this research (2011), based on the reasons given above. Models of MIMO RC prototypes, the CIRA shielded room, and its 1:5 scaled model, are made with the ANSOFT HFSS simulation program, as shown in Fig. 3-5 (all details are stated in Appendix A). The ANSOFT HFSS simulation program has also been used to design all the fittings, and to gain a better understanding of the field structure, in the course of this research (some results are shown in Chapter 2).

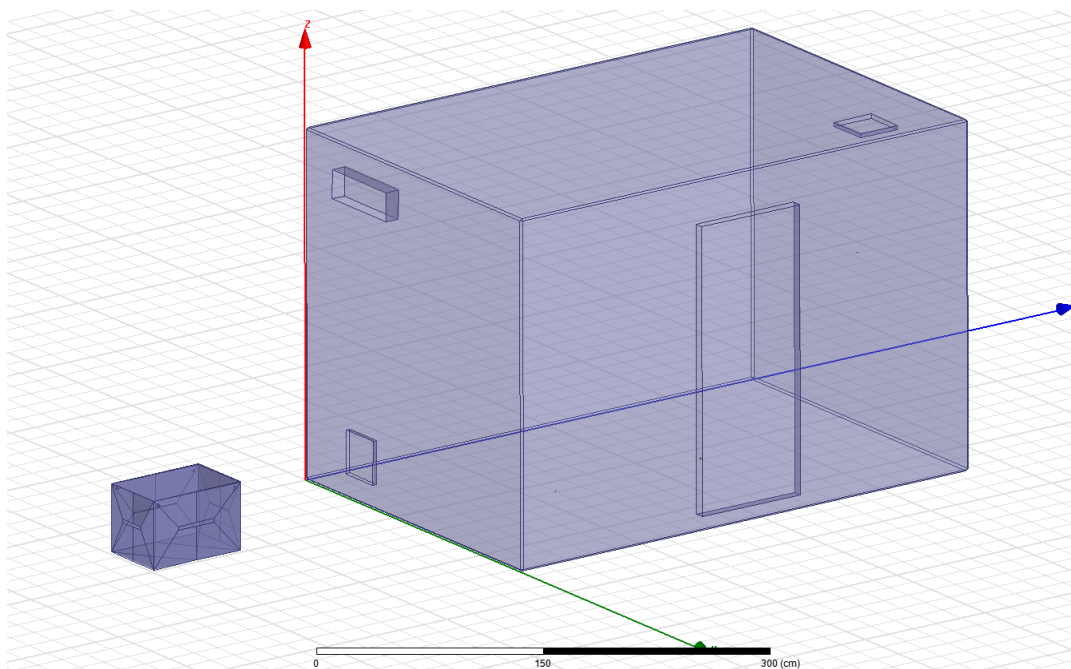


Figure 3-5: Model of the CIRA room and its scaled model (in ANSOFT HFSS).

3.1.3. Composite Q Factors (Q_g) of chambers:

Basically, the quality factor (or Q -factor) is a dimensionless parameter; it is used to characterise of a cavity's bandwidth; the Q -factor is used to quantify the ability of a chamber or cavity to store energy; this ability is determined by the losses present in the chamber. The Q -factor described in this thesis is referred to as a composite or average Q -factor (Q_g). In this thesis, investigation of Q_g can help to:

- 1) reveal the correspondence between the actual room and its scaled model; if their Q_g are related to each other by their linear scaling, all the tools developed on the scaled model can be easily transferred to the actual shielded room.
- 2) understand the behaviour of a MIMO RC below the C-LUF. The Q -factor affects the C-LUF, and the sensitivity of measurement; for example, a higher Q -factor means a lower rate of energy loss relative to the stored energy in the cavity (Eqs. 2-3, 2-46), allowing a more sensitive emission measurement to be performed in the chamber, but the C-LUF becomes higher (as there is less overlapping of modes, see Eq. 2-48).

The Q_g can be determined by both simulation (Eq. 2.48) and calculation (Eqs. 3.1 through 3.3). Investigation is made with three different materials: iron, steel and copper (see Table 3-2).

Table 3-2: Three different materials for investigations.

Material	σ = the electric conductivity	μ_r = relative permeability
Iron (99.8%)	1×10^7 S/m	4000
Iron (rusted)	1×10^6 S/m (10 times lower)	4000
Steel	1×10^6 S/m	1,10,20,50,100 ($\mu_r = 1$, for stainless steel)
Copper	5.8×10^7 S/m	0.999994

Composite Q -factors (Q_g) by Simulation: the ANSOFT HFSS simulation program has been used to find $f_{m,n,l}$ and $\Delta f_{m,n,l}$ of simulation models for both the actual shielded room, and for the 1:5 scaled model; then, Eq. 2.48 is used to determine Q_g . As expected, the simulated Q_g of the actual shielded room and its scaled model are “different” at every scaled frequency (i.e., not proportional, see Table 3-3), for all three chosen materials (at higher frequencies, there is more of a difference). For example, with steel material, the Q_g of the shielded room is 903 at 200 MHz, but the Q_g of the 1:5 scaled model is just 712 at 1,000 MHz (5 times the scaled frequency of 200 MHz of the shielded room). Thus, the simulated results show that Q_g cannot be scaled, i.e., for equivalent frequencies, the Q_g are somewhat different.

Table 3-3: Simulated Composite Q -factors.

Characteristics	1:5 Scaled Model	The Actual Room	Scale
Surface	25 times smaller	48.81m ²	1:25
Volume	125 times smaller	22.61m ³	1:125
The 1 st Resonance	375 MHz (calculated)	75 MHz (calculated)	5:1
Frequencies of Interest	300 MHz -1,000 MHz	60 MHz -200 MHz	5:1
Composite Q-factors			
IRON - Q-Factor @ start FRI	23.54	27.12	1:1.15
- Q-Factor @ end FRI	295.11	507.86	1:1.72
STEEL -Q-Factor @ start FRI	25.73	28.33	1:1.10
($\mu_r = 10$) -Q-Factor @ end FRI	712.50	903.48	1:1.26
COPPER-Q-Factor @ start FRI	26.17	28.56	1:1.09
- Q-Factor @ end FRI	955.86	1050.84	1:1.09

Composite Q -factors (Q_g) by Calculation: Q -factors are determined again from Eq. 2.51 to confirm the results from the ANSOFT HFSS simulation program (in Table 3-3). Ignoring, for now, Q_3 , Q_4 , Q_5 , ..., Eq. 2.51 becomes Eqs. 3.1 through 3.3 [10].

Composite quality factor (Q_g):

$$Q_g = \frac{Q_1 Q_2}{Q_1 + Q_2}, \quad (3.1)$$

Coefficient for the walls:

$$Q_1 = \frac{3V}{2S} \sqrt{\frac{\omega_0 \mu_0 \sigma}{2\mu_r}}, \quad (3.2)$$

Coefficient for one receiving antenna:

$$Q_2 = \frac{2}{\pi} \frac{\omega_0^3}{c^3} V, \quad (3.3)$$

where: V = Volume, S = Surface area of the cavity, σ = the electric conductivity, μ_0 = the permeability of free space, μ_r = relative magnetic permeability, and ω_0 =angular frequency.

To illustrate the analysis, the calculated Q_g of the shielded room and the 1:5 scaled model are shown in Figs. 3-6 and 3-7, respectively.

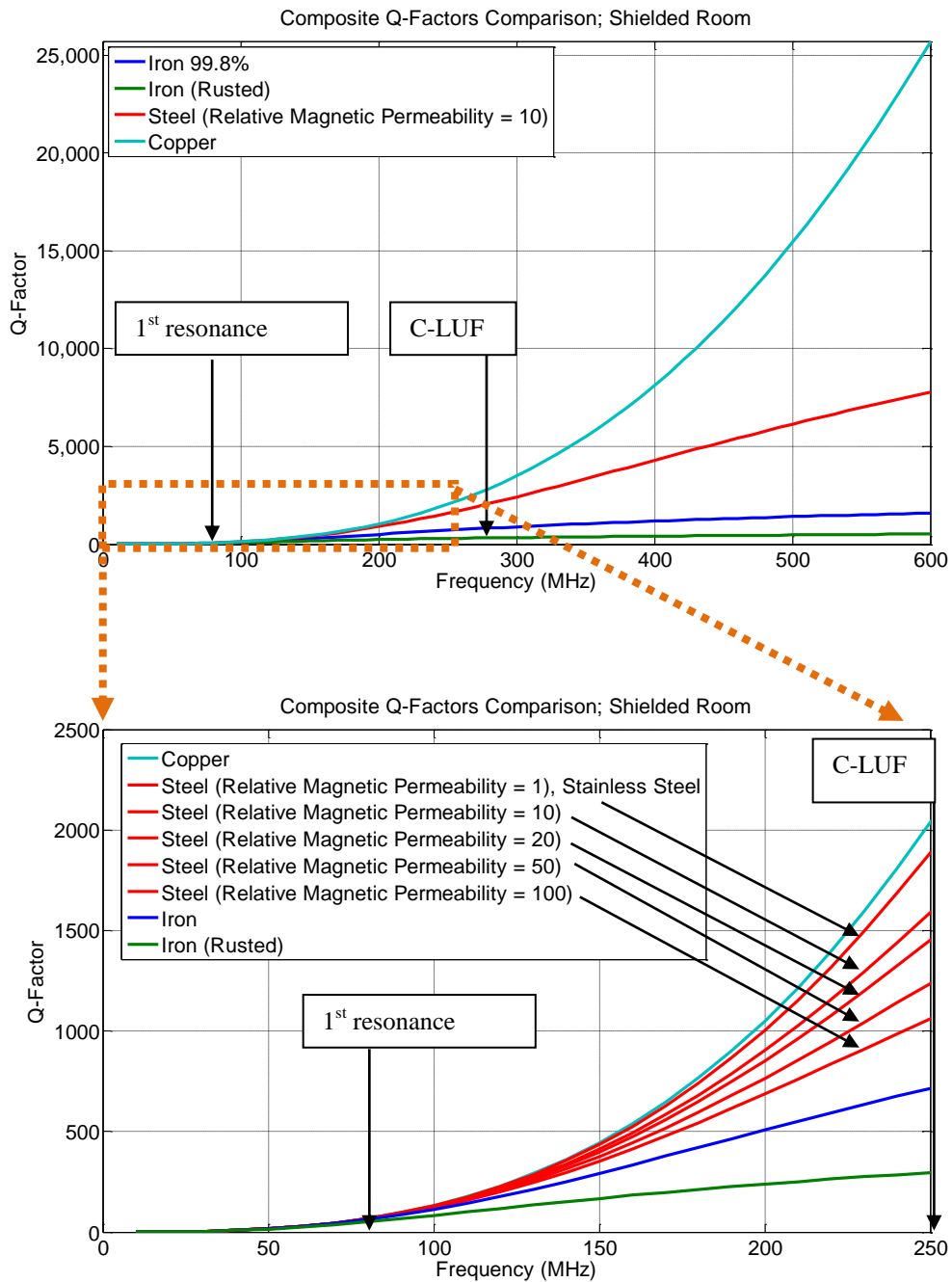


Figure 3-6: Calculated Composite Q -Factors of the Shielded Room.

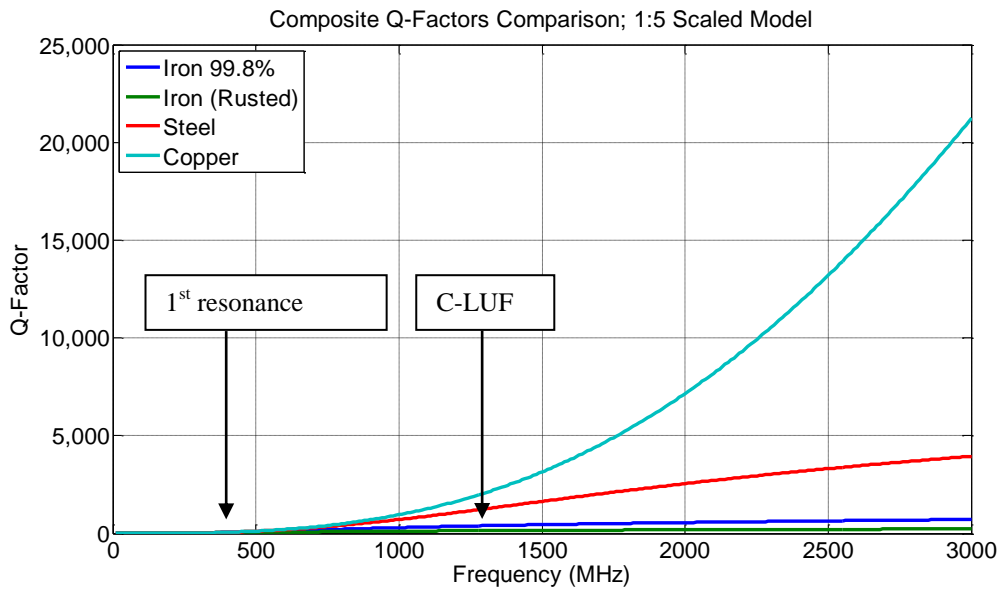


Figure 3-7: Calculated Composite Q -factors of the 1:5 Scaled Model.

Analysis of the results: Fig. 3-8 shows 3 double-plots for 3 different materials. These double plots were constructed to compare the Q_g of the scaled model (lower frequency axis, black curve) with that of the full-size shielded room (upper frequency axis, blue curve) with dimensions 5 times larger. The same modes appear at 5 times the frequency in the scaled model as in the full-size shielded room, and thus appear at the same place along the horizontal axis in Fig. 3-8. For the low order modes (at low frequencies), the Q_g is dominated by Q_2 (antennas), and is not affected by the scaling (5 times larger size results in a 125 times larger volume, but this is compensated for by the influence of ω^3 in Eq. 3.3). At higher frequencies, where the Q_g is dominated by Q_1 (walls), the scaling does affect the results. This can also be explained by Eqs 3.1 through 3.3.

The Q_1 of the enclosures are not proportional to each other. Instead, at any frequency on the frequency in Fig. 3-8, the Q_1 of the shielded room is equal to Q_1 of the 1:5 scaled model multiplied by $\sqrt{5}$. Indeed, they are non-linearly related:

$$Q_1 = \frac{3V}{2S} \sqrt{\frac{\omega_0 \mu_0 \sigma}{2\mu_r}} \rightarrow Q_1 = \frac{V}{S} \sqrt{f_0} \rightarrow Q_1 = \frac{5 \times 5 \times 5}{5 \times 5} \sqrt{\frac{1}{5}} \rightarrow Q_1 = \frac{5}{\sqrt{5}} = \sqrt{5}$$

In contrast, the Q_2 is affected neither by the electrical conductivity (σ) nor by the relative magnetic permeability (μ_r). In fact, the Q_2 is affected by the properties of the antenna (hence the ω_0^3 term) and by the total energy in the room (hence the V); so, their Q_2 -values are independent of scale (i.e. proportional to $\omega_0^3 V$ in Eq. 3.3). For instance, at any normalised frequency in Fig. 3-8, the Q_2 of the scaled model will be approximately equal to Q_2 of the shielded room.

As a result, Q_g — a combination of Q_1 and Q_2 — cannot be linearly scaled. In other words, if two enclosures are in scale, the larger room has a higher Q_g at every scaled frequency; the difference depends on the type of conducting material used. Table 3-4 shows an example of Q_1 , Q_2 and Q_g when copper is used.

Table 3-4: Calculated Q_g , for copper.

Parameter	Scaled Model @1,000 MHz	Shielded Room @200 MHz $\left[\frac{1000 \text{ MHz}}{5}\right]$	Relationship
Chamber Dimensions	0.48×0.48×0.72m	2.4×2.4×3.6m	5 times scaled
Coefficient relative to the Walls (Q_1)	64,600	144,450	$64,599 \times \sqrt{5}$ They are not proportional.
Coefficient relative to the Receiving Antenna (Q_2)	970	970	They are independent of scale.
Composite Quality Factor (Q_g from Eq. 3.1)	956	964	Q_g is result of Q_1 and Q_2 . They are not proportional to each other.

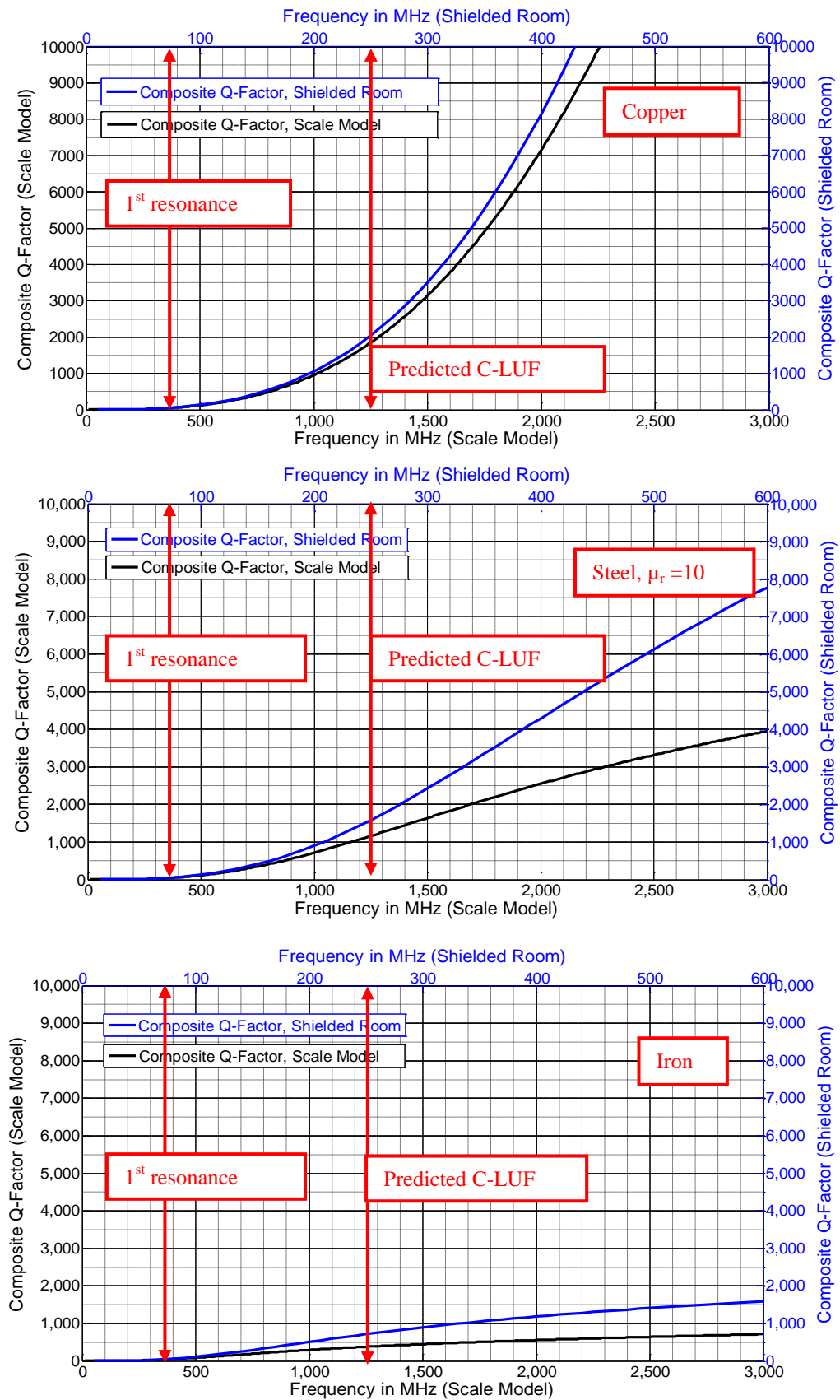


Figure 3-8: Calculated composite Q -factors.

Choice of switch box for increasing Q_g [95]: From Eqs. 3.1 through 3.3, there is a possibility to control Q_g by either changing the value of Q_1 (related to the walls) or Q_2 (related to the antennas). Q_g is dominated by Q_2 at low frequencies. The model of the prototype MIMO RC has 9 antennas installed (explained in Sect. 3.2.1); therefore, changing the value of Q_2 has even more impact than in a conventional RC. For instance, open ports can increase the Q_2 values relative to terminating them with 50 Ohm loads. This can be explained using Eq. 3.4, which is rewritten from Eq. 2.51:

$$\frac{1}{Q_g} = \frac{1}{Q_{wall}} + \frac{1}{Q_{ant1}} + \frac{1}{Q_{ant2}} + \frac{1}{Q_{ant3}} \dots + \frac{1}{Q_{ant9}} + \frac{1}{Q_{Equipment Under Test}}, \quad (3.4)$$

where Q_g is the composite Q-factor, Q_{wall} is the coefficient relative to the walls, $Q_{ant1} - Q_{ant9}$ are coefficients relative to all nine receiving antennas, and $Q_{Equipment Under Test}$ is from the EUT.

Fig. 3-9 shows the results; the composite Q -factors (Q_g) are higher when all receiving antennas (except the one used to measure S_{12}) are open; i.e., unused antennas are opened instead of being terminated with 50 Ohm loads. Therefore, reflective switch boxes are installed in the system. The reason is that the unselected ports on a reflective switch box will be “opened”, which give a higher Q_g , as compared to being terminated by 50 Ohm loads with absorptive switch boxes. As a result, a MIMO RC can make more sensitive measurements with the higher value of Q_g when the unused antenna ports are opened.

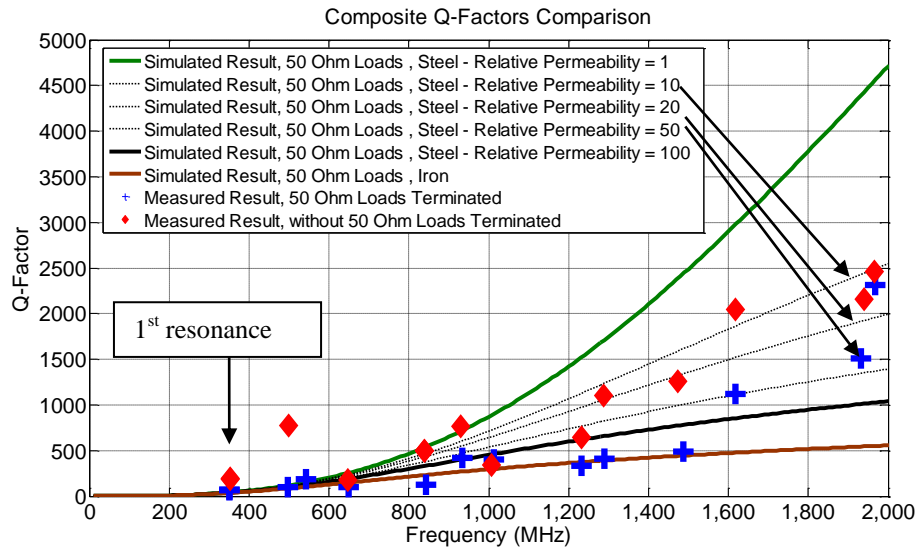


Figure 3-9: Comparison between measured and calculated Q_g , Scaled Model.

In summary, this study of the composite Q -factor (Q_g), and its comparison between the CIRA shielded room and its 1:5 scaled model, has yielded the conclusions listed below:

- 1) The double plots (Fig. 3-8) clearly show that when the physical dimensions are scaled, the Q_g of the chamber will not be linearly scaled. This is because Q_g has a contribution from the RC walls (Q_1), which cannot be linearly scaled, with the result that Q_g also cannot be scaled linearly. Moreover, effects from the relative permeability (μ_r) and conductivity (σ) of materials cannot be scaled linearly either. The calculated results for Q_g show very good agreement with the simulated ones; both demonstrate that Q_g cannot be linearly scaled;
- 2) The differences are only significant when the wall and EUT losses are dominant. At low frequencies, where the Q_g are low and therefore most critical, the antenna losses dominate, and they scale linearly with frequency;
- 3) At low frequencies, the Q_g results for the scaled model and the shielded room are almost identical. At higher frequencies the Q_g in the shielded room will be higher, thus giving more sensitivity; the effect on field uniformity may be adverse but can be expected to be not as critical as at the low end of the FRI;
- 4) Equation 3.4 (rewritten from Eq. 2.51) shows that Q_g can be worse if multiple antennas are installed in the chamber, i.e., more antennas mean a lower sensitivity of a MIMO RC in the transition region. Reducing this effect of the additional antennas can be done when the unused antenna ports are opened.

It should be a good idea to build a scaled model for testing/understanding before transferring any new ideas between the room and its model, as their differences are relatively minor in the transition region (neither are affected above the C-LUF, as the RC chamber can be expected to pass the validation procedure as usual). Thus, a 1:5 scaled model of the CIRA shielded room can be used to test the MIMO technique applied to the RC method; to study the behaviour of a MIMO RC; and to predict results for the shielded room.

3.1.4. Scaled Model

A 1:5 scaled model of the shielded room has been made from steel, which is a common material for RCs (μ_r is about 10). The dimensions of the scaled model are 0.72 m×0.48 m×0.48 m. This scaled model is simulated as explained in Appendix A.



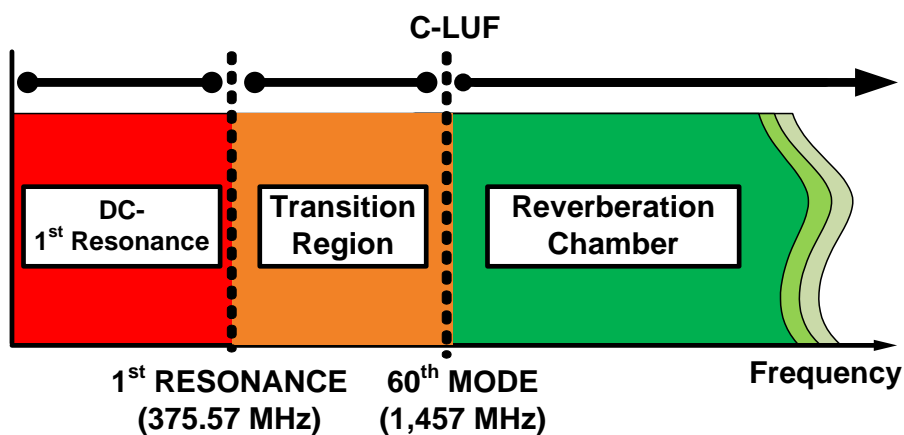
Figure 3-10: Scaled Model (1:5) of the CIRA Shielded Room.

According to Chapter 2, the C-LUF can be approximately predicted from calculations, using either Eq. 2.25, or Eq. 2.45 (at the 60th mode). The calculated C-LUF of the scaled model is 1,457 MHz (the higher frequency predicted from these equations), and the first resonance is expected to be at 375 MHz (tests showed the first resonance to actually be at 365 MHz; the difference between the theoretical or simulated and measured values is due to the magnetic permeability of the material).

The 1:5 scaled model can be used as a conventional RC only above the C-LUF; the frequencies from the 1st resonance to the C-LUF (365 MHz to 1,457 MHz) are called the transition region, where the mode densities are insufficient for any conventional RC to create the required uniform field. The MIMO RC introduced in this study is expected to make the scaled model also usable in the transition region.

Table 3-5: Characteristics of the Scaled Model and the CIRA Shielded Room.

Characteristics	Scaled Model	Shielded Room	Scale
Material	Steel	Steel	-
Surface	1.8432 m ²	48.81 m ²	1:5.13
Volume	0.1659 m ³	22.61 m ³	1:5.02
The 1 st Resonance (MIMO-LUF)	365 MHz (measured)	72 MHz (simulated)	5.06:1
Expected Conventional LUF	1,457 MHz	291.5 MHz	5:1

**Figure 3-11:** MIMO-LUF (1st resonance), C-LUF and transition region of the Scaled Model.

At this point, a 1:5 scaled model and its simulation modelling are available as tools for further research. Next, modifications of the receiving antenna, stirrer, and complementary tools, are discussed in the following Sections.

3.2 Design Characteristics

3.2.1 Receiving Antenna

In the case of conventional RCs, an antenna is needed for the validation procedure (to generate the field inside the working volume), and for emission measurement (to measure radiated emission from the EUT). Generally, it is suggested by the IEC standard [9] that antenna characteristics should be linear/passive; placed at least $\lambda/4$ at the C-LUF from other structures (walls, EUT, stirrer); and pointing to a corner and/or stirrer. A MIMO RC, in contrast, requires multiple antennas to be installed; this brings up a fundamental problem, as their dimensions must be electrically small at low

frequencies, but they should also be usable from the first resonance of the cavity. From that perspective, the dimensions of antennas used in a MIMO RC must be (electrically) small. A research study, [45], recommended that antennas used in RC can have small dimensions, and that there is no need for them to have a very good gain, or a very good reflection coefficient (S_{11} parameter); but it should have wideband operation and a smooth reflection coefficients and antenna factors.

Before designing, all requirements must be listed and considered carefully. Apart from the fundamental requirement for the dimensions of the antennas, it needs to be clarified whether any conventional requirements are still needed, or not, as follows (based on the recommendations of the standard guidelines [9]):

- 1) Linear/passive antenna: in the case of a conventional RC, linearly polarised antennas are actually required in the validation procedure (they may not be required for radiated emission measurements, as the 3 polarised field component strengths are already known to be uniform after the chamber has passed the validation procedure). As a result of this thesis, MIMO RCs will have their own validation procedure (Chapter 4), called the MIMO-RC validation procedure. The new procedures are similar in concept to the conventional ones. Three polarised field strengths are still required to be measured to gauge their STDs. Therefore, linear/passive antennas are also required for MIMO RC;
- 2) Placed at least $\lambda/4$ at the C-LUF from any structure: from the author's understanding, this requirement is to avoid having low field isotropy. This is because each point close to a wall misses some resonance modes resulting in decreasing the field uniformity. In contrast, the field uniformity will be better when the antenna is moved away from any structure's surface by about $\lambda/4$ at the C-LUF. However, this phenomenon does not affect a MIMO RC, because when one antenna starts to miss any resonance, a MIMO system will switch to other receiving antennas to maintain field uniformity. Thus, antennas (in a MIMO RC) can be placed as close as desired to the walls, regardless of the MIMO-LUF, e.g., as fixed wall antennas;
- 3) Pointing to a corner and/or stirrer: placements of multiple receiving antennas in a MIMO RC can cause a serious problem due to available area in the

chamber. Besides, each antenna has to be relatively big compared to chamber's dimensions (antennas must be usable from the first cavity resonance). As a result, in practice, using fixed wall antennas could suit the MIMO RC, as it can provide sufficient area for an EUT placement. In addition, those antennas can use the walls as their ground planes to reduce their dimensions, e.g., a monopole antenna, which uses the benefit of a ground plane, is a half-length of a dipole antenna, at the same operating frequency. However, the direction of the antenna is not relevant in the MIMO case as they are wall mounted; and because of the violation of the standard requirement, the MIMO RC may not work as a conventional RC (i.e., using only one receive antenna) even above the C-LUF.

Design and Installation: After consideration of all these limitations, this research has produced a design of a top-loaded monopole, which is 35 mm long, and is loaded with disks of 30 mm radius (see Fig. 3-12). The antenna characteristic are as for a short monopole (the simplest antenna type), but the reflection coefficient is improved as it is loaded by the disk on the top. This top-loaded antenna is a linear one, and can be used with a Rayleigh field distribution [50, 51, 52, and 53]. Besides, the antenna factor is smooth, and dimensions are small. Any resonance effects up to 1,000 MHz can be expected to come only from the chamber itself, and not from the receiving antennas. All receiving antennas have been installed on the walls (i.e. they are fixed wall antennas). This is to use the walls as ground planes, to provide more available space in the chamber for the use of multiple antennas.

S_{11} parameters (reflection coefficients) of one top-loaded monopole are measured by a mobile network analyser, and by a stationary network analyser: PNA-X Network Analyser N5241A (Agilent Technologies) in an AC and in a shielded room, in which signals can be kept reflecting (Fig. 3-13). The results show that measuring the antenna in an AC gives smoother results (i.e. less fluctuation) than in a shielded room, where the reflections of signals (i.e., standing waves) have an impact on the antenna. However, the measured AC results show very good agreement with those calculated by the ANSOFT HFSS simulation program; the reflection coefficient of a top-loaded monopole is smooth for all frequencies in the transition region.



Figure 3-12: A top-loaded monopole specifically designed for the 1:5 Scaled Model.

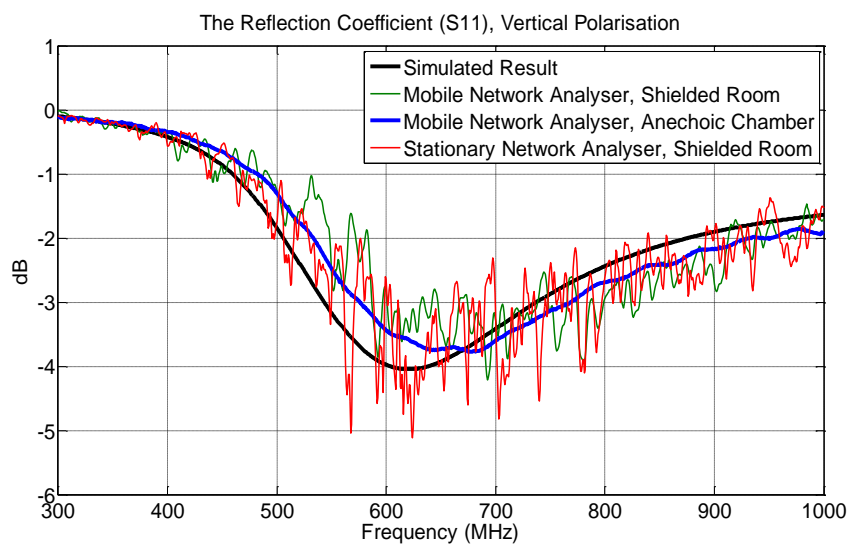


Figure 3-13: Characteristics of the top-loaded monopole placed in the vertical plane.

Number and positions of antennas: In the general case, a minimum of six antennas is suggested by this thesis: at least two antennas for each polarisation to pick up all modes within the transition region. The positions of all receiving antennas in relation to the chamber's field distributions should be one of the primary concerns in the design phase. The MIMO RCs are designed to be used in the transition region, or below the 60th mode ($f_{4,2,2}$); thus, design considerations can be confined to cover field distributions from just mode $f_{1,n,l}$ to mode $f_{4,n,l}$, and mode $f_{m,n,1}$ to mode $f_{m,n,2}$. As a result, it has been found that each polarisation will require two antennas placed at $\lambda/4$ and $5\lambda/16$ from the chamber's corners.

In the case of the scaled model, from the guidelines above, the scaled model is a symmetrical cavity, i.e., it has a square cross-section, with two of its sides having the same length. Then, $f_{m,n,l}$ modes have the same resonance frequency as $f_{m,l,n}$ modes. In this case, antennas on the floor and ceiling are not needed if the EUT is rotated.

However, as many antennas as possible should be installed to study the results of the scaled model as a prototype of a MIMO RC. Fig. 3-14 shows examples of field distributions, whose indices m , n , and l indicate that a half-wave electric field exists along an axis direction. After considering those field distributions, eight antennas will be placed on the X-Y plane (blue colour plane in Fig. 3-15) at half of its height (Z axis). Each antenna is placed at either $\lambda/4$ or $5\lambda/16$ of the length (or width) from a corner for X and Y polarisations, respectively. Only one (the ninth) antenna will be placed on the floor, given that the stirrer will destroy the ‘symmetry’.

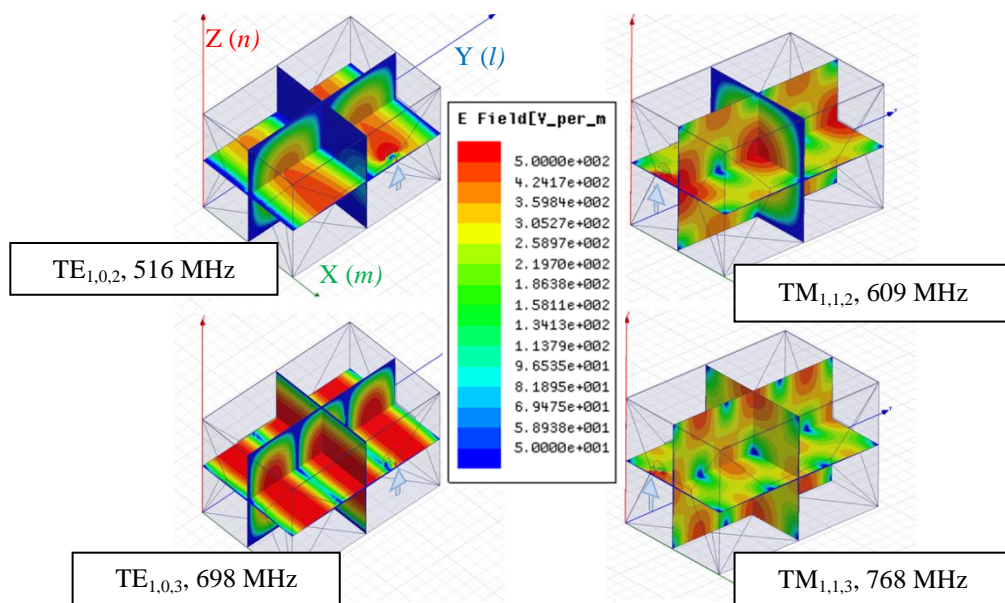


Figure 3-14: Examples of field distributions below the 60th mode frequency.

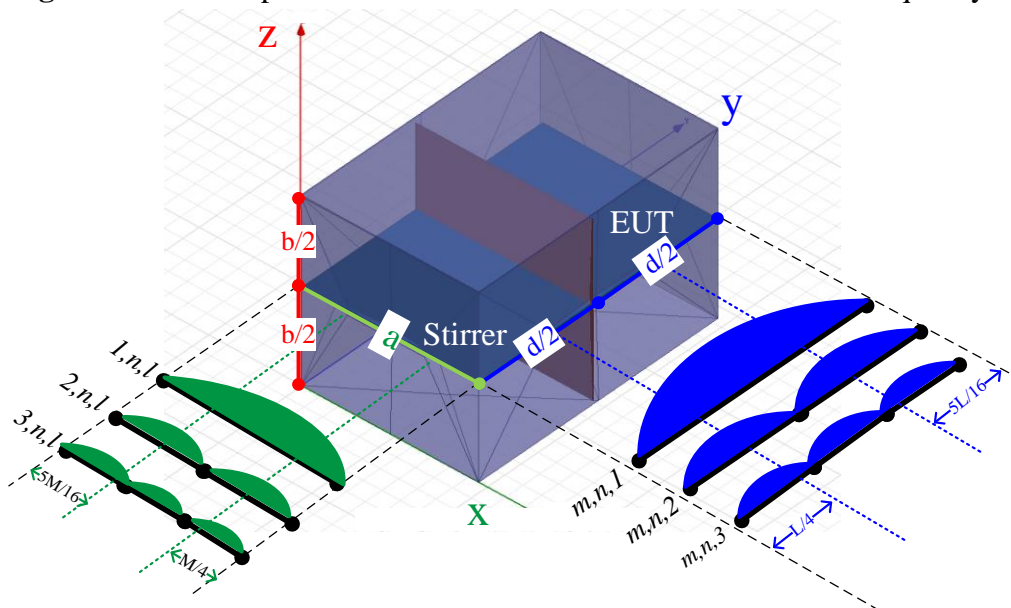


Figure 3-15: Half-wave electric field (in relation to Fig. 3-14).

Figure 3-16 shows the antenna positions as determined based on ANSOFT HFSS simulation results (model's details are in Appendix A). After installation, all receiving antennas can be fed/measured from outside the enclosure. For this configuration, there is still good agreement between S_{11} , measured by the PNA-X Network Analyser N5241A, with the S_{11} calculated by the ANSOFT HFSS simulation program (using FDTD/FEM), see Fig. 3-17.

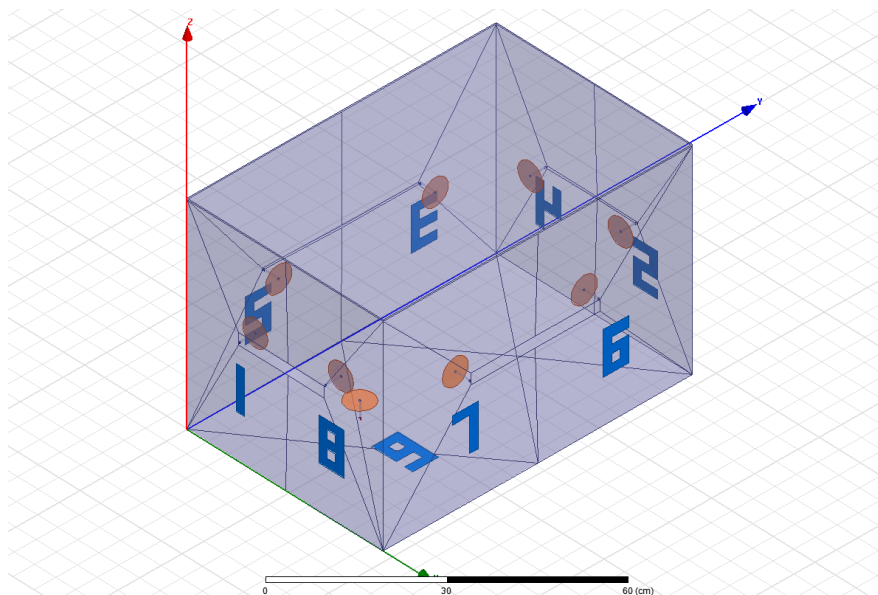


Figure 3-16: Nine top-loaded monopole antennas mounted on the 1:5 Scaled Model.

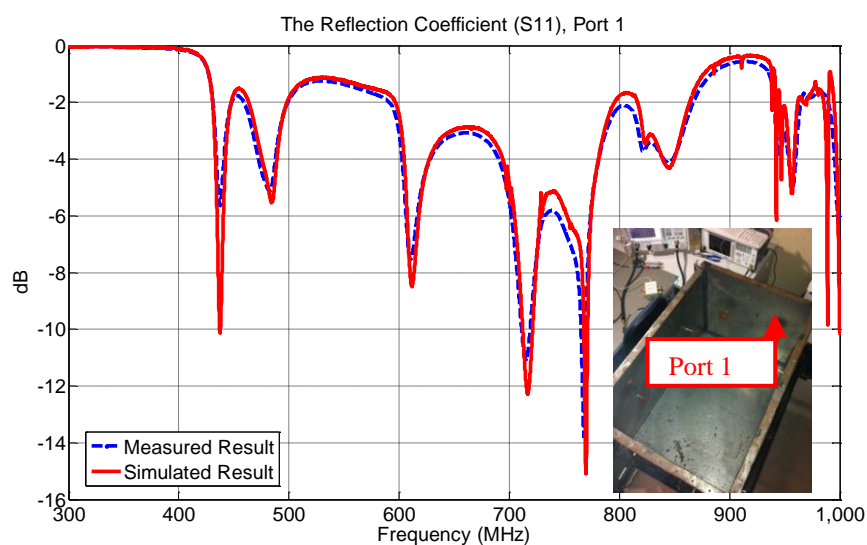


Figure 3-17: Comparison of reflection coefficients (S_{11}) at port 1 (Scaled Model).

3.2.2 Stirrer

As in a conventional RC, a MIMO RC requires a stirrer to alter the field distribution. A well-known and often used stirrer, the Z-stirrer, shows poor performance in the transition region, as mentioned in Sections 2.3 and 2.4. A design of a new stirrer to stir field distributions is required. The first concern in the design is the size of the stirrer in relation to the space available (see Fig. 3-15); up to half of the chamber is made available for the stirrer. Figure 3-18 illustrates that the maximum stirrer length is 260 mm, in order to keep its distance from any antenna $\lambda/4$ at the predicted C-LUF. From the results, the maximum stirrer volume is calculated to be 160 mm×160 mm×250 mm. Based on this design consideration, the scaled model will be able to work as a conventional RC above the C-LUF [9], and also as a MIMO RC below the C-LUF with no need to change the stirrer position.

A Z-shaped stirrer, 250 mm in length, is simulated in the ANSOFT HFSS model at the position shown in Fig. 3-18. The simulated reflection coefficient (S_{11}) determined for port 1 over one revolution of the Z stirrer is shown in Fig. 2-24. The results show poor performance of the Z stirrer in the transition region; the stirrer can barely shift the 1st resonance, and there are only very small changes in the resonance amplitudes in the transition region.

From literature reviews in Chapter 1 [17], a C-shaped stirrer performs well in the transition region of a TEM cell, where one polarised signal dominates the others. However, the fields in a MIMO RC must be uniform for all 3 polarised signals. Modification of a C stirrer to affect more than one polarisation could be suitable for a MIMO RC. As a result, these considerations, a double C stirrer was made with the same volume as the Z stirrer. The resonance frequency for the simulated reflection coefficient (S_{11}) from port 1 over one revolution of this double C stirrer is shown in Fig. 3-19. Eight resonance frequencies from Fig. 3-19 are sampled, from low to high frequency, to investigate more details at these frequencies in Fig. 3-20 and Fig. 3-21.

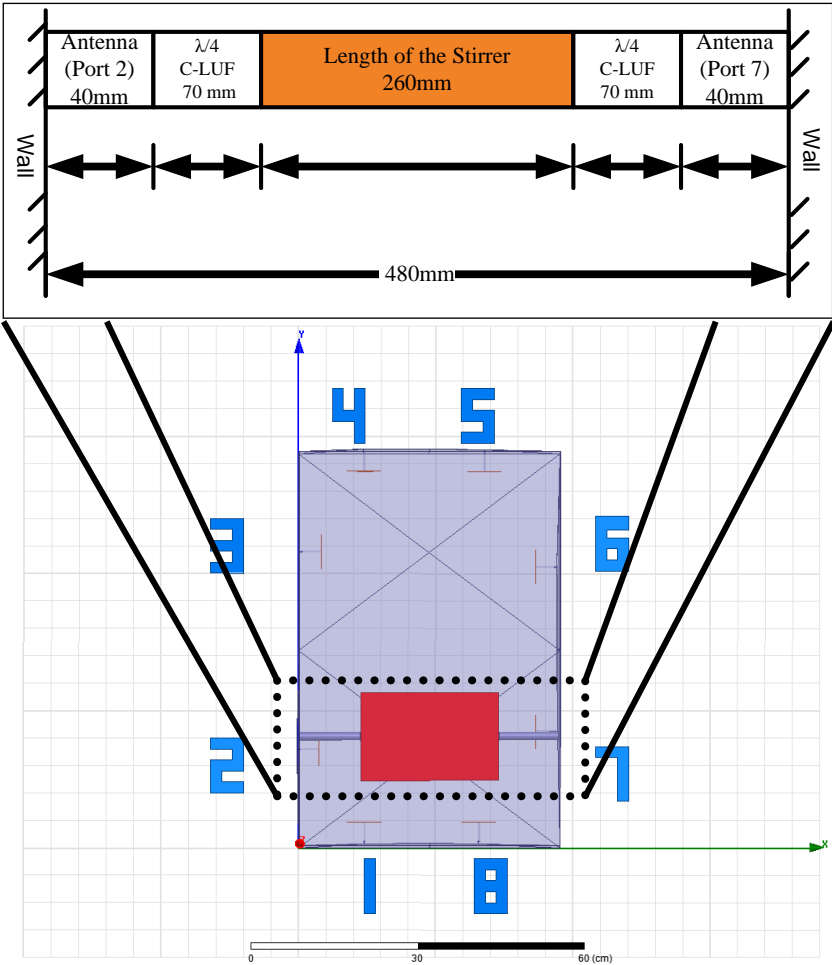


Figure 3-18: Position of the stirrer in the Scaled Model (top view, ANSOFT HFSS).

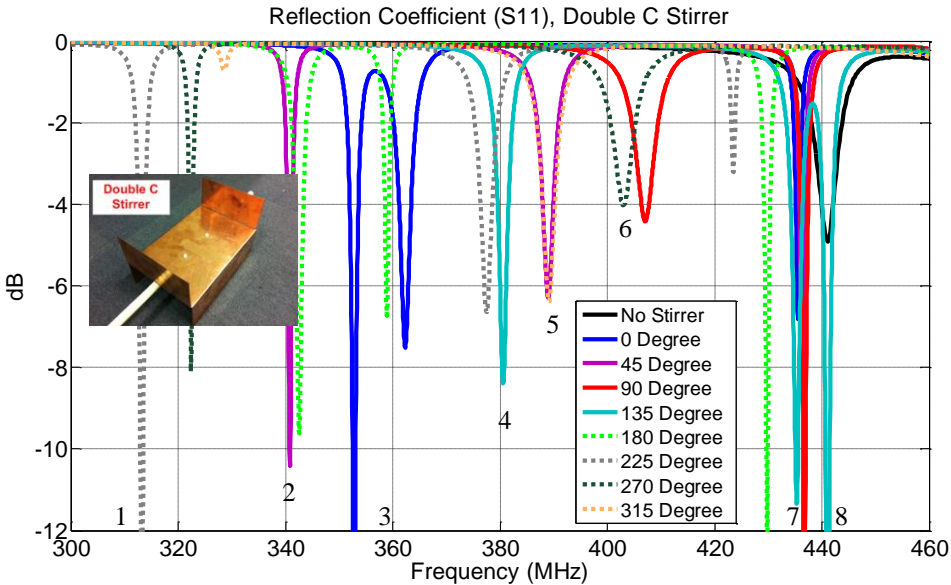


Figure 3-19: Simulated S₁₁ from receiving antenna port 1, Double C stirrer, case A (Fig. 2-19).

Figure 3-20 shows the 8 samples of simulated field distributions, marked in Fig. 3-19 (from low to high frequency, in the transition region). It can be seen that they can be grouped by the pattern of the field distribution into 2 groups, i.e., along the Z axis (marked 1st-6th) and along the X axis (marked 7th and 8th). All resonance frequencies from Fig. 3-19 are plotted in Fig. 3-21, and dots of similar field distribution are connected by the red lines. The results from Z stirrer, shown in Fig. 2-24, are also plotted and connected by the blue lines for comparison. It is obvious that the double C stirrer can shift resonances from mode TM_{110} to TE_{101} much further than the Z stirrer.

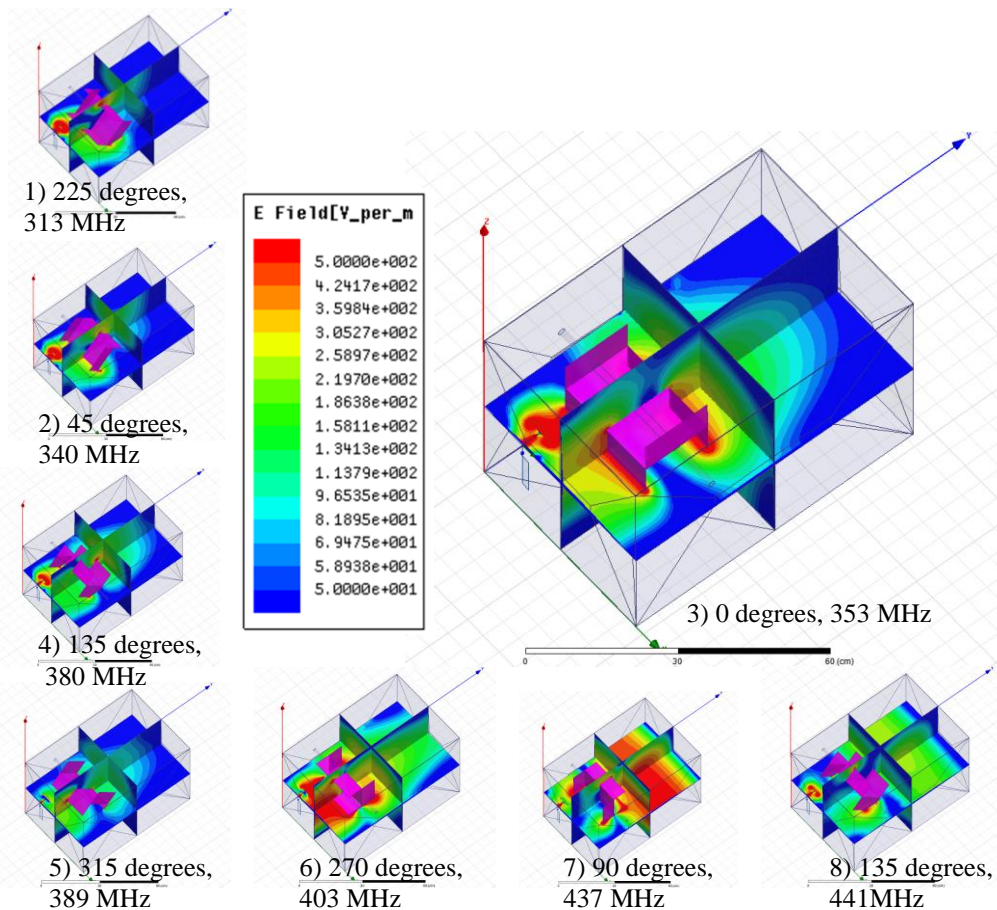


Figure 3-20: *E*-field of 8 marked resonances (from Fig. 3-19), when the Double C stirrer is applied, case A (Fig. 2-19).

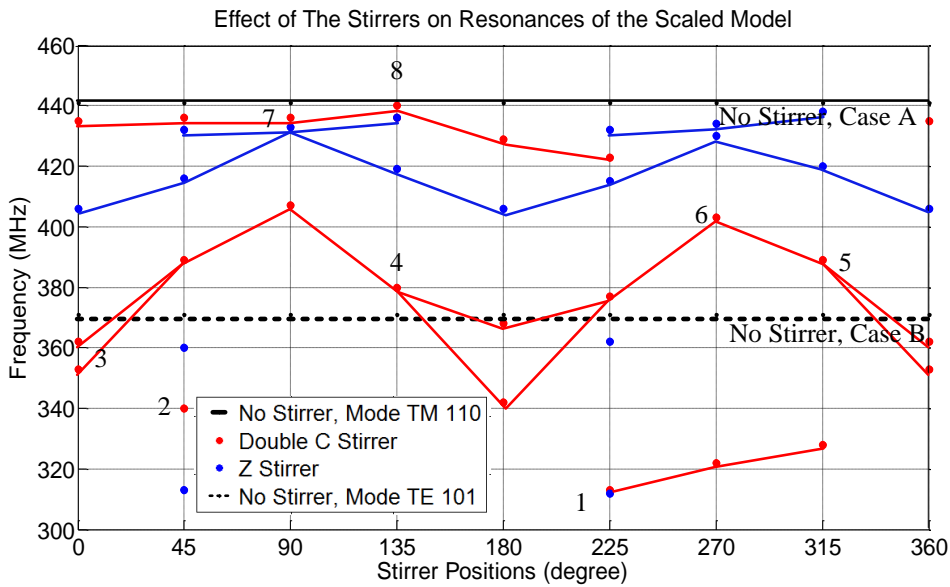


Figure 3-21: Comparison of simulated S_{11} (resonances) for the Z-stirrer & Double C stirrer, one revolution, 45-degree/step, case A (Fig. 2-19).

The comparison of the simulated reflection coefficient S_{11} from both stirrers in Fig. 3-21 confirms that the double C stirrer performs better than the Z stirrer. After studying the simulated results, both stirrers, Z and double C, were built and measurements made. Figure 3-22 shows the measured S_{11} for port 1 over the FRI; the double C stirrer can cover almost the whole FRI except around 420 and 500 MHz (more results are available in Appendix E, Fig. E-5).

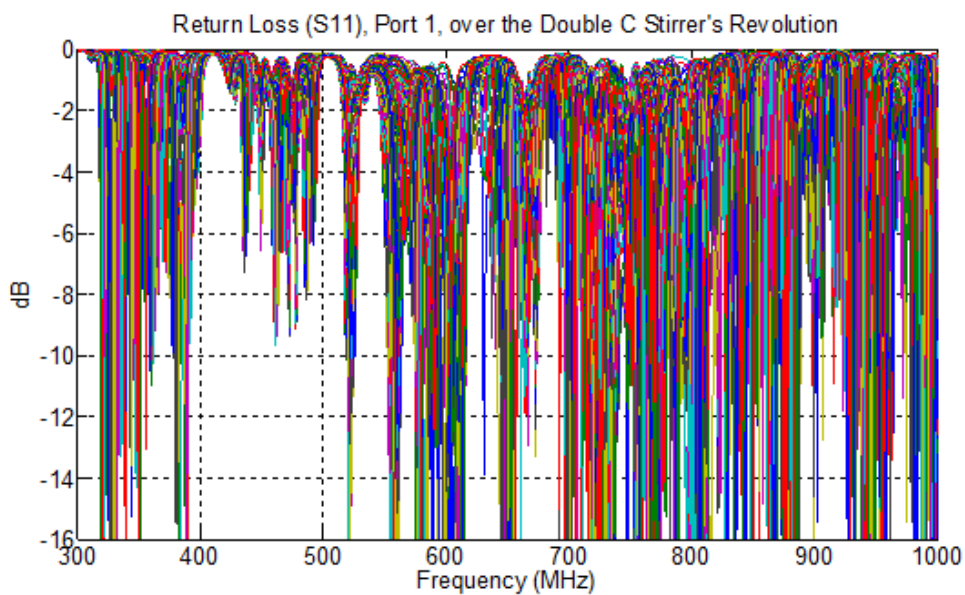


Figure 3-22: Measured S_{11} from receiving antenna case A (Fig. 2-19), Double C stirrer. More results are available in Fig. E-5, Appendix E.

A wideband noise source is made as an EUT similar in concept to that in Fig. 2-26; i.e., the EUT is a shielded aluminium cavity with a monopole antenna on top; the antenna is fed from a noise generator (boosted with two amplifiers) inside of the cavity. Then, the EUT is placed in the scaled model, as for case N2 in Fig. 2-26. The measured voltages from port 1 over one revolution of the Z-stirrer are shown in Fig. 3-23 (a). From a separate test, the measured results over one revolution of the double C stirrer are shown in Fig. 3-23 (b).

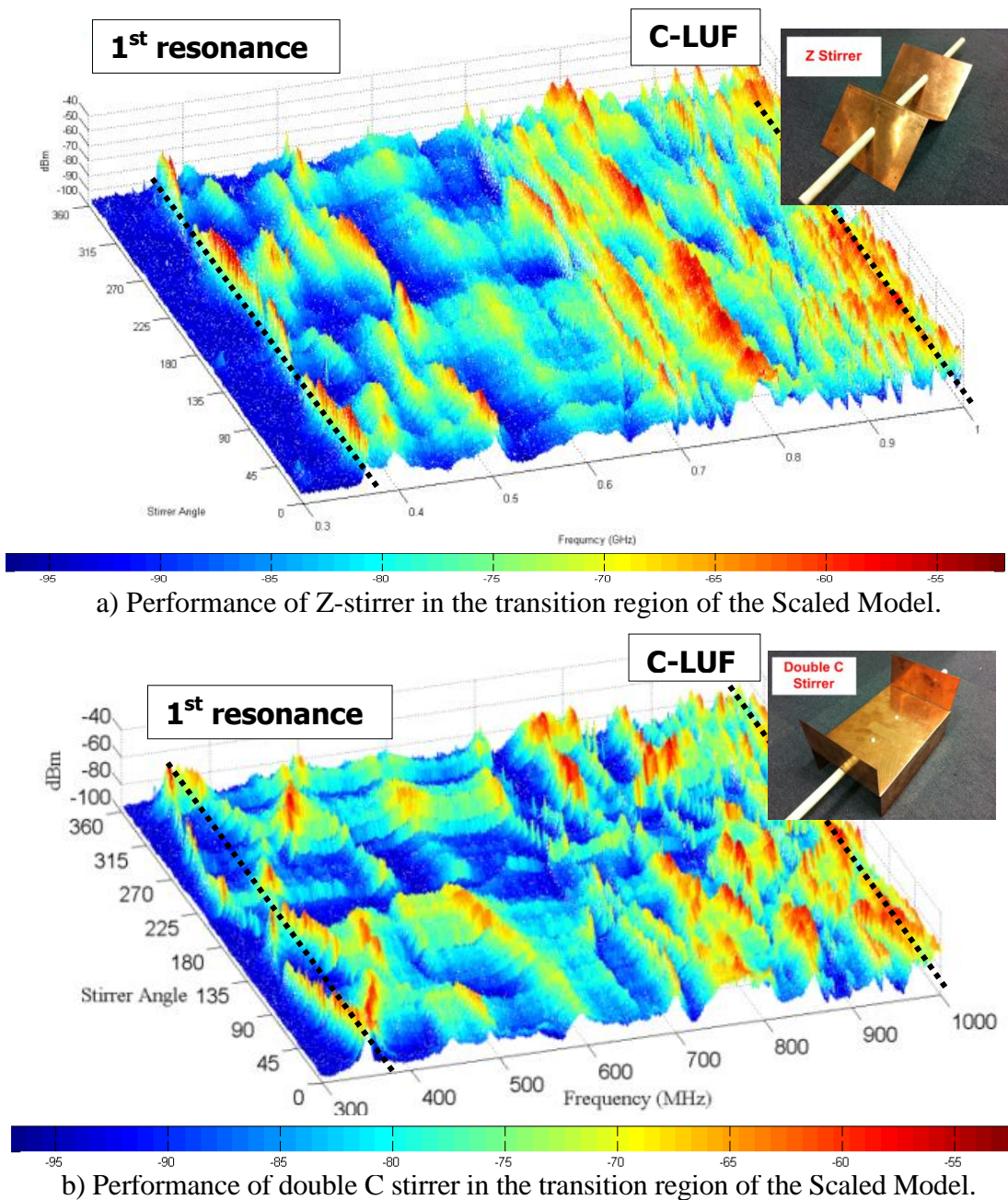


Figure 3-23: Measured Voltages (V) over the stirrer's revolution, case N2 (Fig. 2-26).

Figure 3-23 confirms that the double C stirrer performs very well with regard to changing amplitudes and shifting frequencies in the transition region. The double C stirrer can shift even the first resonance of the scaled model up to 10.95%, while the Z stirrer is almost unable to do so. Therefore, the Double C stirrer will be installed on the scaled model as a prototype of a MIMO RC.

3.2.3 Working Volume & Field Uniformity

The validation procedures are summarised in Fig. 3-3. Basically, a typical RC has to “generate” a statistically uniform environment, within the defined working volume, to meet the conventional validation requirement, as in Fig. 3-24 (see also Appendix F). From the author’s observations, it seems that the conventional validation procedure is designed for immunity tests, as the signal directions are in the opposite direction to those used in making emission measurements. Thus, changing the signal direction to the opposite is more suitable for making emission measurements, and does not affect the results, since $S_{12}=S_{21}$ (assuming reciprocity).

In this thesis, instead of looking at the field uniformity as in conventional RCs, the S_{12} parameter between antennas is investigated here. The S_{12} values (equivalent to a uniform field) should be representative of E -field values for the MIMO validation procedure. Moreover, using antennas instead of probes (as suggested in [9]) can be accommodated more easily in the chamber because the antennas are smaller, and require lower transmitting power. As a result, the concept of the MIMO working volume for the MIMO validation procedure is implemented, as shown in Fig. 3-25; i.e., a cubic working volume rotated by 45 degrees around the X-axis for convenience.

Instead of moving a transmitting antenna around to each of the eight corners, a Validation Set consisting of four small cones attached to the end of a rotatable H-shaft was made (see Fig. 3-26). Characteristics of all four cones are shown in Fig. 3-28. They are not much different; for example, at 650 MHz, the maximum difference in S_{11} is 0.25 (0.8-0.55) dB, which means that there is only 1.5 dB difference in radiated power (-0.8 dB \rightarrow 17% forward power \rightarrow -7.7 dB, and -0.55 dB \rightarrow 12% forward power \rightarrow -9.2 dB). The four small cones of the Validation Set can be fed from outside the scaled model by SMA connectors to the transmitting antennas, resulting in a smaller space required.

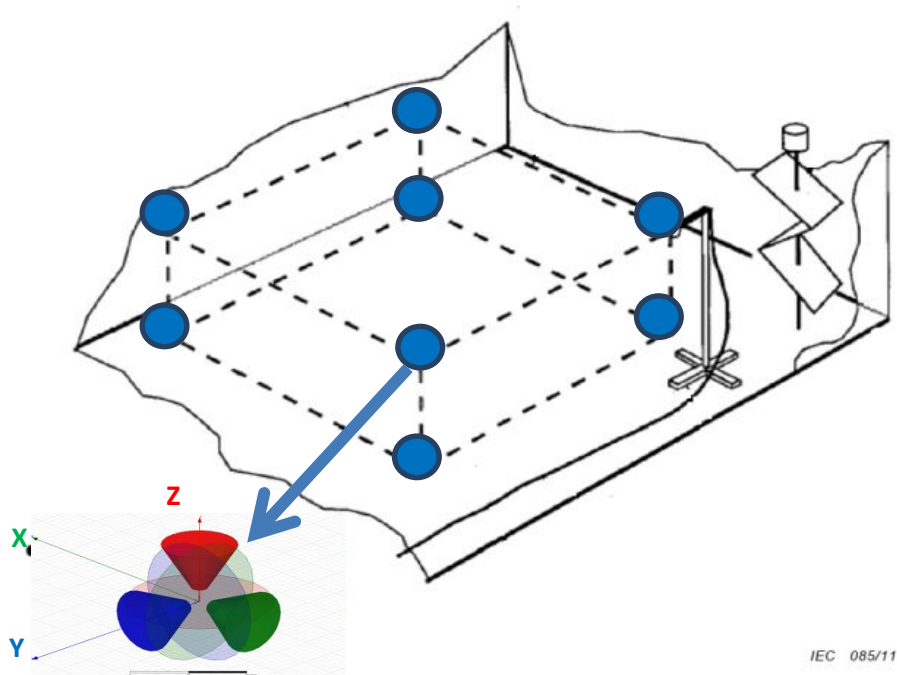


Figure 3-24: Conventional Working Volume validated by probes at each corner.

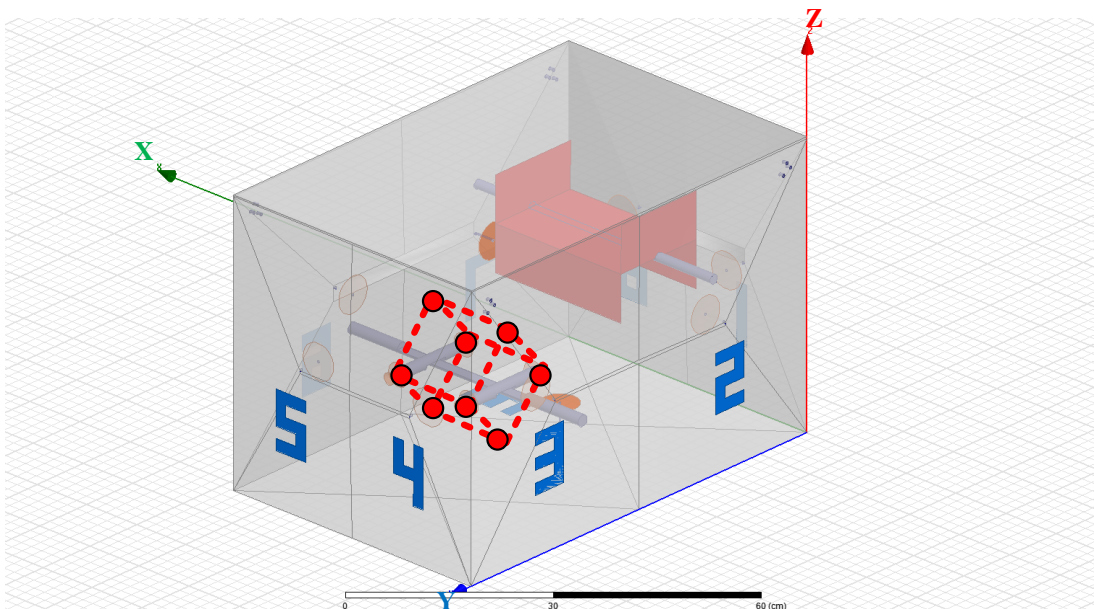


Figure 3-25: Working Volume of the Scaled Model.

As a result, the MIMO working volume is still rectangular in shape, but it no longer looks the same as in the IEC standard concept. The MIMO working volume of

the scaled model will be defined when the H-shaft is rotated by 90 degrees; and the field uniformity can be also determined by antennas at eight corners of the working volume. The ends of the rotatable H-shaft can be replaced with 90 degree connectors, to measure all 3 polarised radiations (see Fig. 3-26). The area of the working volume is defined to be 140 mm × 140 mm × 140 mm; it is 1.65% of the total volume in the scaled model (0.72 m× 0.48 m × 0.48 m). The distances of the boundaries of the MIMO working volume from the chamber walls, receiving antennas, and stirrer exceed $\lambda/4$ at the C-LUF; so the scaled model can still work as a conventional RC above the C-LUF.

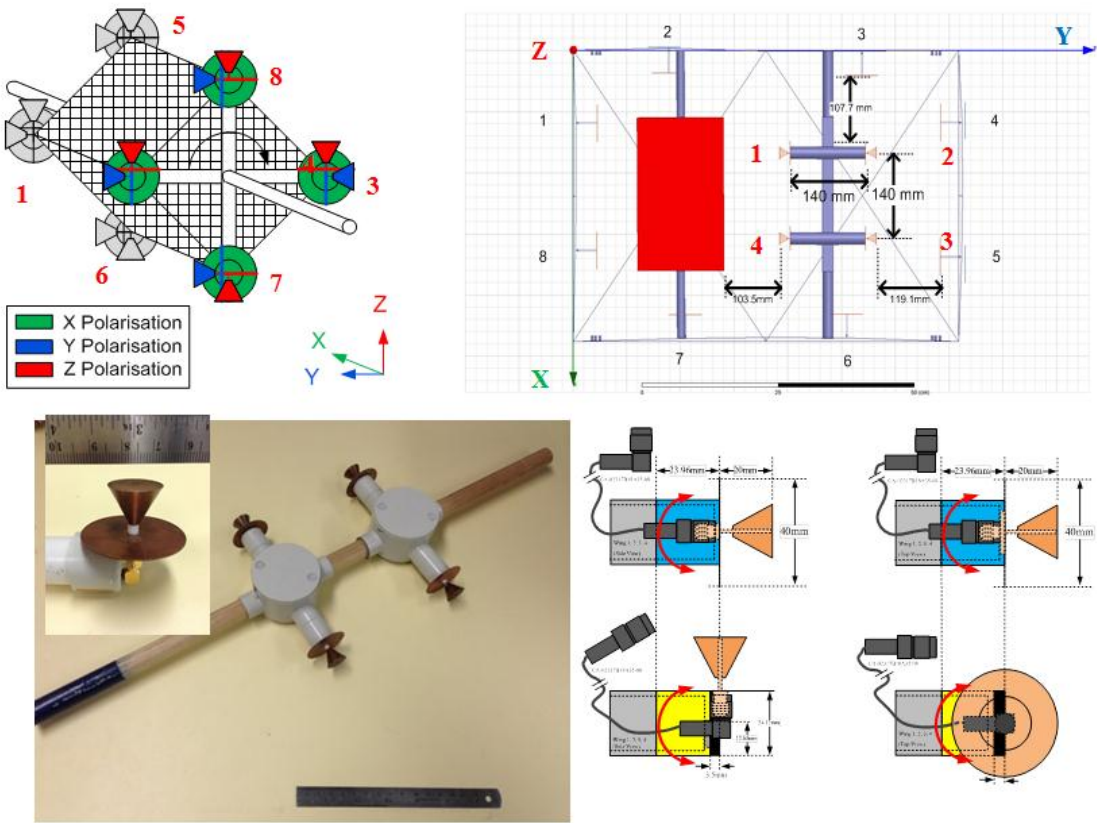


Figure 3-26: The Validation Set; rotatable H-shaft with cone antennas.

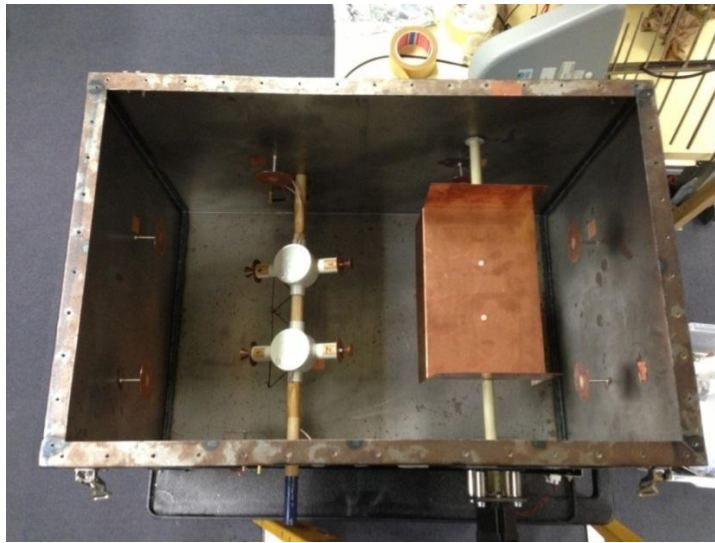
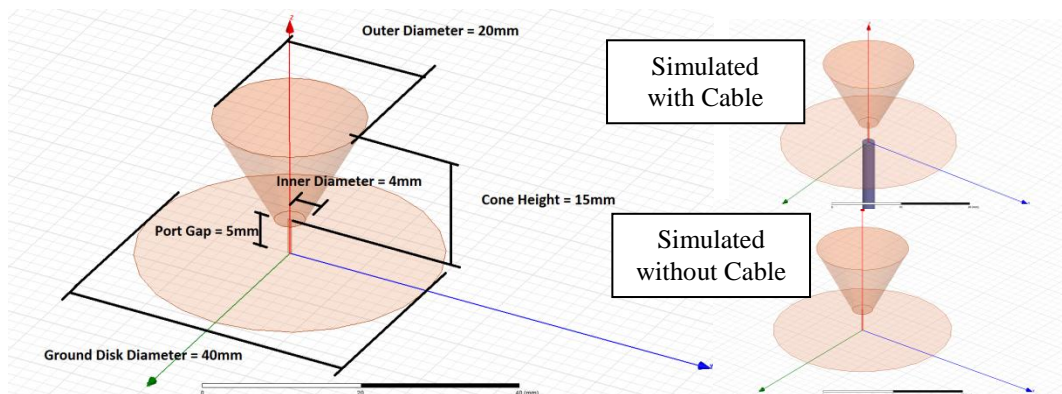
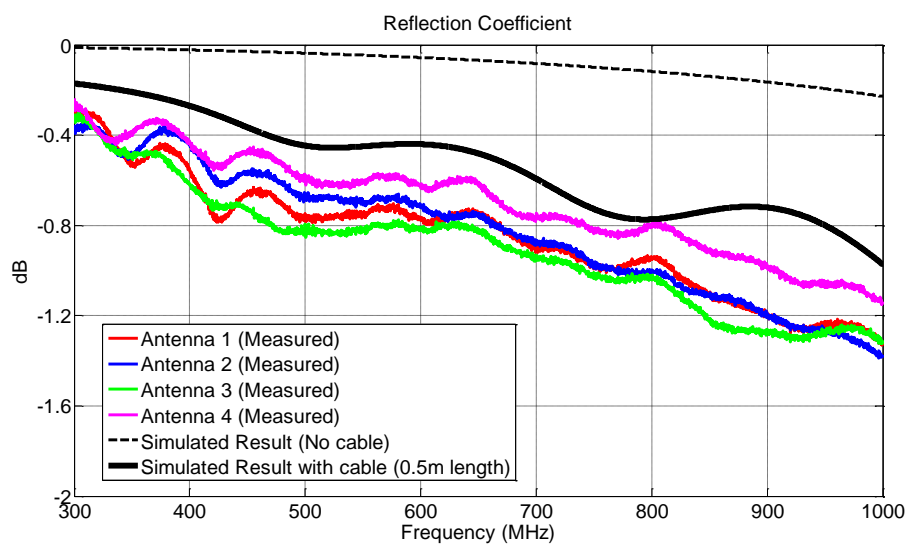


Figure 3-27: The 1:5 Scaled Model with all tools and the Validation Set.



a) Structure of the cone antennas.



b) Reflection coefficient of the cone antennas.

Figure 3-28: Characteristics of the cone antennas.

3.3 Assembly of Components and Control Software

3.3.1 Hardware

The scaled model, with all the described features, becomes the prototype of a MIMO RC. This prototype MIMO RC, a spectrum analyser (HP8594E), a stepper motor, relay-controlled coaxial switches (reflective switches), and all auxiliary equipment are assembled as a system, as shown in Fig. 3-29; the actual system can be seen in Fig. 3-30.

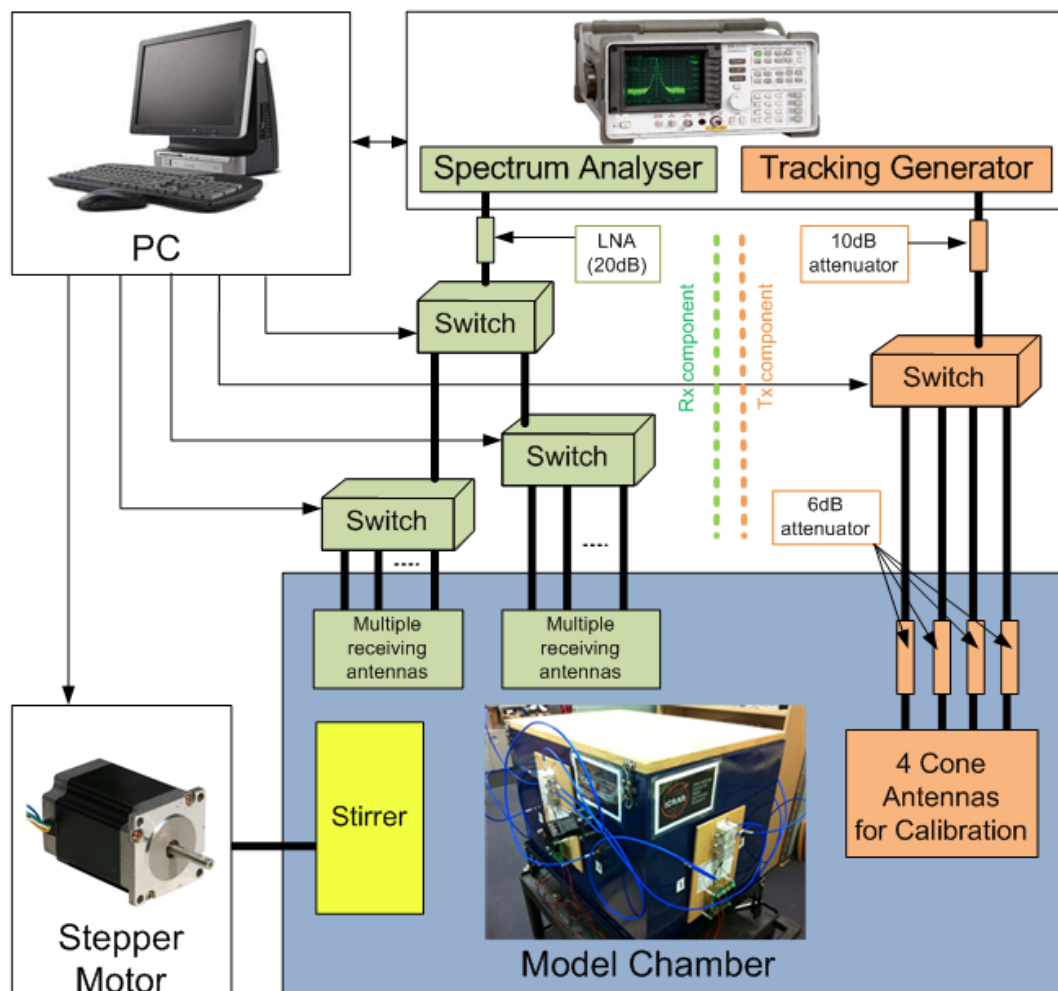


Figure 3-29: Schematic diagram of the automating system.

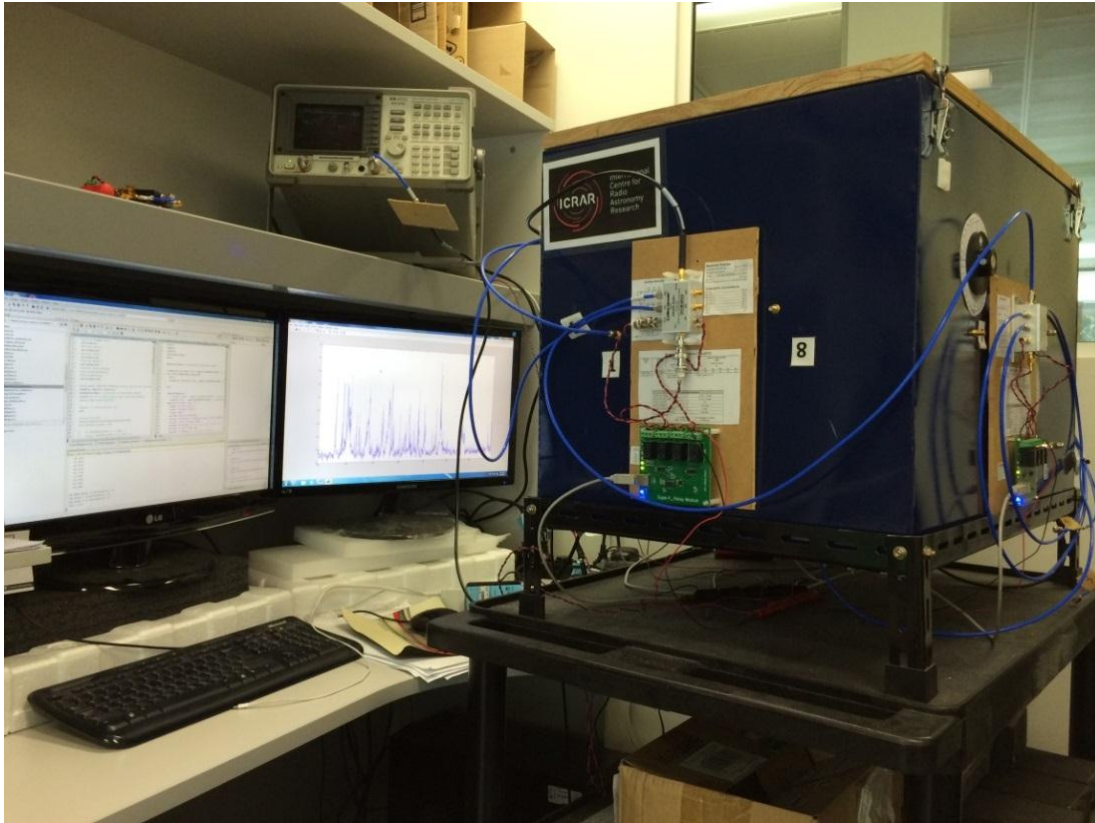


Figure 3-30: The Scaled Model set up for automated measurements.

MIMO RC Procedures: for both a conventional (SISO) RC and a MIMO RC, the field uniformity must be verified before emission measurements are made. While a conventional RC is always a SISO system, the situation for a MIMO RC is different. With respect to field uniformity verification, the MIMO RC is treated as a SIMO system; field uniformity is determined based on the assumption that only one EUT position (Single-Input) is used later during the emission measurements, i.e., a transmitting antenna at each corner of the working volume should produce the same maximum signal in the multiple receiving antennas (Multiple-Output). During an emission measurement, the EUT will be placed at different locations, and the systems thus used a true MIMO system. These distinctions are summarised in Fig. 3-31.

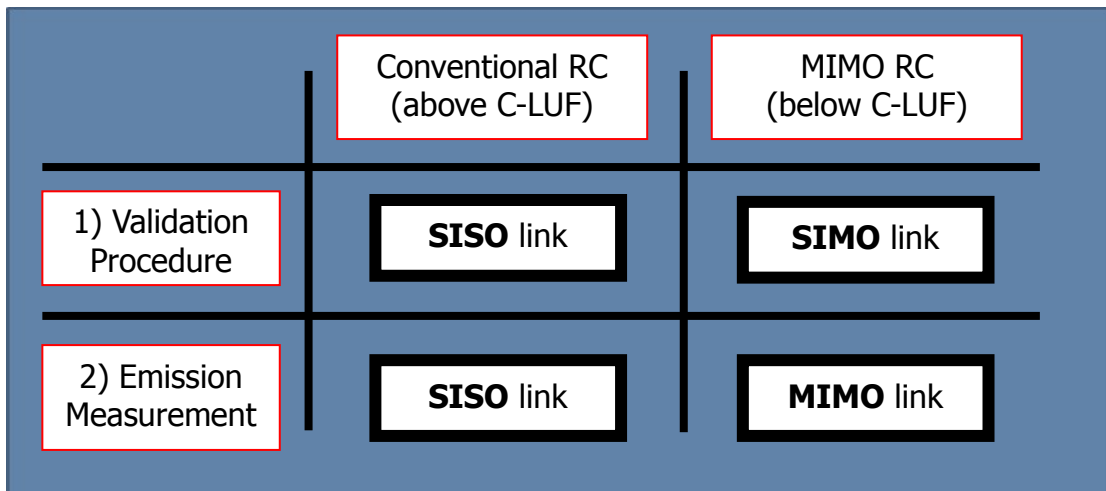


Figure 3-31: Concepts of Conventional RC and MIMO RC — equivalent to basic communication links (see Fig. 3-3).

Figure 3-31 demonstrates that the validation procedure of a MIMO RC is a SIMO system, i.e., one transmitting antenna for all nine receiving ones. The step-by-step explanations of the modified procedure are given as follows:

SISO RC: This is a conventional RC in that there is only one receiving antenna used (Single-Output). The process starts with the first cone antenna of the calibration set becoming a transmitting antenna powered from outside the cavity by the tracking generator (-10 dBm is set as the output power of the tracking generator); the stepper motor brings the stirrer to the desired position, only one top-loaded monopole antenna is selected as the receiving antenna, and the signal at this receiving antenna is measured by the spectrum analyser and saved. Then, the stepper motor turns the stirrer by a certain amount (4.5° in this case), and the signal is measured again. This process is repeated until one revolution of the stirrer (80 steps) is completed. Then, the second cone antenna of the calibration set is selected to be the transmitting antenna; the process is repeated for another revolution of the stirrer, and so on, until the eighth cone position (the last) has transmitted. After that, the whole process is repeated again with another polarisation of the cones, until all 3 cone polarisations are done.

Ultimately, there are 1,920 sets of SISO data; i.e. 80 positions of the stirrer \times 1 receiving antenna \times 3 polarisations \times 8 cone positions. Each data set contains 1,601

frequency points, so there are 3.07 million data points in total. It should be noted that the FRI range is from 300 MHz to 1 GHz, a resolution BW of 100 kHz is used.

SISO RC to SIMO RC: The concept of this thesis looks similar to establishing field uniformity in a conventional RC [9]. The idea of field uniformity in a conventional RC is that regardless of exactly where the EUT is placed within the uniform field volume, it will produce the same signal in the receiving antenna. With several receiving antennas, this requirement is easier achievable; if one antenna does not pick up a 'strong' signal during the stirrer revolution, another one most likely will. For example, when the 1st antenna can measure only the X-polarised signal at a certain frequency, the 2nd antenna might be able to measure only the Y-polarised signal at that frequency; in this way, using all receiving antennas can increase the chances of measuring all polarised signals (X, Y, and Z), even below the C-LUF. This can increase the field uniformity in the transition region. This strategy should be useful for the frequencies in the transition region.

In practice, instead of using only one receiving antenna (Single-Output), 9 receiving antennas will be used (Multiple-Output), i.e., SISO RC procedure is repeated for all nine Rx antennas. As a result, there are 17,280 sets of SISO data; i.e. 80 positions of the stirrer \times 9 receiving antennas \times 3 polarisations \times 8 cone positions. Each data set contains 1,601 frequency points, so there are 27.66 million data points in total. This SIMO RC will be used for the validation procedure steps of a MIMO RC, which will be explained in Chapter 4.

SIMO RC to MIMO RC: Moving the EUT will transform the SIMO system (Single-Input) to a MIMO system (Multiple-Input). Conceptually, if the EUT, when placed at a particular location, does not generate a strong signal in any of the receiving antennas, it should do so when placed somewhere else. Moving the EUT will be used for MIMO emission measurements, which will be explained in Chapter 5.

3.3.2 Software

There are more than 27 million data points generated in each one complete measurement set, which is not possible to analyse manually; to enable this system to work using the procedures designed, it has been automated using MATLAB scripts. The software is designed to be flexible enough for a SISO (conventional) RC, as well

as for a MIMO RC. The programming strategy needed to meet the following demands:

- The process consists of 2 main parts: the data collecting part, and the post-processing part. The system process is shown in Fig. 3-32. The data collecting part uses an automating system (Appendix B) to control all the hardware, sequence the process, and save the data. The post-processing part (Appendix C) is for analysing the data from the first part.
- The collecting part must be able to switch the scaled model to work as a MIMO RC, or as a conventional RC (SISO RC); and also the post-processing part must be able to analyse data collected from both types of RC; i.e., the user can set the automating system to work as a conventional RC by selecting only one receiving antenna; or else by selecting multiple receiving antennas to set the automating system to work as a MIMO RC.

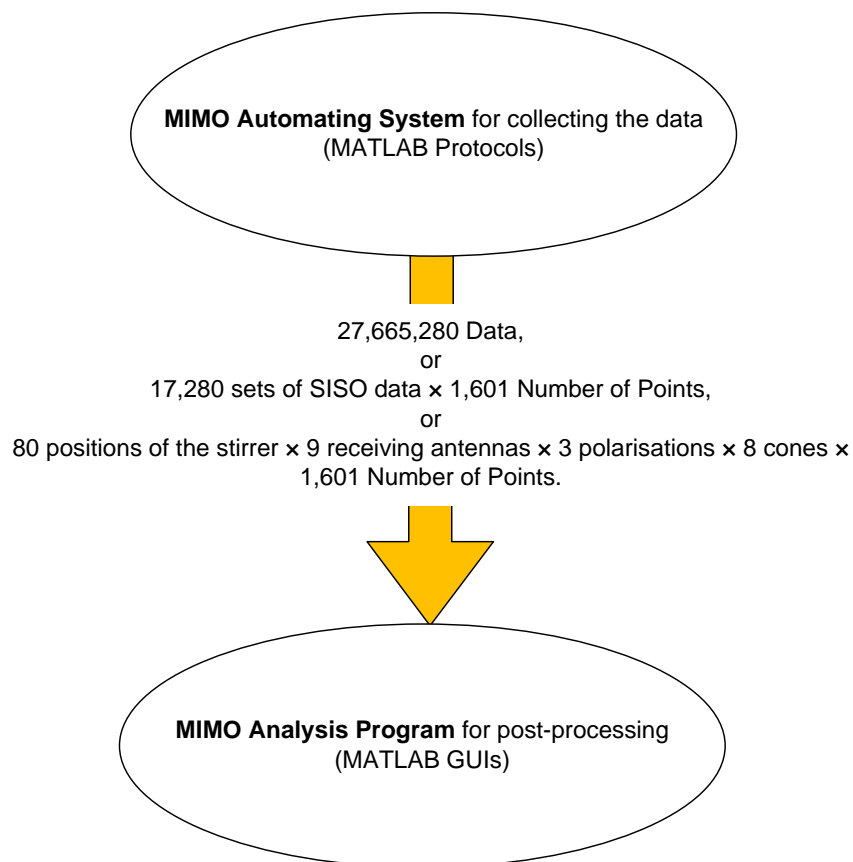


Figure 3-32: Processing steps from data collecting to post-processing.

MIMO Automating System (for collecting data): The codes are separated into the main program and 14 sub-programs for easier understanding, editing, and explanation (Appendix B). If the user wants the program to collect only specified data, they can edit only the main program with no need to edit any subset codes. For example, if the user wants to select only one receiving antenna (SISO system), they can change the value of the “PORT” variable from “9” to “1” in the main program. Overall, the capabilities of this software to control all the tools and instruments in this automating system are:

- 1) To select a cone antenna of the Validation Set by establishing only one cone antenna at a time to be powered by the tracking generator;
- 2) To select a top-loaded antenna to be the receiving antenna, by connecting only one receiving antenna each time to the spectrum analyser;
- 3) To command the stepper motor to turn the stirrer to any desired position;
- 4) To command the spectrum analyser to measure and save the data.

MIMO Analysis System (for post-processing the data): MATLAB User Interfaces (GUIs) have been written to analyse the data. The codes are separated into a main program and 15 subsets (Appendix C). From the interface of the program (see Fig. 3-33), the main part to control is named “CIRA”. When the main part “CIRA” is executed on a computer, the program will pop up with all variables set at default values. There are two sides (blue and orange) for the validation procedure and for emission measurements; both sides work independently; i.e., the user can start from either side.

Now, all the whole system and its tools are available for this research to investigate the MIMO RC performance — in order to extend the operation frequency to cover the transition region (i.e. from C-LUF to the MIMO LUF or the first cavity resonance). All the results and the new procedures are explained and summarised in Chapters 4 and 5.

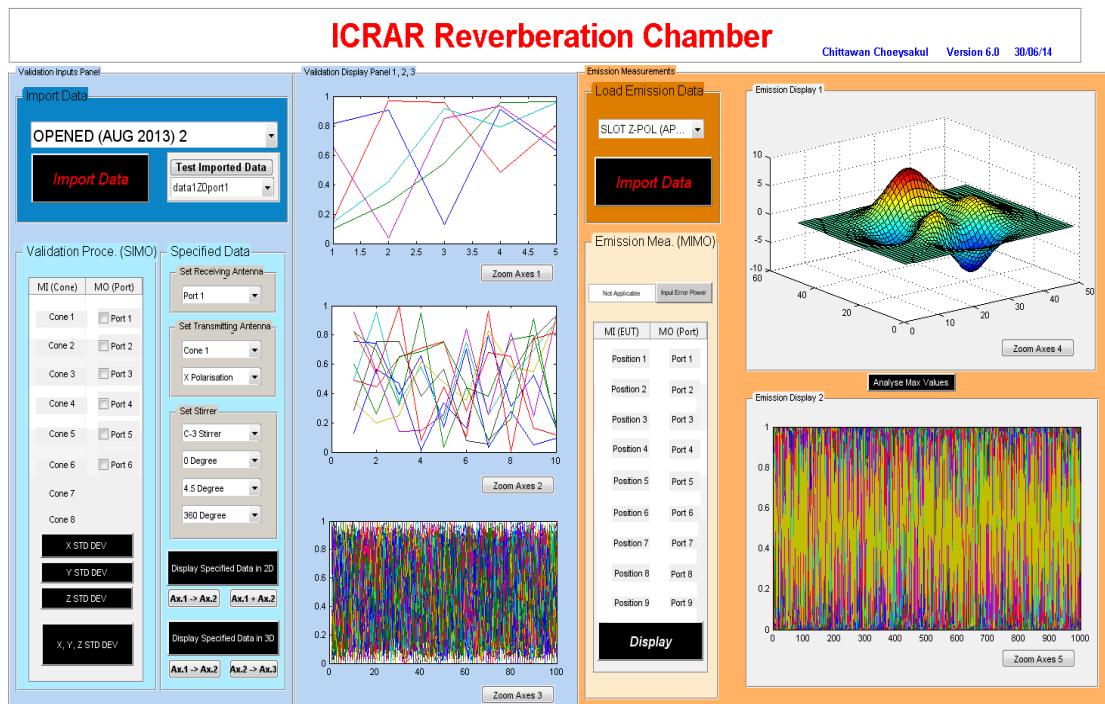


Figure 3-33: GUI version 6.0 (as of 30 June 2014).

3.4 Chapter Summary

Concept designs and implementations of a MIMO RC are outlined in Sect. 3.1. This thesis uses a 1:5 scaled model of the CIRA shielded room for easier and faster investigations. The physical dimensions of the scaled model are 5 times smaller than the actual room (Table 3-5), and its transition region is from 365 MHz (MIMO-LUF) to 1,457 MHz (C-LUF). A FEM simulation software package is chosen. The program helps to understand the relationships between related parameters, such as the composite Q -factor (Q_g).

Section 3.2 explains all the modification ideas developed in this thesis; i.e., using multiple receiving antennas, designing a new stirrer for use in the transition region, and a new idea for the working volume (e.g., using antennas instead of probes; using opposite signal direction; using a rotatable shaft to create the area of the working volume). All the developed tools are installed on the scaled model; then, the model finally becomes the prototype of a MIMO RC. The problem of Q_g is discussed in this Section.

Section 3.3 explains how to assemble all the developed tools, cables, switch boxes, and other complementary objects to make the scaled model work as a MIMO RC. MATLAB protocols are used to automate the system. The Graphical User Interfaces (GUIs) for analysing the collected data are outlined in this Section as well.

CHAPTER 4

FIELD UNIFORMITY OF A MIMO RC

4.1 Introduction

A validation procedure is required to quantify the field uniformity in the working volume; after the field is verified, EUT can be placed anywhere in the working volume for making emission measurements. A conventional RC uses only one receiving antenna to quantify the field uniformity at each corner of the working volume (SISO system); this procedure determines the C-LUF. This Chapter is to show how using multiple receiving antennas (SIMO system) can improve the field uniformity below the C-LUF; then emission measurements are described in Chapter 5.

Basically, although there are some schools of thought for a conventional validation procedure to confirm field uniformity, the use of the standard deviation (STD) method, as shown in Appendix F [9], is more acceptable than the others as all data are considered with the same weight. In this thesis, the STD method is used to quantify the field uniformity for a SISO RC (conventional RC). The SISO RC is considered to pass the field uniformity requirements when the STD for the three individual field components (E_x , E_y , and E_z) and the total data set (E_{Total}) from the 8 locations (corners of the working volume) are within the specified tolerance; i.e., within a limit of 3 dB for the STD above 400 MHz, increasing linearly with the frequency to 4 dB at 100 MHz. This specified tolerance determines the operation frequencies of a conventional RC, and it can be used only above the C-LUF (a conventional RC is unusable in the transition region).

A MIMO RC is designed to increase the field uniformity in the transition region, thus extending the range of operation frequencies. Although the MIMO validation procedure is based on the STD method, and is similar to the conventional procedure, they are different in some respects. The idea of the MIMO validation procedure comes from the author's observation that some requirements of the conventional validation procedure which can be weakened in order to allow a RC to be used below the C-LUF:

- 1) It might not be necessary to quantify field uniformity as good as a standard [9] requires. The requirement is due to some freedom allowed in the placement of the EUT; i.e., it can be placed anywhere in the working volume.
- 2) The field can be more uniform, if more resonances are stirred. So, using multiple (receiving) antennas to excite as many resonances as possible should increase the field uniformity below the C-LUF.

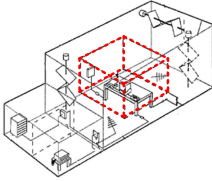
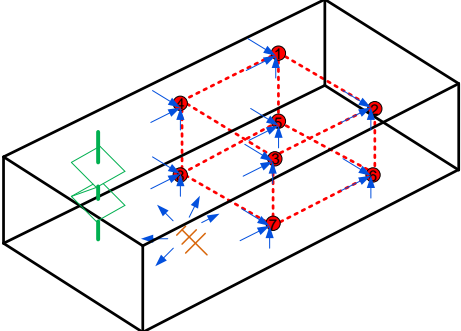
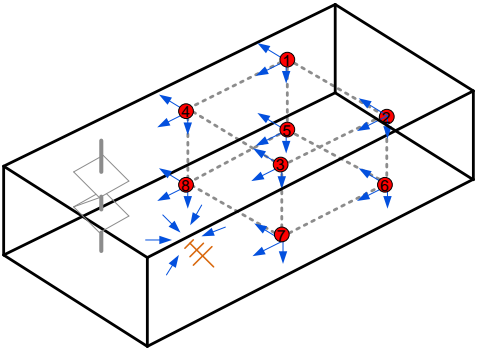
From the considerations above, the proposed MIMO validation procedure, which is equivalent to a SIMO communication system, should be able to increase the field uniformity even in the transition region, as there are more propagation modes excited by the multiple receiving antennas, and by moving the EUT. Table 4-2 explains the step-by-step modification from a SISO system (e.g., the conventional validation procedure) to a SIMO system (e.g., the MIMO validation procedure). Lastly, when the EUT is successively placed at multiple positions, the SIMO system will be transformed into a MIMO system.

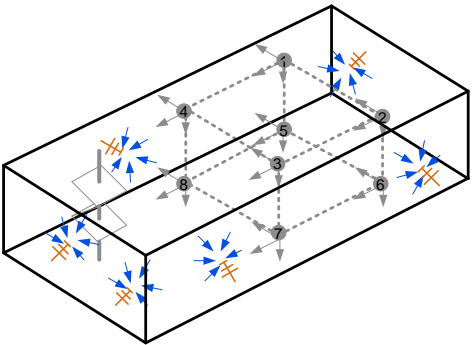
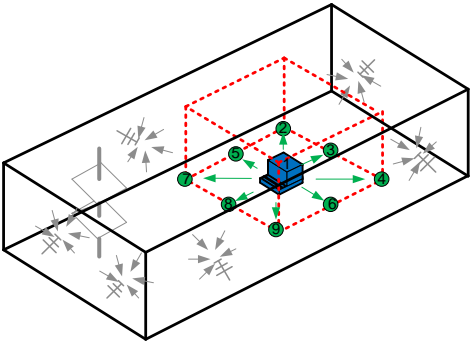
Table 4-1: Implementations of SISO - MIMO Validation Procedures.

	SISO link (Conventional RC)	SIMO link (MIMO RC)	MIMO link
Each corner of the working volume	Fixed position	<u>Fixed position</u>	-not applicable-
Receiving antennas	1 Antenna	<u>Multiple positions</u>	Multiple positions

In this Chapter, Section 4.2 shows implementations and equations. Section 4.3 explains how the MIMO validation procedure extends the lowest operation frequency of the scaled model. This novel MIMO validation procedure is concluded in Sect. 4.4, and is supported by simulated results; the Chapter summary is in Sect. 4.5.

Table 4-2: MIMO RC procedures.

Name	Concept of the system	Conditions and Details
<p>Conventional validation procedure (SISO) [9]:</p> 	<p style="text-align: center;"><u>SISO Link</u></p>  <p>This system is not usable below the C-LUF (confirmed in Sect. 4.3.1).</p>	<p>If the E-field in the working volume is uniform, the EUT can be placed anywhere in this volume; then the antenna and the EUT do not need to be moved.</p> <p>24 sets of data^a (8 corners \times 3 polarisations) are collected from receiving antennas.</p>
<p>Modified SISO validation procedure:</p>	<p style="text-align: center;"><u>Modified SISO Link</u></p>  <p>Same as above; this system also cannot be expected to be usable below the C-LUF (explained in Sect. 4.3.1).</p>	<p>As the 1:5 scaled model is quite small, antennas are used instead of field probes due to their smaller size. Besides, putting Tx antennas at the corners is more intuitive for emission measurements.</p> <p>So the 24 sets of data^a (8 corners \times 3 polarisations) of the received signals from each corner can be measured at the single antenna.</p>

<p>MIMO validation procedure:</p>	<p style="text-align: center;"><u>SIMO Link</u></p>  <p>Better field uniformity can be expected below the C-LUF, ideally down to the first resonance frequency (explained in Sects. 4.3.2 and 4.4).</p>	<p>Multiple (9) receiving antennas are installed to pick up the signal from each corner of the working volume. The pair with the lowest path loss will be selected (only the maximum data is being used in Eq. F.1) to increase the field uniformity.</p> <p>216 sets of data^a (8 corners \times 3 polarisations \times 9 antennas) will be processed with a modified method, based on the previous (SISO) method.</p>
<p>MIMO emission measurements:</p>	<p style="text-align: center;"><u>MIMO Link</u></p>  <p>After verifying the field uniformity in the transition region, moving the EUT should allow the RC to make emission measurements in the region, even if the field uniformity is poor (explained in Chap. 5).</p>	<p>This is for an emission measurement where multiple receiving antennas are used, and the EUT is placed at multiple positions in the working volume (Chap. 5).</p> <p>So 216 sets of data^a (8 corners \times 3 polarisations \times 9 antennas), multiplied by positions of the EUT, will be processed to determine the radiated power of the EUT.</p>

^a 1 set of data must be multiplied by the number of points in the FRI, and also by the number of stirrer steps. For example, in this case, there are 1,601 numbers of points from 300 MHz to 1 GHz, and 80 stirrer steps (per revolution) are used. So, there are 128,080 data points in 1 data set.

Guidelines: According to Table 4-2, the proposed MIMO validation procedure is actually a SIMO link. Therefore, recommendations for setting up the proposed MIMO validation procedure are given as follows:

- 1) **Stirrer:** at least 1 physical stirrer is strongly recommended. Without any stirrers, the chamber becomes a SSRC [35], whose performance is worse than a RC with a stirrer installed. SSRC is discussed and explained in Section 4.4.2;
- 2) **Multiple Receiving Antennas:** these must be linearly polarised antennas, and placed at maximum field strength locations around the chamber. These positions can be located with a program simulating the *E*-field distribution (Sect. 3.2). It is strongly recommended that antennas should be placed for all three polarisations, and that they should not be placed too close to each other;
- 3) **Calibrating Set:** 8 Transmitting Antennas (adjustable for 3 polarisations: X, Y, and Z) are still needed, and placed at the 8 corners of the Working Volume — as in the Conventional Validation Procedure;
- 4) **Working Volume:** this volume (a cubic shape is recommended) should not be too large, as it might be dominated by (i.e., too close to) any of the multiple antennas. It should not be too small, as it might not have enough space for placing the EUT. The boundaries of the working volume should be $\lambda/4$ at the C-LUF (not the MIMO-LUF) from the chamber walls, and from any antenna, stirrer, or other objects;
- 5) **System:** an automated system that is controlled by a computer program is recommended, as there are too many data points to be collected. It is practically impossible to collect all the data manually. Also, using stepper motors ensures that the measurements will be more accurate.

4.2 Setups and Procedures

4.2.1) Setups:

Even though there are 9 receiving antennas installed on the Scaled Model, only one receiving antenna port will be selected each time to measure signals from transmitting antennas at the 8 corners of the working volume (Fig. 4-1). The other

receiving antennas will be set to “open” by reflective switch boxes to increase the Q_g (as explained in Sect. 3.3). The system is controlled by MATLAB scripts.

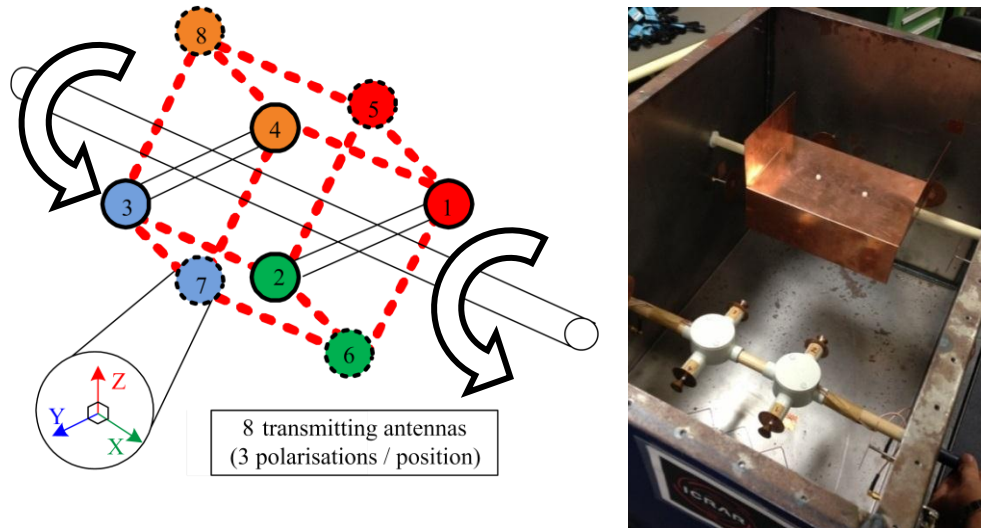


Figure 4-1: The Working Volume defined by the Validation Set.

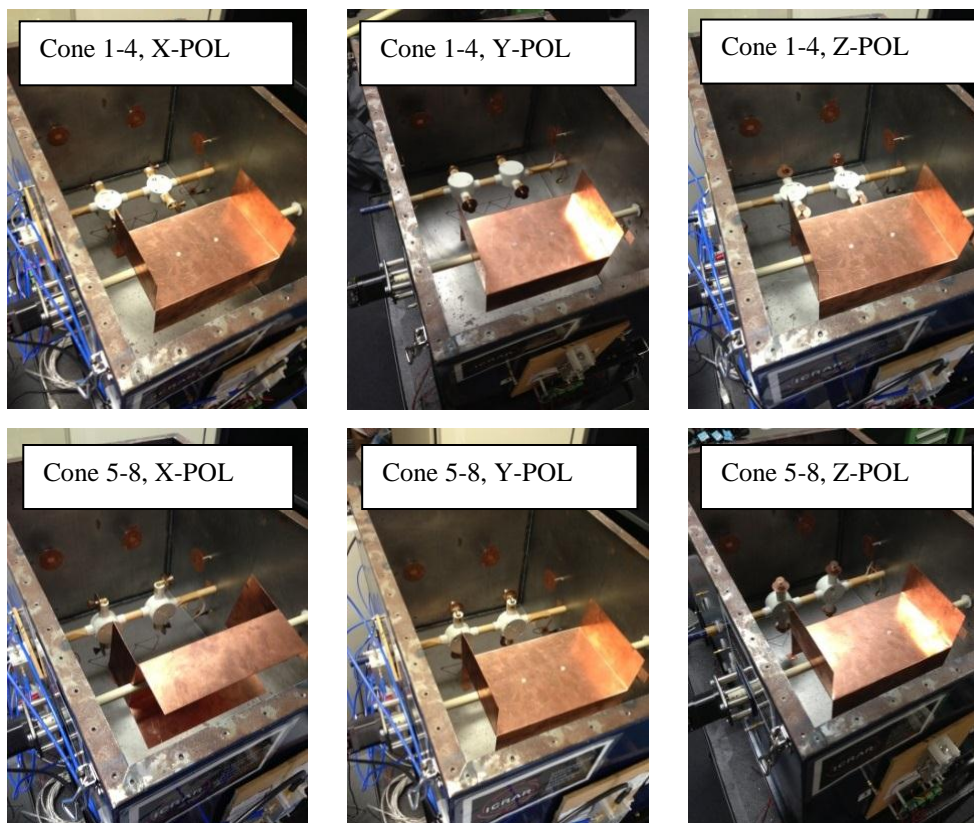


Figure 4-2: Setting up for validation procedures.

4.2.2) The Procedures

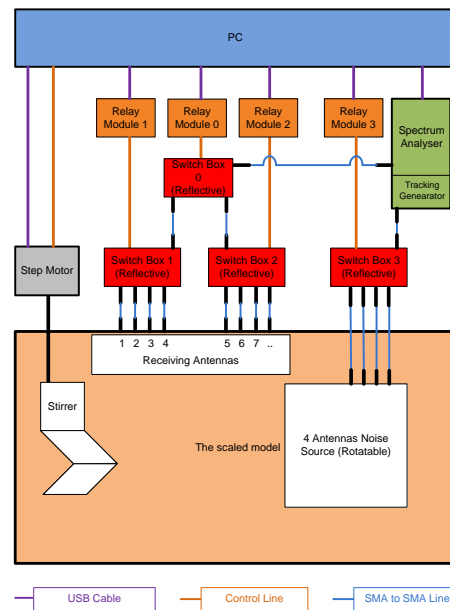


Figure 4-3: Connection diagram of the validation procedures.

The Process:

- 1) Starting from the first transmitting antenna, one polarisation is selected and powered;
- 2) The stepper motor brings the stirrer to the desired position;
- 3) Record the maximum received signal at the first receiving antenna, and so on, until the signals at all receiving antennas have been measured. For example, in this research, there are 9 receiving antennas in total;
- 4) Repeat the above procedure (from 1 to 3) again, the second transmitting antenna is selected, and so on, until all 8 transmitting antennas have been used;
- 5) Rotate the stirrer by a certain amount, and measure the signals at all receiving antennas (repeat the above procedure (from 1 to 4)); this process is repeated until a full revolution of the stirrer has been completed. It is recommended by [9] that the minimum number of positions should be 12 per revolution. However, this research used 80 positions per revolution (4.5 degrees per step);
- 6) Repeat the above procedure (from 1 to 5) again, to complete all 3 polarisations of transmitting antennas.
- 7) For MIMO RC (SIMO system), repeat the above procedure (from 1 to 6) again, to complete all receiving antennas.

Analysis of the results (based on the Conventional Procedure, Appendix F):

- 1) Normalise each of the maximum received signals by;

$$\vec{P}_{x,y,z} = \frac{P_{max\ x,y,z}}{P_{mean}}, \quad (4.1)$$

where:

$\vec{P}_{x,y,z}$ is the normalised maximum received power (W), defined as the maximum received signal from all receiving antennas over one stirrer revolution, divided by the input power, while Tx antenna polarised for X, Y or Z.

$P_{max\ x,y,z}$ is the maximum received signal of all receiving antennas, over the stirrer revolution; i.e., from 17,280 SISO sets of measured results (8 corners \times 3 polarisations \times 9 receiving antennas \times 80 stirrer steps),

P_{mean} is the average received power (W) in which $P_{Max\ x,y,z}$ is recorded.

- 2) Calculate the average of the normalised maximum values for each polarisation of the cone antennas;

$$\langle \vec{P}_x \rangle_8 = \frac{(\sum \vec{P}_x)}{8}, \quad \langle \vec{P}_y \rangle_8 = \frac{(\sum \vec{P}_y)}{8}, \quad \langle \vec{P}_z \rangle_8 = \frac{(\sum \vec{P}_z)}{8}, \quad (4.2)$$

where:

$\langle \ \rangle$ denotes the arithmetic mean across a number of antenna positions and/or antenna axes.

- 3) Calculate the average of the normalised maximum of all the measured data;

$$\langle \vec{P} \rangle_{24} = \frac{(\sum \vec{P}_{x,y,z})}{24}, \quad \sum \vec{P}_{x,y,z} = \sum \vec{P}_x + \sum \vec{P}_y + \sum \vec{P}_z, \quad (4.3)$$

where:

$\langle \ \rangle$ denotes the arithmetic mean across all axes (X, Y, and Z).

- 4) The field uniformity is specified as standard deviation (STD) from the normalised mean value of the normalised maximum values obtained at each of the eight locations during one stirrer rotation. The STD is calculated using data from each polarisation independently, and the total data set.

For example, for the X-vector:

$$\sigma_x = \sqrt{\frac{\sum(\vec{P}_{x,i} - \langle \vec{P}_x \rangle_8)^2}{8-1}}, \quad (4.4)$$

where:

- $\vec{P}_{x,i}$ is the individual measurement of X vectors,
 $\langle \vec{P}_x \rangle_8$ is the arithmetic mean of the normalised $P_{Max\ x}$ vectors for all eight measurement locations, and
 σ_x is the standard deviation of all X vectors.

And for all the vectors:

$$\sigma_{24} = \sqrt{\frac{\sum_{m=1}^8 \sum_{n=1}^3 (\vec{P}_{m,n} - \langle \vec{P} \rangle_{24})^2}{24-1}}, \quad (4.5)$$

where:

- $\vec{P}_{m,n}$ is the individual measurement of all vectors ($m =$ transmitting antenna locations 1 – 8, and $n =$ isotropic probe axes 1-3, i.e., x , y , and z),
 $\langle \vec{P} \rangle_{24}$ is the arithmetic mean of the normalised $P_{max\ x,y,z}$ vectors from all 24 measurements, and
 σ_{24} is the standard deviation of all vectors (X, Y, and Z).

Finally, the standard deviation is expressed relative to the mean, and then converted to dB:

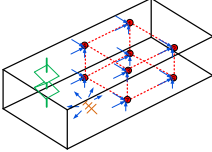
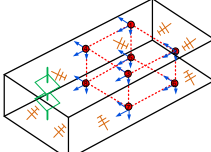
$$\sigma(dB) = 10 \log_{10} \left\{ \frac{\sigma + \langle \vec{P}_{x,y,z} \rangle}{\langle \vec{P}_{x,y,z} \rangle} \right\}, \quad (4.6)$$

- 5) The chamber passes the MIMO field uniformity requirement if the standard deviation for the X, Y, Z and total data set ($\sigma_x, \sigma_y, \sigma_z$, and σ_{24}) are within the specified tolerance (this is later analysed, and given in Table 4-4); e.g. within a limit of 4 dB from the standard deviation above 400 MHz, increasing linearly with the logarithm of the frequency, to 5 dB at 100 MHz. If the margin by which the chamber fails to meet the criteria is small, it may still be possible to meet the requirements by:

- Increasing the stirrer steps per revolution by 10% to 50%, and / or
- Reducing the size of the working volume.

All equations are summarised in Table 4-3. The equations of the MIMO validation procedure are based on those of the conventional (SISO) validation procedure.

Table 4-3: Comparison of all equations.

Equation / concept	Conventional Validation procedure (SISO Link)	MIMO Validation procedure (SIMO Link)
	 <p>24 SISO data sets (8 corners \times 3 polarisations) are used in the process.</p>	 <p>216 SISO data sets (8 corners \times 3 polarisations \times 9 antennas) are used in the process.</p>
Normalise each maximum signal over 1 stirrer revolution	$\vec{E}_{x,y,z} = \frac{E_{Max\ x,y,z}}{\sqrt{P_{Input}}}$ <p>*E_{Max} is the maximum received value over 1 revolution of stirrer(s).</p>	$\vec{P}_{x,y,z} = \frac{P_{Max\ x,y,z}}{P_{Mean}}$ <p>*P_{Max} is the maximum received value of 9 antennas over 1 revolution of stirrer(s).</p>
Normalise values in terms of dB	$\vec{E}_{x,y,z}(\text{dB}) = 20\log_{10} \left\{ \frac{E_{Max\ x,y,z}}{\sqrt{P_{Input}}} \right\}$	$\vec{P}_{x,y,z}(\text{dB}) = 10\log_{10} \left\{ \frac{P_{Max\ x,y,z}}{P_{Mean}} \right\}$
Average of the normalised maximum value of each axis	$\vec{E}_8 = (\Sigma \vec{E}) / 8$	$\vec{P}_8 = (\Sigma \vec{P}) / 8$
Average of the normalised maximum value of all	$\vec{E}_{24} = (\Sigma \vec{E}_{x,y,z}) / 24$	$\vec{P}_{24} = (\Sigma \vec{P}_{x,y,z}) / 24$
Standard deviation of individual axis	$\sigma = \sqrt{\frac{\Sigma(\vec{E}_i - \langle \vec{E} \rangle)^2}{n-1}},$ <p>For example, $\sigma_x = \sqrt{\frac{\Sigma(\vec{E}_{x,i} - \langle \vec{E}_x \rangle_8)^2}{8-1}}$</p>	$\sigma = \sqrt{\frac{\Sigma(\vec{P}_i - \langle \vec{P} \rangle)^2}{n-1}},$ <p>For example, $\sigma_x = \sqrt{\frac{\Sigma(\vec{P}_{x,i} - \langle \vec{P}_x \rangle_8)^2}{8-1}}$</p>
σ of total data set	$\sigma_{24} = \sqrt{\frac{\Sigma_{m=1}^8 \Sigma_{n=1}^3 (\vec{E}_{m,n} - \langle \vec{E} \rangle_{24})^2}{24-1}}$	$\sigma_{24} = \sqrt{\frac{\Sigma_{m=1}^8 \Sigma_{n=1}^3 (\vec{P}_{m,n} - \langle \vec{P} \rangle_{24})^2}{24-1}}$
σ in terms of dB	$\sigma(\text{dB}) = 20\log_{10} \left\{ \frac{\sigma + \langle \vec{E}_{x,y,z} \rangle}{\langle \vec{E}_{x,y,z} \rangle} \right\}$	$\sigma(\text{dB}) = 10\log_{10} \left\{ \frac{\sigma + \langle \vec{P}_{x,y,z} \rangle}{\langle \vec{P}_{x,y,z} \rangle} \right\}$
Requirement to meet the criterion	<p>σ is below a limit of 3 dB for the standard deviation above 400 MHz, increasing linearly with the log of the frequency, to 4 dB at 100 MHz.</p>	<p>σ is below a limit of 4 dB for the standard deviation above 400 MHz, increasing linearly, with the log of the frequency, to 5 dB at 100 MHz.</p>

* All the maximum and average values, maximum field strength must be in linear values (i.e., Watts, not dB).

4.3 Measured Results

4.3.1) Conventional Validation Measurements

The process:

- 1) One cone antenna (at X-polarisation) of the calibration set becomes a transmitting antenna (the other cones are opened) powered by the tracking generator (-10 dBm is set as the output power of the tracking generator);
- 2) The stepper motor brings the stirrer to the desired position, and only the first receiving antenna (Fig. 4-4) is selected to measure the signal by the spectrum analyser, and the signal is saved;
- 3) Then, the second cone antenna of the calibration set is selected to repeat the whole process, and so on until the last cone;
- 4) Then, the stepper motor rotates the stirrer by a certain amount (4.5° for each step, 80 positions for one revolution), and the signals are measured again;
- 5) This process is repeated for a full revolution of the stirrer. After that, all the above processes are repeated with Y and Z polarisations.

Finally, there are 1,920 sets of SISO data; i.e. 80 positions of the stirrer \times 1 receiving antenna \times 3 polarisations \times 8 cones. All results will be analysed and displayed using Graphical User Interfaces (GUIs).

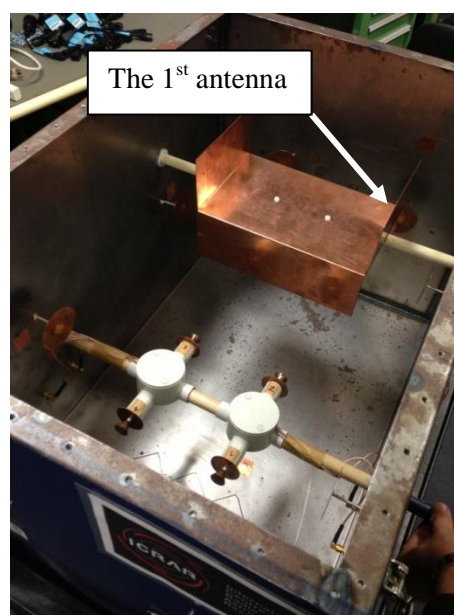


Figure 4-4: Setting up for the SISO validation procedure.

Figure 4-5 shows all received signals over one revolution of the stirrer, when cone 1 (X-polarisation) is the transmitting antenna and port 1 is the receiving antenna. The second highest values of those results will be used, instead of the highest maximum, for more stability. The second highest values of the received signals from cone 1 to cone 8 (X-polarisation) from each corner of the working volume are plotted in Fig. 4-6.

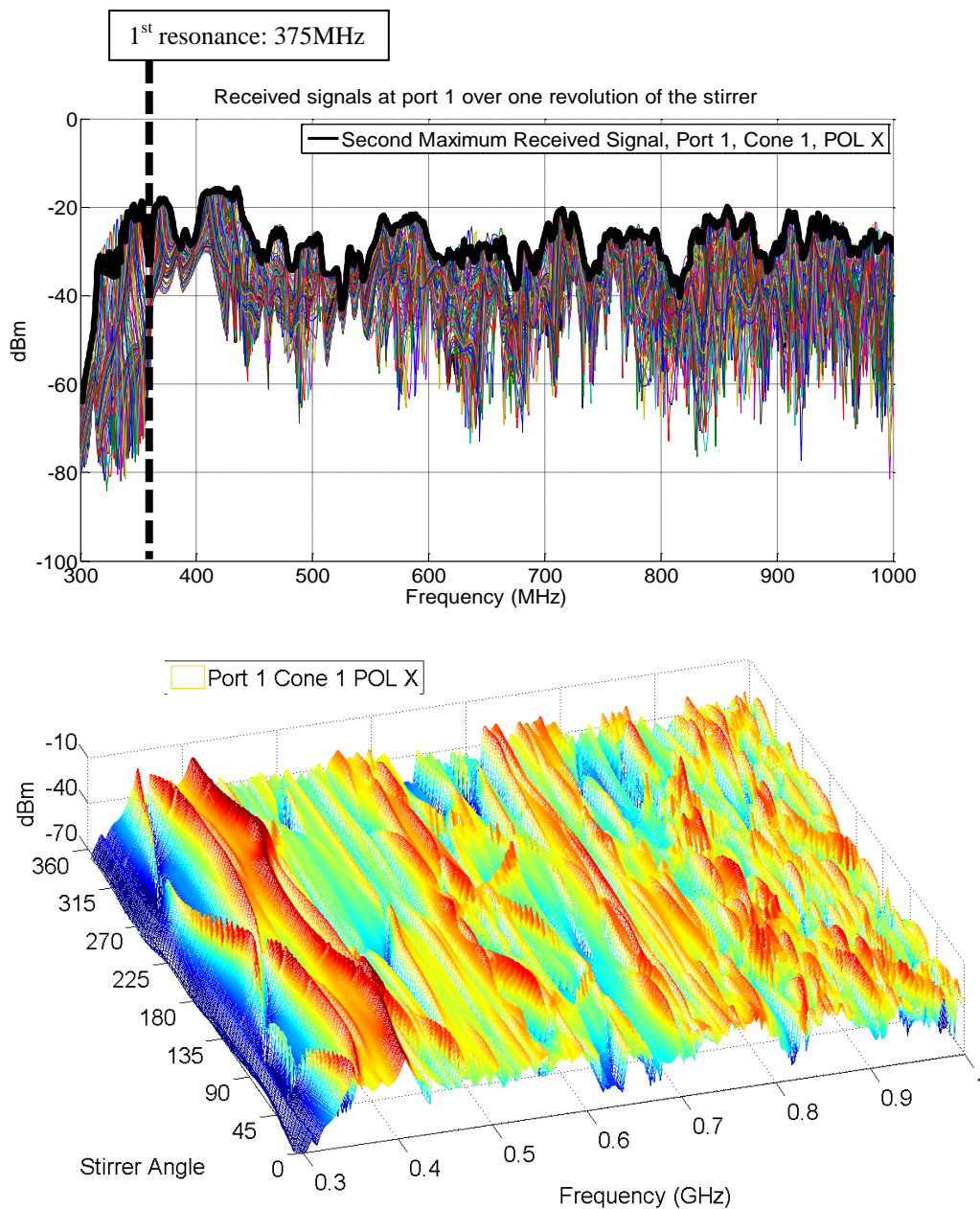


Figure 4-5: Signals received by antenna Port 1, X-polarisation.

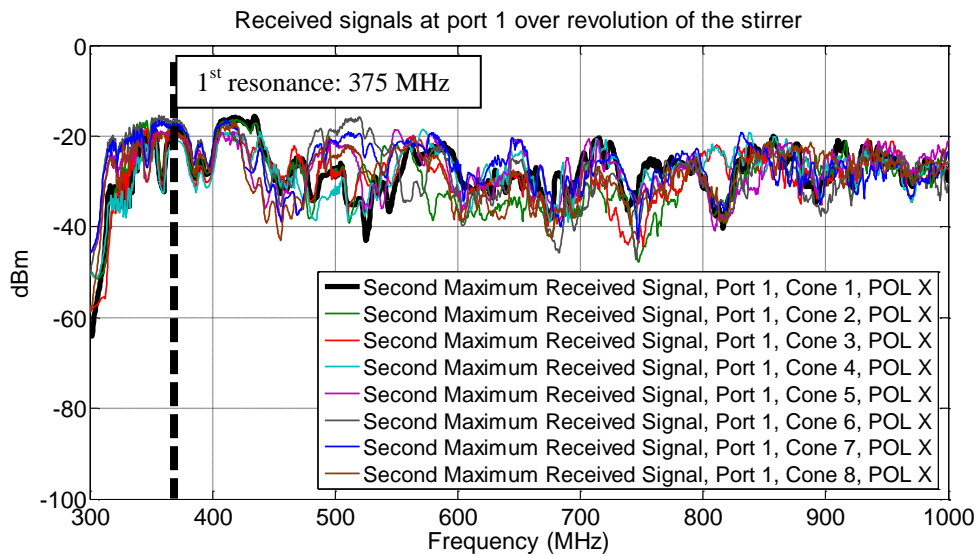


Figure 4-6: Maximum received signals (from 8 corners of the working volume) by receiving antenna Port 1, X-polarisation.

Then, the field components (E_x , E_y , and E_z) and the total data set (E_{Total}) processed by the GUI — following Sect. 4.2.2 — are shown in Fig. 4-7; none of them can meet the requirements of [9] in the transition region. In other words, most of them are over the proposed limit; this is as predicted for the Scaled Model, i.e. when strictly the following the IEC standard, this conventional RC method cannot work lower than the C-LUF, although the field shows better field uniformity at higher frequencies.

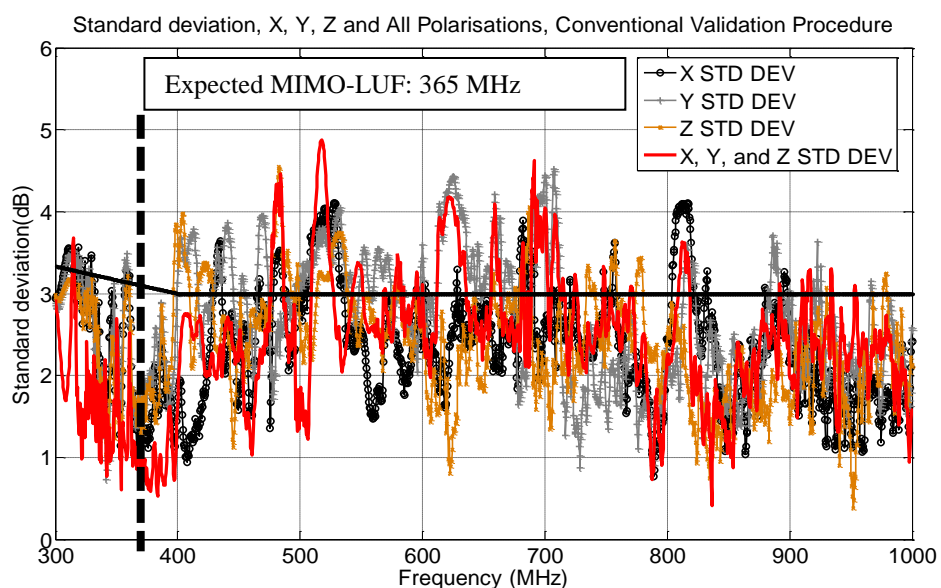


Figure 4-7: STDs of X, Y, Z and total over one revolution of the double C stirrer, following the IEC standard.

To sum up, this SISO validation procedure confirms the scaled model is not suitable as conventional RC below its C-LUF. In the results, there are too few resonances excited at low frequencies, resulting in poor field uniformity.

From Fig. 4-7, it can be concluded that:

- The STD results fail to meet the criteria below the C-LUF. All STDs of P_x , P_y , P_z , and P_{Total} are over the proposed limit in the transition region;
- At high frequencies, near the C-LUF, the results almost meet the criteria, as expected;
- Although the results seem better at ~ 300 MHz, they actually are not. The reason is that their characteristics (reflection coefficients) are all worse at lower frequencies (see Fig. 3-28).
- As expected, the Scaled Model cannot work as a conventional RC below the C-LUF due to the limitations of standard (fixed position of the receiving antenna).

The Scaled Model, when following the Conventional Validation Procedure [9], which is a SISO link, is unable to be used below the C-LUF even with a double C stirrer implemented. The main reason is that using only one fixed-position receiving antenna cannot select/measure excited resonances in the transition region. It can be concluded that the limitation of the C-LUF comes from the conventional procedure itself, not from the performances of fittings or tools.

4.3.2) MIMO Validation Measurements

The MIMO validation procedure is a modified one based on the conventional (SISO) validation procedure. The setup for the MIMO validation procedure on the 1:5 Scaled Model is demonstrated in Fig. 4-8. All tools and instruments are the same as those used in the conventional validation procedure in Sect. 4.3.1, except multiple receiving antennas are used. Thus, comparison of both results can show the differences which arise from using these procedures only; there is no variation due to other factors.

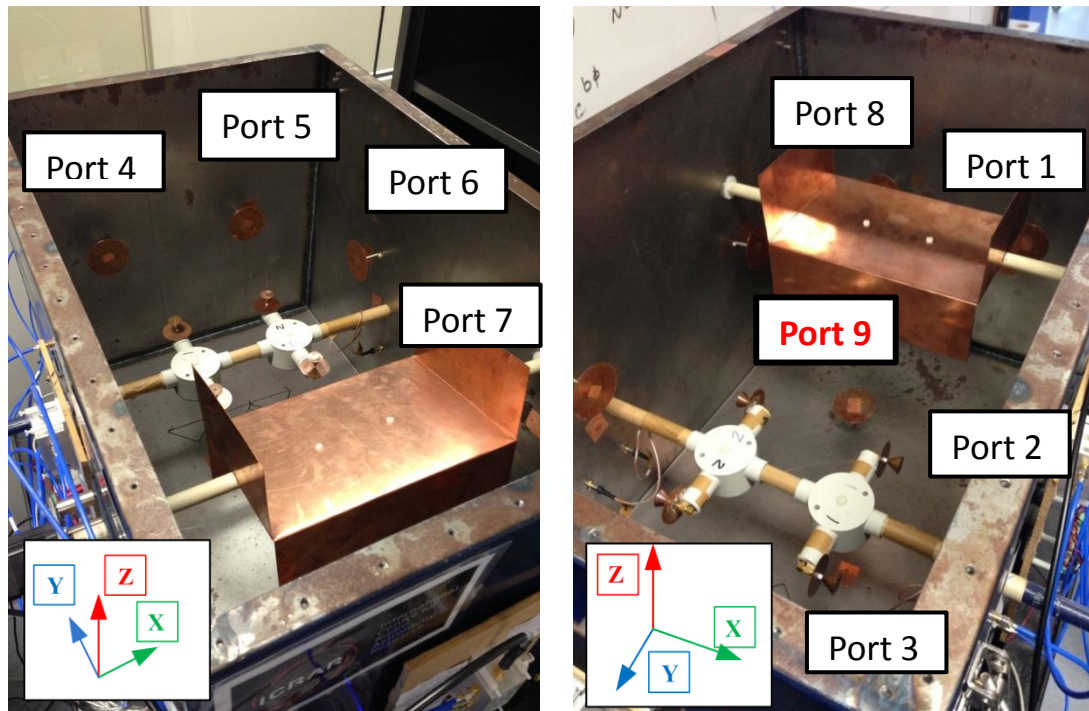


Figure 4-8: Setting up for the MIMO validation procedure.

The process:

The process is exactly the same as Sect. 4.3.1 except the second step, it is changed to be

“

2) The stepper motor brings the stirrer to the desired position, and only the first receiving antenna (Fig. 4-4) is selected to measure the signal by the spectrum analyser, and the signal is saved by all the 9 receiving antennas;

”

Therefore, there are 17,280 sets of SISO data; i.e. 80 stirrer positions \times 9 receiving antennas \times 3 polarisations \times 8 cones. Each set of SISO data consists of 1,601 numbers of points in the FRI (from 300 MHz to 1 GHz). Again, all collected data (more than 18 million individual points) are analysed by the GUI program.

In practice, this research investigates the MIMO validation procedure by using only 6 receiving antennas, due to reasons stated in Section 3.2.1, i.e. to optimise the number of receiving antennas, and to speed up the system. The receiving antennas are selected to cover all three polarisations. As a result, the 1st, 2nd, 3rd, 4th, 5th and 9th receiving antennas are chosen; the other receiving antennas are left as open ports. Only the maximum received signal (i.e., with the lowest path loss) will be analysed to calculate the STD, and determine the field uniformity.

As the results, field uniformity from MIMO validation procedure is shown in Fig. 4-9. This Figure clearly shows that the MIMO validation procedure (i.e., the use of multiple receiving antennas) can improve the field uniformity of the Scaled Model for the X, Y, Z and total polarisations (σ_x , σ_y , σ_z , and $\sigma_{x,y,z}$). Thus it has been demonstrated that the MIMO validation procedure can improve the field uniformity in the transition region.

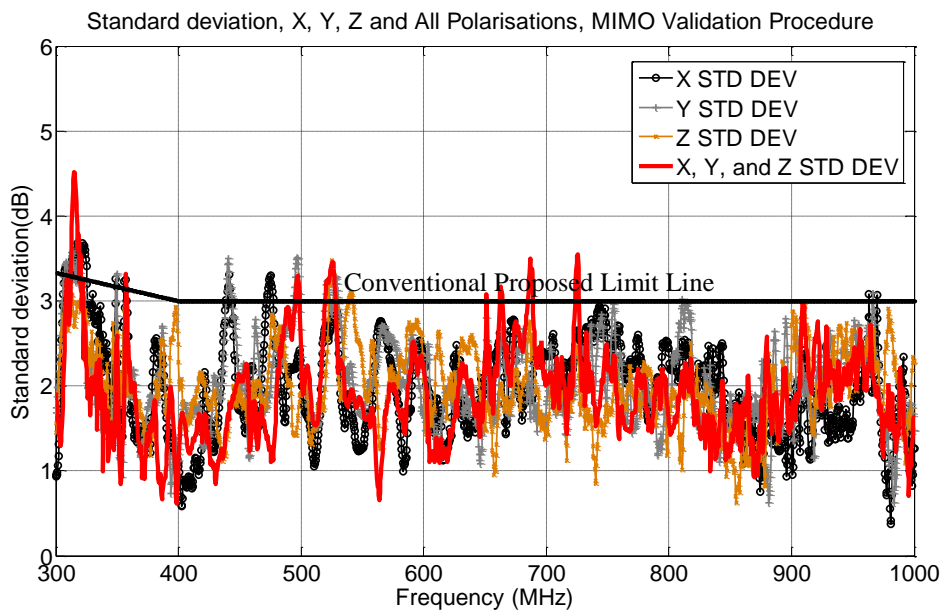


Figure 4-9: Standard deviations of X, Y, Z and total for the MIMO validation procedure. More measured results are available in Appendix E.

4.4 Analysis of the Measured Results

4.4.1) Analysis

A comparison of STDs, for Z polarisation, between following the conventional validation procedure and the MIMO validation procedure is shown in Fig. 4-10. The MIMO validation procedure shows good results for the whole transition region; i.e., no single frequency has a STD exceeding the required tolerance of [9] by more than 1 dB (Table 4-4). In following MIMO validation procedure, however, the field uniformity is still not good enough to pass the tolerance requirements (Table 4-4), although it is much better than for the conventional validation procedure. STDs at a few frequencies are over the proposed limit line; more resonances are still required to improve the field uniformity to make emission measurements.

In fact, emission measurements on the scaled model could be done because the EUT will be later moved to excite more resonances, i.e., make the SIMO (link) system become a MIMO (link) one. However, field uniformity of a MIMO RC cannot be checked after applying the strategy of moving the EUT; thus, this thesis recommends checking the field uniformity of a MIMO RC before making MIMO emission measurements (i.e. before moving the EUT) based on the conventional IEC standard limits (Table 4-4); i.e., the MIMO tolerance requirements can be a “loose” version of the SISO tolerance requirements.

As an arbitrary suggestion, The MIMO tolerance requirements, or “loose” version, are chosen 1 dB less strict than the conventional tolerance requirements stated in the Standard [9]. These modified “loose” criteria are used just as a reference to confirm that the field uniformity is still good enough to make MIMO RC emission measurements, i.e., by moving the EUT.

Table 4-4: Field uniformity tolerance requirements (Appendix F) [9].

Frequency range (MHz)	Tolerance requirements for standard deviation
80 to 100	4 dB ^a
100 to 400	4 dB at 100 MHz decreasing linearly to 3 dB at 400 MHz ^a
Above 400	3 dB ^a
^a A maximum of three frequencies per octave may exceed the allowed standard deviation by an amount not exceeding 1 dB above the required tolerance.	

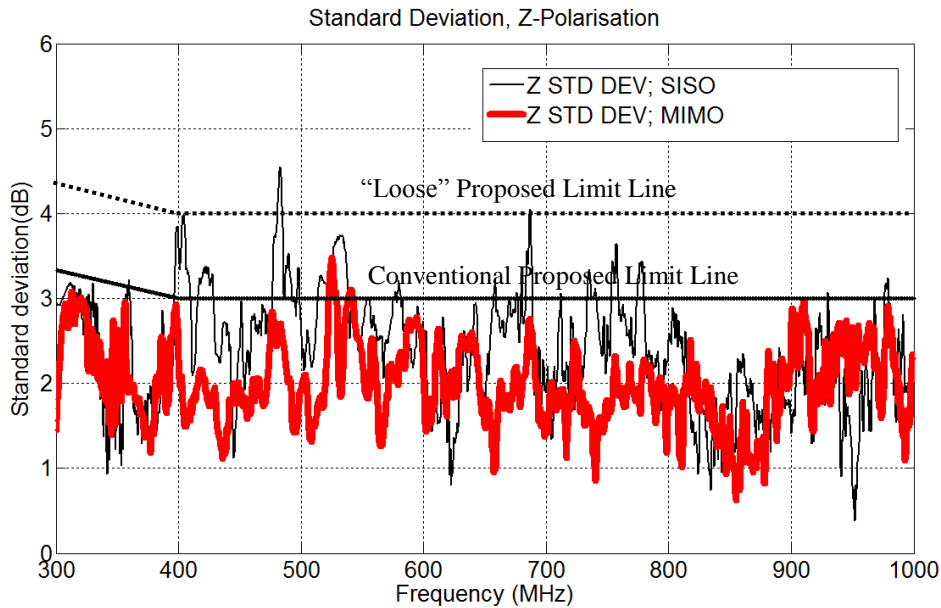


Figure 4-10: Comparison of σ_z between the conventional RC (SISO link) and MIMO RC (SIMO link) validation procedures.

4.4.2) Simulated Field Distribution

The simulated field distribution can reveal how multiple receiving antennas can improve the uniformity of the field distributions. The stirrer is removed (Fig. 4-11) in order to investigate how the field distributions are affected by using multiple receiving antennas only. The Scaled Model, after the stirrer is removed, becomes a Source Stirring Reverberation Chamber, or SSRC [35].



Figure 4-11: The Scaled Model without stirrer—this can be called a Source Stirring Reverberation Chamber (SSRC) [35].

Figure 4-12 shows the comparison of the field uniformity, for Y polarisation, with and without stirrers; the results clearly show that the stirrer can make the field more uniform (approximately 1-1.5 dB better). This Figure also shows that the MIMO RC is better than the SSRC in the transition region, and why using at least one physical stirrer is strongly recommended for a MIMO RC. The maximum difference between the results, with and without the stirrer, is at around 600-700 MHz. It can be theoretically assumed that the signals from the 8 corners of the working volume are the most different at these frequencies. In other words, there is at least radiation from one corner of the working volume which is relatively weak, while the rest of them are fine. Thus, 650 MHz will be selected to simulate the E-field inside the Scaled Model (using the ANSOFT HFSS simulation program).

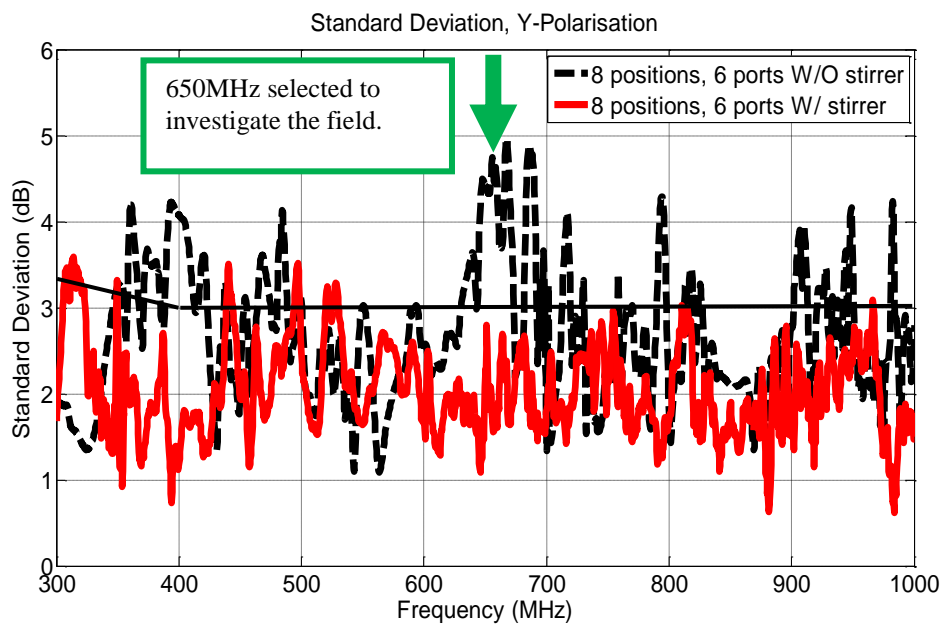
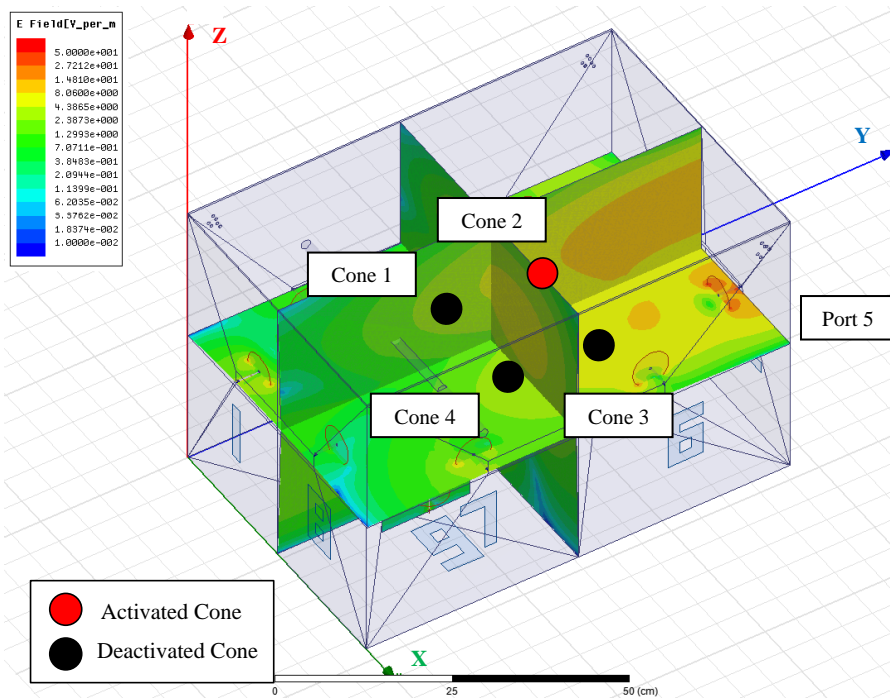


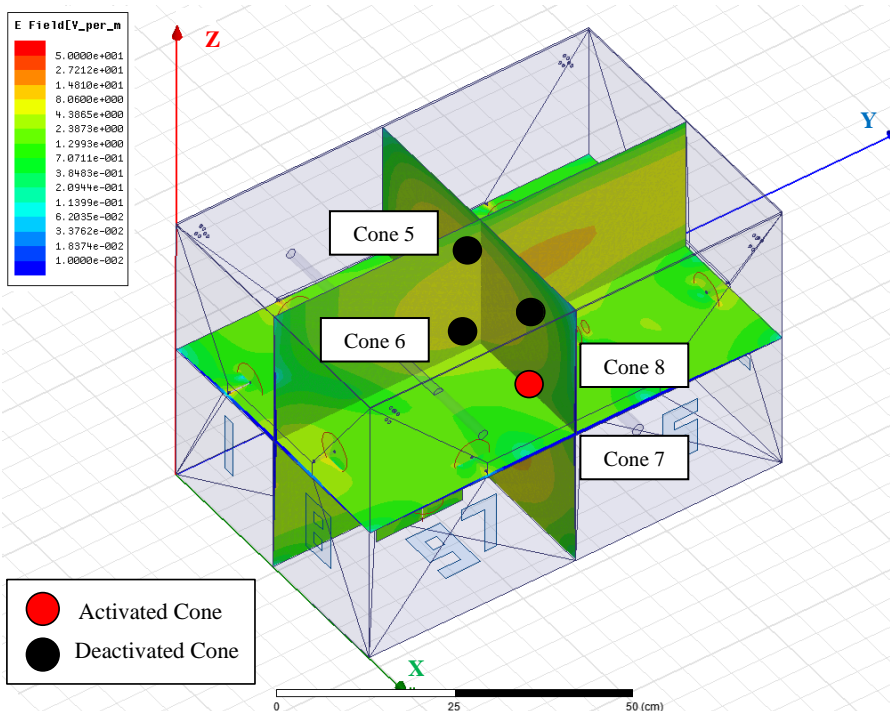
Figure 4-12: Measured STD of the Scaled Model, with and without the stirrer.

The field distribution pattern in the Scaled Model without the stirrer at 650 MHz, Y-polarisation, looks similar to the $TM_{1,1,2}$ mode (Fig. 3-13); thus, the 1st, 4th, 5th and 8th receiving antennas should be most able to pick up signals. Figure 4-13(a) shows that when cone 2 radiates, the 5th receiving antenna can pick up the best signal. The ANSOFT HFSS program also shows that when cone numbers 1, 2, 3, 4, 5, and 8 each radiate in turn, there is at least one receiving antenna which can pick up a strong signal. However, Fig. 4-13 (b) shows that when either cone 6 (or cone 7) radiates, none of the receiving antennas can pick up a good signal. When there is no receiving

antenna to pick up signals from the 2 corners (cone numbers 6 and 7), the field is not uniform at 650 MHz, as shown in Fig. 4-12.



a) When Cone 2, Y-POL, radiates, Port 5 receives a “VERY GOOD” signal.



b) When Cone 7, Y-POL radiates, all ports receive a “POOR” signal.

Figure 4-13: Field distributions at 650 MHz, Y-Polarisation.

The simulation results confirm the importance of using a physical stirrer, as well as multiple receiving antennas. They can effectively make a MIMO RC become usable in the transition region. Note: the colour scale in Fig. 4-13 is 10 times weaker than those in Chapters 2 and 3, as the radiation of the cone antennas is about 10 times lower than from the receiving antenna (Fig. 3-26). However, this will not affect the accuracy of the results, as their characteristics (i.e., S_{11}) are similar, and the purpose of the validation procedure is to measure the field uniformity (not absolute emissions).

4.5 Chapter Summary

According to the conventional RC method [9], the criterion of the SISO (conventional) validation procedure is to quantify the field uniformity within the working volume. After the field uniformity is verified, the EUT can be placed at any position in the working volume. In practice, the field uniformity is verified when the standard deviations (STDs) of the E -field of 3 mutually orthogonal axes ($\sigma_x, \sigma_y, \sigma_z$, and $\sigma_{x,y,z}$) at the corners of the working volume become better than a specified value; i.e. within a limit of 3 dB for the standard deviation above 400 MHz, increasing linearly with the frequency, to 4 dB at 100 MHz. This procedure determines the C-LUF; i.e., the chamber is unusable below the C-LUF, if the current conventional RC standards are strictly followed.

The C-LUF of the Scaled Model is about 1.2-1.4 GHz (Chapter 2). Following the conventional validation procedure (which uses a SISO link system) in Sect. 4.3.1, it was confirmed that the E -field within the working volume will not be uniform below the C-LUF. Section 4.3.2 shows that, after applying the MIMO validation procedure (which uses a SIMO link system), the E -fields of the Scaled Model in the transition region become more uniform than those in the conventional validation procedure. As a result, this research introduces a MIMO RC which can perform more effectively than a SISO (conventional) RC, with regard to the field uniformity below the C-LUF. A comparison of measured results clearly shows that using multiple receiving antennas can increase the field uniformity of a RC in the transition region.

The conclusions of this Chapter are as follows:

- 1) Following the conventional (SISO link system) validation procedure, the field uniformity is poor in the transition region.
- 2) Following the MIMO validation procedure (SIMO link system, using multiple receiving antennas; MO) can improve the field uniformity in the transition region.
- 3) Although the MIMO validation procedure can improve the field uniformity, there are still a few frequencies in the transition region which are not uniform enough to meet the conventional tolerance requirements (Table 4-3). A MIMO RC will require moving the EUT to improve/smooth the fields for making MIMO emission measurements. As a result, the field uniformity cannot be measured when the strategy of moving the EUT is applied for making MIMO emission measurements.
- 4) This thesis recommends that the MIMO RC fields should meet the suggested MIMO tolerance requirements, before applying the strategy of moving the EUT for MIMO emission measurements. This field uniformity validation is to confirm the positions of the receiving antennas, stirrer, and working volume as a kind of a reference, with somewhat less stringent than for the conventional tolerance requirements. The MIMO tolerance requirements are suggested to be a “1 dB loose version” of the conventional tolerance requirements (i.e., the MIMO RC validation limit is set 1 dB higher than the conventional RC limit—see Table 4-4).

CHAPTER 5

MIMO RADIATED EMISSION MEASUREMENTS

“For emissions measurements, the typical primary quantity of interest is the average transmitted radiated power density, integrated over all spatial directions and propagation and polarisation. Occasionally, the maximum power density, or the field strength (average or maximum) is the quantity of interest that can be derived from the measured transmitted power.”

- IEC Standard 61000-4-21:2011

5.1 Introduction

The MIMO validation procedure, which uses a SIMO communication link, is explained in Chapter 4. Using a double C stirrer can increase the field uniformity in the transition region, although fields at some frequencies are not as uniform as required. In other words, the E -fields of 3 mutually orthogonal axes (x , y , and z) in the working volume have not met the lowest acceptable field uniformity, as specified in the conventional RC requirements. This means that different positions of the EUT in the working volume might give different measured results. A technique to smooth these different results is required to increase measurement accuracy; and the previous conventional field uniformity requirements need to be replaced by new ones for MIMO RCs. This can be summed up by: (1) using multiple receiving antennas (MO) is to increase field uniformity, and (2) changing EUT positions (MI) is to make emission measurements more reliable when field uniformity cannot be improved anymore.

When the EUT is moved from one position to another, as the fields in the chamber are slightly over the tolerance requirements (Sect. 4.3.2), the measured signals can be different between each EUT position. Some of those measured results (i.e., from few EUT positions) will be further away from the mean value than others. Thus, using the mean value, calculated from different EUT positions, should provide more accurate emission measurements for a MIMO RC. Thus, MIMO emission measurements should follow certain procedures to find the best possible emission estimates among those different results. In practice, the key procedures are as follows:

- 1) Procedure to change the position of the EUT (Sect. 5.2.1); for instance, moving or rotating the EUT;
- 2) Procedure to process the measured results (Sect. 5.2.2): i.e., a strategy to find the best possible emission estimates from the different results generated by moving the EUT position.

5.2 Procedure Developments

5.2.1) Procedure to move the EUT:

First of all, a solution needs to be designed for how to change the position of the EUT, e.g., moving or rotating. Two examples for measurement and radiation procedures from existing standards are given. In the case of TEM cells, as only one polarisation can be done at a time, the EUT needs to be successively rotated to each of the 3 polarisations; i.e., choose any column in Fig. 5-1 [82], finish that column for a complete measurement, and use Eq. 2.1 to find the final result. In other words, rotating the EUT is a “must do” for TEM cells.

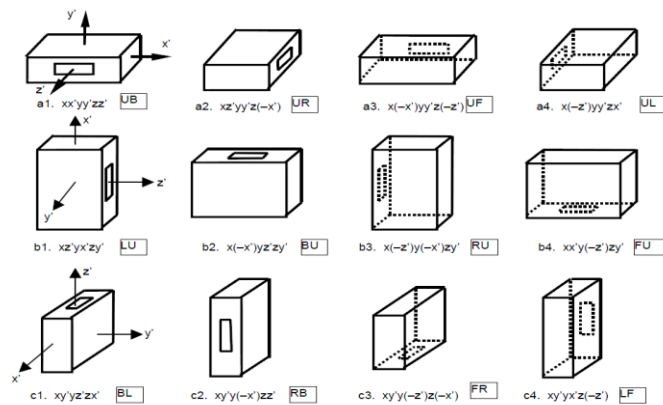


Figure 5-1: Canonical 12-face/axis orientations for a typical EUT for TEM cells [82].

Another technique, in the case of ACs, uses the concept of a Uniform Field Area (UFA), shown in Fig. 5-2, which is used for the calibration of the field [63]. A field is considered uniform if its magnitude measured at grid points is within ± 0 dB of the nominal value for not less than 75 % of all grid points (e.g. if there are at least 12 of the 16 points of an $1.5 \text{ m} \times 1.5 \text{ m}$ UFA measured within the tolerance).

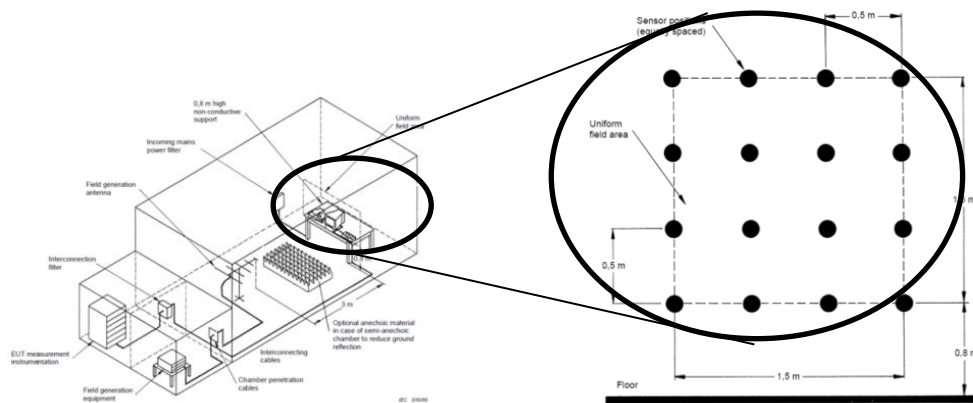


Figure 5-2: Concept of a Uniform Field Area (UFA), in ACs [63].

Rotating the EUT in TEM cells (Fig. 5-1), and verifying a uniform field area in ACs (Fig. 5-2), are the “key” techniques for the two methods. A MIMO RC has a Rayleigh distribution [24, 25, and 26]; thus, moving the EUT is theoretically more suitable for a MIMO RC, than rotating the EUT. In addition, the simulated results in Fig. 2-27 show that moving the EUT can excite different resonances below the C-LUF. However, tests should be done to confirm that moving the EUT is more suitable to be adopted on MIMO RC.

Making tests [96]: a battery-operated broadband noise source in a hollowed biconical antenna is made, and used as the EUT. A noise source (generator), a battery and 2 amplifiers are placed inside the antenna, with overall dimensions of 150×120 mm; the smallest diameter of the cone is 30 mm, and the widest diameter is 120 mm. There is no cable from the chamber walls (in the 1:5 Scaled Model) to the biconical antenna, which could result in resonances; thus, there are no resonance effects due to cables or the transmitting system below 1,000 MHz. The schematic diagram, radiated power, and radiation pattern of the biconical noise source are shown in Fig. 5-4. The radiated power is about -50 dBm and the antenna is linearly polarised. It must be noted that simulated result, and Z_{in} measured results (Fig. 5-4 b) are combined with input power (forward power) generated from the noise generator.

The biconical Noise Source is well designed (see Fig. 5-3). The radiated power is smooth, and the radiation pattern is similar over the whole transition region (from 300 MHz to 1,000 MHz), as shown in Fig. 5-4. The noise source is placed inside the

working volume of the Scaled Model (Fig. 5-5) in 9 different configurations (3 positions \times 3 polarisations). The measured results are processed and shown in Figs. 5-6 to 5-7.

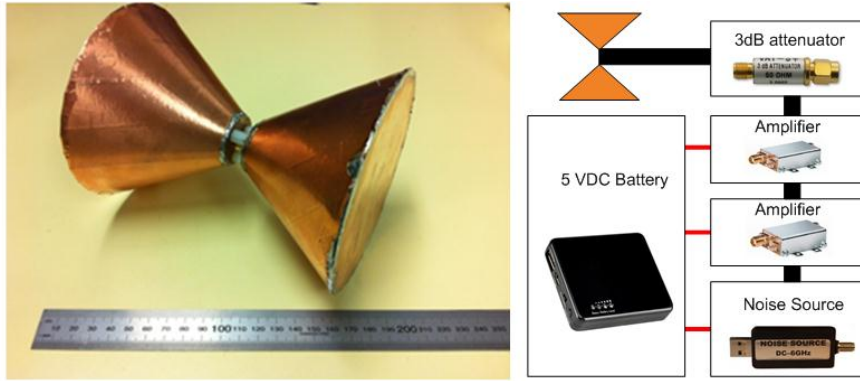


Figure 5-3: The Biconical Noise Source.

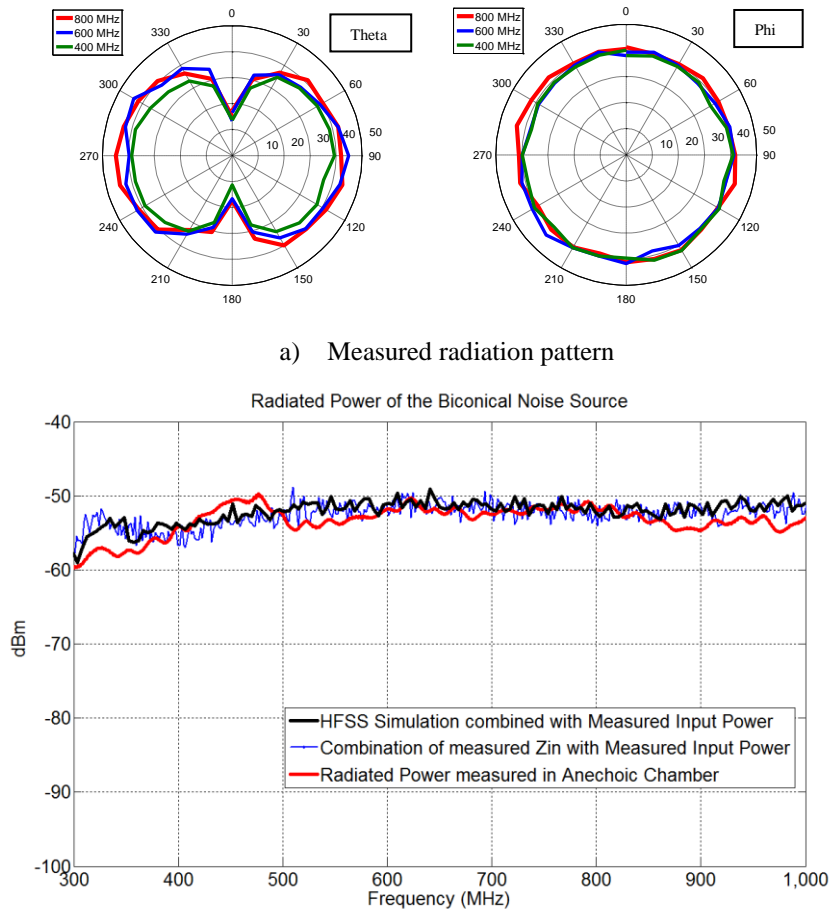


Figure 5-4: Characterisations of the Biconical Noise Source.

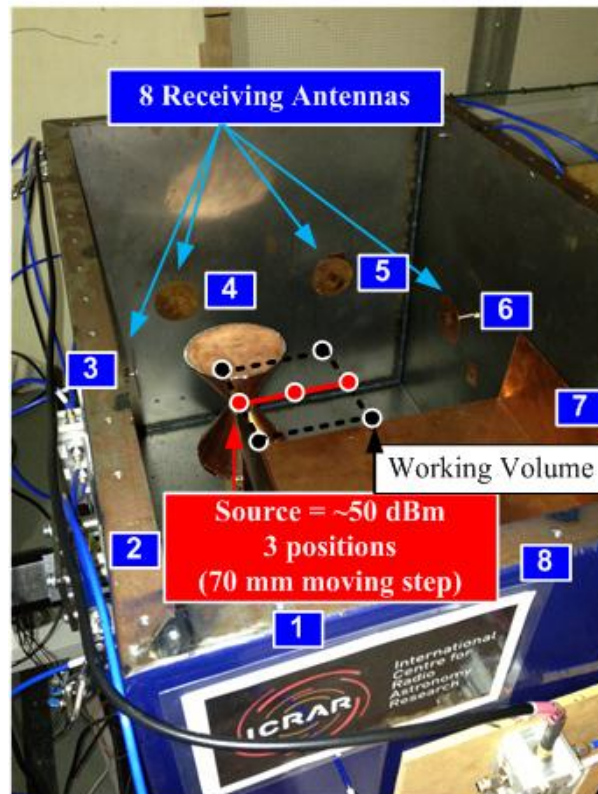


Figure 5-5: The Biconical Noise Source placed for 3 positions \times 3 polarisations.

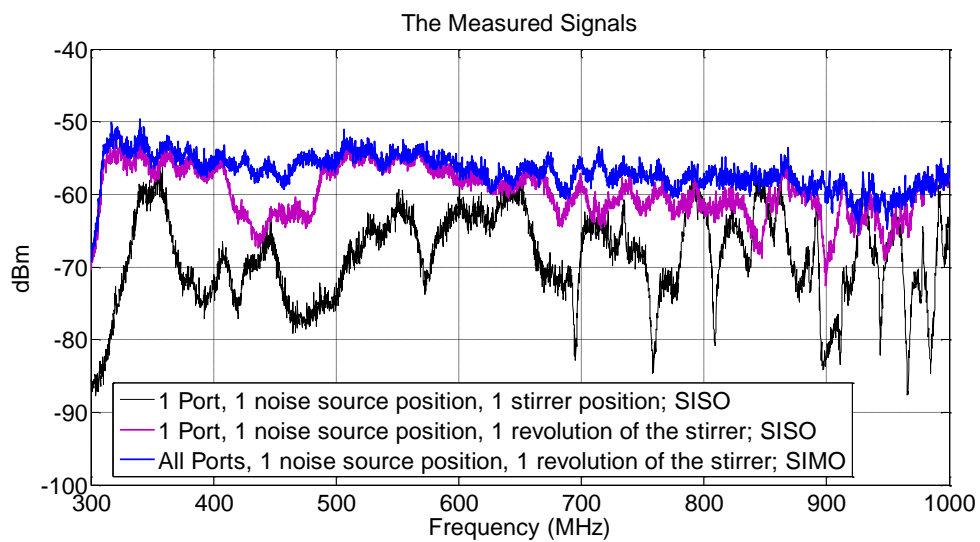
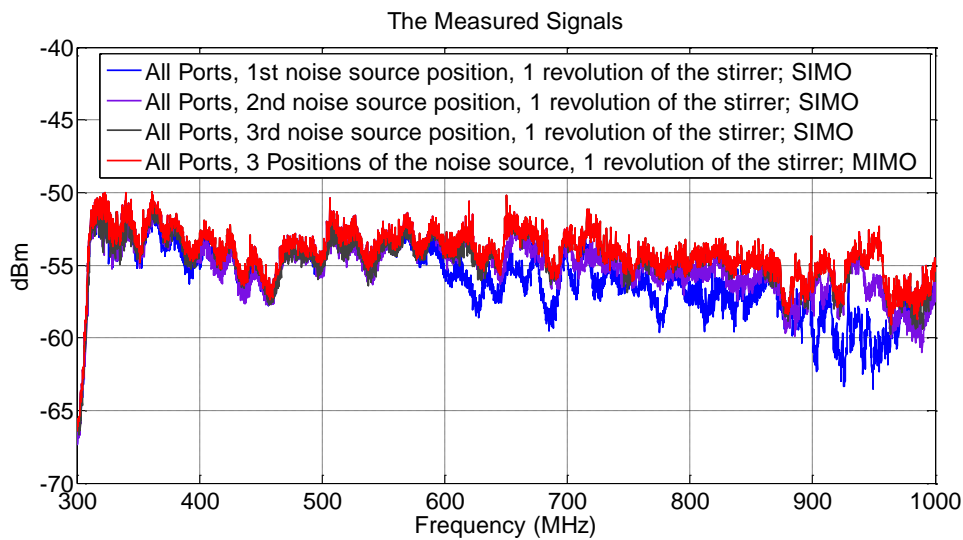
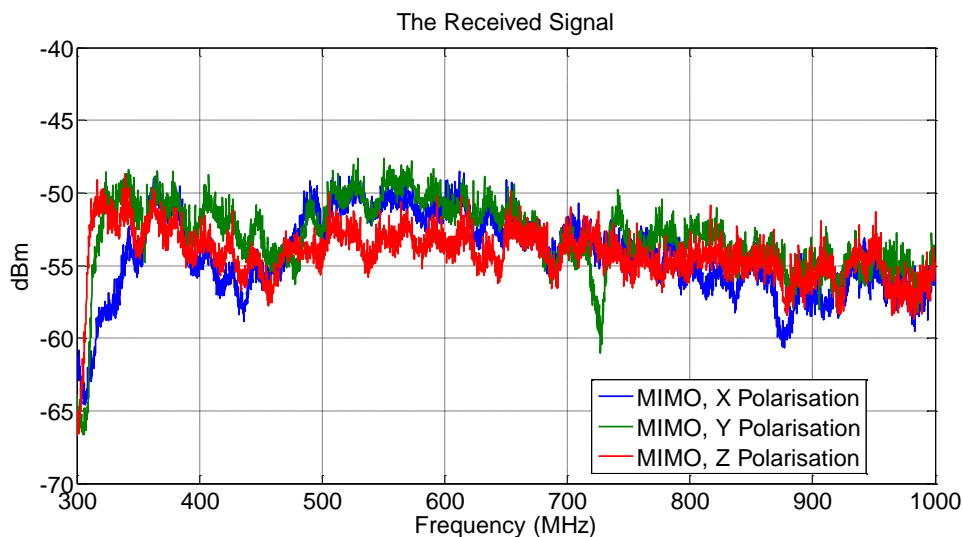


Figure 5-6: Maxima of eight SISO results (receiving antennas, raw results without CVF).



(a) Maxima of three SIMO result becomes one MIMO results, Z-polarisation.



(b) MIMO, 3 polarisations.

Figure 5-7: Comparisons of SIMO and MIMO results (Q_g is not compensated).

Conclusions of the tests: the results could be another indication that a stirrer is needed in MIMO RC (this was confirmed by the simulation program in Sect. 4.4.2); the maximum values over all 80 stirrer angles are much smoother than the signals for individual stirrer angles (see Fig. 5-6). However, using only one receiving antenna (i.e., single-input and single-output (SISO) — shown as the purple line in Fig. 5-6), even at the high frequency end the variation is more than 15 dB for port 1, which is not as smooth as in Fig. 5-4. Now considering all receiving antennas (i.e., single-input and multiple-output, SIMO) in Fig. 5-6, their output is smoother than those from the

individual ports. Moreover, using the concept of multiple-input and multiple-output (MIMO), i.e. a combination of moving the EUT and using multiple receiving antennas (see the red line in Fig. 5-7), an even smoother noise spectrum can be derived from the power maxima than for the SISO and SIMO cases, at the resonance frequencies. After completing the Z polarisation, the whole measurement process is repeated again with the EUT placed in the X and Y polarisations. Figure 5-7 shows that the variation of each polarisation is less than ~ 5 dB, which indicates that each of the 3 polarisations can provide similar results.

Decision made on moving the EUT: Fig. 5-7 shows that rotating the EUT can be a partial solution, while moving the EUT can adequately smooth the results (if the EUT is placed at sufficiently many positions). Moreover, rotating the EUT is often not easy in practice, due to the size, dimensions, and shapes of most equipment. As a result, moving the EUT has been decided to be suitable for a MIMO RC.

Therefore, the procedures for moving the EUT are as follows:

- 1) Moving the EUT should cover most of the MIMO RC working volume;
- 2) The EUT should be moved in a “pattern” (along 3 axes, i.e., x , y , z , is preferred, while 2 axes is more convenient);
- 3) The motion may be in one plane for convenience;
- 4) Changing the polarisation (or rotating) of the EUT (during moving) is optional; but this may be impractical;
- 5) From the test in Fig. 5-5, the results show that 3 positions should be the minimum number for moving the EUT.

The measured results from each position of the EUT should not be much different from each other because the field uniformity of the Scaled Model is just slightly over the tolerance requirements (Sect. 4.4). In other words, the measured results from most positions of the EUT should be close to each other, while just a few might be different.

5.2.2) Procedure to process the Measured Signals

Conventionally, there are 2 ways to determine the radiated power of the EUT from the measured results in a RC: one is to use the mean of the received signals over one stirrer revolution, and the other is to use the maximum thereof. This thesis will explore both methods, starting from the conventional procedures; then, the practical application of both procedures will be quantified with regard to finding a suitable MIMO RC emission measurements technique.

Conventional procedure: mean (average) of received signals: this procedure is extracted from the IEC standard [9]. When the EUT is placed in the working volume, the radiated power of the EUT is determined from the received signals by Eqs. 2.49 and 2.50.

MIMO procedure: mean (average) of received signals: when the MIMO RC concept is applied to a conventional RC, it will affect two variables, i.e. $P_{AveRec,EUT}$ and CVF . Firstly, the procedure to measure the CVF for a MIMO RC is a modified one based on the IEC standard [9] (Sect. 2.3.2). In the case of a MIMO RC, the CVF can be determined by using one of the antennas as a transmitting (Tx) antenna fed (with P_{Input}) from outside the chamber, instead of using an additional antenna; then, the received signals from the other antennas are averaged over one revolution of the stirrer. After that, another polarised antenna is swapped for the transmitting antenna, and the process is repeated again. At least two transmitting antennas are recommended to find the mean value ($P_{AveRec,Tx\ antenna}$) for determining the CVF . Only the concept is explained here, the CVF process will be demonstrated in Sect. 5.3.2.

Secondly, for the $P_{AveRec,EUT}$, after finishing one complete MIMO emission measurement process for the EUT, the output is one set of MIMO data. This means that “ N_p ” positions of the EUT give “ N_p ” sets of SIMO results. For instance, when the EUT is moved over 9 positions, there are $N_p = 9$ complete SIMO measurements; each SIMO measurement is for 1 position of the EUT, with data collected from multiple (N_a) receiving antennas. If “ N_a ” receiving antennas are used, 1 set of SIMO data consists of “ N_a ” sets of SISO data. In other words, one complete emission measurement for an EUT provides 1 set of MIMO data, which is equal to N_p sets of SIMO data (single-

input: 1 EUT position, and multiple-output: N_a receiving antennas). Ultimately, there is total of $(N_p \times N_a)$ sets of SISO data in 1 MIMO RC measurement data set.

To process these results, for all the measured signals from each EUT position, it can be assumed that the majority of them are correct, and so a minority of them may contain some errors, because the field uniformity of the Scaled Model is just slightly over the tolerance requirements. Thus, the purpose of processing all these data is to “ELIMINATE” all the erroneous result; which is not as simple as finding the mean value from all of them (as in conventional emission measurements on RCs). Again, this may benefit from using an “off-the-shelf” (i.e. known) technique; e.g., the technique of UFA for ACs in Fig. 5-2. An AC would require the technique of UFA to confirm field uniformity for one plane. The IEC 61000-4-3:2011 [63] standard requires that 75% of the results must lie inside the \pm_6^0 dB criterion; otherwise, the chamber is not usable. When an AC passes this criterion, the field on the plane can be considered to be sufficiently uniform.

For a MIMO RC, each EUT position provides 1 set of SIMO data, which equals “ N_a ” sets of SISO data (from “ N_a ” receiving antennas). The mean value of each SISO set of data must be calculated; the maximum value of these mean values, from the same position of the EUT, becomes 1 SIMO result. In total, there are N_p SIMO sets of data from N_p positions of the EUT. Most of them should be similar (due to field uniformity), while only a few of them will not be; these will be flagged as unusable results; in this way, the validation procedure to verify field uniformity in an AC will be adopted for a MIMO RC. Figure 5-8 shows an example of the UFA technique when the EUT is moved over 9 positions; i.e., 75% of the 9 SIMO results (or about 6 out of 9), one from each EUT position, must lie inside a “6 dB” band for every frequency; and the mean of those 75% will be used as $P_{AveRec,EUT}$ to find the total radiated power from the EUT.

To explain the technique in Fig. 5-8, step by step:

- 1) at any particular frequency, results from $N_p=9$ sets of SIMO data are sorted (Fig. 5-8b); then, the “6 dB band” strategy is applied starting from the maximum values (in this case, it is -64 dBm from EUT position 2);
- 2) When EUT position 2 is chosen, there are only 4 positions (45%) which comply; i.e., $(-64 \text{ dBm}) - (6 \text{ dB}) = (-70 \text{ dBm})$, or only EUT positions 2, 5, 1, and 3. Thus, the result from EUT position 2 will be ignored;

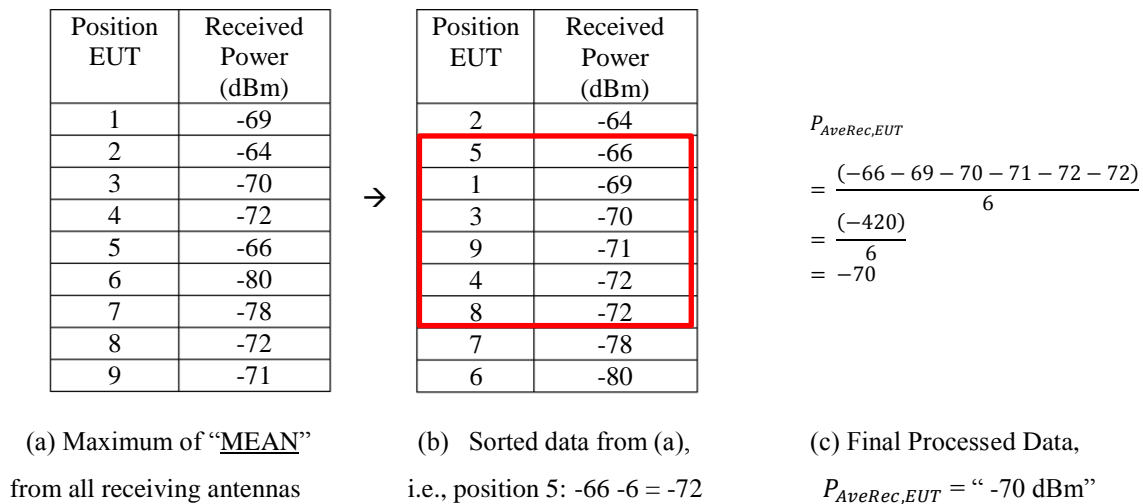


Figure 5-8: Example of the “6 dB band” strategy at a particular frequency.

- 3) The next position down from position 2 is selected. Position 5: (-66 dBm) – 6 dB= (-72 dBm). so -72 dBm will be set as the minimum value, if EUT position 5 is selected. There are 6 EUT positions (66%) which comply; i.e. positions 5, 1, 3, 9, 4, and 8. This is usable.
- 4) The EUT measuring positions 2, 7 and 6 lie outside the “6 dB band” criterion, but at least 6 out of 9 positions (positions 5, 1, 3, 9, 4, and 8) are within the criterion. Thus, -70 dBm is chosen as the $P_{AveRec,EUT}$ value for this particular frequency.
- 5) In practice, at some frequencies, the results might fall short of the 75% requirement, or the criterion might be perfectly satisfied (i.e., 100% lie inside 6 dB); so, Table 5-1 suggests solutions for these extra situations. Also, Key Performance Indicators (KPIs) will be evaluated as performance of the criterion.

Table 5-1: KPIs suggested from the “6 dB band” criterion (at a particular frequency).

KPI (equivalent to)	Solution to find the processed result
100%, Perfect	The mean of all 100%
90%, Very Good	The mean of those 90%
80%, Good	The mean of those 80%
75%, Acceptable	The mean of those 75%
Not meet the criterion	The mean of all 100%

Conventional procedure: maximum of received signals: from the IEC standard [9], $P_{Radiated}$ of the EUT can also be determined from the maximum signal (Eq. 5.1).

$$P_{Radiated} = \frac{P_{MaxRec,EUT} \times \eta_{Tx}}{CLF \times IL} \quad (5.1)$$

$$CLF = \frac{CVF_{Chamber\ with\ EUT}}{AVF_{Empty\ chamber}} \quad (5.2)$$

$$AVF = \left\langle \frac{P_{AveRec,Tx\ antenna}}{P_{Input,Average}} \right\rangle_{N_a, Empty\ chamber} \quad (5.3)$$

$$IL = \left\langle \frac{P_{MaxRec,Tx\ antenna}}{P_{Input,Average}} \right\rangle_{N_a, Empty\ chamber} \quad (5.4)$$

where $P_{Radiated}$ is the radiated power (in W) from the EUT within the measurement bandwidth,

P_{AveRec} is the received power (in W) as measured by the reference antenna averaged over the stirrer steps,

P_{MaxRec} is the maximum power received (in W) over the stirrer steps,

CLF is the Chamber Loading Factor,

CVF is the Chamber Validation Factor,

AVF is the Antenna Validation Factor,

$P_{Input, Average}$ is the forward averaged power over a stirrer rotation,

IL is the chamber Insertion Loss,

η_{Tx} is the Antenna Efficiency Factor (dimensionless) for the Tx antenna used in validating the chamber, and can be assumed,

N_a is the number of antenna locations (i.e., $n=N_a$).

MIMO procedure: maximum of received signals: when a MIMO RC method is applied to a conventional RC, every relevant variable will be determined from the maximum data from multiple (N_p) EUT positions and multiple (N_a) receiving antennas. For instance, $P_{MaxRec,EUT}$ is the maximum received signal of all the EUT positions measured by all receiving antennas, over one stirrer revolution. CLF and IL are determined with the same perspective (demonstrated in Sect. 5.3.2).

5.3 MIMO Radiated Emission Measurements

Making MIMO radiated emission measurements consists of a procedure for moving the EUT, and one for processing the measured results; both are developed in Sect. 5.2. This Section describes a sample EUT used in a test, and how to measure all the relevant variables for making emission measurements following the developed procedures. Emission measurement results from a MIMO RC will be tested by comparing with results from an AC. This Section will start with making the EUT, measuring its characteristics, and measuring the *CVF*, *CLF*, *AVF* and *IL* of the Scaled Model.

5.3.1) The EUT for Measurements

Slot Noise Source: a battery-operated noise source in a hollowed aluminium cavity is used as a sample EUT, which is more realistic (and not just a dipole). A noise source, a battery, a monopole antenna, and 2 amplifiers are placed inside the cavity, which has overall dimensions of 55 mm×115 mm×90 mm; the monopole antenna fed by the noise source feeds the slot antenna on the cavity. Also, there is no cable from the chamber walls (in the 1:5 Scaled Model) to the antenna, which could result in any resonances.

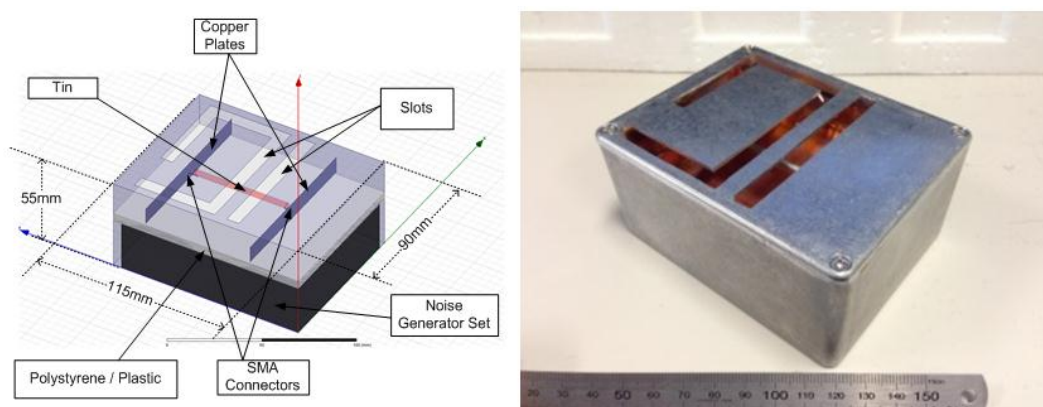
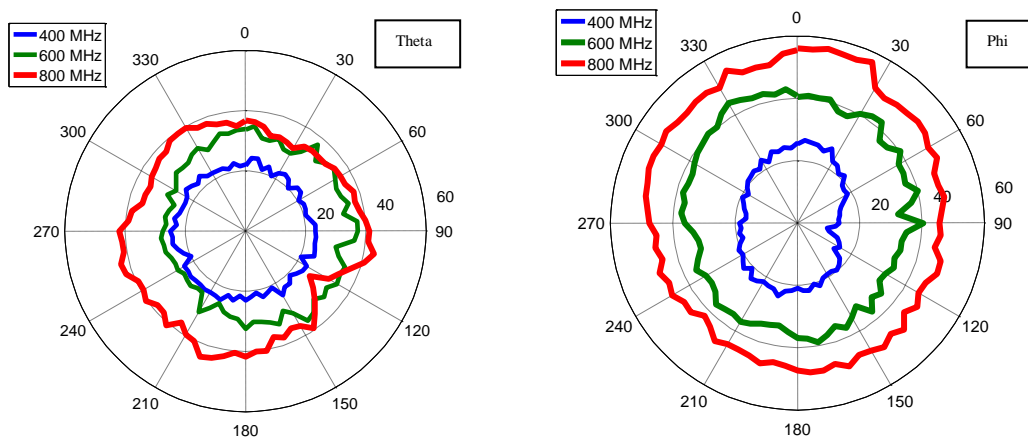
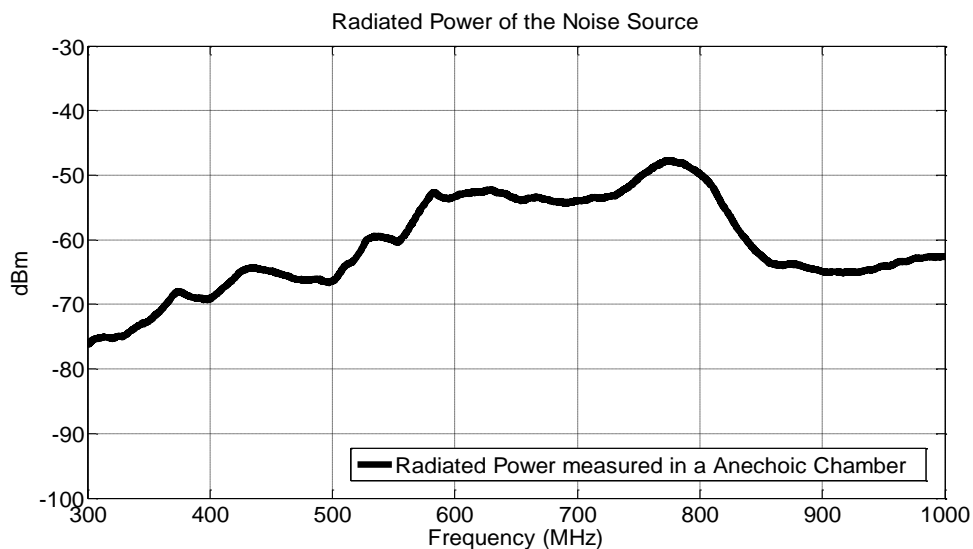


Figure 5-9: Diagram of the EUT: Slot Noise Source.

The schematic diagram, radiated power, and radiation pattern of the slot noise source, as expected, are shown in Figs. 5-9 and 5-10. The slot noise source is more realistic than the biconical noise source (dipole) in Figs. 5-3 to 5-4.



a) Measured radiation pattern.



b) Measured radiated power of the Slot Noise Source.

Figure 5-10: Characteristics of the EUT: Slot Noise Source.

5.3.2) Measuring CVF , CLF , AVF and IL

The EUT can be considered as a small EUT (0.34% of the total chamber volume), and its aluminium surface can be assumed to have a very low loading effect on the Scaled Model chamber. Thus, according to Sect. 5.2.2, the Antenna Validation Factor (AVF) is assumed to be equal to the CVF , and the Chamber Loading Factor (CLF) is 1. As a result, only the CVF and IL will be measured in this Section.

CVF and IL are determined from Eq. 2.49 and Eq. 5.4 respectively. Fig. 5-11 shows the setting up for measuring the CVF and IL on the Scaled Model (MIMO RC), in which multiple receiving antennas are installed. One of the receiving antennas is used

as transmitter, and the other eight antennas as receivers. For port 1 transmitting, the received signals over one stirrer revolution are shown in Figure E-6 (and Figure E-7, for port 2 transmitting). The plots also show the source power of the tracking generator (as delivered into a 50Ω load), and the average and maximum received signals.

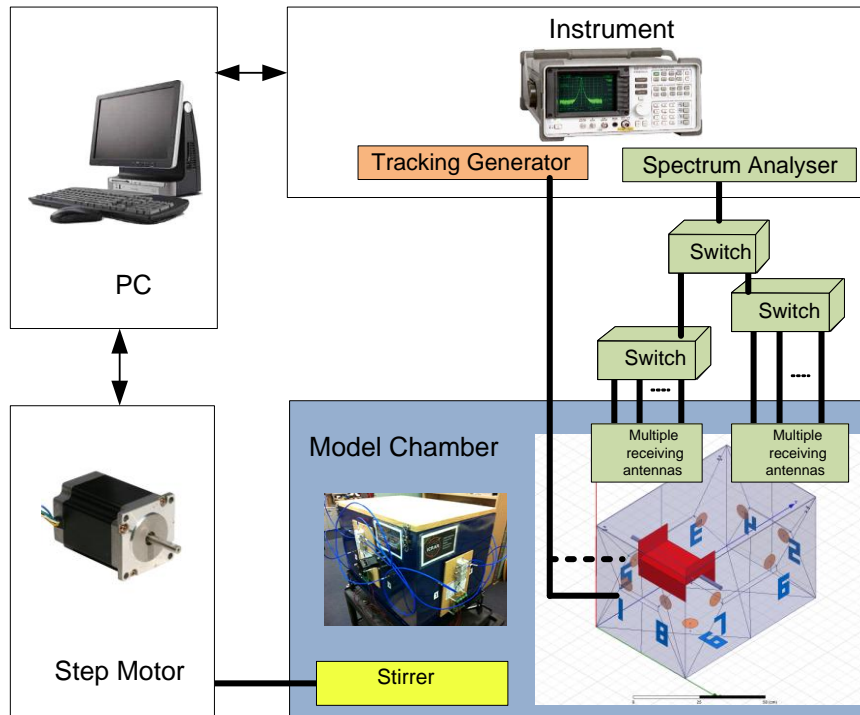


Figure 5-11: Setting up for *CVF* measurements.

P_{input} used in Eqs. 2.49 and 5.4 is the input power to the transmitting antenna. The input power is calculated from the source power of the tracking generator and the reflection coefficient, S_{11} , of the transmitting antennas (Fig. 3-22 and Fig. E-5) by Eq. 5.5, measured over a stirrer revolution. Then, P_{input} are shown in Figs. E-8 to E-10.

$$P_{Input} = P_{Source}(1 - |S_{11}|^2). \quad (5.5)$$

Thus, Fig. 5-12 shows the values for CVF and IL based on antenna 1 and antenna 2 as transmitter, respectively, and as a combination of both. The average of the two average values (for antenna 1 and antenna 2 transmitting) is used for CVF in Eq. 2.49, and the maximum of the two maximum values for IL in Eq. 5.4.

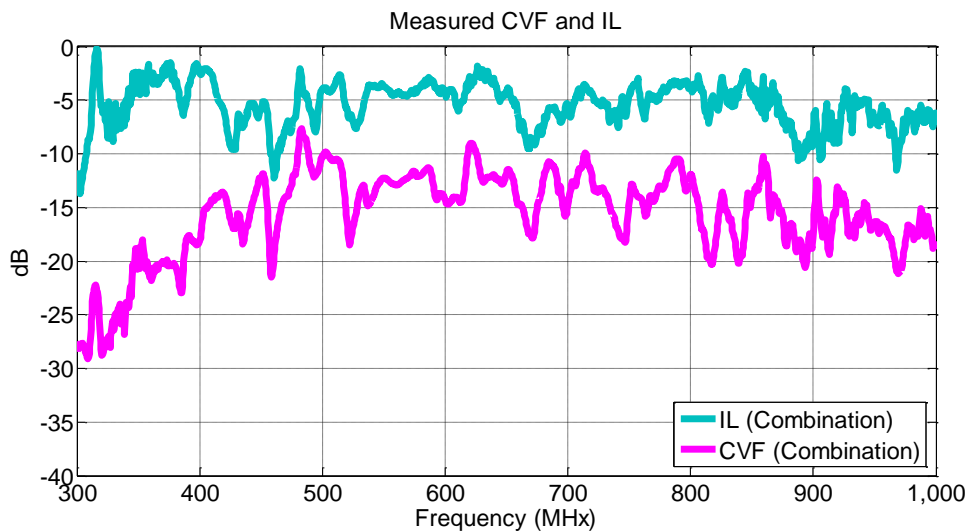
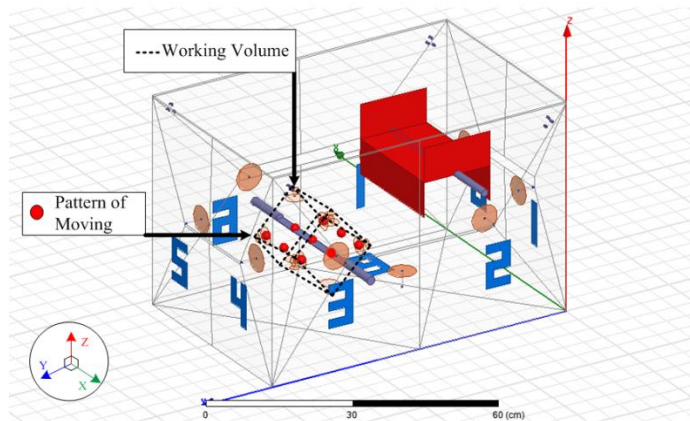


Figure 5-12: Measured *CVF* and *IL* of the Scaled Model for the combination of antennas 1 and 2.

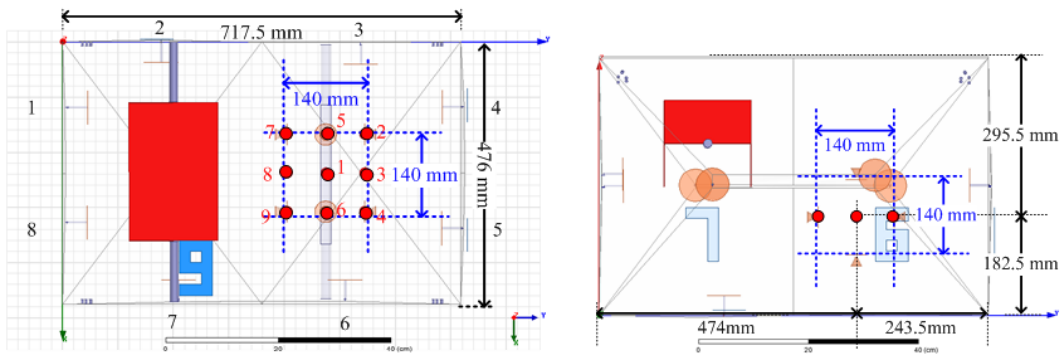
5.3.3) Setting Up for MIMO Radiated Emission Measurements

Following the procedure of moving the EUT (Sect. 5.2.1), the EUT will be moved over $N_p = 9$ positions (3×3) in one (X-Y) plane. The pattern of moving the EUT over 9 positions is demonstrated in Fig. 5-13. The starting position is at a corner of the working volume; then, the EUT is moved for two steps along an axis to another corner. After that, the EUT will be moved along another axis by the same distance, and thereafter moving until it arrives at the last corner of the working volume.

Measuring: The setup is as in Fig. 5-14, which shows the initial position of the slot noise source in the Scaled Model. When the EUT is placed at the 1st position, the automating system will start to measure the signal radiated from the EUT by using multiple ($N_a=9$) receiving antennas (at ports 1 through 9) for 1 revolution of the stirrer. After that, the EUT will be moved to the 2nd position for another measurement. The process will be repeated until the EUT finishes at the 9th position (Fig. 5-14). Then, $N_p=9$ sets of SIMO data will be available for post-processing with the GUI (see Appendix C).



a) General view



b) Top view and side view

Figure 5-13: Pattern of moving the EUT over $N_p = 9$ positions.

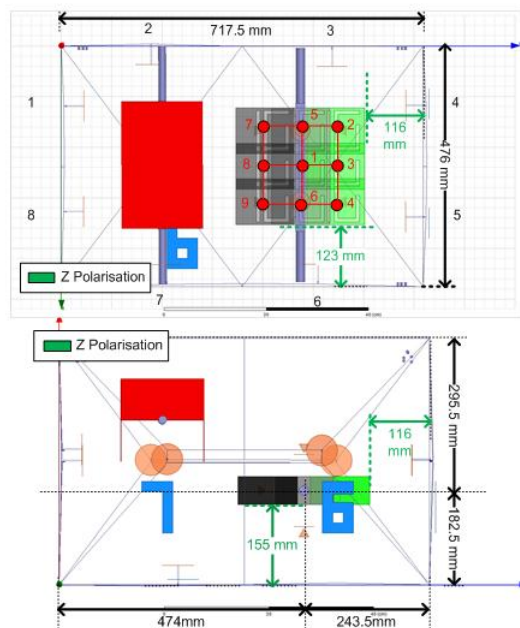
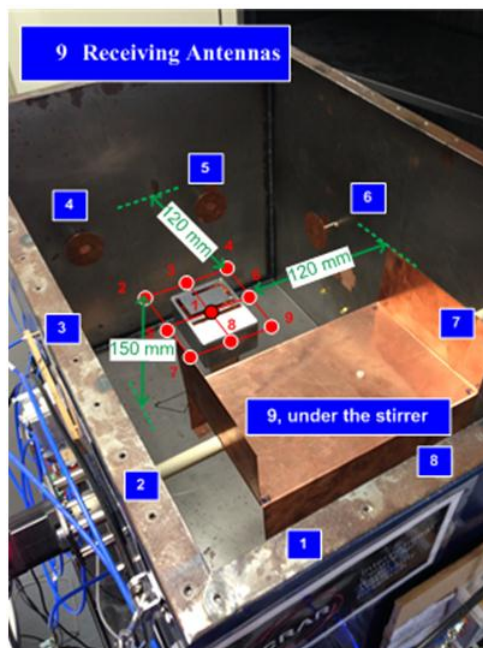


Figure 5-14: Setup for moving the EUT over 9 positions.

5.3.4) Processing Received Signals by using Mean Values

After completing the MIMO emission measurements, $N_p=9$ sets of SIMO data are available. Each set of SIMO data consists of $N_a=9$ sets of SISO data; each set of SISO data consists of the received signals from one position of the EUT measured by one receiving antenna over 80 steps of the stirrer (i.e., one revolution).

- 1) For each position of the EUT, find the mean value of the received signal measured by each receiving antenna over one stirrer revolution. Note: these mean values should be calculated from the linear values, not from the dB values. The measured results from receiving antenna port 1, and the mean values thereof, are shown in Fig. 5-15. In a similar way, the mean values from all $N_a = 9$ receiving antennas are determined (see Fig. E-4).

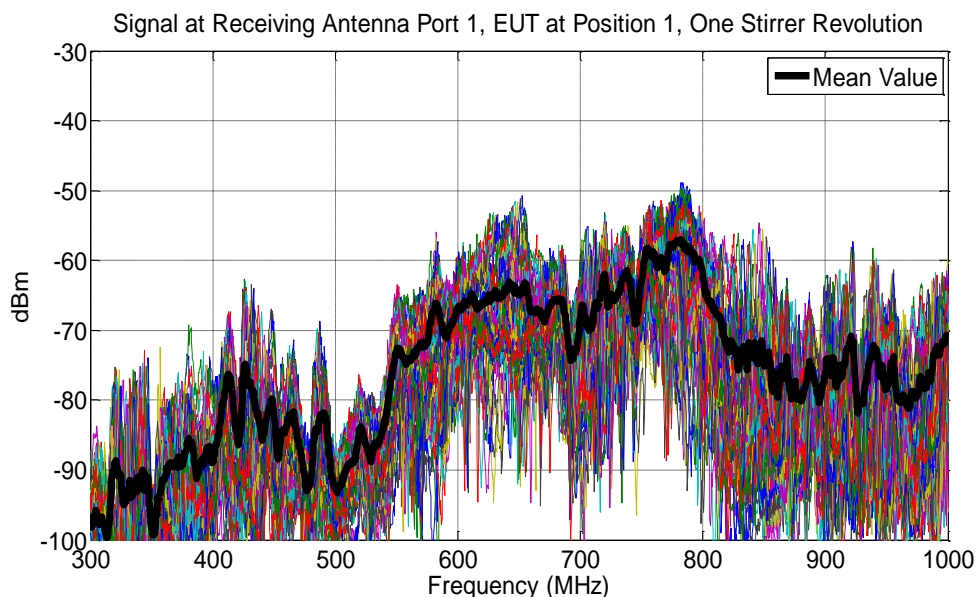


Figure 5-15: Receiving antenna 1 only, EUT position 1, over 1 stirrer revolution (the rest of all the measured results are in Appendix E).

- 2) The maximum value of all $N_a = 9$ mean values from the first step is determined. The blue line (Fig. 5-16) is the maximum of the means from all $N_a = 9$ receiving antennas at the 1st EUT position. This blue line is the output value of the 1st EUT position.
- 3) The 2 previous steps are repeated for all $N_p = 9$ positions of the EUT. At this stage, 9 maxima of the means of the received signals for 9 positions of the EUT have been recorded, and are shown in Fig. 5-17 (the blue lines in Figs. 5-16 and 5-17 are the same). Fig. 5-17 clearly shows that all the spectra are not too

different from each other. This is due to the fact that the field uniformity of the Scaled Model is just slightly over the tolerance requirements (Sect. 4.4); the field inside the MIMO working volume is more or less uniform.

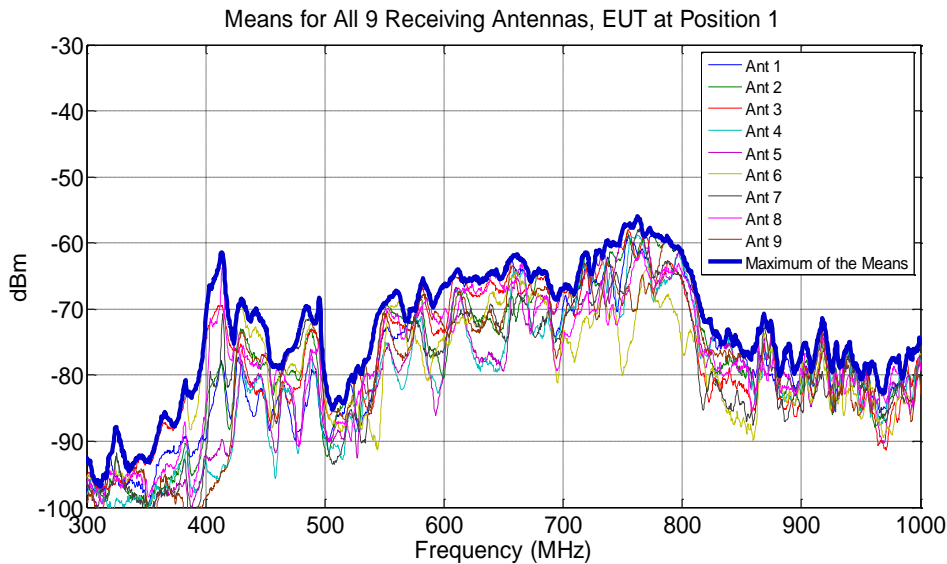


Figure 5-16: All 9 receiving antennas (mean value in each case), EUT position 1; 1st EUT Position, 1 stirrer revolution.

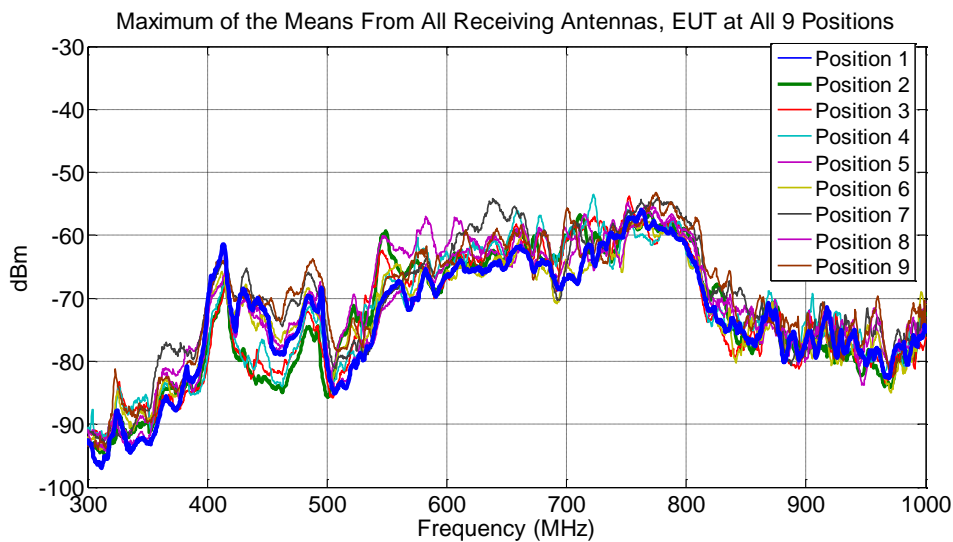


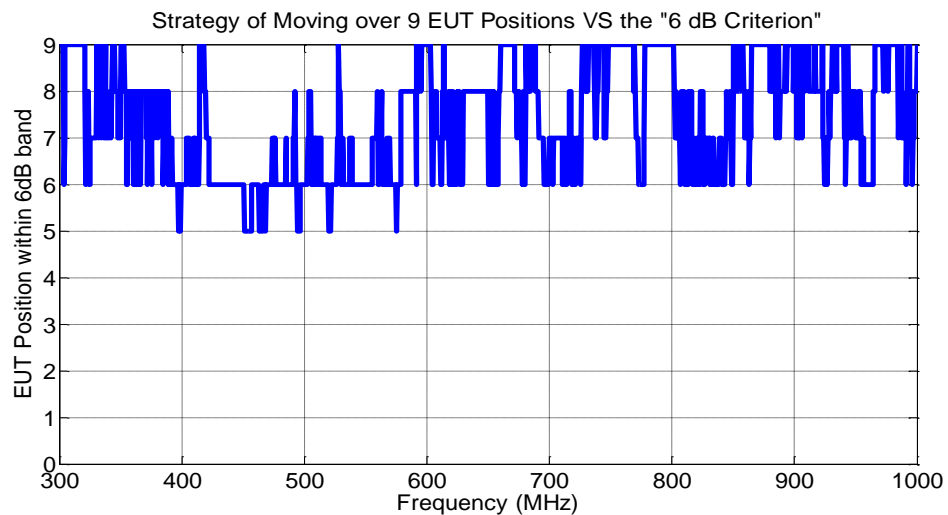
Figure 5-17: All 9 EUT positions (maximum of means from all 9 receiving antennas in each case).

- 4) The next step is to find the best P_{AveRec} out of these 9 spectra. This can be done calculating the mean value from all results (common mean) or from all results within a “6 dB band” (modification mean value).

Table 5-2: KPIs after applying the “6 dB band” criterion to 9 EUT positions.

Number of EUT positions met the criterion (out of 9 positions)	KPI (equivalent to)	Solution to find the processed result
9	100%, Perfect	The mean of those 100%
8	89%, Very Good	The mean of those 89%
7	78%, Good	The mean of those 78%
6	67%, Acceptable	The mean of those 67%
Fewer than 6	Not meet the criterion	The mean of all values

5) Fig. 5-18 shows the numbers of results from Fig. 5-17 that meet the “6 dB criterion”.



There are 1,373 points in the reduced FRI (365 MHz– 1,000 MHz);
 KPI of 32 points (2.22%) do not meet the criterion;
 KPI of 213 points (15.51%) are acceptable;
 KPI of 271 points (19.71%) are good;
 KPI of 365 points (26.71%) are very good; and
 KPI of 492 points (35.83%) are perfect.

Figure 5-18: KPI strategy that 67% (or 6 out of 9 data points) must lie inside 6 dB.

Therefore, 97.78% of the data points passed the criterion; only 2.22% of the results might contain some errors. If less than 6 of the 9 results lie within a “6 dB band” the results are considered unreliable. This does not mean that the other 2.22% are faulty, but it means that errors “MIGHT” occur up to 9.787 dB (the maximum error is calculated to be 9.787 dB, as explained in Sect. 5.4).

- 6) The processed results for the MIMO emission measurements are shown in Fig. 5-19; the red line is called the “modified mean received value”. This processed result is compared to all 9 maxima of the mean values (from Fig. 5-17).

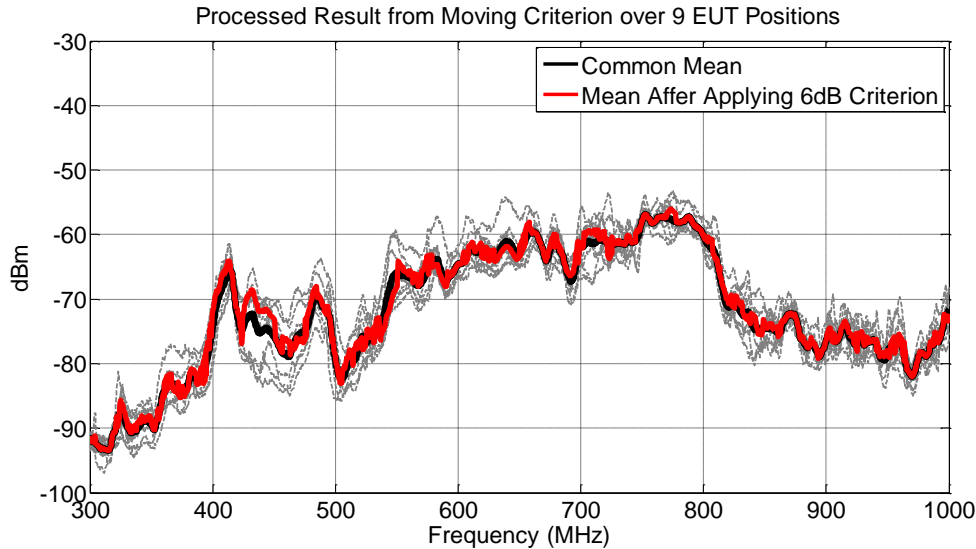


Figure 5-19: Common and modified means (6 dB band) for all 9 results of Fig. 5-17.

- 7) The “modified mean received value” from Fig. 5-19 is applied to Eq. 2.50 to determine the radiated power of the EUT, as shown in Fig. 5-20.

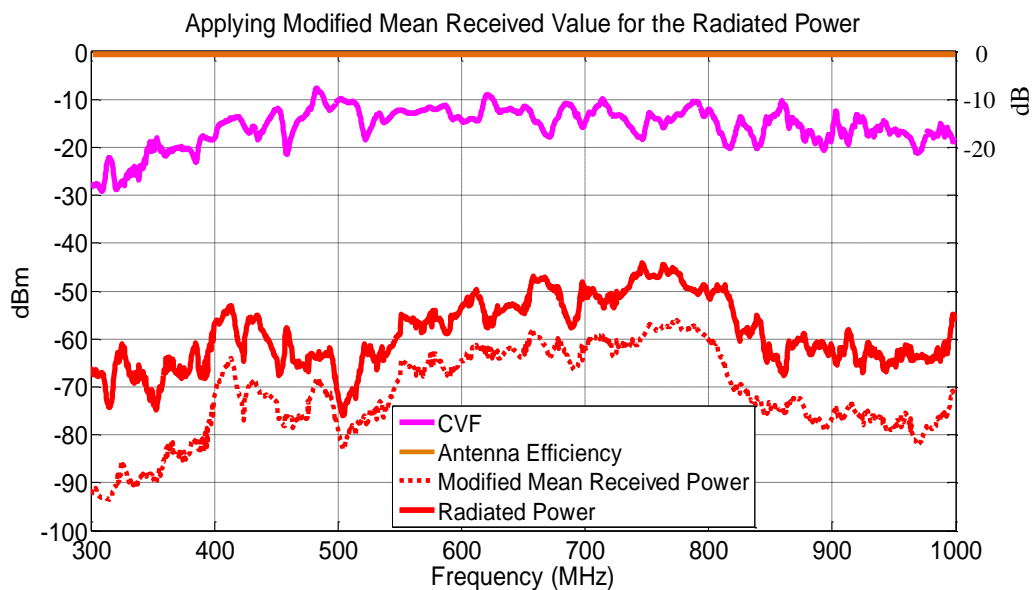
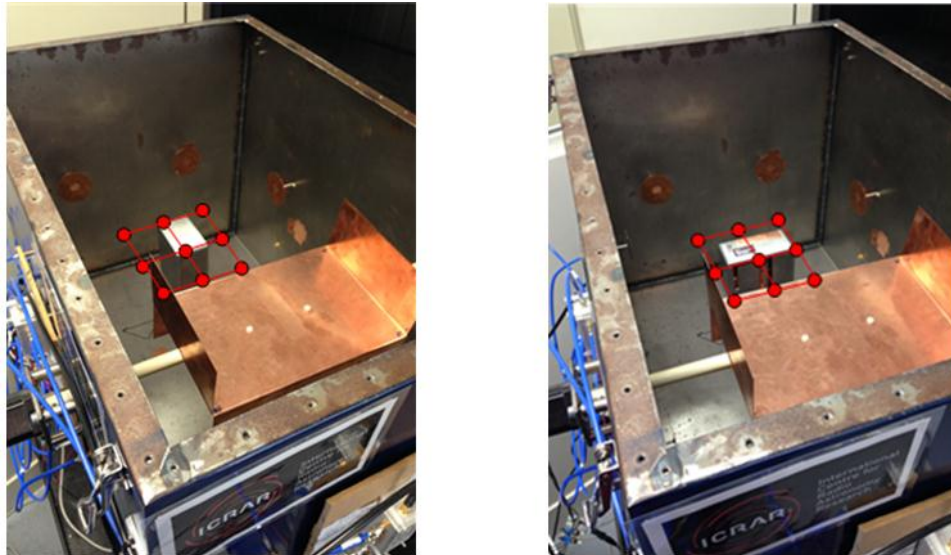


Figure 5-20: The Radiated Power of the EUT, determined from the processed results in Fig. 5-19.

- 8) Step 1 to 7 are repeated with the EUT placed in the 2 other polarisations (i.e., X and Y polarisations).



a) X Polarisation

b) Y Polarisation

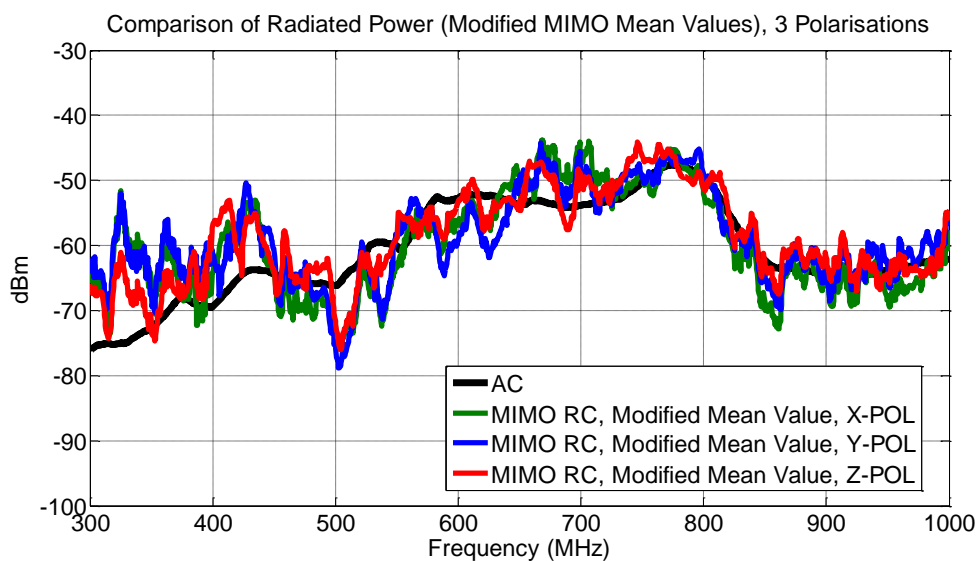


Figure 5-21: Radiated power (CVF method), when EUT is placed in different polarisations.

In summary, from the procedures above, a MIMO RC shows the capability to make radiated emission measurements in the transition region, which ranges from the first resonance to the C-LUF. Fig. 5-21 shows good agreement of the results from the MIMO RC (in all 3 polarisations) with those from the AC. The errors in the 450-550

MHz range are consistent with the field uniformity results shown in Chapter 4 (Fig. 4-9). It should be noted that the differences between the RC and AC results can be up to 7 dB [97].

5.3.5) Processing Received Signals by using Maximum Values

The maximum signals can also be used to determine the radiated power of the EUT by Eqs. 5.1 to 5.4. Using the maximum values is more suitable for measuring weak signals, especially close to the noise floor. For instance, Koepke et al. [100] stated that using the maximum received signal could provide more sensitive results above the C-LUF. Using maximum instead of mean values might be better for RA applications. In this thesis, using maximum received signals is demonstrated in order to more fully investigate the characteristics of MIMO emission measurement below the C-LUF.

From Eqs. 5.1 to 5.4, the P_{MaxRec} is the maximum received signal of the measured signals from all receiving antennas, and all EUT positions, over one stirrer revolution. Again, the Antenna Validation Factor (AVF) is assumed to be equal to the CVF , due to the small dimensions and aluminium surface of the EUT; thus, the Chamber Loading Factor (CLF) is 1. The Insertion Loss (IL) is determined in the same way as the CVF (IL is about -6 dB, Fig. 5-12).

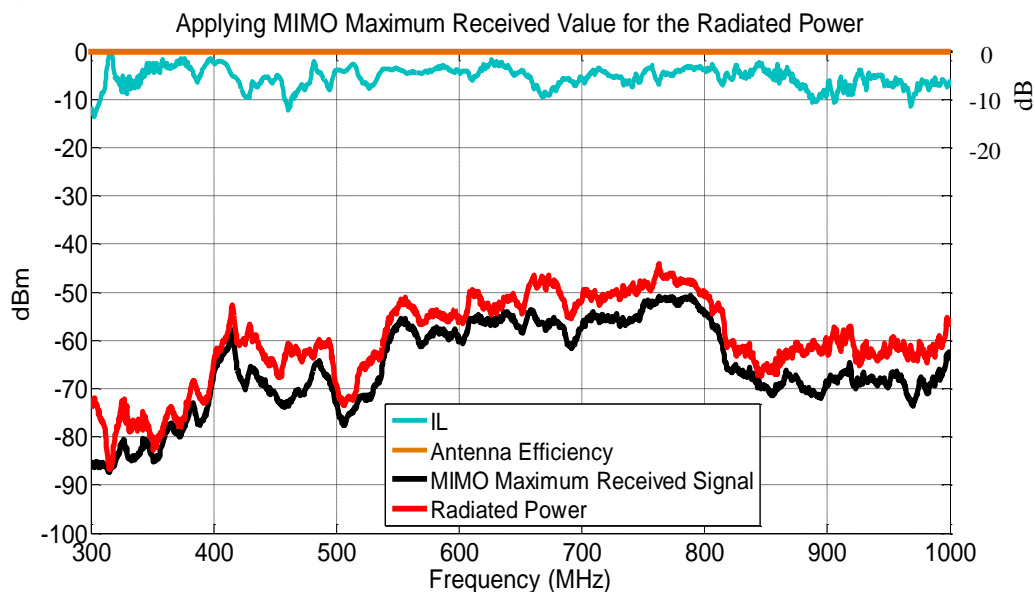


Figure 5-22: The Radiated Power determined by Equation 5.1, EUT placed in Z-Polarisation.

Equations 5.1 to 5.4 are used for all 3 polarisations of the EUT, and the results are shown in Fig. 5-23. The results are similar to those in Fig. 5-21, which are based on modified mean values. A comparison between them is shown in Fig. 5-24 (only the Z polarisation is plotted). In summary, using either MIMO modified mean values or MIMO maximum received signals give almost the same results, while the conventional RC method gives poor results in the transition region.

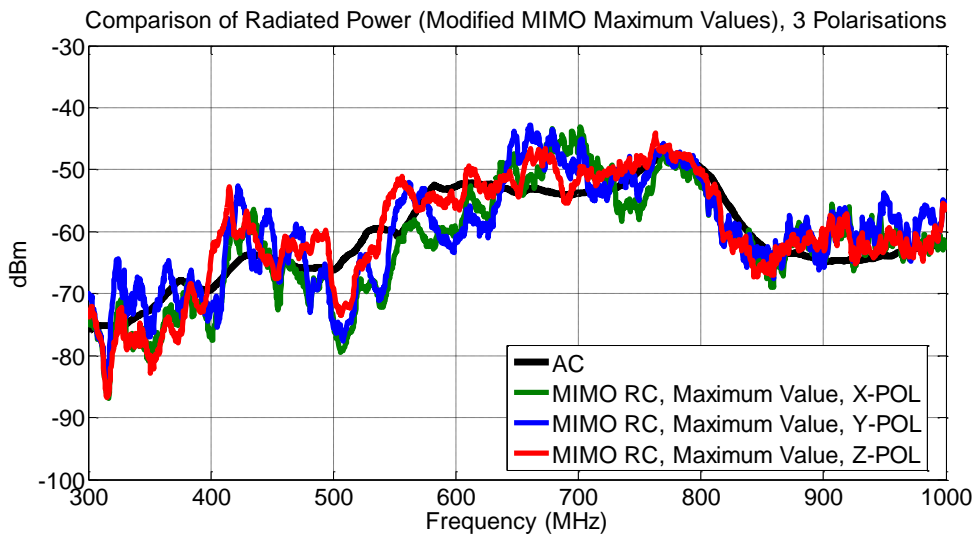


Figure 5-23: Radiated power (IL method), when the EUT is placed in different polarisations.

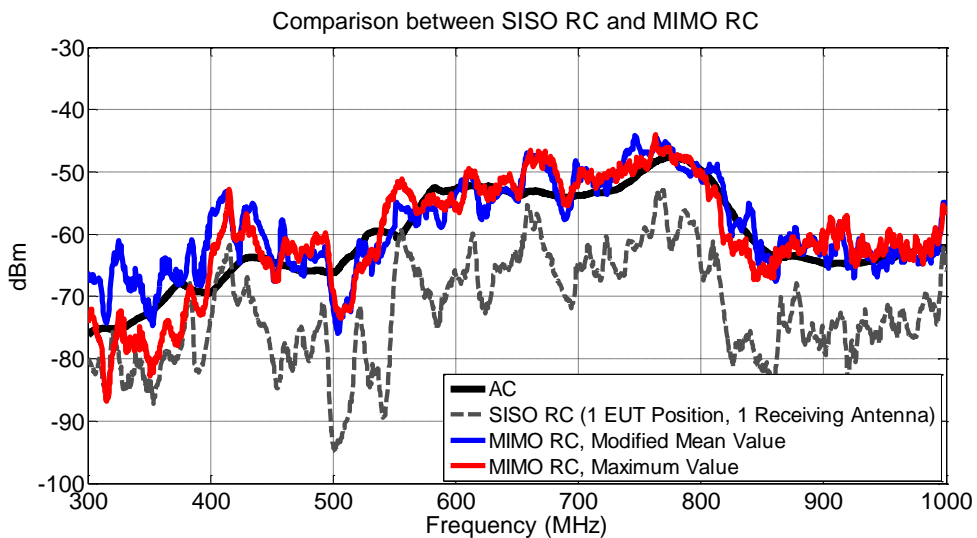


Figure 5-24: Comparison of Radiated power (absolute values, Z polarisation) between MIMO RC, Conventional RC, and AC results.

5.4 Scientific Validation of the Results: Sensitivity and Accuracy

Fig. 5-25 presents an analysis of the “Accuracy” of the MIMO RC method. The Figure shows the differences between the MIMO RC and SISO RC relative to AC results; MIMO RC results for radiated power are more accurate. However, at some frequencies, the results show differences of up to ~ 8 dB. There are 3 possible reasons causing these differences. Firstly, the structure of the stirrer might not be able to shift resonances at these frequencies (see Fig. 5-26). Secondly, the frequency gaps between modes are wide here. Lastly, the results from the AC method might contain some errors due to the estimations made in the AC measurement method itself.

In addition, MIMO RC can provide better sensitivity than AC, as shown in Fig. 5-27. The Figure shows absolute raw signals at the receiver input, without considering antenna factor (AC results) or CVF and IL (MIMO RC). The signals in a MIMO RC are up to 20 dB or 15 dB higher than in an AC when applying average or maximum values, respectively.

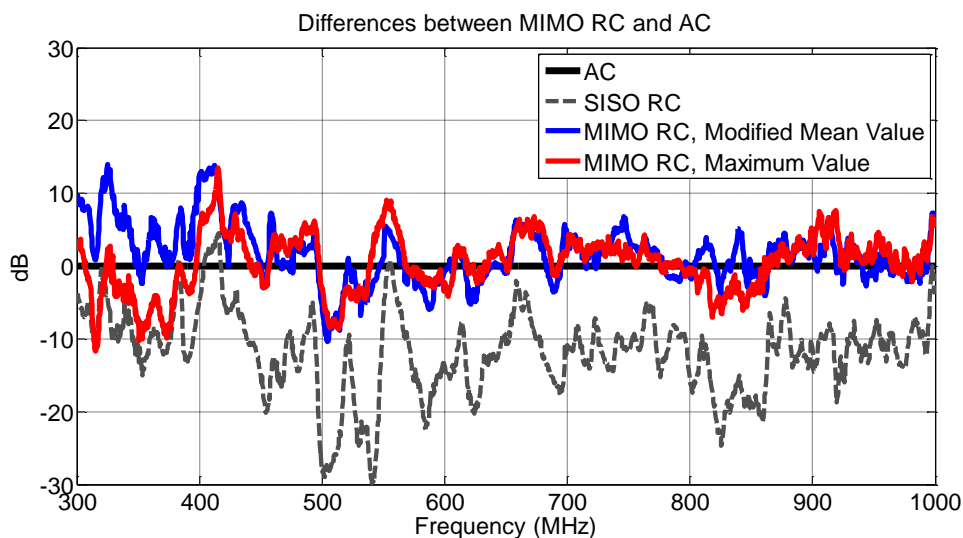


Figure 5-25: Comparison of Radiated power (relative differences) between MIMO RC, Conventional RC, and AC results.

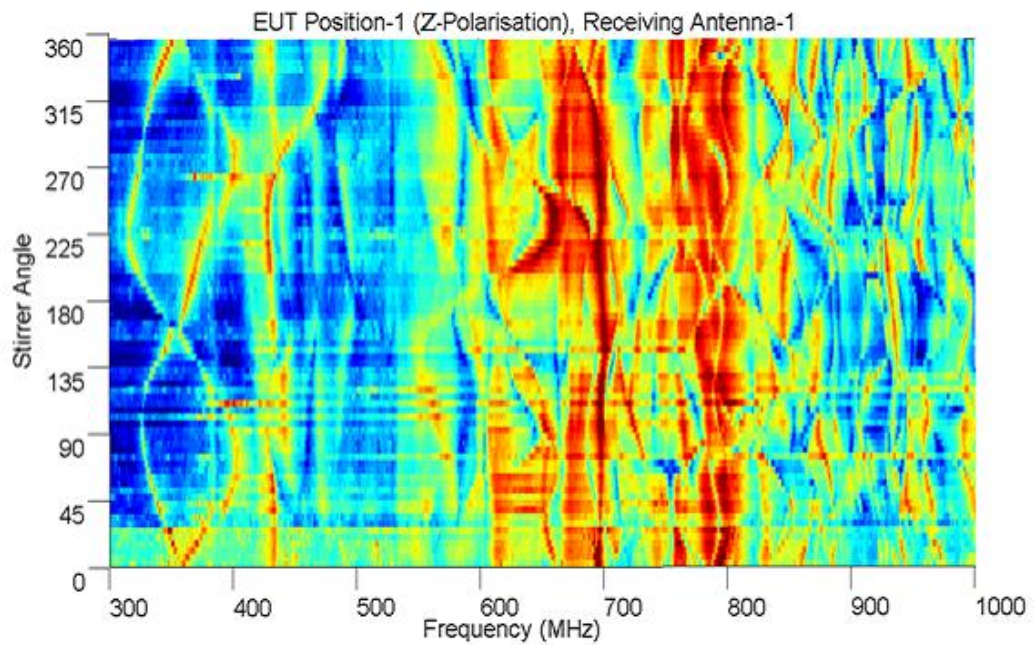


Figure 5-26: Performance of Double C Stirrer from Fig. 3-20.

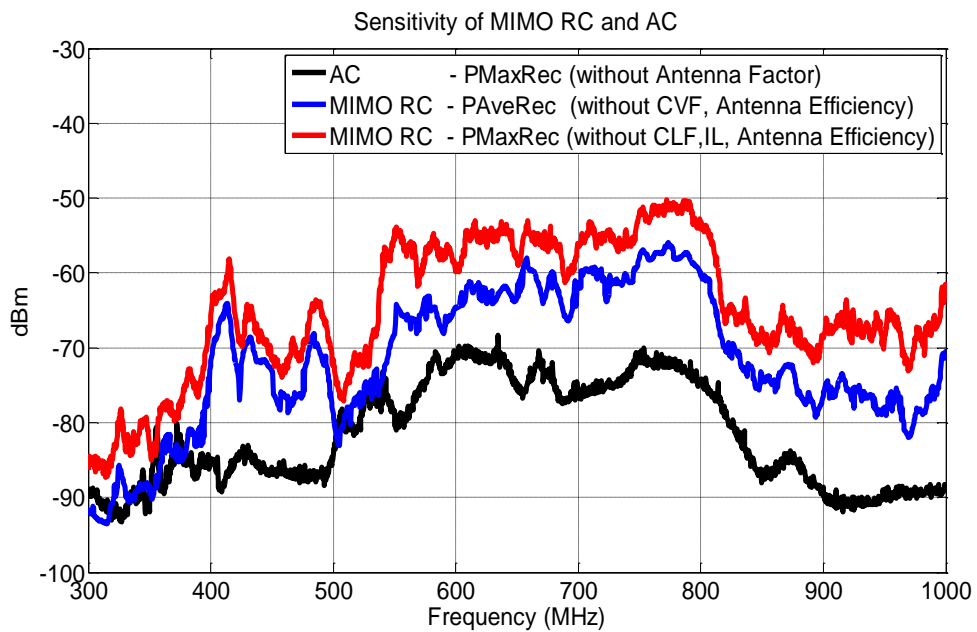


Figure 5-27: Sensitivities of MIMO RC and AC.

Scientific Validation of the Results: the RC method provides a statistically averaged result. This subsection aims to validate and explain accuracy of MIMO RC by comparing the maximum error which can occur in conventional RCs to the maximum error which can occur in a MIMO RC. It is clear that when conventional RCs pass the validation procedure (i.e., meet the conventional tolerance requirements for the measured STD; Table 4-4), this means that the field in the conventional working volume is just “acceptably” uniform. Theoretically, the difference in the standard deviations between the E -field components of 3 mutually orthogonal axes (x, y, z) is under the limit; i.e., 4 dB at 100 MHz decreasing linearly to 3 dB at 400 MHz. In other words, placing the EUT at different positions (within the conventional working volume) can provide “acceptable” though different measured results; i.e., some errors still occur even though the chamber passed the conventional validation procedure — they are still acceptable.

The maximum error that can occur in the conventional procedure can be calculated by considering the worst situation. This is when signals from 7 corners of the working volume are exactly the same; then, the conventional validation procedure allows the last corner to be different by as much as possible, as allowed by the prescribed STD limits of “ 3 dB ” and “ 4 dB ”. To investigate this case, the equations used for the conventional validation procedure are calculated backward from Eqs F.7 back to F.1 (see Appendix F) to find out the maximum amount of the error. Starting from Eq. F.7, and looking at only one polarisation (X-polarisation, for instance):

$$\sigma(\text{dB}) = 20\log_{10}\left(\frac{\sigma + \langle \vec{E}_x \rangle}{\langle \vec{E}_x \rangle}\right). \quad (\text{F.7})$$

There are two cases: 3 dB and 4 dB . So, when the 4 dB limit applied (for $f \leq 100\text{ MHz}$);

$$\begin{aligned} 4 &= 20\log_{10}\left(\frac{\sigma_x + \langle \vec{E}_x \rangle_8}{\langle \vec{E}_x \rangle_8}\right) \\ 10^{\frac{4}{20}} &= \frac{\sigma_x + \langle \vec{E}_x \rangle_8}{\langle \vec{E}_x \rangle_8} \\ 10^{\frac{4}{20}} \times \langle \vec{E}_x \rangle_8 - \langle \vec{E}_x \rangle_8 &= \sigma_x \\ 0.5849 \langle \vec{E}_x \rangle_8 &= \sigma_x \end{aligned}$$

Using the value of σ_x in Eq. F.5:

$$\begin{aligned} \sigma_x &= \sqrt{\frac{\sum (\vec{E}_{x,i} - \langle \vec{E}_x \rangle_8)^2}{8-1}} \\ 0.5849 \langle \vec{E}_x \rangle_8 &= \sqrt{\frac{\sum (\vec{E}_{x,i} - \langle \vec{E}_x \rangle_8)^2}{8-1}} \end{aligned} \quad (\text{F.5})$$

$$(0.5849\langle\vec{E}_x\rangle_8)^2 = \frac{\sum(\vec{E}_{x,i} - \langle\vec{E}_x\rangle_8)^2}{8-1}$$

$$0.3421\langle\vec{E}_x\rangle_8^2 \times 7 = \sum(\vec{E}_{x,i} - \langle\vec{E}_x\rangle_8)^2$$

$$2.3947\langle\vec{E}_x\rangle_8^2 = \sum(\vec{E}_{x,i} - \langle\vec{E}_x\rangle_8)^2$$

Now, assuming that the worst error happens, i.e., when the signals from 7 corners ($\vec{E}_{x,1-7}$) are exactly the same, and the last corner ($\vec{E}_{x,8}$) is so different that it makes a 4 dB (requirement) of standard deviation (σ) occur. So: $\langle\vec{E}_x\rangle_8 = \frac{(7\times\vec{E}_{x,1-7}) + \vec{E}_{x,8}}{8}$, then,

$$2.3947\langle\vec{E}_x\rangle_8^2 = 7 \times (\vec{E}_{x,1-7} - \langle\vec{E}_x\rangle_8)^2 + (\vec{E}_{x,8} - \langle\vec{E}_x\rangle_8)^2$$

$$2.3947 \left(\frac{(7\times\vec{E}_{x,1-7}) + \vec{E}_{x,8}}{8} \right)^2 = 7 \times \left(\vec{E}_{x,1-7} - \frac{(7\times\vec{E}_{x,1-7}) + \vec{E}_{x,8}}{8} \right)^2 + \left(\vec{E}_{x,8} - \frac{(7\times\vec{E}_{x,1-7}) + \vec{E}_{x,8}}{8} \right)^2$$

Using a computer to determine the relation, so:

$$3.08561\vec{E}_{x,1-7} = \vec{E}_{x,8}$$

Thus, the maximum error that the last corner, $\vec{E}_{x,8}$, can be different from the other corners, $\vec{E}_{x,1-7}$, can be up to;

$$20\log_{10} \left(\frac{E_{x,8}}{\vec{E}_{x,1-7}} \right) = 20\log_{10} 3.08561 = 9.787 \text{ dB}$$

Therefore, it is found that, in the worst case (assumed at corner 8), $E_{x,8}$ can have an error of up to 9.78 dB from the other corners (in the case of a 3 dB limit, by following all the equations above, $E_{x,8}$ can have an error of up to 7.48 dB from the others). Thus, meeting the 3 dB and 4 dB tolerance requirements of conventional RCs means that 7.48 dB and 9.78 dB, respectively, are acceptable errors on emission measurements, when the EUT is placed at different positions in the working volume.

In the case of MIMO RC, the field uniformity is just slightly over the conventional tolerance requirements; i.e., the field uniformity is not higher than 1 dB above the conventional tolerance allowed. Then, the results can be smoothed later by moving the EUT, and applying a “6 dB band” strategy; all the procedures are explained in Section 5.2. Then, 75% of the mean values from 9 positions of the EUT (or at least about 6 out of 9) must lie inside 6 dB for each frequency, and the mean of those 75% will be used to find the total radiated power. Thus, the maximum acceptable error which can occur in MIMO RCs is within 6 dB, meaning that the errors of MIMO RC (limited to 6 dB) can never be worse than those of conventional RCs, which can be up to 9.78 dB.

5.5 Summary of MIMO RC Procedure for Emission Measurements

In Chapters 2 and 3, this thesis showed that using multiple receiving antennas improves field uniformity. Figure 5-28 shows that moving the position of even a single transmitting antenna can stir the field distribution at the same frequency (below the C-LUF). On the other hand, moving the EUT can excite different modes. The use of multiple positions for the receiving antenna (MO), and moving the position of the EUT (MI), leads to the technique called MIMO RC.

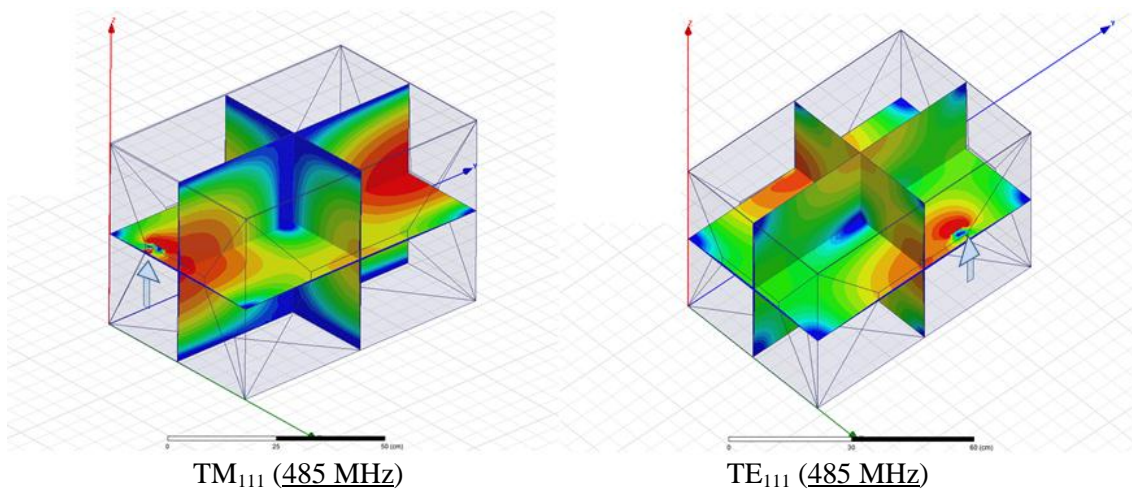


Figure 5-28: Field distribution is changed when the Tx antenna position is moved.

In practice, MIMO RC requires its own procedures, i.e., the MIMO validation procedure and MIMO emission measurements, to measure emission of the EUT. This thesis developed both procedures based on the conventional ones. From this perspective, MIMO RC can be understood easily; all conventional RCs can be easily modified to MIMO RCs (to be usable below the C-LUF), and all the results can obviously be compared to the conventional ones. The MIMO validation procedure was demonstrated in Chap. 4, and MIMO emission measurements were confirmed in this Chapter.

All MIMO RC procedures, i.e., MIMO RC validation procedure and MIMO RC emission measurements, developed in this thesis are summarised in Fig. 5-29.

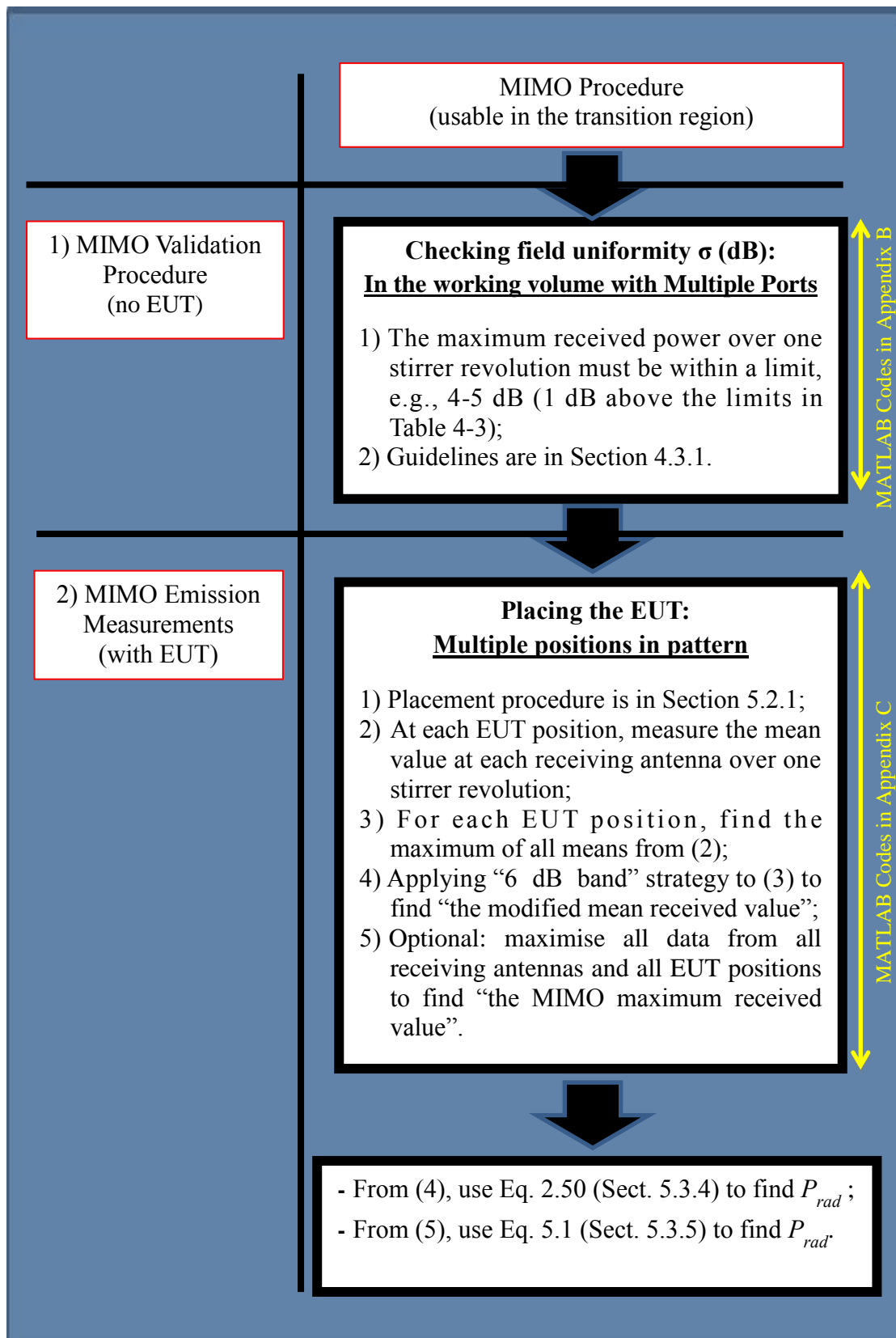


Figure 5-29: MIMO RC procedure for emission measurements.

5.6 Chapter Summary

The purpose of this Chapter is to develop and test procedures for making MIMO radiated emission measurements in a MIMO RC, in the transition region. In Chapter 4, it was shown how multiple receiving antennas can improve the field uniformity of the Scaled Model chamber in the transition region (from 375 MHz to 1,000 MHz). Placement of the EUT at selected positions might not always give the correct results, but the majority of them will be significantly close to the actual radiated power, and thus useful for emission measurements.

In this Chapter, a technique for moving the EUT is applied in a MIMO RC to make an emission measurement. This technique is based on the concept of calibrating a Uniform Field Area (UFA) in an AC [63], which is discussed in Sect. 5.1. Although the technique is applied to MIMO RCs in Sect. 5.2, the MIMO RC technique for moving the EUT and the UFA technique are not related to each other (this is because the UFA technique is concerned with maximum error, not to find the average value). Thus, technique for moving the EUT has been detailed in Sect. 5.2; for instance, the number of positions for moving the EUT, the pattern for moving the EUT, and how to process all the measured results. In this way, procedures for making MIMO RC emission measurements have been established in this Section.

Sect. 5.3 demonstrates the results from testing these procedures, as well as comparing the results to those from conventional RC and AC methods. The accuracy and sensitivity of the MIMO RC method are explored in Sect. 5.4. Finally, Sect. 5.5 summarises the procedures necessary to make emission measurements using a MIMO RC.

CHAPTER 6

CONCLUSION AND SCOPE FOR FUTURE WORK

6.1 Introduction

Radio astronomy (RA) is concerned with the measurement of extremely weak electromagnetic signals; the sensitivity of radio telescopes is one of the key factors in their success. Increasing sensitivity usually means more problems with radio frequency interferences (RFI); e.g. from amplifiers, power lines, and computers. In order not to interfere with very faint astronomical signals, electrical and electronic equipment close to, or at, RA sites must have an exquisitely low level of electromagnetic emission over a wide frequency range (50 MHz to 20 GHz at the Murchison Radioastronomy Observatory (MRO) site in Western Australia, for example). All electronic devices installed at modern RA sites are required to undergo an Electromagnetic Compatibility (EMC) assessment. A traditional, or conventional, Reverberation Chamber (RC), defined by the International Electrotechnical Commission (IEC) [9], is suitable for testing instruments used in RA, since a conventional RC method can deliver a way of making very sensitive, reliable, repeatable, and stable emission measurements at a lower cost than for other methods, except at lower frequencies. For similar chamber dimensions, applying the RC method is cheaper than using an Anechoic Chamber (AC). For example, the costs for an AC with dimensions of 7 m \times 4 m \times 3 m, equipped with ferrite absorbers, are currently ~ \$200K, while a RC costs at least 3 times less for similar linear dimensions. However, the RC method comes with the limitation of the Conventional Lowest Usable Frequency (C-LUF): a lower C-LUF requires larger chamber dimensions. This dimension requirement also renders the conventional RC method to be impractical to apply to low-frequency RA applications, e.g. at 50-350 MHz for The Square Kilometre Array, SKA [7].

6.2 Practical Outcomes and Considerations

This thesis is a study into the feasibility of a new way of using small RCs for low-frequency RA EMC applications. Normally, a conventional RC has to be large,

so that the chamber can maintain a uniform field strength within a working volume, over the revolution of a field stirrer. This field uniformity requirement determines the Conventional Lowest Usable Frequency (C-LUF); the larger the chamber, the lower the C-LUF. This thesis introduces the possibility of using a RC below the C-LUF, with techniques to increase the field uniformity below the C-LUF; this modified approach is initially intended for RA applications, whose need for sensitivity justifies longer measurement time, thus allowing non-standard procedures to be acceptable.

This research has found an approach to convert a conventional RC into a multiple-input multiple-output (MIMO) RC that is up to 6 times smaller (in linear dimensions) than the conventional requirements; the new approach is suitable to be applied to any existing conventional RC so as to make it usable below the C-LUF. Although the primary outcome is initially intended for RA applications at the MRO, widening the range of tested frequencies could provide reliable radiated tests (immunity and emission in shielded room down to VHF).

Chapters 1 and 2 explain the relevant theories, starting with introductions, objectives, the origin of conventional RCs, the MIMO communication link system, up to the initial setup of a MIMO RC. Theoretically, the conventional RC method cannot alter the field distribution by using only a stirrer(s) at low frequencies; i.e., the field uniformity derived from measurements of the standard deviation (STD) for three polarisations cannot meet the specified limits in the IEC Standard criterion (Appendix F). This research invokes Maxwell's equations (Chapter 2) to explain the field distribution in a cavity; moving the position of an antenna can theoretically "excite" more resonances even below the C-LUF. Then, the use of multiple positions for the receiving antenna (multiple-output: MO), and moving the position of the EUT (multiple-input: MI), have been adopted to increase the field uniformity in the transition region (i.e. from the 1st chamber resonance to the C-LUF). Thus, the E-fields of 3 mutually orthogonal axes (x, y, z) become more uniform, even in the transition region. This leads to the new MIMO RC technique. Chapter 3 shows implementations and designs of all fittings for a prototype of a MIMO RC; all designs are supported by a simulation program (a FEM code), and a series of experimental results are presented. A MATLAB prototype program is used to automatically control the experimental system, and to investigate all the validation and measurement procedures described in Chapters 4 and 5.

Chapter 4 shows that the prototype MIMO RC can perform with better field uniformity compared to the conventional RC technique. The 1:5 scale prototype model passed the conventional measurement criterion below the C-LUF. This means that the *E*-fields of 3 mutually orthogonal axes (x, y, z) in the working volume in the MIMO RC became effectively uniform. In fact, by the conventional definition, the field uniformity is just slightly over the proposed IEC Standard limit; the majority of measured results from when the EUT is placed in different positions are correct, but a minority may contain errors. To account for this shortcoming, a procedure of moving the EUT to identify the correct results is demonstrated in Chapter 5. The tests have been done by comparing the MIMO RC measurements to those from using the AC method—they are in good agreement (i.e., mostly within ~ 5 dB) with each other. This confirms the feasibility of using this new MIMO RC technique in the transition region; and the MIMO RC concept can be applied to any conventional RC to increase its effective size by 3-6 times (in its linear dimensions).

6.3 Implications/Utilisation of the Study to Related Areas

After designing and building a MIMO RC, this thesis has used a range of contemporary Electrical and Computer Engineering practices to undertake the research work, with some important implications:

- For RA (ICRAR/CIRA): the outcome of this research can be applied to typical shielded rooms to make them function as a RC with smaller dimensions than usual; e.g., for the ICRAR/CIRA shielded room, usable frequencies range up from 70 MHz, which increases the sensitivity of RF emission measurements for low-frequency RA applications at the MRO. The guidelines for applying MIMO RC methods to the shielded room at ICRAR/CIRA are available in Appendix D.

- For the wider EMC community: this research project provides guidelines on how to improve the accuracy of emission measurements in small shielded rooms; for instance, the solution of using multiple antennas in a shielded room to avoid nulling effect, the solution for having low composite Q factor (Q_g) when multiple antennas are used.

- For Navy and related fields: although MIMO RC is explained in this thesis only for emission measurements, it can also be used for immunity tests; for

example, the high-level immunity tests needed on NAVY warships. The outcome shows a promising possibility of MIMO RC being useful to NAVY RF applications, i.e. from VHF (30 MHz) to Ku band (up to 18 GHz).

6.4 Problems and Suggestions for Future Research

1) Measurement time: MIMO RC technique requires much longer measurement times and more sophisticated signal processing. A possible solution to achieve faster measurement times is to use a high-speed, multi-channel analogue-to-digital conversion system to allow parallel measurements.

2) Shape of chamber: the width and height of the shielded model in this thesis are more or less symmetrical (Appendix A), which reduces the number of modes from being excited; an asymmetrical room could have a more uniform field distribution (see Sect. 3.2.1). Exploration of improved form factors would be worthwhile.

6.5 A Final Word

This thesis has demonstrated an advance in the methods of using a RC, allowing radiated emission measurements to be more sensitive allowing sensitive and reliable emission measurements at much lower frequencies than conventionally possible. Although the conventional reverberation chamber (RC) method requires lower cost (~3 times) per square metre compared to an anechoic chamber (AC), the issue of the C-LUF makes a conventional RC become large. The new approach and MIMO techniques developed in this thesis enable smaller dimensional requirements, and thus cost, for the MIMO RC chamber. The feasibilities of these new MIMO RC techniques have been confirmed by theory, simulated results, and measurements on a prototype.

As well as being applicable to new installations, this novel method can extend the performance of existing RCs. Long-range communication systems, such as in the NAVY, which also require highly sensitive, reliable, repeatable and stable emission measurements could benefit from this outcome.

REFERENCES

- [1] C. Wilson, "RFI Standards for Equipment to be Deployed on the MRO," Feb. 2009, [Online]. Available: http://snebulos.mit.edu/projects/mwa/file_cabinet/0/01080/01080_r05m.pdf.
- [2] "Requirement for the Control of Electromagnetic Interference Characteristics of Subsystems and Equipment," MIL-STD-461F, Department of Defense Interface Standard, USA, 2007.
- [3] J.N. Chengalur, Y. Gupta, and K.S. Dwarakanath, "Low Frequency Radio Astronomy," 3rd Edition, NCRA and TIFR, India, pp. 21-38, 2007.
- [4] W.N. Christiansen, and J.A. Hogbom, "Radiotelescopes," 2nd Edition, Cambridge University Press, London, UK, pp. 1-16, 1985.
- [5] J. D. Kraus, "Radioastronomy," 2nd Edition, Cygnus-Quasar Books, USA, 1986.
- [6] "Characteristics of Radio Quiet Zones," ITU-R RA.2259, International Telecommunication Union, Sep. 2012.
- [7] SKA, [cited Oct. 17, 2014]. Available from URL: <https://www.ska.gov.au>.
- [8] CSIRO, [cited Oct. 17, 2014]. Available from URL: <https://www.csiro.au>.
- [9] "Reverberation chamber test method," IEC 61000-4-21: 2011, EMC, Part 4-21: Testing and Measurements Technique, Apr. 2011.
- [10] P. Besnier, and B. Démoulin, "Electromagnetic Reverberation Chambers," ISTE Ltd, London, UK, pp. 140-184, 2011.
- [11] P. Corona, G. Latmiral, E. Paolini, and L. Piccioli, "Use of a Reverberating Enclosure for Measurements of Radiated Power in the Microwave Range," *IEEE Transactions on EMC*, vol. 18, no. 2, pp. 54-59, May, 1976.
- [12] J. L. Bean, and R. A. Hall, "Electromagnetic susceptibility measurements using a mode-stirred chamber," *International Symposium on EMC*, Atlanta, GA, USA, pp. 143-150, Jun. 20-22, 1978.
- [13] M. T. Ma, M. Kanda, M. L. Crawford, and E. B. Larsen, "A Review of Electromagnetic Compatibility/Interference Measurement Methodologies," *IEEE Transactions on EMC*, vol. 73, no. 3, pp. 388-411, Mar. 1985.
- [14] M. Bäckström, O. Lundén, and P-S. Kildal, "Reverberation chambers for EMC susceptibility and emission analyses," *Review of Radio Science 1999-2002*, pp. 429-452, 2002.
- [15] E. Broström, "Investigation of the EM Field Distribution in an Undermoded Reverberation Chamber," report no. FOI-R-0823-SE, ISSN 1650-1942, Mar. 2003. – Master's thesis [FOI-Swedish Defence Research Agency]

- [16] F. Schlagenhauser, and P. Kay, "Graphical Presentation of Simulated Field Data for a Hybrid TEM/Reverberation Chamber," *IEEE 2007 International Symposium on Microwave, Antenna, Propagation, and EMC Technologies for Wireless Communications*, Hangzhou, China, Aug. 16-17, 2007.
- [17] P. Kay, "A Hybrid TEM-Reverberation Chamber for Electromagnetic Immunity Testing," Ph.D. dissertation, Department of Electrical and Information Engineering, University of South Australia, Jul. 2009.
- [18] A. Walters, T. Doan, and C. Denton, "Field Characterisation of an Aircraft Sized TEM Cell," *Electromagnetic Compatibility Symposium*, Adelaide, Australia, pp. 47-52, Aug. 16-18, 2009.
- [19] K. Goldsmith, "Reverberation Chambers – What Are They?," *IEEE EMC Society Newsletter*, Fall, IEEE EMC Society, 1999.
- [20] J.W. Nijenhuis, A.P.J. V. Deursen, "Characterization of a contest 5 x 4 x 3 m reverberating chamber," *EMC Europe*, Poland, Sep. 13-17, 2010.
- [21] A. Cozza, "The Role of Losses in the Definition of the Overmoded Condition for Reverberation Chambers and Their Statistics," *IEEE Transactions on Electromagnetic Compatibility*, Vol. 53, Issue 2, pp. 296-307, May 2011.
- [22] Y. Cui, S. Y. Wang, and Y. Mao, "Study of the Effect of Chamber Shape and Loading Position on Reverberation Chamber Performance," *Asia-Pacific EMC Symposium; APEMC*, Singapore, May 21-24, 2012.
- [23] D. I. Wu, and D. C. Chang, "The Effect of an Electrically Large Stirrer in a Mode-Stirred Chamber," *IEEE Transactions on Electromagnetic Compatibility*, Vol. 31, no. 2, pp. 164-169, May 1989.
- [24] D. A. Hill, "Electronic mode stirring for reverberation chambers," *IEEE Transaction on EMC*, Vol 36, Issue 4, pp. 294-299, Nov. 1994.
- [25] J. Clegg, A. C. Marvin, J. F. Dawson, and S. J. Porter, "Optimization of Stirrer Designs in a Reverberation Chamber," *IEEE Transactions on EMC*, vol. 47, no. 4, pp. 824-832, Nov. 2005.
- [26] E. B. Ibrahim, S. Lalléchère, P. Bonnet, J. Benoit, and F. Paladian, "Computing total scattering cross section from 3-D reverberation chambers time modeling," *Asia-Pacific EMC Symposium; APEMC*, Singapore, May 21-24, 2012.
- [27] S. Pfennig, and H. G. Krauthäuser, "A General Method for Determining the Number of Independent Stirrer Positions in Reverberation Chambers," *EMC EUROPE 2012*, Rome, Italy, Sep. 17-21, 2012.
- [28] A. Adardour, G. Andrieu, and A. Reineix, "Influence of a Stirrer on the Cavity Modes Within a Reverberation Chamber," *EMC EUROPE 2012*, Rome, Italy, Sep. 17-21, 2012.

- [29] J. Perini, and L. Cohen, "Extending the Operation of Mode Stirred Chambers to Low Frequencies," *IEEE International Symposium on EMC*, Volume 2, pp. 964 – 965, Aug. 19 – 23, 2002.
- [30] R. Serra, and F. Canavero, "A One-Dimensional Interpretation of the Statistical Behavior of Reverberation Chambers," *ICEAA*, Italy, Sep. 17-21, 2007.
- [31] W. J. Krzysztofik, and S. Wolny, "Design of small reverberation chamber for handsets testing," Microwave, *International Conference on Radar and Wireless Communications; MIKON 2008*, Wroclaw, Poland, May 19-21, 2008.
- [32] J.-S. Kim, and R. Mittra, "Performance Evaluation of a Mode-Stirred Reverberation Chamber Using the Finite Difference Time Domain (FDTD) Simulation," *Asia-Pacific EMC Symposium; APEMC*, Singapore, May 21-24, 2012.
- [33] H. Zhao, Z. Shen, and E. Li, "Hybrid numerical modelling of reverberation chambers," *Asia-Pacific EMC Symposium; APEMC*, Singapore, May 21-24, 2012.
- [34] J. Perini, and L. Cohen, "An Alternative Way to Stir the Fields in a Mode Stirred Chamber," *IEEE International Symposium on EMC*, vol. 2, pp. 633 – 637, Aug 21 – 25, 2000.
- [35] L. Shuanggang, X. Jiadong, D. Jianjin, and H. Yanning, "Experiment Investigation of the Antenna Layout in Source Stirring Reverberation Chamber," *IEEE Transactions on EMC*, vol. 978-1-4244-5623-9/10, pp. 594-597, 2010.
- [36] F. B. J. Leferink, "Using reverberation chamber for EM measurements," *SoftCOM*, Croatia, Sep. 23-25, 2010.
- [37] A. Cozza, W. J. Koh, Y. S. Ng, and Y. Y. Tan, "Controlling the State of a Reverberation Chamber by means of a Random Multiple-Antenna Stirring," *Asia-Pacific EMC Symposium; APEMC*, Singapore, May 21-24, 2012.
- [38] Z. Bo, Y. Zhiyong, H. Jinliang, "Comparison on the Test Results between Reverberation Chamber and Anechoic Chamber," *Asia-Pacific EMC Symposium; APEMC*, Singapore, May 21-24, 2012.
- [39] E. Amador, C. Lemoine, and P. Besnier, "A Probabilistic Approach to Susceptibility Measurement in a Reverberation Chamber," *Asia-Pacific EMC Symposium; APEMC*, Singapore, May 21-24, 2012.
- [40] F. Moglie, and V. M. Primiani, "Numerical analysis of a new location for the working volume inside a reverberation chamber," *IEEE Transactions on Electromagnetic Compatibility*, vol. 54, no. 2, pp. 238–245, 2012.
- [41] G. Gradoni, V. M. Primiani, and F. Moglie, "Reverberation chamber as a statistical relaxation process: Entropy analysis and fast time domain simulations," *EMC EUROPE 2012*, Rome, Italy, Sep. 17-21, 2012.

- [42] D. Senić, and A. Šarolić, “Shielding Effectiveness Measurements in Resonant Enclosure based on Loaded Reverberation Chamber in a GTEM Cell,” *EMC EUROPE 2012*, Rome, Italy, Sep. 17-21, 2012.
- [43] Q. Wang, R. Jia, and E. Cheng, “Experimental Research on Immunity Test Method Using Reverberation Chamber and Relevance with other Platform,” *Asia-Pacific EMC Symposium; APEMC*, Singapore, May 21-24, 2012.
- [44] V. M. Primiani, P. Russo, and G. Cerri, “Experimental Characterization of a Reverberation Chamber Excited by the Source Stirring Technique,” *EMC EUROPE 2012*, Rome, Italy, Sep. 17-21, 2012.
- [45] R. Vogt-Ardatjew, S. V. D. Beek, and F. Leferink, “Wide-band Antennas for Reverberation Chambers,” *EMC EUROPE 2012*, Rome, Italy, Sep. 17-21, 2012.
- [46] S. V. D. Beek, R. Vogt-Ardatjew, H. Schipper, and F. Leferink, “Vibrating Intrinsic Reverberation Chambers for shielding effectiveness measurements,” *EMC EUROPE 2012*, Rome, Italy, Sep. 17-21, 2012.
- [47] J. Carlsson, K. Karlsson, and A. Johansson, “Validation of Shielding Effectiveness Measurement Method Using Nested Reverberation Chambers by Comparison with Aperture Theory,” *EMC EUROPE 2012*, Rome, Italy, Sep. 17-21, 2012.
- [48] A. Manicke, and H. G. Krauthäuser, “Pulse Excitations of Reverberation Chambers Simulations with an Approach Using Time Domain Plane Waves,” *EMC EUROPE 2012*, Rome, Italy, Sep. 17-21, 2012.
- [49] M. Magdowski, R. Vick, and M. Aidam, “Alternative Field Leveling and Power Control of Immunity Tests in a Reverberation Chamber,” *EMC EUROPE 2012*, Rome, Italy, Sep. 17-21, 2012.
- [50] K. Rosengren, P. Bohlin, and P.-S. Kildal, “Multipath Characterization of Antennas for MIMO Systems in Reverberation Chamber Including Effects of Coupling and Efficiency,” *IEEE on AP Society International Symposium*, Monterey, California, Jun. 20-25, 2004.
- [51] P.-S. Kildal, and K. Rosengren, “Correlation and capacity of MIMO systems and mutual coupling, radiation efficiency and diversity gain of their antennas: Simulations and measurements in reverberation chamber,” *IEEE Communications Magazine*, vol. 42, no. 12, pp. 102-112, Dec. 2004.
- [52] P.-S. Kildal, and C. Orlenius, “Characterization of Mobile Terminals in Rayleigh fading by using Reverberation Chamber,” *18th International Conference on Applied Electromagnetics and Communications*, 2005. Dubrovnik, Russia, Oct. 12-14, 2005.
- [53] A. A. H. Azremi, H.-G. Shiraz, and P. S. Hall, “Small Antenna Efficiency using the Reverberation Chamber and the Wheeler Cap methods,” *Malaysia International Conference on Communications*, Kuala Lumpur, Malaysia, 2005.

- [54] A. A. H. Azremi, H.-G. Shiraz, and P. S. Hall, "A Comparative Study of Small Antenna Efficiency Measurements," in *Proceeding of the 2005 Asia Pacific Conference on Applied Electromagnetics*, Malaysia, Dec. 20-21, 2005.
- [55] A. A. H. Azremi, "An Investigation of Rayleigh Distribution in Reverberation Chamber," *International RF and Microwave Conference 2006; RFM 2006*, Malaysia, Sep. 12-14, 2006.
- [56] C. L. Holloway, D. A. Hill, J. M. Ladbury, P. Wilson, G. Koepke, and J. Coder, "On the use of reverberation chambers to simulate a controllable Rician radio environment for the testing of wireless devices," *IEEE Transactions on Antennas and Propagation*, vol. 54, no. 11, pp. 3167-3177, Nov. 2006.
- [57] C. Orlenius, N. Aijaz, and M. Franzen, "Active MIMO Performance Measurements in Connected Reverberation Chambers," *Proceedings of the Fourth European Conference on Antennas and Propagation; EuCAP*, Spain, Apr. 12-16, 2010.
- [58] K. A. Remley, H. Fielitz, H. A. Shah, and C. L. Holloway, "Simulating MIMO Techniques in a Reverberation Chamber," *International Symposium on EMC*, Italy, Aug. 14-19, 2011.
- [59] D. Jianjin, G. Enquan, Z. Chuxin, and X. Ning, "Performance comparison of Source Stirring Reverberation Chamber and Mechanical Stirring," *Asia-Pacific EMC Symposium; APEMC*, Singapore, May 21-24, 2012.
- [60] C. L. Holloway, R. S. Smitch, C. R. Dunlap, R. J. Pirke, J. Ladbury, W. F. Young, D. A. Hill, W. R. Hansell, A. Shadish, and K. B. Sullivan, "Validation of a two-antenna reverberation-chamber technique for estimating the total and radiation efficiency of antennas," *EMC EUROPE 2012*, Rome, Sep. 17-21, 2012.
- [61] C. Choeysakul, F. Schlagenhauer, and P. Hall, "Characterisation and Design of a Reverberation Chamber for Electromagnetic Emission Measurements for Radio Astronomy Applications," *EMC Society of Australia Newsletter*, Issue no. 59, Dec. 2012.
- [62] R. Rehammar, A. Skårbratt, and C. Orlenius, "Measuring 4x4 MIMO capability in reverberation chambers," *Proceedings of the Seventh European Conference on Antennas and Propagation; EuCAP*, Gothenburg, Sweden, Apr. 8-12, 2013.
- [63] "Radiated, radio-frequency, electromagnetic field immunity test," IEC 61000-4-3, EMC, Part 4-3: Testing and Measurement Techniques, 2008.
- [64] International Electrotechnical Commission (IEC), "Electromagnetic compatibility/ Basic concept," [cited Feb. 10, 2012]. Available from URL: <http://www.electropedia.org>.
- [65] R. D. Ehrbar, J. M. Fraser, R. A. Kelley, L. H. Morris, E. T. Mottram, and P. W. Rounds, "The SD Submarine Cable System," *The Bell System Technical Journal 1922-1983*, vol. 43: 4, Paris, France, pp. 1243-1273, Jul. 1964.
- [66] M. Schwartz, "Carrier-wave telephony over power lines: Early history [History of Communications]," *IEEE Comm. Mag.*, vol. 47, Issue 1, pp. 14-18, Jan. 2009.

- [67] M. Schwartz, "Improving the Noise Performance of Communication Systems: Radio and Telephony Developments of the 1920s," *IEEE Communications Magazine*, vol. 47, Issue 12, pp. 16-20, Dec. 2009.
- [68] M. Schwartz, "Improving the Noise Performance of Communication Systems: 1930s to early 1940s," *History of Telecommunications Conference 2008; HISTELCON 2008*, Paris, France, Sep. 11-12, 2008.
- [69] T. Johnson, "Naval Aircraft Radio," *Proceedings of the Institute of Radio Engineers*, vol. 8, no. 2, pp. 87-134, Apr. 1920.
- [70] G. Levy, "Loop Antennas for Aircraft," *Proceedings of the Institute of Radio Engineers*, vol. 31, no. 2, pp. 56-66, Feb. 1943.
- [71] D. E. C. Möhr, "History of EMC," [cited Oct. 17, 2014]. Available from URL: http://www.emtest.com/what_is/emv-emc-basics.php.
- [72] D. S. Friday, "Radio-Frequency Metrology from NBS to NIST: The Legacy," *Microwave Symposium Digest: 2001 IEEE MTT-S International*, Phoenix, AZ, USA, May 20-25, 2001.
- [73] E. W. Allen, and H. Garlan, "Evolution of Regulatory Standards of Interference," *Proceedings of the Institute of Radio Engineers*, Vol. 50, no. 5, pp. 1306-1311, May 1962.
- [74] L. F. Curtis, "Electrical Interference in Motor Car Receivers," *Proceedings of the Institute of Radio Engineers*, vol. 20, no. 4, pp. 674-688, Apr. 1932.
- [75] A. C. Kucukozyigit, "Electronic Warfare (EW) Historical Perspectives and its Relationship to Information Operation (IO)-Considerations for Turkey," Naval Postgraduate School, Monterey, CA, USA, Sep. 2006.
- [76] The Forrestal Fire, July 29, 1967 Ship's Logs contributed by Ken Killmeyer, USS Forrestal Association Historian, aboard July 29, 1967, [cited Sep. 26, 2013]. Available from URL: <http://www.navsource.org/archives/02/cv-59/59f-0729.htm>.
- [77] T.J. Duggan, "Military Aircraft Electromagnetic Compatibility: Release to Service Testing in the United Kingdom, Past, Present and Future," *IEEE International Symposium on EMC 2007: EMC 2007*, Honolulu, HI, USA, Jul. 9-13, 2007.
- [78] R. T. Schilizzi, P. E. F. Dewdney, and T. J. W. Lazio, "The Square Kilometre Array," *Proc. of SPIE*, vol. 7012, 701211-13, 2008.
- [79] S. Mazzola, "MIL-STD-461: The basic military EMC specification and its evolution over the years," *Systems, Apps. and Tech. Conf., 2009: LISAT '09*, NY, USA, May 2009.
- [80] International Electrotechnical Commission (IEC), "IEC and EMC/ How the IEC is organized for EMC," 2013, [cited Sep. 17, 2013]. Available from URL: <http://www.iec.ch/index.htm>.
- [81] M. L. Crawford, "Generation of standard EM fields using TEM transmission cells," *IEEE Transactions on Electromagnetic Compatibility*, vol. EMC-16, no. 4, pp. 189-195, Nov. 1974.

- [82] "Emission and Immunity Testing in Transverse Electromagnetic (TEM) Waveguides," IEC 61000-4-20:2007, Ed 1.1, EMC, Part 4-20: Testing and Measurement Techniques, 2007.
- [83] M. Debowski, "Measurement of electromagnetic compatibility using GTEM chambers," *The Eighth International Conference on Environment and Electrical Engineering; IEEEIC 2009*, Madrid, Spain, May 10-13, 2009.
- [84] D. K. Cheng, "Field and Wave Electromagnetics," Addison-Wesley Publishing Company, Canada, pp. 486-493, 1983.
- [85] W. H. Hayt, and J. A. Buck, "Engineering Electromagnetics," 6th Edition, McGraw-Hill, New York, USA, 2001.
- [86] D. M. Pozar, "Microwave Engineering," 2nd Edition, John Wiley and Sons, Crawfordsville, IN, USA, 1998.
- [87] S. Wang, Z. Wu, G. Wei, Y. Cui, and L. Fan, "A New Method of Estimating Reverberation Chamber Q-Factor with Experimental Validation," *Progress In Electromagnetics Research Letters*, vol. 36, pp.103-112, 2013.
- [88] "Radio frequency susceptibility (radiated and conducted)," RTCA/DO-160D: Environmental Conditions and Test Procedures for Airborne Equipment, Radio Technical Commission for Aeronautics, US Federal Aviation Administration, USA, 2000.
- [89] M. Vollmer, "Physics of the microwave oven," *Physics Education*, vol. 39, No. 1, pp. 74-81, 2004.
- [90] W. Wallyn, F. Olyslager, E. Laermans, and D. D. Zutter, "Fast Evaluation of the Shielding Efficiency of Rectangular Shielding Enclosures," *IEEE International Symposium on EMC*, vol. 1, Seattle, WA, USA, pp. 311-316, Aug. 2-6, 1999.
- [91] X. Zhou, J. Li, H. Fan, A. Bhohe, K. Taunk, J. Yu, and P. Sochoux, "Validating EMC Simulation by Measurement in Reverberation Chamber," *Signal integrity in serial interconnect designs; DesignCon 2013*, Santa Clara, CA, USA, Jan. 28-30, 2013.
- [92] Concept-II, "Advance Electromagnetic Field Simulation", [cited Aug. 10, 2014]. Available from URL: <http://www.tet.tuhh.de/concept/?lang=en>.
- [93] FEKO, [cited Aug. 10, 2014]. Available from URL: <https://www.feko.info/product-detail/overview-of-feko>.
- [94] CST Microwave Studio, [cited Aug. 10, 2014]. Available from URL: <https://www.cst.com/Products/CSTMws/IntegralEquationSolver>.
- [95] C. Choeyesakul, F. Schlagenhauser, P. Rattanakreep, and P. Hall, "EMC Applications for Military: Reverberation Chamber Tests," *The 20th Asia-Pacific Conference on Communications; APCC*, Pattaya, Thailand, Oct. 1-3, 2014.

- [96] C. Choeysakul, F. Schlagenhauser, and P. Hall, "Reducing the LUF of a Reverberation Chamber based on the concept of MIMO for Electromagnetic Emission Measurements for Radio Astronomy Applications," *Asia-Pacific EMC Symposium; APEMC*, Melbourne, VIC, Australia, May 20-23, 2013.
- [97] C. L. Holloway, P. F. Wilson, G. Koepke, and M. Candidi, "Total Radiated Power Limits for Emission Measurements in a Reverberation Chamber," *2003 IEEE International Symposium on EMC*, vol. 2, pp.838-843, Aug. 18-22, 2003.
- [98] "CRAF Handbook for Radio Astronomy," Committee on Radio Astronomy Frequencies (CRAF), European Science Foundation, Third edition, 2005.
- [99] R. Sitch, "The Dish," Roadshow Entertainment, Australia, 19 Oct. 2000.
- [100] G. H. Koepke, and J. M. Ladbury, "New electric field expressions for EMC testing in a reverberation chamber," *17th Digital Avionics Systems Conference (DASC) 1998*, pp. D53/1-D53/6, vol. 1, 31 Oct. 1998-7 Nov.1998.
- [101] Q. Maofei, W. Na, L. Zhiyong, and C. Maozheng, "Flux density measurements of 23 pulsars," *International Conference on Electronics and Optoelectronics; ICEOE*, Dalian, China, Jul. 29-31, 2011.
- [102] M. Ryle, "The Cambridge 1 mile radiotelescope," *Electronics and Power*, vol. 13, no. 6, pp. 208-212, Jun. 1967.
- [103] "Coordination of Apparatus Licensed Services within the Australian Radio Quiet Zone Western Australia," RALI-MS-32, Radiocommunications Assignment and Licensing Instruction, AUS, Dec. 2014.
- [104] H. Garbe, and D. Hansenlon, "The GTEM Cell Concept; Application of this new EMC test Environment to Radiated Emission and Susceptibility Measurements," *International Conference on EMC*, York, UK, Aug. 28-31, 1990.
- [105] Lord Rayleigh, "On the passage of electric waves through tubes, or the vibrations of dielectric cylinders," *Philosophical Magazine*, vol. XLIII, pp. 125-132, 1897.
- [106] J. R. Hampton, "Introduction to MIMO Communications," Cambridge University Press, London, UK, 2013.
- [107] J. D. North, "Cosmos: an illustrated history of astronomy and cosmology," University of Chicago Press, pp.661, 2008.
- [108] R. A. Batchelor, D. L. Jauncey, K. J. Johnston, V. A. Efanov, L. R. Kogan, V. I. Kostenko, K. I. Matveenko, I. G. Moiseev, S. H. Knowles, A. Kh. Papatsenko, R. Preston, J. Spenser, A. N. Timofeev, N. Fourikis, and R. W. Schilizzi, "First Global radio telescope," *Sov Astronom Letters*, vol. 2, No 2, Sep-Oct, 1976.

"Every reasonable effort has been made to acknowledge the owners of copyright material. I would be pleased to hear from any copyright owner who has been omitted or incorrectly acknowledged."

APPENDIX A

COMPUTATIONAL ELECTROMAGNETIC MODELLING
(ANSOFT HFSS SIMULATION PROGRAM)

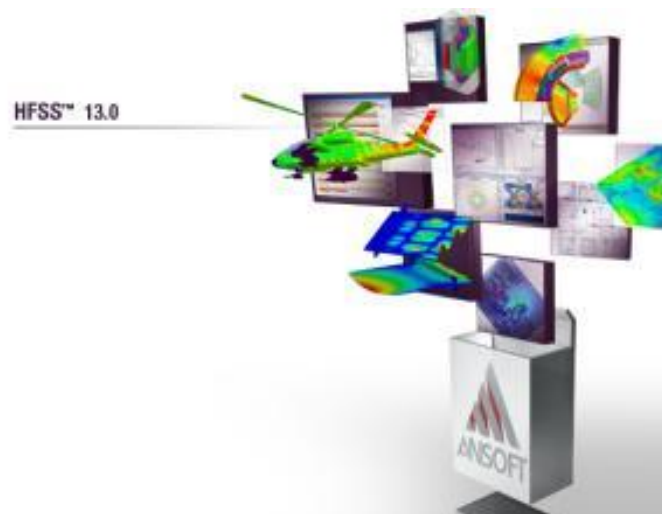


Figure A-1: ANSOFT HFSS V.13 is deployed to make a model of the actual shielded room (3.6m by 2.4m by 2.4m).

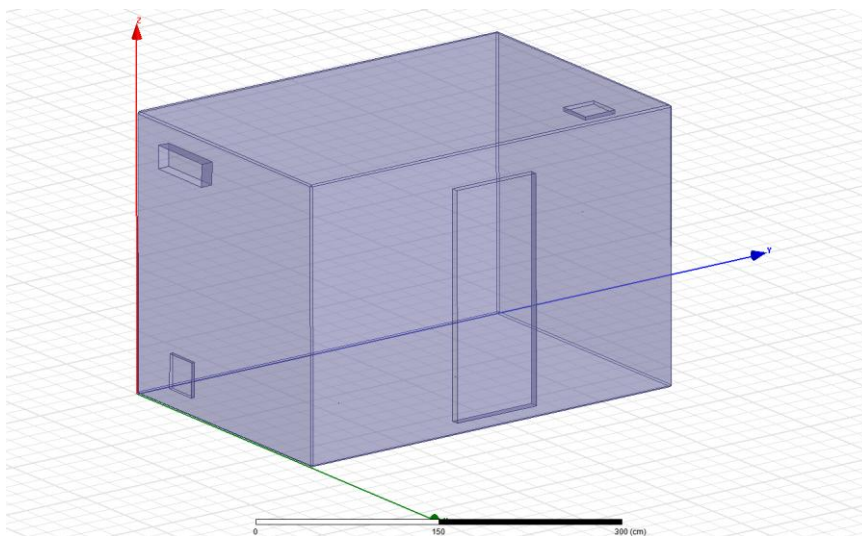
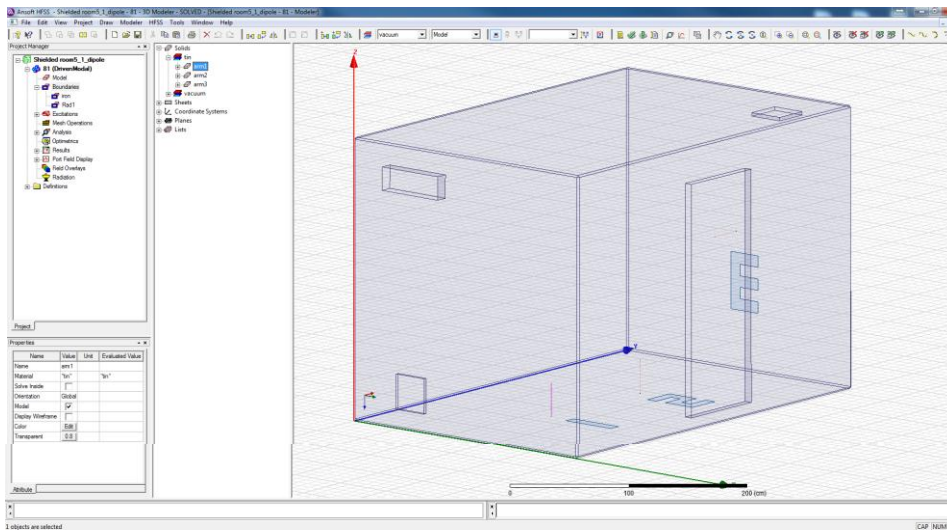
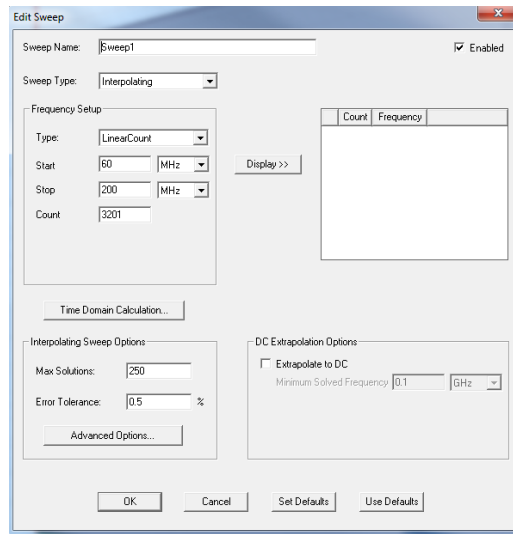


Figure A-3: A model of the existing shielded room in ANSOFT HFSS (with set-up parameters).

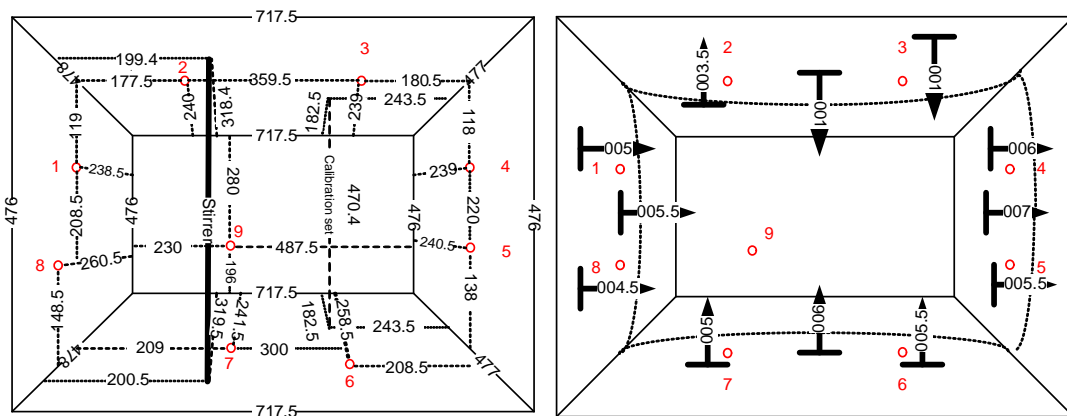
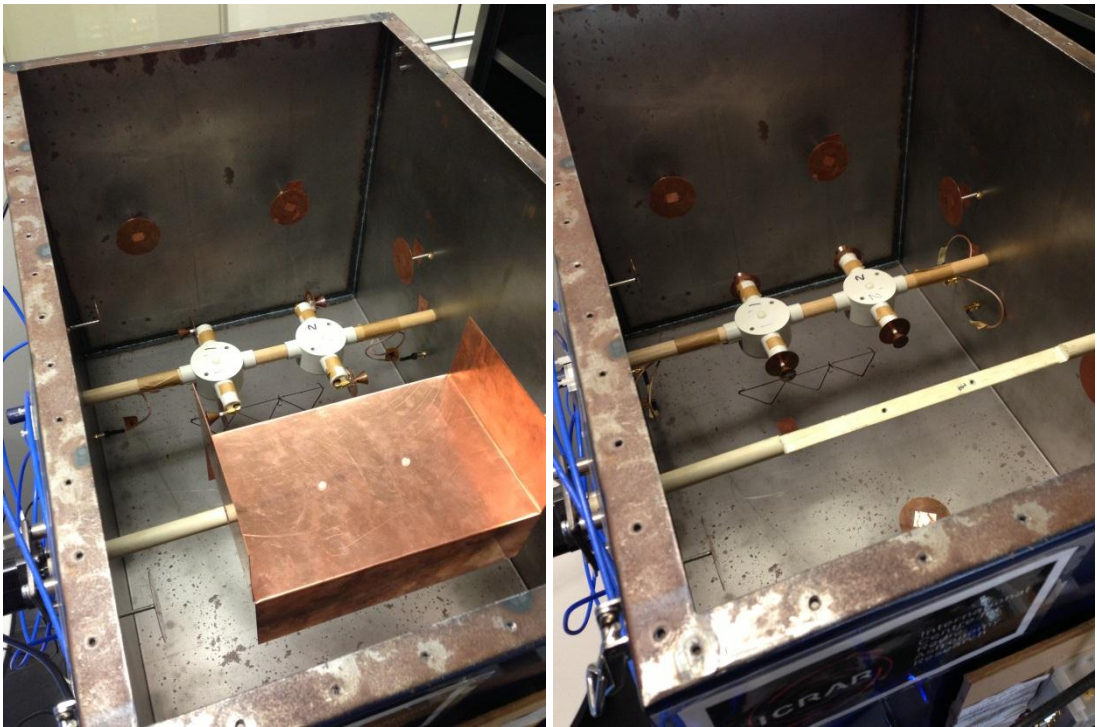


Figure A-4: Dimensions of the 1:5 Scaled Model (in mm) with positions of 9 receiving antennas, stirrer, and calibrating set.

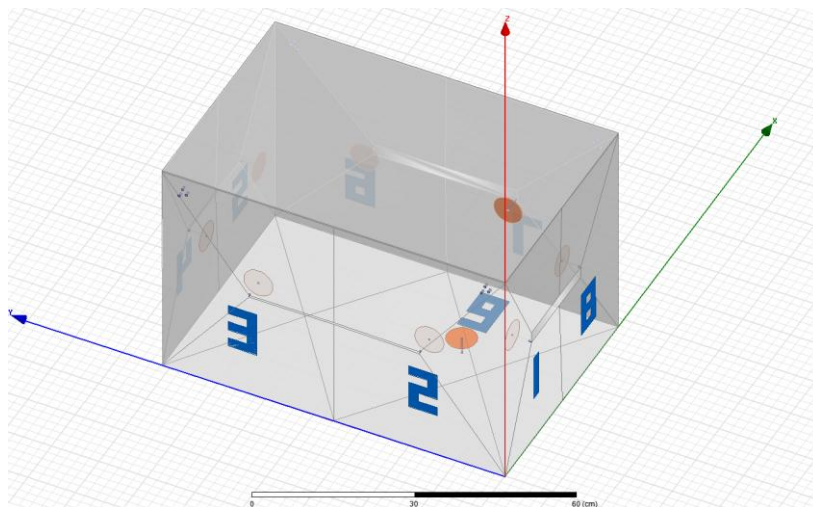
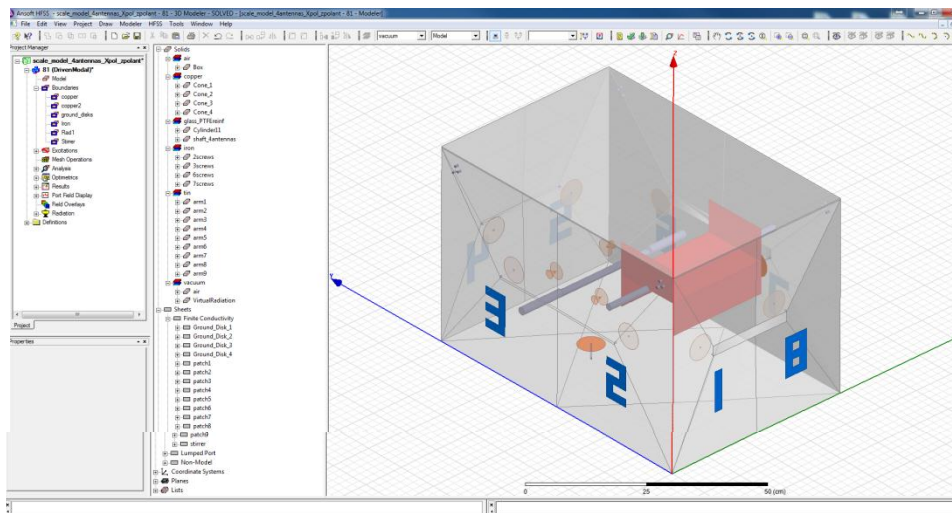
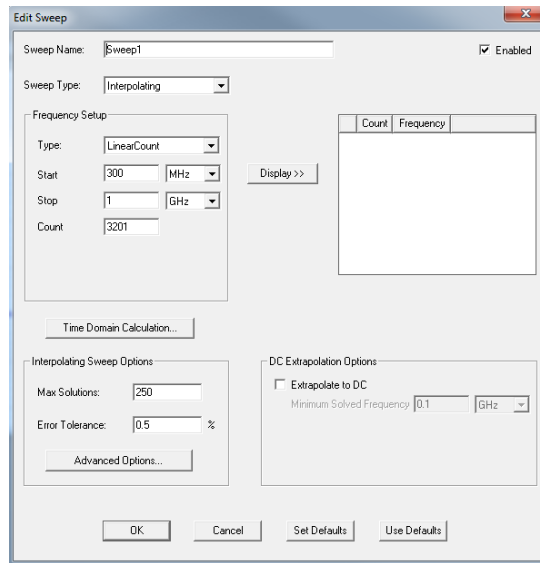
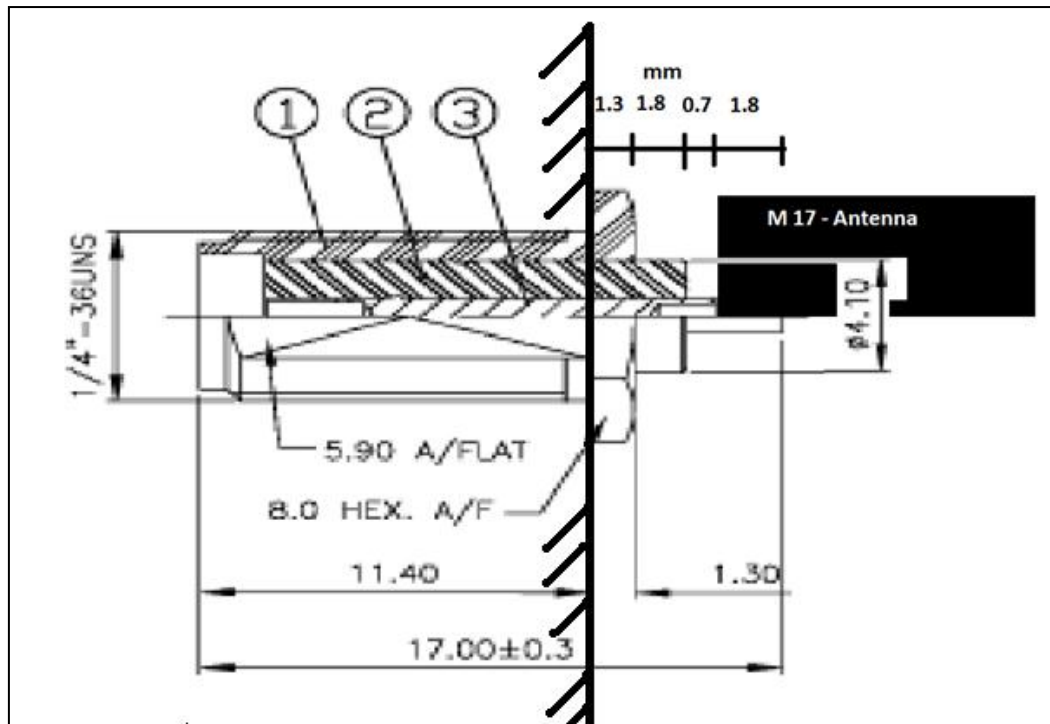
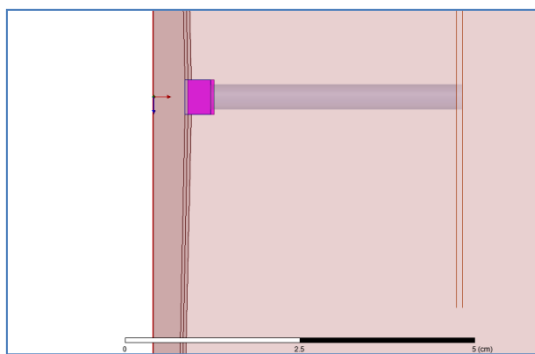


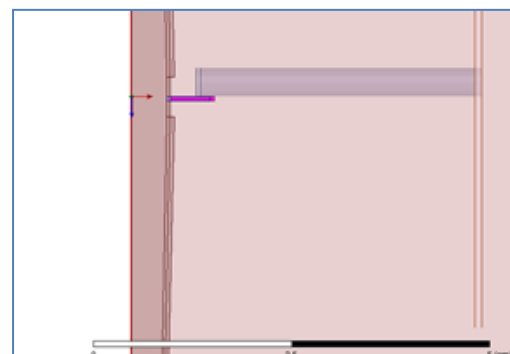
Figure A-5: A model of the 1:5 scaled model in ANSOFT HFSS (with set-up parameters).



a) SMA port and the antenna (in practice)



b) Feeding ports for normal used



c) Feeding ports used on the models

Figure A-6: Feeding Ports used with all models in this research in ANSOFT HFSS simulation program.

APPENDIX B

MATLAB AUTOMATING SYSTEM FOR COLLECTING THE DATA

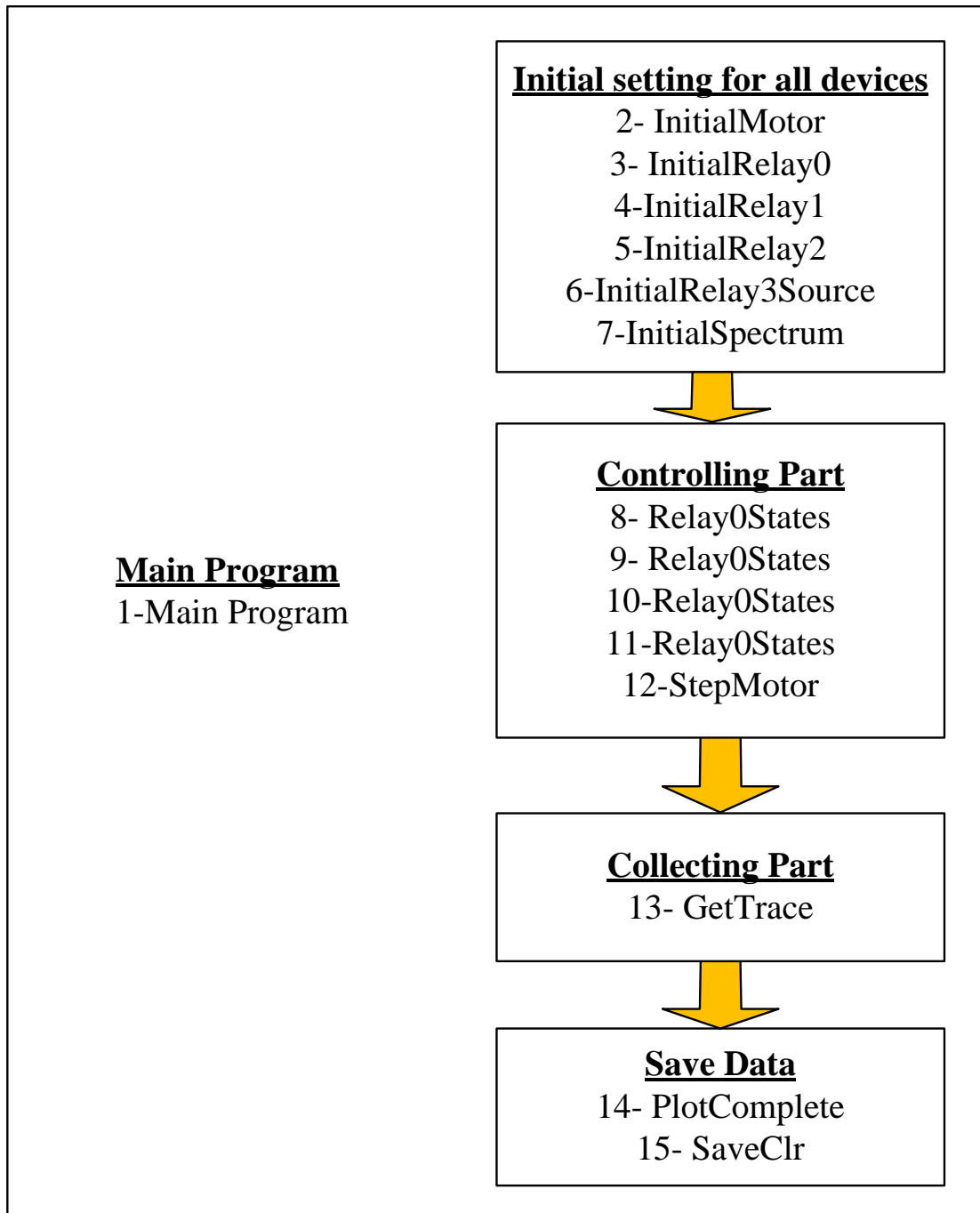


Figure B-1: All 15 sub codes of the Automating System for collecting the data.

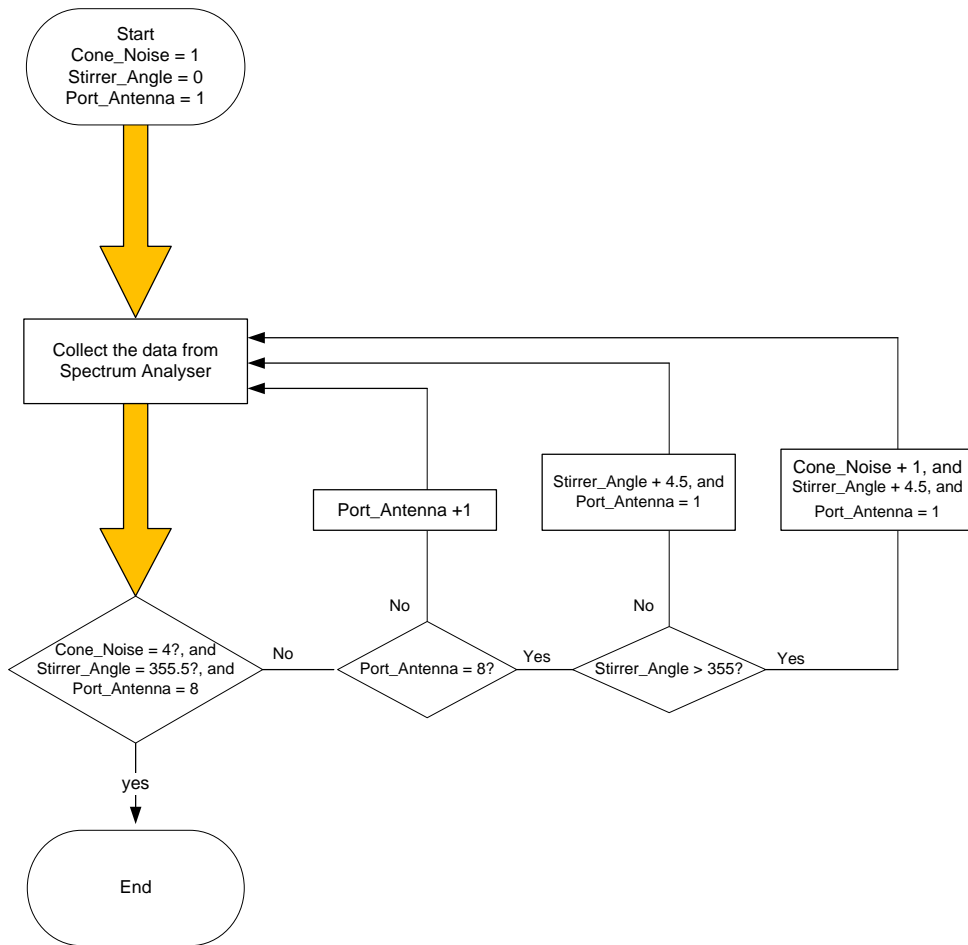


Figure B-2: MIMO Automating System for collecting the data.

APPENDIX C

THE GUI CODE FOR PORT-PROCESSING THE DATA

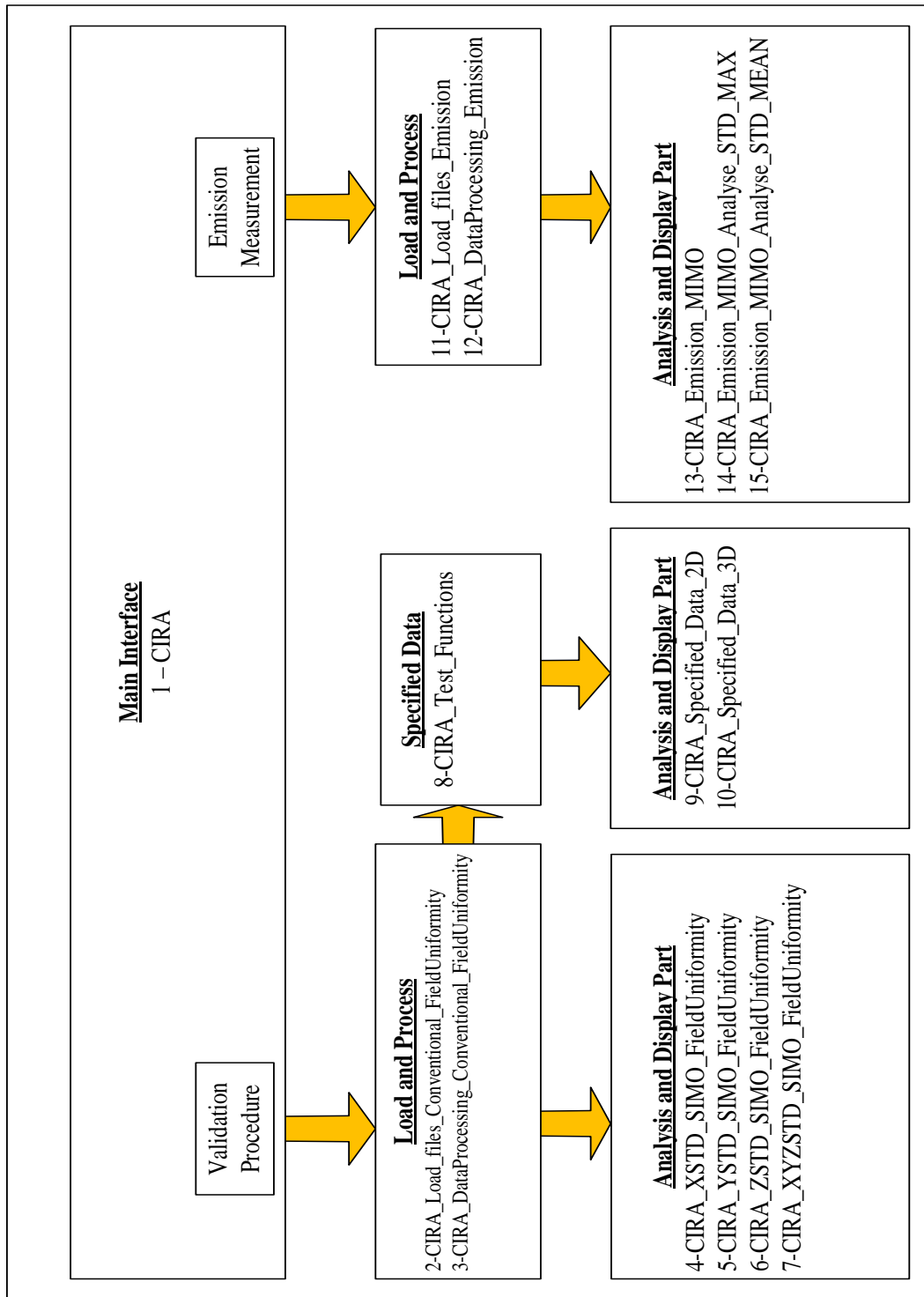


Figure C-1: All 15 sub codes of MATLAB Analysis System for post-processing the recorded data.

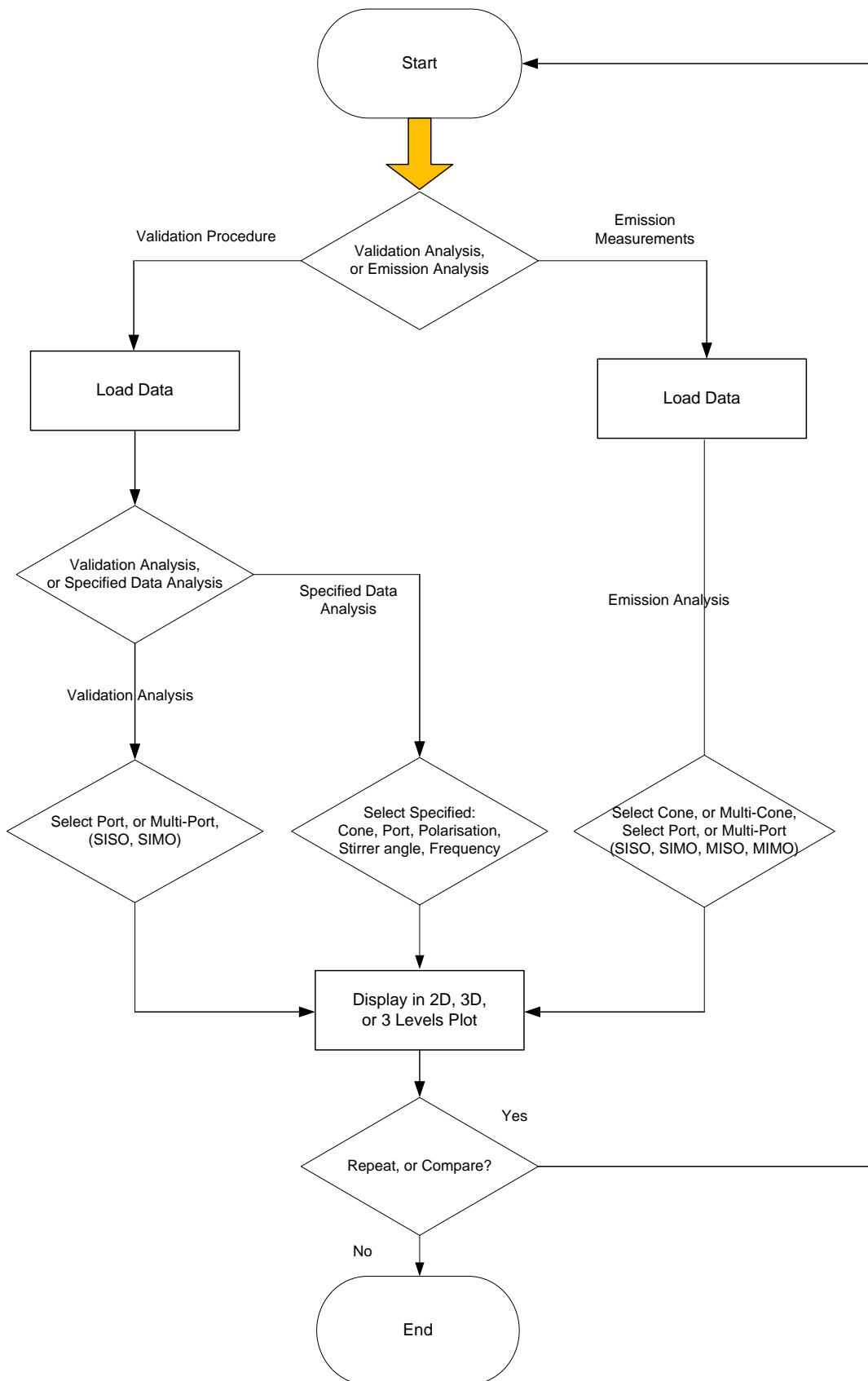


Figure C-2: MIMO Analysis System for post-processing the data.

Part of Validation Procedure: The left hand-side of the program (light blue colour, Fig. C-3) is to analyse data from validation procedure that is for calculating field uniformity. This part consists of 3 input panels with 1 display panel which has 3 multi-purposed screens. The first panel is for loading data. This panel is written separately for users to add/edit new data. The MATLAB code of this panel is written separately and it is named "CIRA_Load_files_Conventional_Fielduniformity." The second panel is Validation Procedure panel. This panel allows users to choose how many receiving antennas added into MIMO RC. If users choose only 1 receiving antenna, the system will become SISO system or conventional RC. Note, this panel does not allow users to choose number of cone antenna, as the system always wants 8 cone antenna positions to validate the field uniformity. The lowest area of the panel is for commands to display standard deviation (field uniformity) within working volume. The graphic can show for E_x , E_y , E_z , and E_{total} (all X, Y, and Z polarisations). The third panel is for specified data which allows users to investigate every specified loaded data. Conceptually, if standard deviation of a polarisation is bad, this will be a very useful panel to understand what cause the problem. This panel can show data in both ways; 2D or 3D. If user chooses 2D for display, user can compare 2 of whatever data in the third screen as well.

The newest version (6.0) has main capabilities:

- Maximum data analyses for validation procedure;
- Sub-functions for all codes;
- Display in 2D or 3D
- Validation procedure supported on left hand side (light blue screen);
- Load function for any new data;
- Separation load functions for validation procedure and emission testing;
- Drop-down menus can automatic change value of valuable;
- Specified data for any stirrer angle, or specified range of angle;
- Zoom plots;
- Comparison between 2 of any couple;
- Self-test.

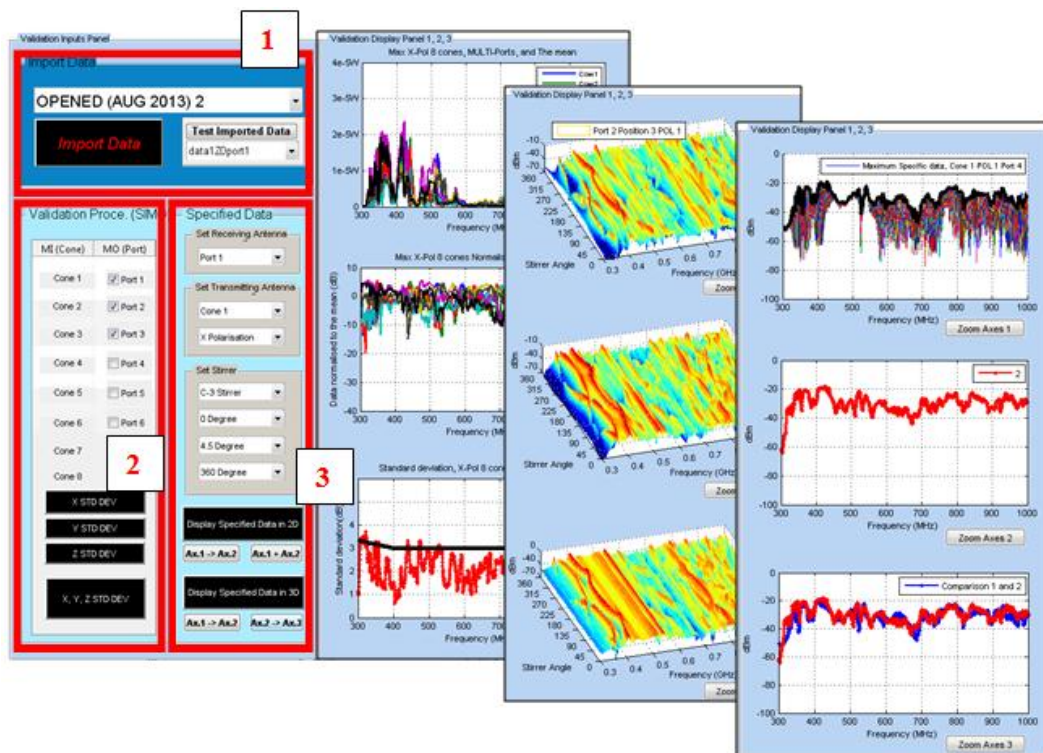


Figure C-3: Validation Procedure Analysis on GUI version 6.0.

Part of Emission measurement: The right hand-side of the GUI (orange colour, Fig. C-4) is to analyse data from emission measurement for calculating radiated power. When the chamber (without EUT) passed the validation procedure, an EUT can be placed in the working volume for emission measurements. The first panel is for loading recorded emission data. This panel is written separately for user to edit/add any new data. The MATLAB code for this panel is named “CIRA_Load_files_Emission.” The second panel is panel of MIMO emission measurements. This panel is planned to allow users to select number of receiving antenna in the future. Then, the user will have to click on “display” button to display information in the display panel. The mean values will be shown on the upper screen of the display panel, while the addition information will be displayed on the lower screen. User can still switch to see maximum value by clicking on “Analyse Max Value”.

The newest version (6.0) has main capabilities:

- Mean values analyses for emission measurement;
- Max values analyses for emission measurement;
- “ -0 / $+6$ dB strategy” support;
- Sub-functions for all codes;
- Display in 2D
- Emission measurements supported on right hand side (light yellow screen);
- Load function for any new data;
- Separation load functions for validation procedure and emission testing;
- Drop-down menus can automatic change value of valuable;
- Zoom plots;

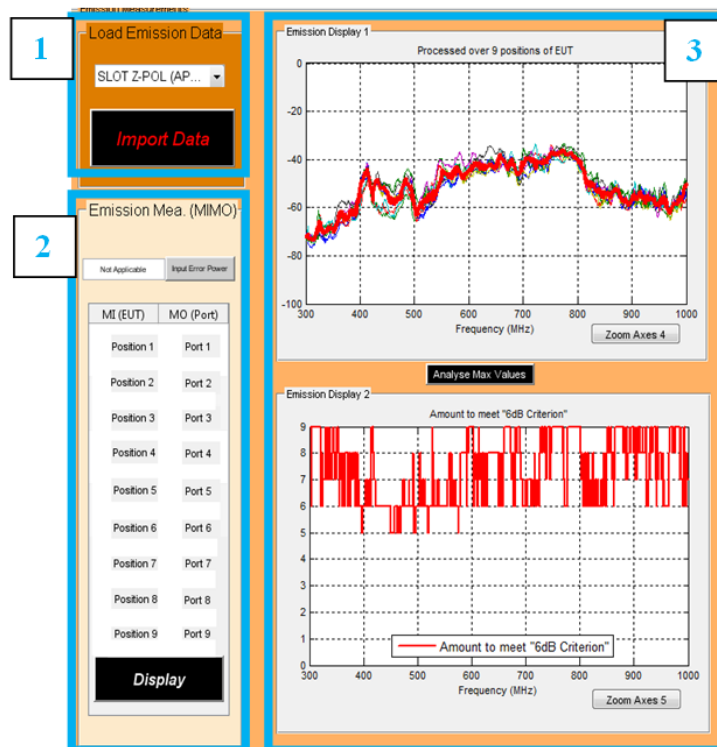


Figure C-4: Emission Measurement Analysis on GUI version 6.0.

APPENDIX D

MANUAL FOR MIMO REVERBERATION CHAMBER
(GUIDELINE FOR APPLYING MIMO RC TO THE ACTUAL ROOM OR OTHERS)

D.1 Introduction

Once design guidelines of MIMO RC have been found and analysis tools for MIMO RC have been developed on 1:5 scaled model, all procedures and developed tools can be transferred to the actual shielded room (or other RC) with some modifications. So, MIMO validation procedure and MIMO emission measurements could allow the shielded room to work as a MIMO RC.

D.2 Installation and Implementation

Characteristics of the actual shielded room and its model are stated in Chapter 3. The model's walls are made from steel, and the dimensions are about 3.6 m by 2.4 m by 2.4 m. The room has 3 honeycomb air vents and 1 door which are expected to influence the field distribution at low frequencies only slightly. Each wall's edge connected to another is covered by 45 degree metal brackets. The simulation model could be useful for studies before applying the MIMO RC concept on the actual shielded room to simulate the effect of; for example, changing material, antenna positions, working volume area, etc.

D.2.1) Receiving Antenna:

All receiving antennas should be placed close to the walls, similar as in the scaled model. Instead of using of fixed wall-mounted antennas as in the scaled model they may be installed on separate ground planes, which in turn are connected to the walls, to avoid the need to drill holes in the shielding structure. The antennas should be linear, passive, and electrically small. There is no need to have very good gain or very good reflection coefficient (S_{11} parameters), rather they should allow wideband operation and have smooth reflection coefficient (also smooth antenna factor).

The number of antennas should be at least 6, 2 antennas for each polarisation. Each position of them should be the same as in the scaled model (Figure 3-15); i.e., ideally placing around $1/4$ or $5/16$ along the length axis and the width axis from each corner on half of the height plane (suggested in Section 3.2.1). All antennas should be placed at least $\lambda/4$ at the C-LUF (290 MHz) from any structure, except from the

chamber walls, i.e., approximately 0.3 m. to allow use as conventional RC, above the C-LUF.

D.2.2) Stirrer:

The double C stirrer which has been found to provide better results compared to some other stirrers shapes (explained in Section 3.3.2) is scaled up and installed into the actual shielded room. The layout of the room allows an installation that does not obstruct access through the door.

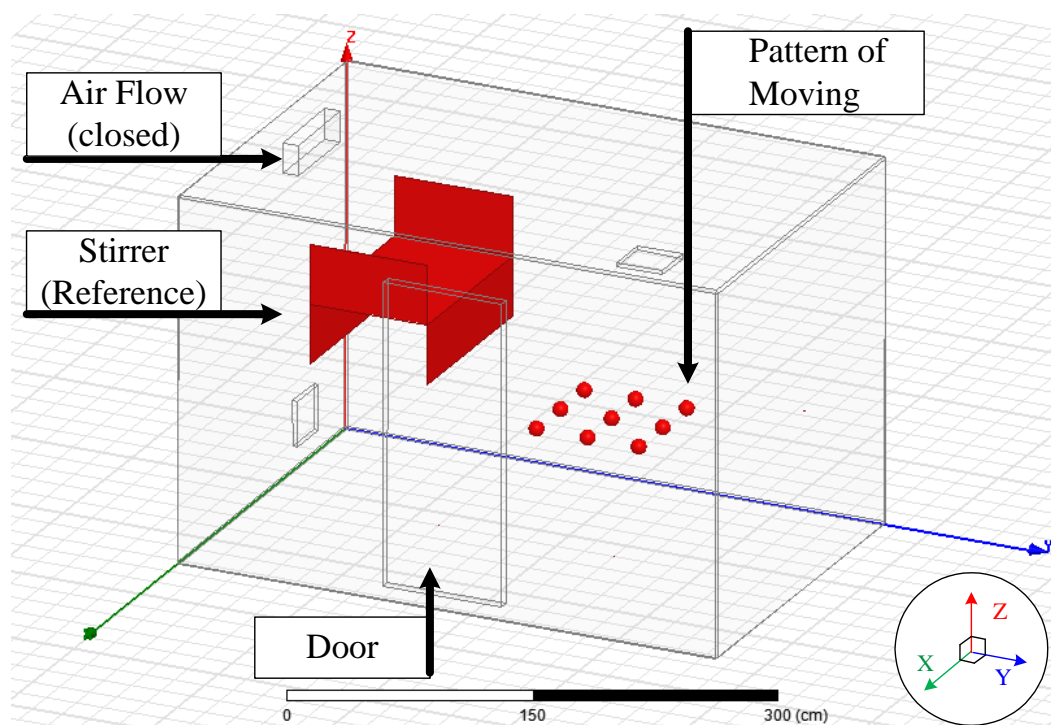


Figure D-1: The actual Shielded Room with its 1:1 model in ANSOFT HFSS.

D.2.3) MIMO-LUF:

At low frequencies the quality factor is dominated by the losses in the antennas and scales with frequency, i.e. at the quality factor in the full sized room is very similar to the factor in the scaled model at the respective frequencies. Also, the field distribution will not be affected significantly by the irregularities of the room (e.g. the door or the air vents). It can be expected that the performance of the full size room is

similar to the scaled model, at respective frequencies, and the MIMO-LUF scales accordingly, i.e. 1:5.

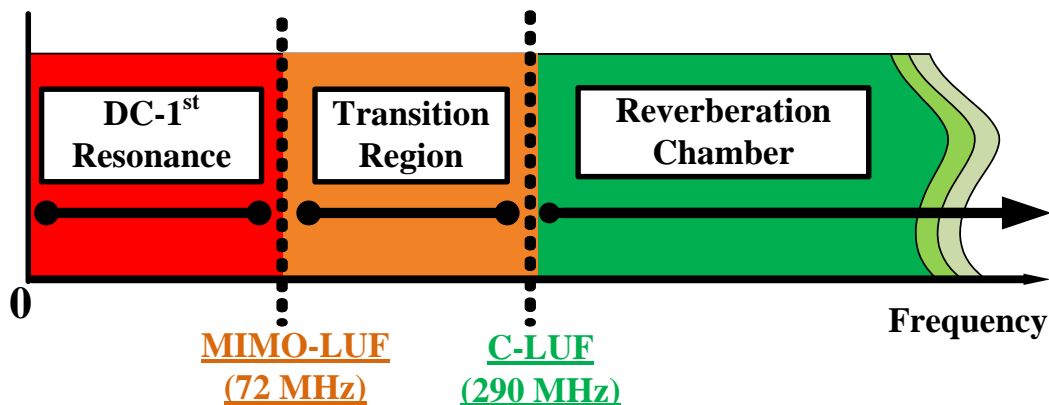


Figure D-2: Expected conditions of the actual Shielded Room when MIMO RC technique is applied.

D.2.4) Working Volume & Field uniformity:

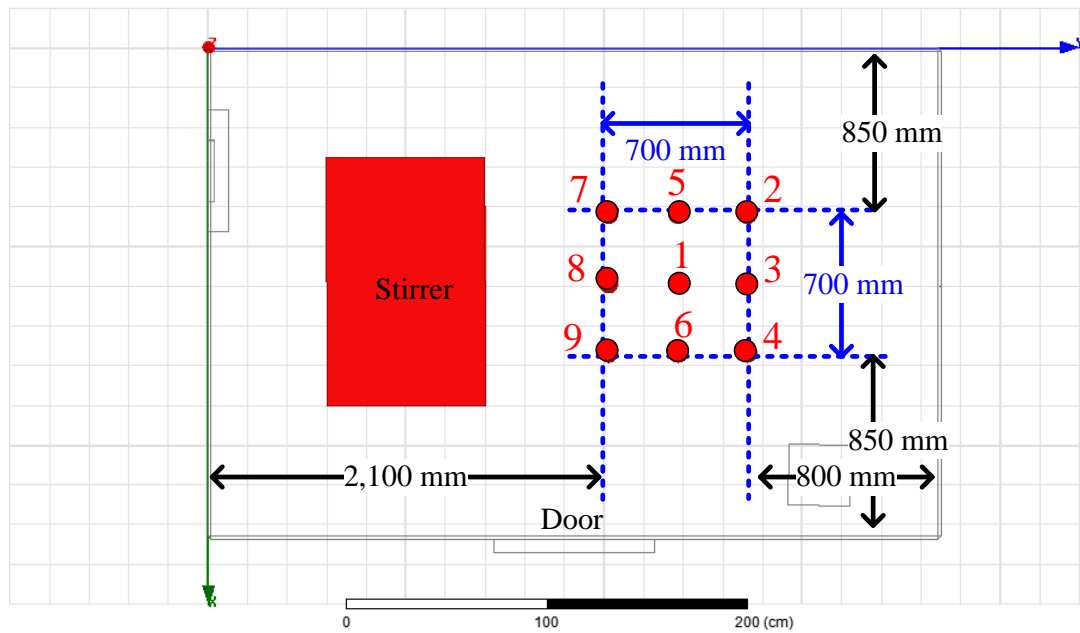
The quality factor in the shielded room will be only slightly higher than in the scaled model at low frequencies; emission measurements could therefore be slightly more sensitive, at respective frequencies, but otherwise the performance of the full size room and the scaled model should be very similar. Working volume and EUT positions can be chosen as in the scaled model.

D.2.5) Software and Programming:

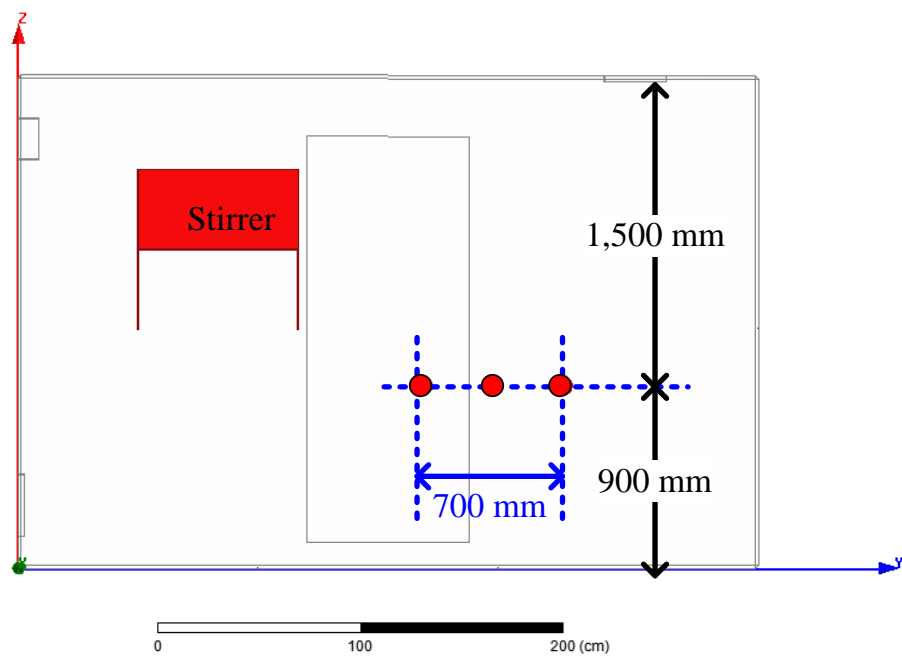
The MATLAB codes for collecting data and MATLABs GUI for analysing the data developed for the 1:5 scaled model can be used without the need for modifications.

D.3 Pattern of moving the EUT

Figure D-3 shows the actual shielded room being ready for testing. Guidelines for moving the EUT are stated in Section 5.2.2; the EUT is suggested to be moved for 9 positions. Then, all the measured data are going to be analysed by MATLABs GUI for the final result.



a) Top view



b) Side view

Figure D-3: Pattern on moving EUT for 9 positions in the actual Shielded Room.

APPENDIX E

KEY MEASURED RESULTS

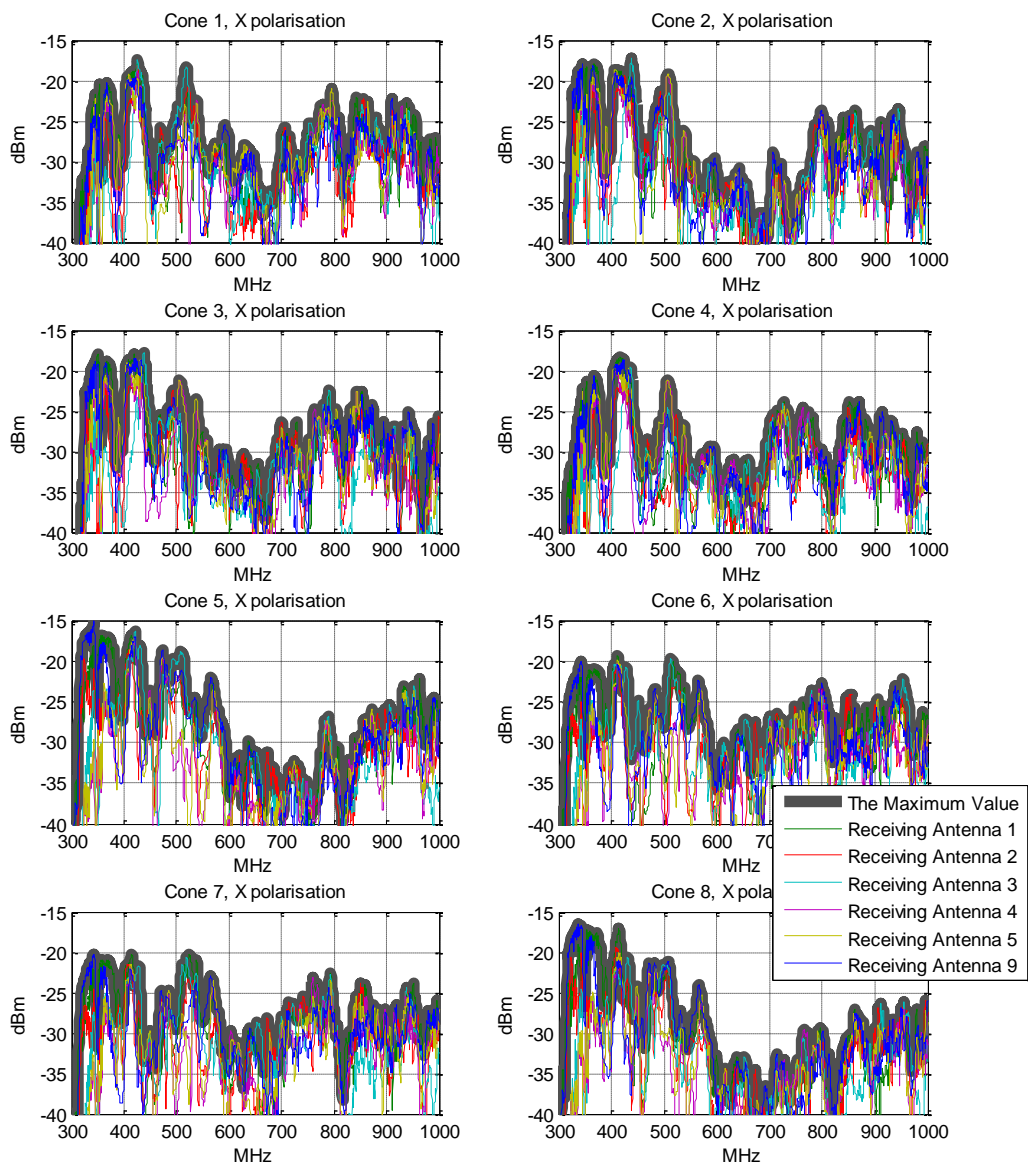


Figure E-1: from Section 4.3.2, MIMO Validation Procedure: Raw data, from each cone to receiving antennas, only X-polarisation (the maxima are used).

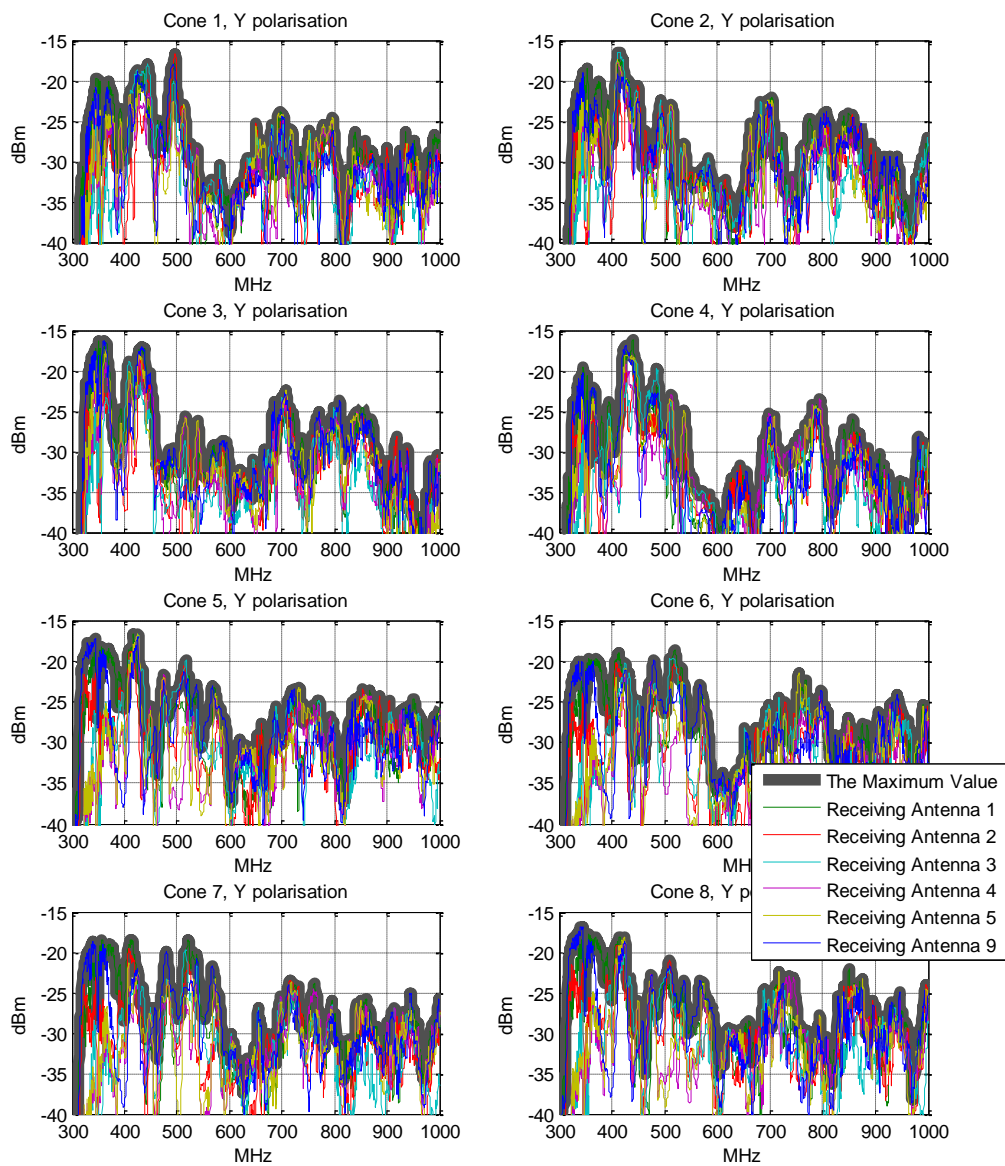


Figure E-2: from Section 4.3.2, MIMO Validation Procedure: Raw data, from each cone to receiving antennas, only Y-polarisation (the maxima are used).

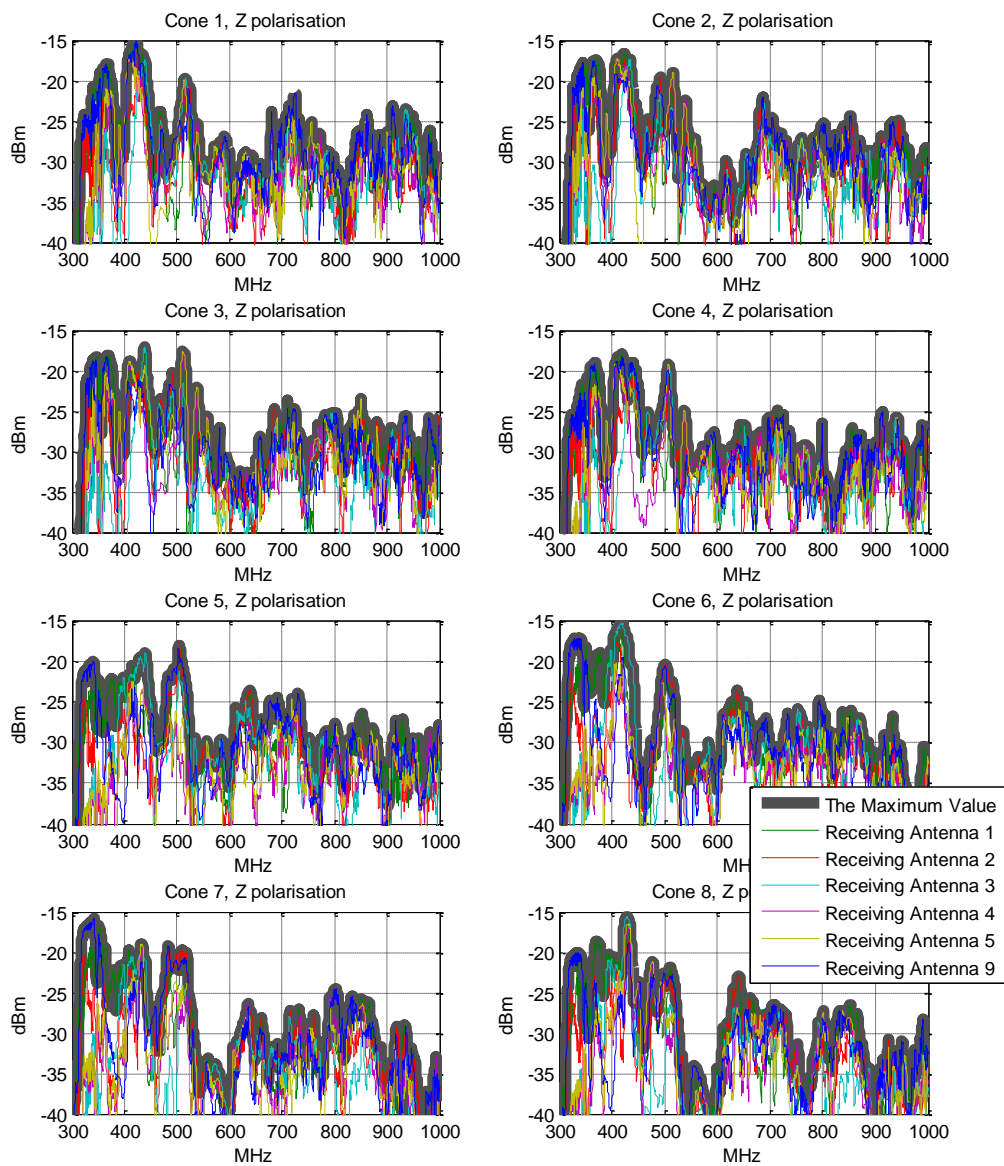


Figure E-3: from Section 4.3.2, MIMO Validation Procedure: Raw data, from each cone to receiving antennas, only Z-polarisation (the maxima are used).

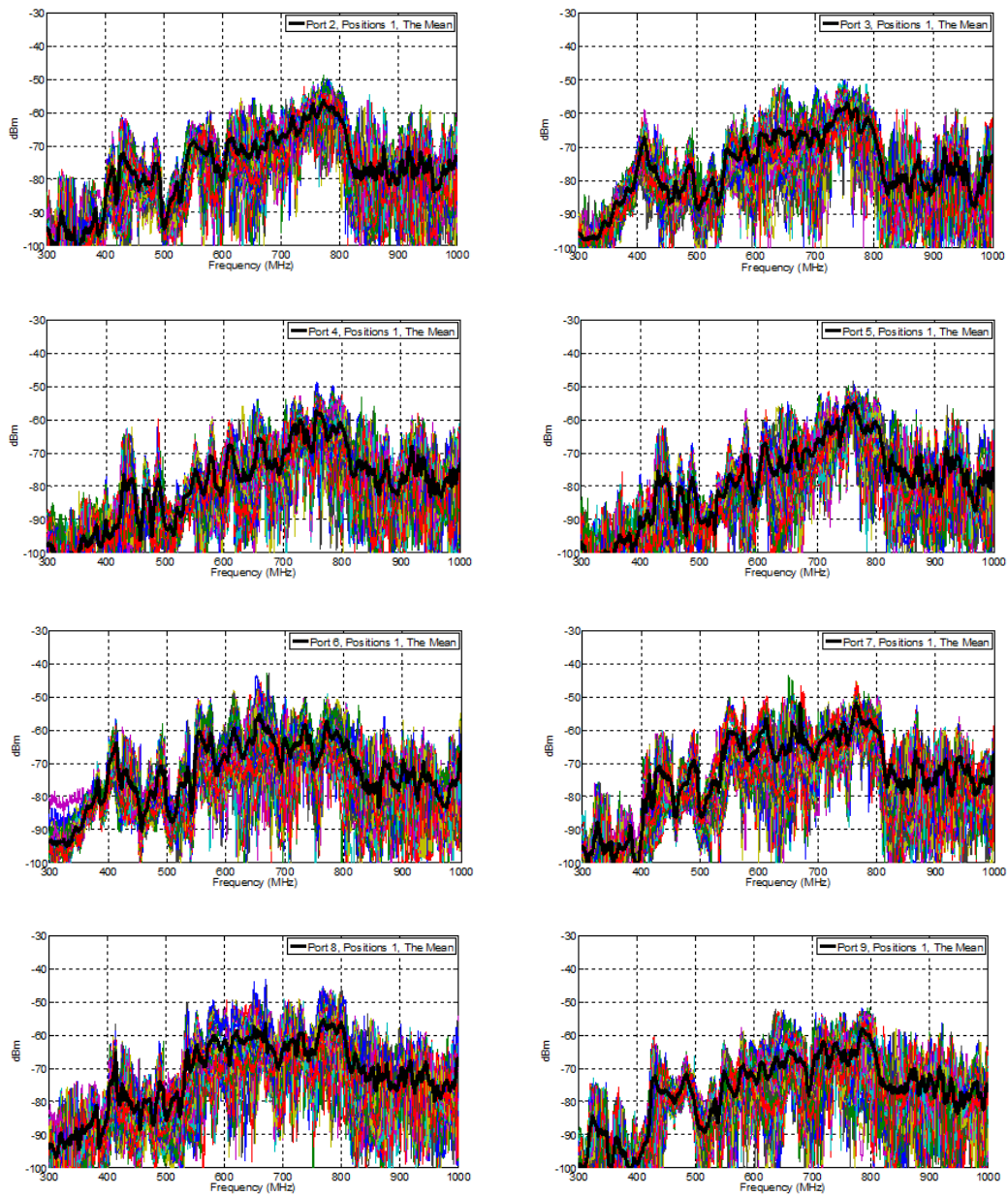


Figure E-4: from Section 5.3.3, MIMO emission measurement:
Z-polarisation, 1st EUT position, 2nd – 9th antenna

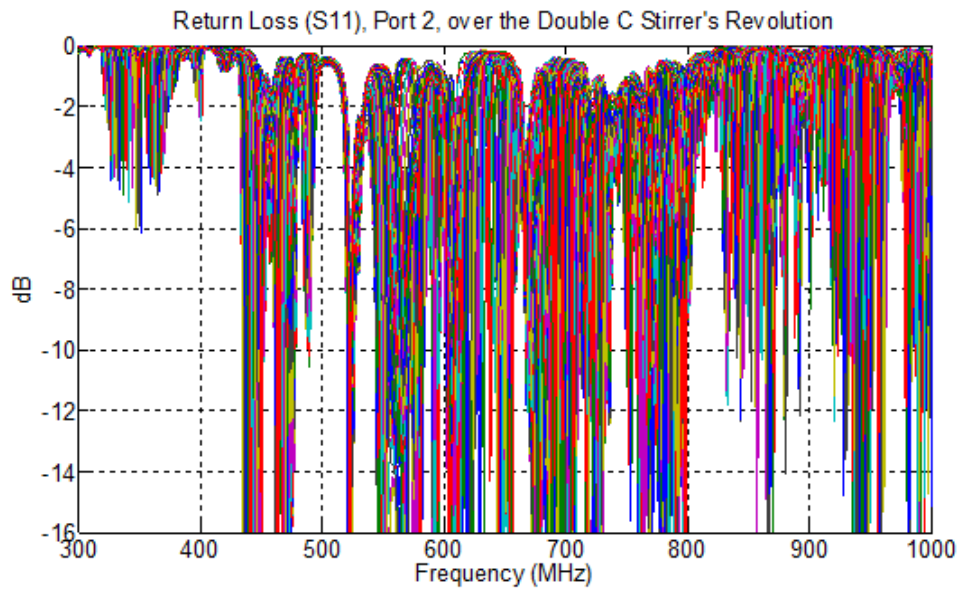


Figure E-5: from Section 3.2.2, Measured S_{11} from receiving antenna port 2, Double C stirrer, case A (Fig. 2-19).

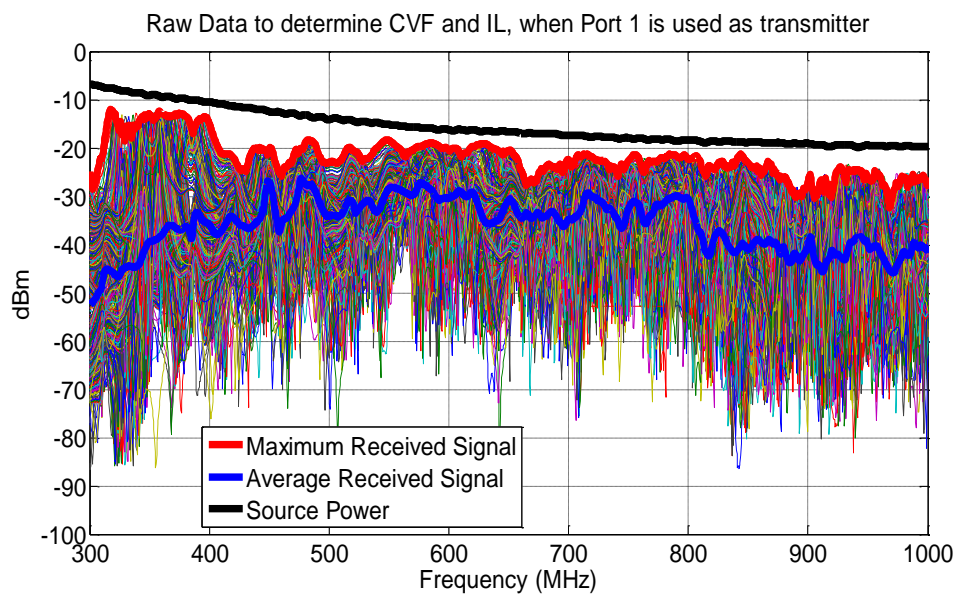


Figure E-6: from Section 5.3.2, Received signals over one stirrer revolution, when Port 1 is used as Tx (the red line is the second maximum value).

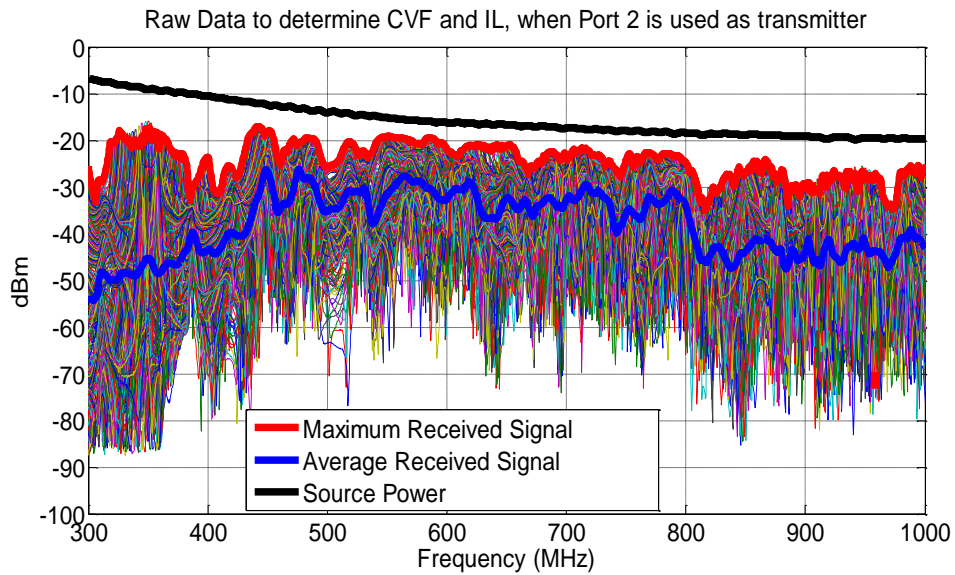


Figure E-7: from Section 5.3.2, Received signals over one stirrer revolution, when Port 2 is used as Tx (the red line is the second maximum value).

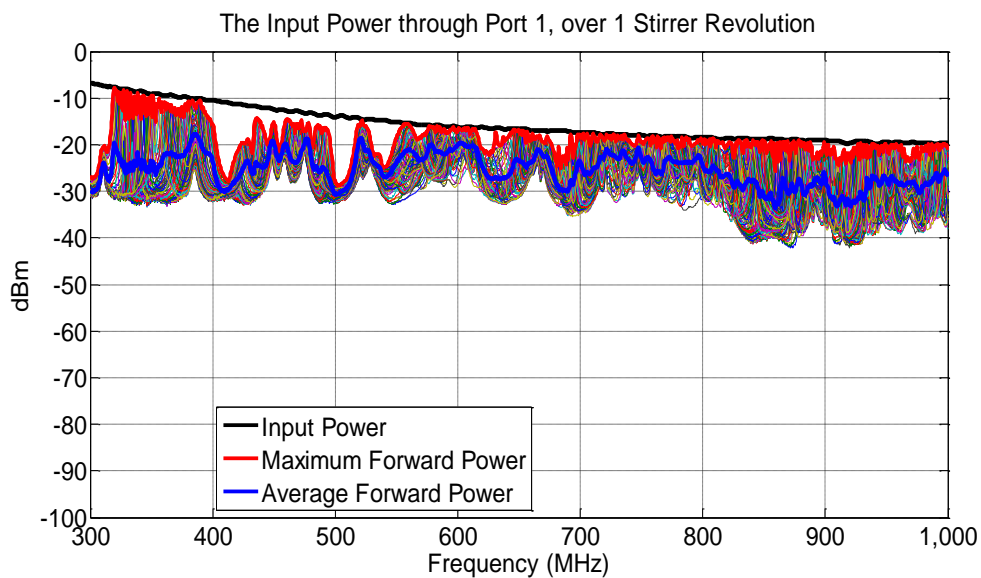


Figure E-8: from Section 5.3.2, The forwarded power go through the antenna port 1 over one stirrer revolution (the red line is the second maximum value).

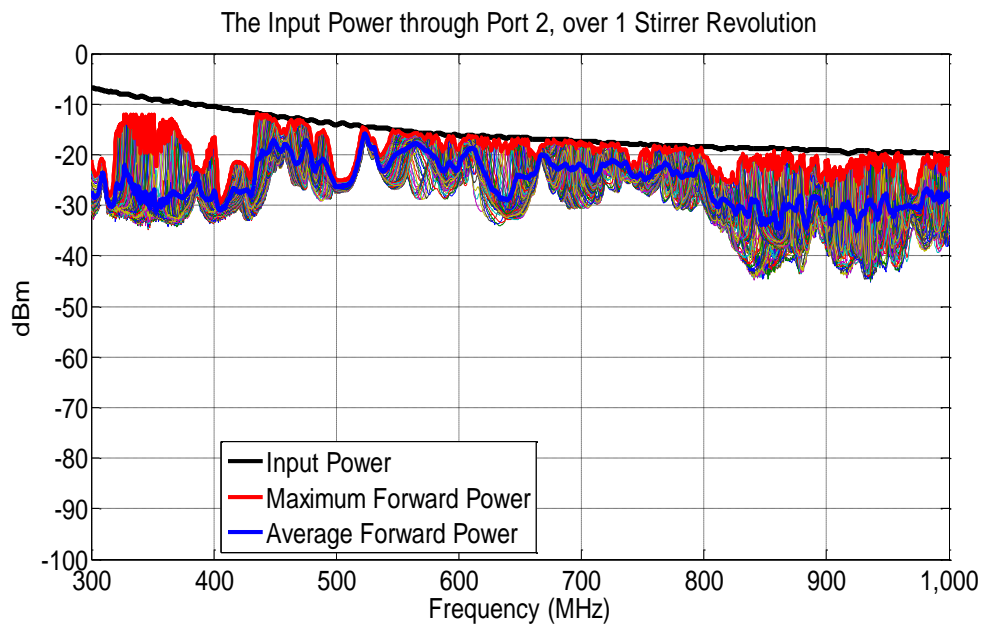


Figure E-9: from Section 5.3.2, The forwarded power go through the antenna port 2 over one stirrer revolution (the red line is the second maximum value).

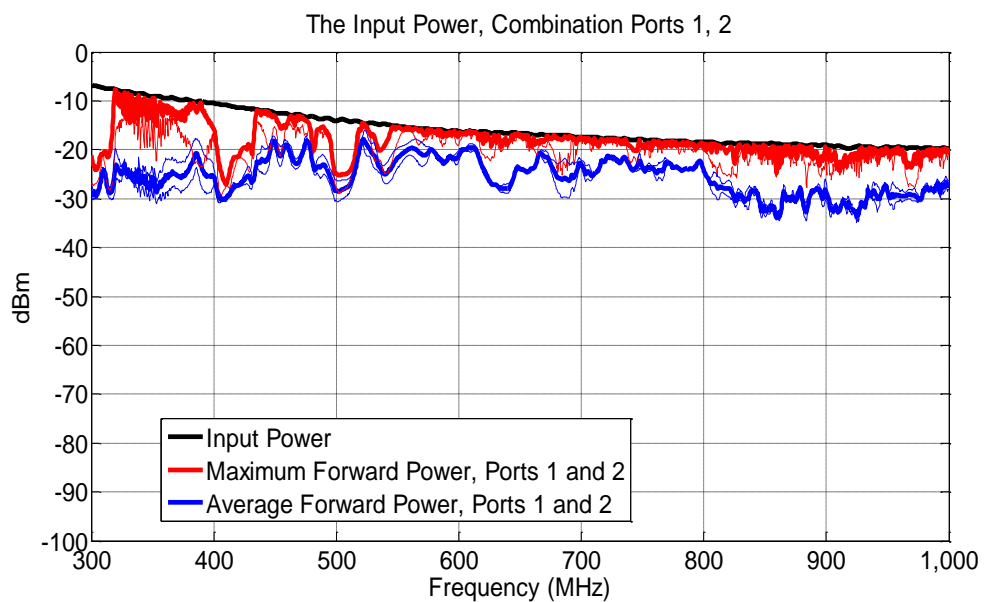


Figure E-10: from Section 5.3.2, The forward power, combination between ports 1 and 2, over one stirrer revolution.

APPENDIX F

CONVENTIONAL VALIDATION PROCEDURE
FROM IEC STANDARD 61000-4-21:2011

This appendix summarised procedures to validate a conventional RC [9]. All conventional results shown in this thesis (especially Section 4.2) follow the procedures below:

Process and Calculations for validation procedure:

- 1) The field strength is measured at each of the eight points at the extremities of the working volume, using a 3 axis probes.
- 2) At each test frequency, the tuner is stepped through a specified number of positions
- 3) For each step, the E-field sensor monitors the field strength, and the forward power to the chamber's transmitting antenna is recorded in order to find the average input power during the stirrer rotation.
- 4) The maximum E field in each of the three axes ($E_{Max\ x,y,z}$) for each position is normalised to the square root of the average input power (i.e. the average input power over all stirrer positions).
- 5) At each frequency, the average of the normalised maxima (over the 8 sample locations) is determined, for each of the three axes.
- 6) At each frequency, the average of all E-field measurements is determined, for all polarisations together.

Analysis the results:

- 1) Normalise each of the maximum E-field probe measurements to the square-root of the average input power by;

$$\vec{E}_{x,y,z} = \frac{E_{max\ x,y,z}}{\sqrt{P_{input}}}, \quad (F.1)$$

Where

$E_{max\ x,y,z}$ is the maximum measurement (in V/m) from each probe axis (i.e., 24 or 8 measurements) over the stirrer revolution,

$\vec{E}_{max\ x,y,z}$ is the normalised maximum field, defined as the maximum measurement from each probe axis data divided by the square root of the input power, and

P_{input} is the average input power (in W) to the chamber for which $E_{max\ x,y,z}$ is recorded.

- 2) Calculate the average of the normalized maximum values for each probe axis;

$$\langle \vec{E}_x \rangle_8 = \frac{(\sum \vec{E}_x)}{8}, \quad \langle \vec{E}_y \rangle_8 = \frac{(\sum \vec{E}_y)}{8}, \quad \langle \vec{E}_z \rangle_8 = \frac{(\sum \vec{E}_z)}{8}, \quad (\text{F.2})$$

$\langle \quad \rangle$ denotes arithmetic mean across a number of probe positions and/or probe axes.

- 3) Calculate the average of the normalized maximum of all the measured;

$$\langle \vec{E} \rangle_{24} = \frac{(\sum \vec{E}_{x,y,z})}{24}, \quad (\text{F.3})$$

$\langle \quad \rangle$ denotes arithmetic mean across a number of probe positions and/or probe axes.

- 4) The field uniformity is specified as a standard deviation from the normalized mean value of the normalized maximum values obtained at each of the eight locations during one rotation of the stirrer. The standard deviation is calculated using data from each probe polarisation independently and the total data set.

$$\sigma = \sqrt{\frac{\sum (\vec{E}_i - \langle \vec{E} \rangle)^2}{n-1}}, \quad (\text{F.4})$$

where

n is the number of measurements i ,

\vec{E}_i is the individual E -field measurement normalised, and

$\langle \vec{E} \rangle$ is the arithmetic mean of the normalised maximum E -field measurements.

For example, for the x-vector:

$$\sigma_x = \sqrt{\frac{\sum (\vec{E}_{x,i} - \langle \vec{E}_x \rangle_8)^2}{8-1}}, \quad (\text{F.5})$$

where

$\vec{E}_{x,i}$ is the individual measurement of x-vector,

$\langle \vec{E}_x \rangle_8$ is the arithmetic mean of the normalised $E_{max \ x}$ vectors for all eight measurement locations.

And for all vectors:

$$\sigma_{24} = \sqrt{\frac{\sum_{m=1}^8 \sum_{n=1}^3 (\vec{E}_{m,n} - \langle \vec{E} \rangle_{24})^2}{24-1}}, \quad (\text{F.6})$$

where

$\vec{E}_{m,n}$ is the individual measurement of all vectors (m = probe locations 1 -8 and n = isotropic probe axis 1-3, i.e., x , y , and z),

$\langle \vec{E} \rangle_{24}$ is the arithmetic mean of the normalised $E_{max\ x,y,z}$ vectors from all 24 measurements, and

σ_{24} is the standard deviation of all vectors (x, y, and z).

Finally, the standard deviation is expressed relative to the mean and converted to dB:

$$\sigma(\text{dB}) = 20 \log_{10} \left(\frac{\sigma + \langle \vec{E}_{x,y,z} \rangle}{\langle \vec{E}_{x,y,z} \rangle} \right), \quad (\text{F.7})$$

- 5) The chamber passes the field uniformity requirement if the standard deviation for both the individual field components and the total data set is within a specified tolerance of 3 dB for the standard deviation above 400 MHz, increasing linearly, with frequency, to 4 dB at the 100MHz (Table F-1).

Table F-1: Field uniformity tolerance requirements

Frequency range MHz	Tolerance requirements for standard deviation
80 to 100	4 dB ^a
100 to 400	4 dB at 100 MHz decreasing linearly to 3 dB at 400 MHz ^a
Above 400	3 dB ^a
^a A maximum of three frequencies per octave may exceed the allowed standard deviation by an amount not to exceed 1 dB of the required tolerance.	

- 6) If the chamber fails to meet the requirement, it may not be possible for the chamber to operate at the desired lower frequency. If the margin by which the chamber fails to meet the criteria is small, it may be possible to obtain the requirement by:

- Increasing the number of samples (i.e., tuner steps),
- Normalising the data to the average net chamber input power ($P_{\text{Net}} = P_{\text{Input}} - P_{\text{Reflected}}$),
- Reducing the size of the working volume.

APPENDIX G
PUBLICATIONS

Publications

- 1) C. Choeyesakul, F. Schlagenhauser, and P. Hall, "Characterisation and Design of a Reverberation Chamber for Electromagnetic Emission Measurements for Radio Astronomy Applications," *Postgraduate Electrical Engineering and Computing Symposium; PEECS2012*, Perth, Nov 09, 2012.
- 2) C. Choeyesakul, F. Schlagenhauser, and P. Hall, "Characterisation and Design of a Reverberation Chamber for Electromagnetic Emission Measurements for Radio Astronomy Applications," *EMC Society of Australia Newsletter*, Issue Number 59, Dec. 2012, (won the best student paper award).
- 3) C. Choeyesakul, F. Schlagenhauser, and P. Hall, "Reducing the LUF of a Reverberation Chamber based on the concept of MIMO for Electromagnetic Emission Measurements for Radio Astronomy Applications," *Asia-Pacific Symposium on EMC; APEMC*, Melbourne, May 20-23, 2013.
- 4) C. Choeyesakul, F. Schlagenhauser, and P. Hall, "EMC Applications for the Navy: Reverberation Chamber Tests," *Royal Thai Naval Academy Journal of Science and Technology*, Issue Number 1, Aug. 2014.
- 5) C. Choeyesakul, F. Schlagenhauser, P. Rattanakreep, and P. Hall, "EMC Applications for Military: Reverberation Chamber Tests," *The 20th Asia-Pacific Conference on Communications; APCC*, Pattaya, Oct. 1-3, 2014.
- 6) C. Choeyesakul, F. Schlagenhauser, and P. Hall, "EMC Applications for the Military: Reverberation Chamber Tests," *Royal Thai Air Force Journal of Science and Technology*, Issue Number 10, Nov. 2014.
- 7) C. Choeyesakul, F. Schlagenhauser, and P. Hall, "Emission Measurements in a Reverberation Chamber at Low Frequencies for Radio Astronomy Applications," *IEEE Transactions on EMC*, [in progress].

Posters

- 1) "Characterisation and Design of a Reverberation Chamber for Electromagnetic Emission Measurements for Radio Astronomy Applications," *Postgraduate Electrical Engineering and Computing Symposium; PEECS2012*, Perth, Nov. 09, 2012
- 2) "Reducing the LUF of a Reverberation Chamber based on the concept of MIMO for Electromagnetic Emission Measurements for Radio Astronomy Applications," *Asia-Pacific Symposium; APEMC*, Melbourne, May 20-23, 2013.
- 3) "EMC Applications for the Navy: Reverberation Chamber Tests," *Royal Thai Naval Academy Academic Expo 2014; RTNA Academic Expo 2014*, Samutprakarn, Aug. 22, 2014.

External Presentations

- 1) *Asia-Pacific EMC Symposium; APEMC*, Melbourne, May 22, 2013.
- 2) *RTNA Academic Expo 2014*, Samutprakarn, Thailand, on 22/Aug/2014.